AD-A016 684

PROCEEDINGS OF GAS TURBINE MATERIALS 1972 CONFERENCE HELD AT THE NAVAL SHIP ENGINEERING CENTER, HYATTSVILLE, MARYLAND IN OCTOBER 1972

Charles L. Miller

Naval Ship Engineering Center
Hyattsville, Maryland

October 1972

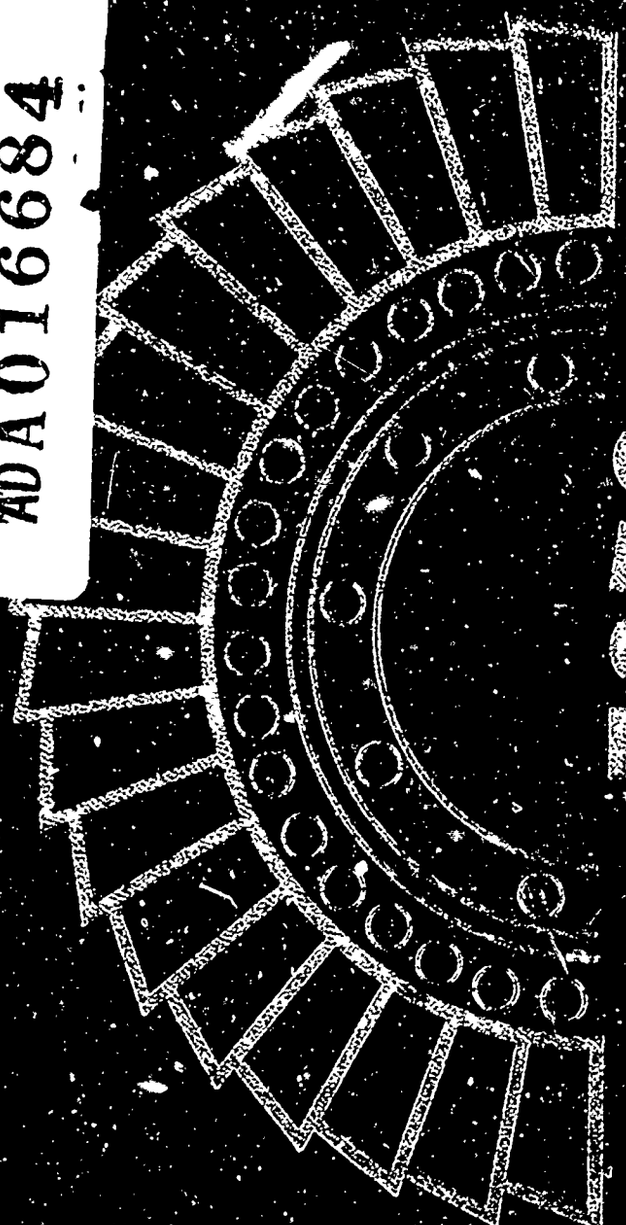

GAS TURBINE MATERIALS CONFERENCE PROCEEDINGS

NAVAL SHIP ENGINEERING CENTER
NAVAL AIR SYSTEMS COMMAND

WASHINGTON, D.C.
OCTOBER 1972

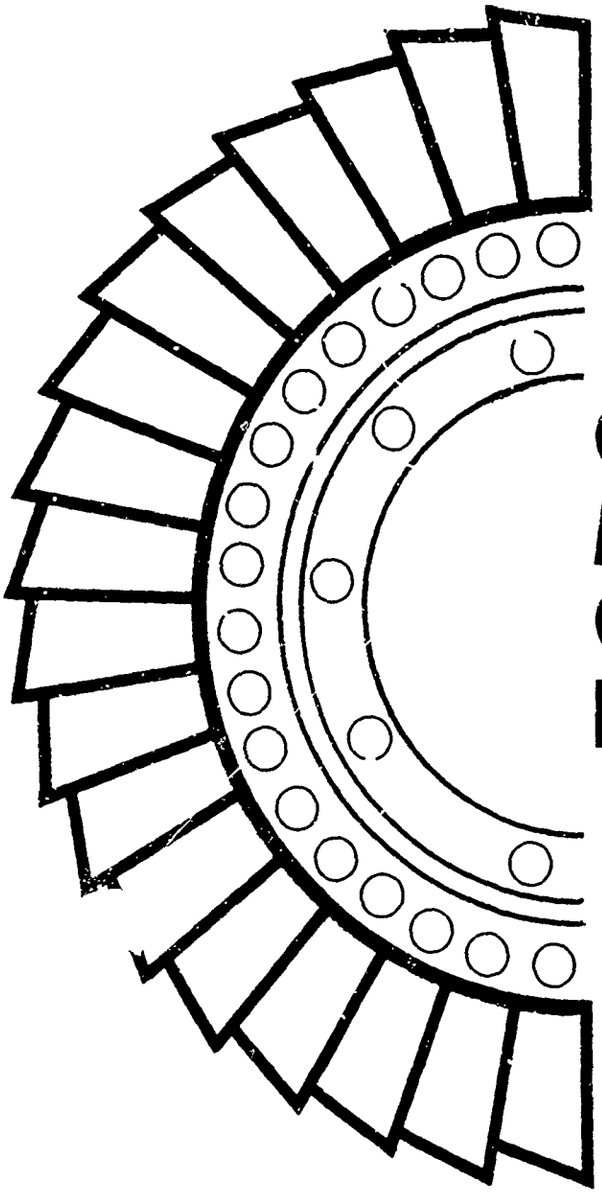

GAS TURBINE MATERIALS CONFERENCE PROCEEDINGS

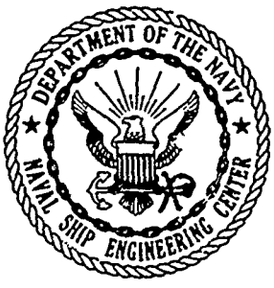

NAVAL SHIP ENGINEERING CENTER

NAVAL AIR SYSTEMS COMMAND

COLOR ILLUSTRATIONS REPRODUCED IN BLACK AND WHITE

WASHINGTON, D.C.
OCTOBER 1972

The Gas Turbine Materials Conference convened at the Naval Ship Engineering Center, Hyattsville, Md in October 1972 was jointly sponsored by the Naval Ship Engineering Center and the Naval Air Systems Command. The Conference addressed the life limiting materials and maintenance problems common to aircraft jet engines and marine gas turbines. Government and industry experts in hot-section metallurgy, coatings and testing from the United States and the United Kingdom presented technical papers.

I was most gratified by the technical expertise and cooperative spirit of all persons connected with the Conference and I commend to you this compilation of the technical papers presented.

Reviewed and approved

F. C. Jones
Rear Admiral, USN
Commander
Naval Ship Engineering Center

Preceding page blank

NAVAL SHIP ENGINEERING CENTER
CENTER BUILDING
PRINCE GEORGE'S CENTER
HYATTSVILLE, MARYLAND 20782

IN REPLY REFER TO

This conference was organized to provide a forum for technically responsible representatives of government and industry to discuss the many facets of sulfidation corrosion and methods of reducing its effects. In his opening remarks, Rear Admiral F.C. Jones, Commander, Naval Ship Engineering Center, articulated the Navy's committment to extensive gas turbine use. He also discussed some new concepts in naval surface ships which will require advanced gas turbines. Admiral Jones identified the major problem encountered operating gas turbines in the marine environment as sulfidation, which limits engine life and restricts performance improvements. The conference co-host, Captain A.D. Williams, Commanding Officer of the Naval Air Propulsion Test Center, indicated that sulfidation is also a significant problem with naval aircraft jet engines. He went on to outline some of the projects related to this problem that the Naval Air Systems Command is sponsoring. These programs of common interest with the surface forces including accelerated salt ingestion testing, non-destructive test techniques and reprocessing of air-cooled blades and vanes.

The opening session was on the mechanism of sulfidation corrosion with renowned investigators as both authors and discussors. This session produced the best technical discourse on this topic ever conducted and helped place in perspective both the commonalty and diverse interpretations of this complex phenomenon.

After the problem was placed in perspective, speakers intimately involved with materials development and engine use discussed materials and coatings which ameliorated engine resistance to the sulfidizing environment. The high level of success of the conference is directly attributable to the willingness of the engine manufacturers to discuss the state-of-the art in high temperature coatings and substrate alloys. The detailed discussions of mutual problems by the highly knowledgable participants were particularly interesting. The description of the NAVSEC sponsored program with high-rate sputter deposition stimulated considerable interest in this new process to coat vanes and blades.

The third session was devoted to various testing techniques to determine sulfidation resistance and engine life. The non-destructive technique of microdefect detection was quite interesting. Also, test cell results at NAPTC were of considerable interest.

On behalf of the Naval Air Propulsion Test Center and the Naval Ship Engineering Center, I would like to express the Navy's sincere appreciation of the outstanding presentations by both authors and discussors. The extensive willingness and unbounded co-operation of the participants made this meeting the most meaningful gas turbine conference that I have attended in my sixteen years in this field. I should like to hoist the "Bravo-Zulu" pennants, which is the Navy's flag code for "Well done", for the conference organizer, John Fairbanks.

Charles L. Miller
Conference Chairman

Preceding page blank

The Major Problem with Marine Gas Turbines–Sulfidation–Illustrated with 2 Superalloys used in Aircraft Engines Exposed to Na_2SO_4 Crucible Test at 1700°F.

Session I

MECHANISM OF HOT CORROSION

Session Chairman:

John Fairbanks
NAVSEC Hyattsville, Maryland

WEDNESDAY, OCTOBER 25, 1972

Accelerated Corrosion in Gas Turbine Engines

N. S. Bornstein, M. A. DeCrescente and H. A. Roth
United Aircraft Research Laboratories
East Hartford, Connecticut

ABSTRACT

The relationship between oxide ion content of Na_2SO_4 and the accelerated oxidation phenomenon termed sulfidation attack was investigated. It was previously shown that oxides such as Cr_2O_3 which decrease the oxide ion content of Na_2SO_4, inhibit sulfidation attack. It was found that the oxides MoO_3 and V_2O_5 like Cr_2O_3 react with and thereby decrease the oxide ion content of fused Na_2SO_4. It was also shown that binary nickel-vanadium and nickel-molybdenum alloys like nickel-chromium alloys are more resistant to Na_2SO_4 attack than unalloyed nickel.

The reactions between V_2O_5 with metal oxides and the salt Na_2SO_4 were also investigated. V_2O_5 readily fluxes Al_2O_3 and slowly reacts with Na_2SO_4. The relationship between accelerated oxidation attack, oxide ion content of the fused melt and fluxing of the normally protective oxide scale by liquid metal oxides is discussed.

INTRODUCTION

Accelerated oxidation, hot corrosion, or sulfidation attack of gas turbine alloys occurs when a salt composed primarily of Na_2SO_4 deposits onto turbine components (1). It has been postulated that the accelerated rates of oxidation are due to the rapid oxidation of sulfide phases (2) or loss of oxidation inhibition by chromium-depletion through formation of chromium rich sulfide precipitates (3,4). Simons, et al (2) postulated a reducing agent in the alloy which reacts with Na_2SO_4 to produce sulfides, although Quets and Dresher (5) indicate that the formation of alkali compounds, i.e. $NaAlO_2$, Na_2CrO_4, etc. is the necessary driving force to release sulfur for sulfide formation.

Bornstein and DeCrescente (6,7,8,9) have shown that the accelerated rates of oxidation associated with sulfidation attack are not related to the preferential oxidation of either the sulfur rich phases or the alloy depleted zone and have shown that the accelerated rates of oxidation are due to the inability of the alloy to form a protective oxide scale due to the presence of oxide ions in the Na_2SO_4 melt. Gobel and Pettit (10) confirmed that the products of the reaction between the normally protective oxide scale and oxide ions is nonprotective, and then postulated that the self-sustaining nature of the attack appears to be caused by alloying elements that are present in the alloy.

The superalloys employed in gas turbine engines are quite complex, often consisting of five or more alloying elements. Aluminum, titanium, and chromium are common alloying elements to almost all of the commercially available nickel base superalloys. In addition, one or more of the refractory metals such as molybdenum, tungsten and vanadium are present in concentrations from less than one to more than 18 weight percent.

During oxidation the refractory metals present in the alloy contribute to the formation of the oxide scale. During sulfidation, the oxides of these refractory metals can interact with the fused salt. The objectives of this study are to determine the relationship between refractory metal oxides, oxide ion concentration in fused Na_2SO_4 and sulfidation attack of some nickel base alloys and nickel aluminide which is the most commonly employed protective coating for superalloys.

EXPERIMENTAL PROCEDURES

The nickel base superalloy B-1900 and five binary nickel base alloys were chosen for this study. The nominal compositions are presented in Table I.

Test specimens approximately 1 X 1 X 0.090 in. in the "as cast" condition were polished with 600 grit emery, washed and rinsed with acetone immediately prior to all experiments. The method of inducing sulfidation attack, i.e. application of Na_2SO_4 and subsequent exposure at elevated temperatures, has been described in detail in a previous publication (8). Continuous oxidation studies were performed using an Ainsworth thermobalance and a three zone Marshall furnace all of which have also been described elsewhere (8).

The NiAl specimens were prepared by hot pressing finely divided (-325 mesh) NiAl powders. Consolidation was achieved by pressing at 1250°C for one hour in argon at an applied pressure of 5000 psi.

NiAl alloyed with either Cr, Mo, or V was obtained by mixing the respective metal powders with the NiAl powder prior to consolidation.

EXPERIMENTAL RESULTS

BINARY NICKEL ALLOYS

Sulfidation attack occurs when oxide ions present in the melt react with the normally protective oxide scale to form product(s) which are nonprotective with respect to the

Table I
Nominal Composition of Alloys

Alloy	Elements w/o								
	Ni	Cr	Co	Ti	Al	Mo	Ta	C	V
B-1900	Bal	8	10	1	6	6	4	0.1	
Ni-1V	99								1
Ni-5V	94.5								5.5
Ni-10V	89								11
Ni-4Mo	96					4			
NiAl	67				33				

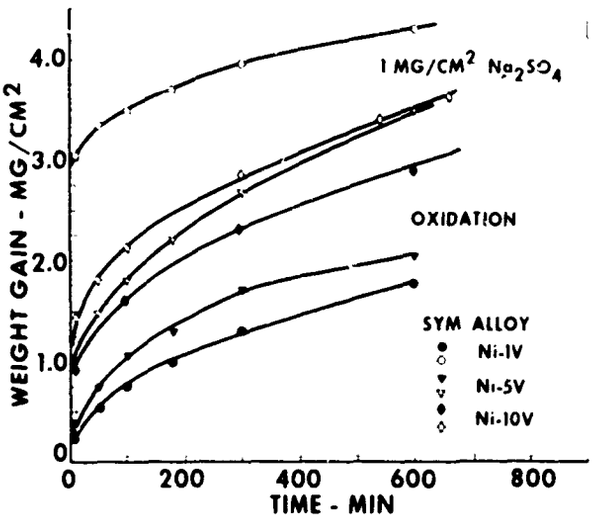

Figure 1. Oxidation behavior of uncoated and Na_2SO_4 coated Ni-V alloys exposed at 900°C in O_2.

metallic substrate (8). Sulfidation attack is prevented by reducing the oxide ion concentration of the fused melt so that this reaction does not occur (8).

It was shown that oxides such as Cr_2O_3 and SnO_2 react with and sufficiently reduce the oxide ion concentration of Na_2SO_4 to allow the fused salt and the oxide scale to coexist. In a recent publication it was shown that oxides such as MoO_3 and V_2O_5, like Cr_2O_3 react with and decrease the oxide ion content of Na_2SO_4 (9). It has been determined by thermodynamic calculations that the oxides of tungsten, titanium and silicon can react with and reduce the oxide ion content of the fused melt. This has not been verified by the electrochemical techniques previously used to measure relative oxide ion concentrations in Na_2SO_4 (7,15). The extent to which the reactions can occur will be discussed later in detail.

Ni-V Alloys

It has been shown that whereas Na_2SO_4 significantly increases the rate of oxidation of unalloyed nickel, the corrosivity of the fused salt is significantly decreased and depending upon the Cr content of the alloy the rate of oxidation of salt free and Na_2SO_4 coated Ni-Cr alloys are for all practical purposes identical (7). Since both Cr_2O_3 and V_2O_5 decreased the oxide ion content of fused Na_2SO_4, it was expected that the behavior of Ni-V alloys would be similar to Ni-Cr alloys. In order to verify that the behavior of vanadium is similar to that of chromium, the oxidation kinetics of uncoated and Na_2SO_4 coated Ni-1V, Ni-5V and Ni-10V alloys exposed at 900°C were studied.

The effect of vanadium on the oxidation behavior of nickel is shown in Fig. 1 where the filled symbols represent the oxidation of Ni-1V, Ni-5V and Ni-10V exposed at 900°C in flowing oxygen. It is observed that as the vanadium content of the alloy increases, the rate of oxidation also increases. These results agree with those of a previous study (11).

The open symbols represent the rates of oxidation of the Na_2SO_4 coated (sulfidation) Ni-V alloys. It is observed that as the vanadium content of the alloy increases the degree to which the alloy is affected by Na_2SO_4 decreases. Thus, vanadium inhibits sulfidation in nickel-vanadium alloys. Although the data are not shown in Fig. 1, the rate of oxidation of 1 mg/cm^2 Na_2SO_4 coated unalloyed nickel at 900°C is extremely rapid. After 10 min exposure, the weight gain is approximately 10 mg/cm^2.

The surfaces of the Na_2SO_4 coated Ni-V alloys were chemically analyzed after test, to determine the amount of unreacted Na_2SO_4 and water soluble vanadium formed. These results are summarized in Table II. Little difference was found in the amount of sodium present prior to and after test, although the amount of sulfate found was dependent to some degree upon the vanadium content in the alloy. Although it is not possible to establish the identity of the soluble vanadium compound, the salts present on the Ni-1V alloy based upon electro-neutrality, are Na_2SO_4 and Na_3VO_4, while those present on the Ni-5V and Ni-10V alloy are $NaVO_3$ and Na_2SO_4.

Table II
Quantitative Chemical Analyses of Salt Coated Ni-V Alloys

Alloy	Salt Applied (millimoles)		Chemical Analyses (millimoles)		
	Na	SO_4	Na	V	SO_4
Ni-1V	.1240	.0618	.108	.0180	.0025
Ni-5V	.1305	.0652	.1272	.0712	.0291
Ni-10V	.1285	.0642	.1165	.0628	.0307

It was shown in Ref. (7) that when Cr_2O_3 is codeposited with Na_2SO_4 onto nickel or nickel base superalloys, the accelerated rate of oxidation associated with sulfidation attack are attenuated or prevented. Weight gain experiments were performed in which V_2O_5 was codeposited with Na_2SO_4 onto Ni-V alloys. These results are shown in Fig. 2. It is seen that when either V_2O_5 (or MoO_3) are codeposited onto nickel-vanadium alloys the differences in the rates of oxidation between the salt coated and salt free specimens are quite small. When 12.5 w/o V_2O_5 was added to the Na_2SO_4 coated Ni-1V alloy, the rate of oxidation of the salt coated specimen was identical for all practical purposes to that of the salt free specimen, Fig. 2. Metallographical examination of Na_2SO_4 coated and Na_2SO_4 + 12.5 w/o V_2O_5 coated Ni-V revealed in the case of the former the presence of numerous nickel-vanadium rich sulfide precipitates in the matrix and a continuous film of a nickel-vanadium sulfur phase (as identified by electron microbeam studies) directly beneath the oxide scale and in the adjacent grain boundaries, Fig. 3. In the case of the latter, the presence of an internal oxidation zone was noted, however, noticeably lacking was the sulfur rich phases which were so prominent when only Na_2SO_4 was present (Fig. 3).

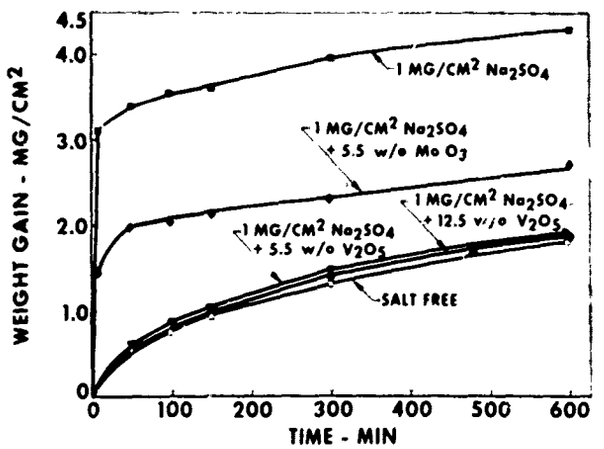

Figure 2. Effect of decreasing the [O⁼] on the oxidation behavior of Na_2SO_4 coated Ni-1V at 900°C.

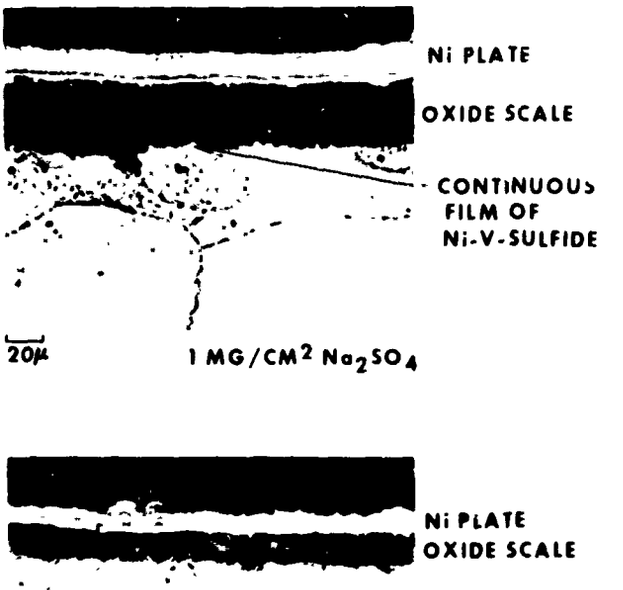

Figure 3. Microstructure of salt coated Ni-1V alloy exposed at 900°C.

Ni-4Mo

Since MoO_3 was shown to behave similar to Cr_2O_3 and V_2O_5 with respect to lowering the oxide ion content of Na_2SO_4, the oxidation behavior of the binary alloy Ni-4Mo was also studied. A comparison of the oxidation behavior at 825°C of Na_2SO_4 coated Ni and Na_2SO_4 coated Ni-4Mo is shown in Fig. 4. In the absence of Mo, the rate of oxidation of the nickel is very rapid, however, similar accelerated rates of oxidation are not noted with the salt coated Ni-4Mo alloy specimen.

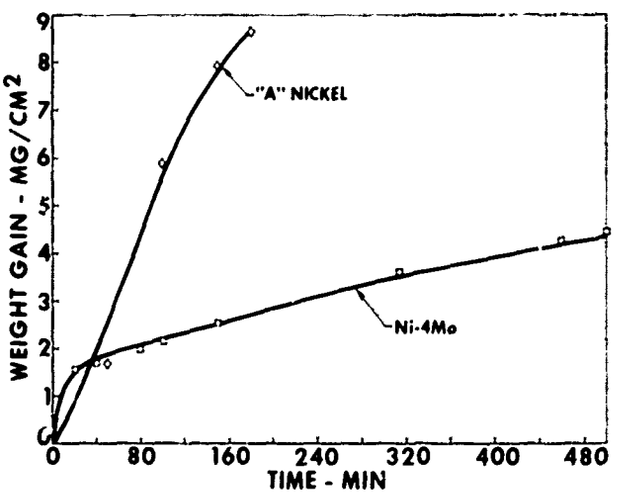

Figure 4. Oxidation of Na_2SO_4 coated alloys at 825°C in O_2.

NiAl

Oxidation–The introduction of Cr, Mo, or V to NiAl in almost all cases adverseiy affected the oxidation behavior of the intermetallic compound. However, whereas the effect of Cr (1 and 5 w/o) was minimal, significantly large

increases in the rates of oxidation were noted for vanadium or molybdenum additions, Fig. 5.

Na_2SO_4-Accelerated Oxidation - The intermetallic compound NiAl, like the nickel base superalloys, undergoes accelerated rates of oxidation when coated with Na_2SO_4. The comparison between uncoated and Na_2SO_4-coated NiAl at 1000°C is shown in Fig. 6. Again, the effect of Cr is beneficial with respect to sulfidation attack. These results are shown in Fig. 6. It is observed that as the Cr content of the NiAl is increased the difference in magnitude of the weight gains between that of Na_2SO_4 accelerated oxidation and simple oxidation decreases, and at 10 w/o Cr, a continual weight loss is noted. The latter behavior had previously been observed during sulfidation of Ni-17Cr alloys (7,8) and is attributed to the loss of SO_2 and evaporation of the more volatile salt, Na_2CrO_4.

It was demonstrated earlier in this report that additions of vanadium and molybdenum to nickel decreased the rate of oxidation of Na_2SO_4-coated specimens and in effect these elements performed like chromium. Their behavior is in agreement with the predicted behavior based upon the electrochemical studies which showed that the oxides of Cr, V, and Mo react with and decrease the oxide ion content of fused Na_2SO_4. However, when Na_2SO_4 was applied onto the NiAl + Mo or NiAl + V specimens, inhibition was not observed. On the contrary the rate of sulfidation of NiAl was significantly increased when these elements were present, Fig. 7.

After test, the salts present on the surface of the Na_2SO_4-coated NiAl-10 w/o Mo specimen were analyzed by wet chemical techniques. The results are presented in Table III.

Initially, 45μ moles of Na^+ and 22.5μ moles of $SO_4^=$ (as Na_2SO_4) were applied onto the NiAl + 10 w/o Mo specimen. After exposure for approximately 30 min at 1000°C the specimen was cooled and immersed into water. The solution was analyzed and found to contain 43.5μ moles of Na^+ and 20.6μ moles of $SO_4^=$ in good agreement with the original amount applied. In addition to soluble sodium and sulfate, a significant quantity of soluble molybdenum, 15.72μ moles, was noted. The fact that no significant quantity of sulfate was consumed during the experiment

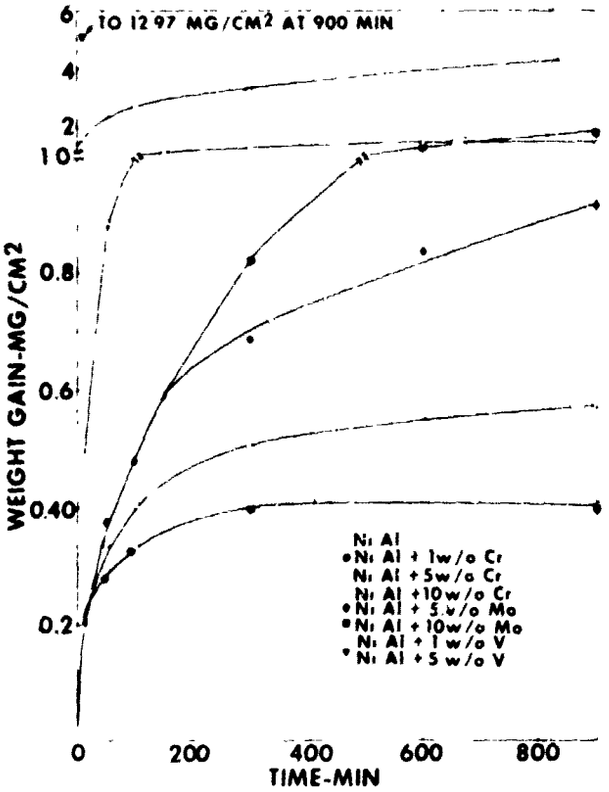

Figure 5. Oxidation of 1 mg/cm^2 Na_2SO_4 coated NiAl at 1000°C.

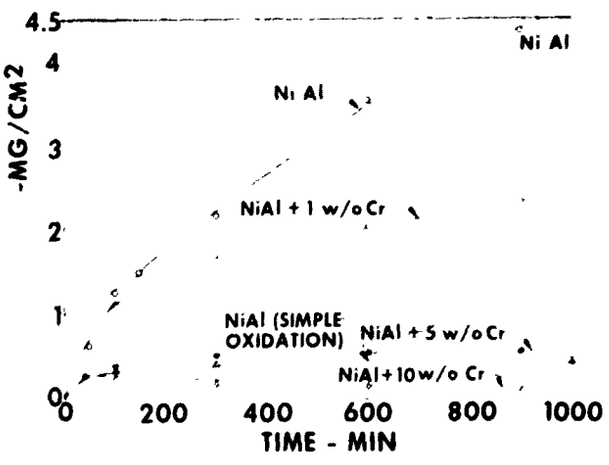

Figure 6. Comparison of the oxidation behavior of 1 mg/cm^2 Na_2SO_4 coated in NiAl at 1000°C.

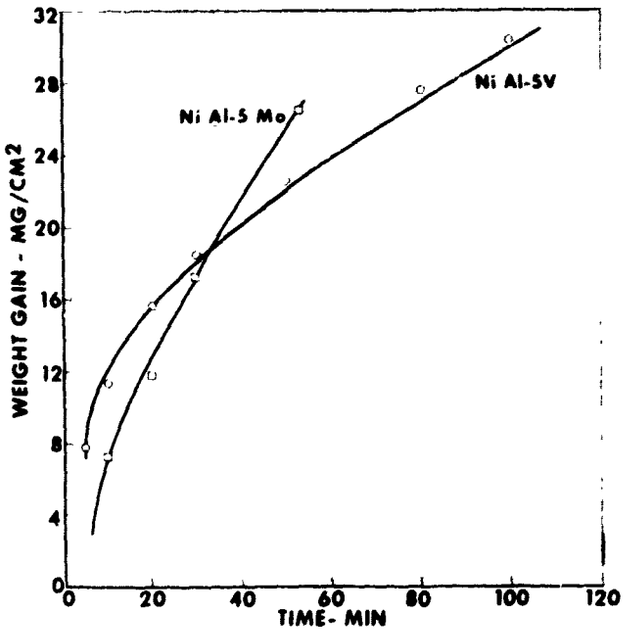

Figure 7. Oxidation of NiAl at 1000°C in flowing O_2.

Table III
Quantitative Chemical Analyses of
Na_2SO_4 Coated NiAl - 10 w/o Mo

Initial Amount of Salt Applied	
Na^+ (μ moles)	$SO_4^=$ (μ moles)
45	22.5

Initial Molar Ratio $Na/SO_4^=$ 2/1

After Test		
Na^+ (μ moles)	$SO_4^=$ (μ moles)	Mo^+ (μ moles)
43.5	20.6	15.72

Final Molar Ratio $Na/SO_4^=$ 2/1

indicates that the reaction $SO_4^= + MoO_3 \rightarrow MoO_4^= + SO_3$ had not occurred. Instead, the presence of soluble molybdenum in the wash solution after test is due to the dissolution of MoO_3, a water soluble oxide.

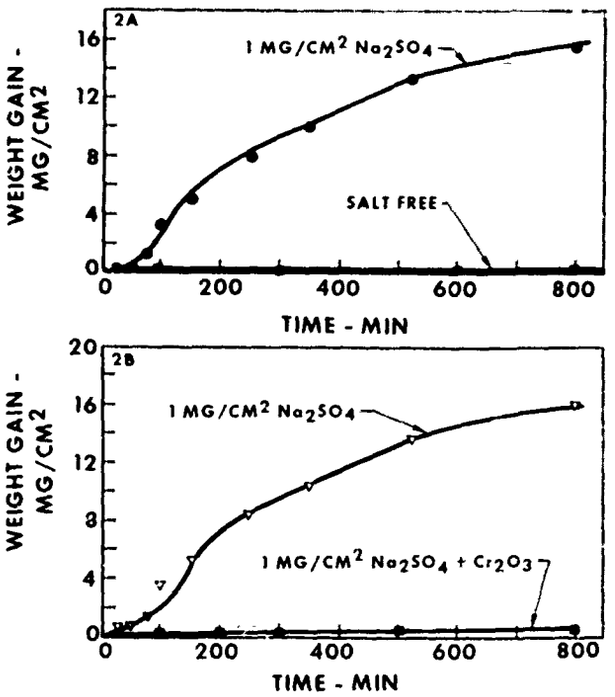

Figure 8. Oxidation of B-1900 alloy at 900°C.

SUPERALLOYS

A comparison of the oxidation behavior of uncoated and 1 mg/cm^2 Na_2SO_4 coated B-1900 at 900°C is shown in Fig. 8a. When Cr_2O_3 or SnO_2 are codeposited with Na_2SO_4, no accelerated rates of oxidation are observed, Fig. 8b. However when MoO_3 or V_2O_5 are codeposited with Na_2SO_4, the inhibition previously observed with Cr_2O_3 and SnO_2 is not observed, and the alloy oxidizes at an accelerated rate, Fig. 9.

When the oxide SiO_2 is codeposited with Na_2SO_4 onto B-1900, the rate of oxidation of the alloy is comparable to that of simple oxidation, i.e. as observed with the Cr_2O_3 or SnO_2 additions, Fig. 10. However, if the specimen is thermally shocked (removal and then reinsertion into the hot zone of the furnace), rapid rates of oxidation ensue. This is also shown in Fig. 10.

Specimens coated with 1 mg/cm^2 each of SiO_2 and Na_2SO_4 were after 1000 min exposure at 1000°C washed and the solutions quantitatively chemically analyzed. Only trace quantities of Na_2SO_4 were found. The surface of the specimen was coated with a glassy scale.

Specimens similarly coated and exposed for 300 min at 900°C were also immersed in water and the solutions were quantitatively analyzed. The solutions were found to contain soluble sodium and silicon. The silicon was inferred to be present as $Na_2Si_2O_5$, which is water soluble. This is based on quantitative chemical analyses of the reaction products present on Si_3N_4 after sulfidation.

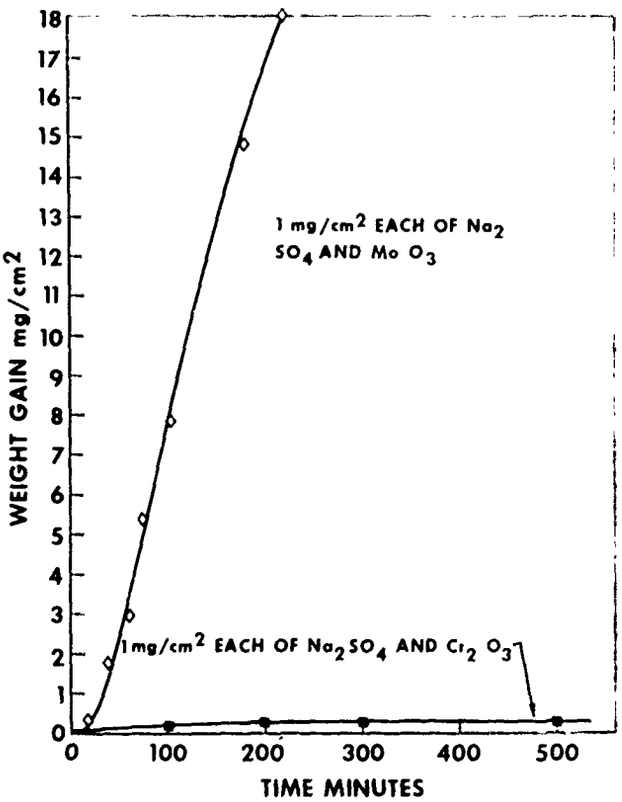

Figure 9. Oxidation of salt coated B-1900 at 900°C.

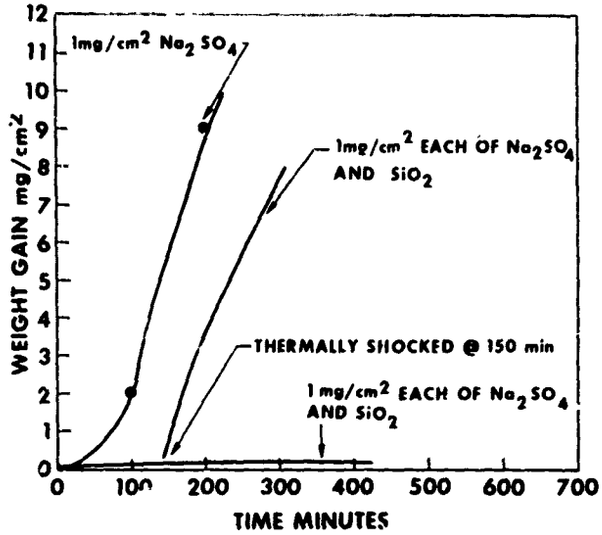

Figure 10. Oxidation of salt coated B-1900 at 900°C.

FUSED SALT EXPERIMENTS

Al_2O_3 Dissolution

In order to determine the relative rate of dissolution of Al_2O_3 in fused salts, a series of experiments was performed in which coupons of high purity Al_2O_3, approximately 1/2 in. X 1/2 in. X 0.10 in., were immersed into Na_2SO_4, and into Na_2SO_4 containing various concentrations of either Na_2O, V_2O_5 or MoO_3. The experimental procedure consisted of heating the salt(s) in Pt crucibles to 900°C ± 10°C and allowing the fused melt to equilibrate for 45 minutes. During this time the Al_2O_3 specimen, suspended from a platinum wire, was then immersed into the fused melt and held for a predetermined period, removed and then stripped of retained melt by immersion into boiling water.

The experimental results are presented in Table IVA. It is noted that no measurable weight changes were detected when the Al_2O_3 was immersed into the pure salt. With either V_2O_5 or Na_2O contained in the Na_2SO_4, dissolution of Al_2O_3 occurred. The amount of Al_2O_3 which dissolved in the V_2O_5-Na_2SO_4 (.5-1 m/o) melts was small, whereas significant losses were observed when Na_2O was present. The experiment was repeated with the following changes in the experimental procedure. The platinum crucible containing the Na_2SO_4 was heated to 900°C and then a smaller platinum crucible containing either MoO_3 or V_2O_5 which was already at 900°C was lowered into the Na_2SO_4-filled crucible. At the same time, the Al_2O_3 specimen which was maintained at 900°C was also lowered into the Na_2SO_4-filled crucible. Thus, the Al_2O_3 specimen could at no time directly contact the V_2O_5 (MoO_3) and yet due to subsequent chemical reactions, the effect of these oxides on the dissolution of Al_2O_3 in Na_2SO_4 could be evaluated. The results of this experiment are summarized in Table IVB. It is seen that no weight loss of Al_2O_3 occurred when either V_2O_5 or MoO_3 were added to the Na_2SO_4 in such a way that direct contact was prevented even though the amount of V_2O_5 present was more than 5 times greater than that in the previous experiment. Based upon subsequent chemical analysis of the fused melt, the concentration of vanadium in the melt was at least 2 mol percent which indicates that mixing and reaction of the two fused salts did occur.

When Al_2O_3 was immersed into either pure V_2O_5 or MoO_3 the rate of dissolution is extremely rapid as shown in Table IVB.

V_2O_5-Na_2SO_4 Reaction Studies

According to the phase diagram published in Ref. 12, there exists in the V_2O_5-Na_2SO_4 system only one compound containing 25 m/o Na_2SO_4 which melt congruently at 700°C and is separated from the terminal phases by two eutectics which occur at 10 m/o Na_2SO_4 (630°C) and 80 m/o Na_2SO_4 (650°C). The melting point of Na_2SO_4 is 884°C and that for V_2O_5 is 672°C. In order to determine if the rate of the reaction between V_2O_5 and Na_2SO_4 is rapid or proceeds slowly, an experiment was performed in which V_2O_5 and Na_2SO_4 mixture was melted in a quartz tube.

The powders, 90 m/o Na_2SO_4 and 10 m/o V_2O_5, were mixed and then placed into a quartz tube open on one end which was heated for 1 hr at 900°C in air.

After heating for 1 hr, the quartz tube was quickly removed from the furnace, chilled and then broken. It was observed that the "cap," that portion of the melt in contact with the bottom of the quartz tube, was yellow in appearance and the rest of the melt steel gray in color. The cap is shown in Fig. 11. A cross section through the cap is shown in Fig. 11b and the microstructure of the salt mixture is shown in Fig. 11c. The large grains are alloyed Na_2SO_4 and the bright yellow grains (which appear white in the photomicrograph) are a vanadium rich compound whose identity was not established. In the interstices of the grains lies a purple phase. The concentration of this purple phase is significantly greater at the bottom (i.e. cap) than in the center and quite sparse at the top, in agreement with the relative densities of V_2O_5 and Na_2SO_4, i.e. the more dense V_2O_5 tended to separate from the less dense Na_2SO_4.

Na_2SO_4-MxOy Nickel Base Superalloys

A mixture of the salt, Na_2SO_4 and one of the following oxides Cr_2O_3, MoO_3, V_2O_5, and WO_3 were applied onto one face of a B-1900 alloy specimen and exposed for up to 6 hrs at ± 900°C in static air. The amount of salt applied was approximately 1 mg/cm² of Na_2SO_4 and a comparable amount of metal oxide. After test, the specimens were removed from the furnace, washed and examined. The specimens coated with Na_2SO_4, Na_2SO_4 + MoO_3, and Na_2SO_4 + V_2O_5 exhibited the typical sulfidation

Table IV
Stability of Al_2O_3 in Na_2SO_4 Melts at 900°C ± 10°C

	A. Series I (Salts and Oxides in Physical Contact)								
Run No.	Salt Composition (mole percent)			Weight Loss (mg) after					
	Na_2SO_4	V_2O_5	Na_2O	30 min	60 min	6 hrs	10 hrs	24 hrs	65 hrs
1	100					0	0	0	0
2	99.5	.5		3	6	7	7.5		
3	99	1.		4.5	8	8.5		8.5	
4	95		5			105		300	

	B. Series II (V_2O_5 and MoO_3 Physically Separated from Al_2O_3)							
Run No.	Salt Composition (mole percent)			Weight Loss (mg) after				
	Na_2SO_4	V_2O_5	MoO_3	2 min	5 min	15 min	25 min	45 min
5	100			0	0			0
6	97	3			0	0		0
7		100			7.25		89	216
8			100	50				

morphology, i.e. loose non-adhering oxide scale. The specimens coated with Na_2SO_4 + Cr_2O_3 or Na_2SO_4 + WO_3 exhibit a tight, adherent oxide scale, similar to that expected for simple oxidation. No visual evidence of sulfidation attack or accelerated oxidation was noted. Photographs of the specimens are shown in Fig. 12.

DISCUSSION

Sulfidation attack can occur when a salt composed primarily of Na_2SO_4 is deposited onto superalloy gas turbine components. It has been shown that oxide ions present in the melt react with the normally protective oxide scale rendering it nonprotective. The normally protective oxide scale formed on the high strength nickel base superalloys is composed chiefly of alumina. The subsequent reaction between the salt and the substrate results in the formation of the sulfur rich precipitates which are associated with sulfidation attack. The decrease in sulfur potential as a result of sulfide formation is synonymous with an increase in the oxide ion concentration in the melt thereby preventing reformation of a protective oxide scale.

Chromium oxide has been shown to preferentially react with oxide ions present in the melt (7). The reaction product is Na_2CrO_4. The lowering of the oxide ion concentration allows the fused melt to coexist with the normally protective oxide scale.

Vanadium pentoxide and MoO_3 have also been shown by electrochemical techniques to decrease the oxide ion content of sodium sulfate (8). Available thermodynamic data indicate that the oxides of tungsten, titanium and silicon would also react with and therefore decrease the oxide ion concentration of Na_2SO_4. The relative ranking order of oxides capable of reducing the oxide ion content of Na_2SO_4 can be determined by electrochemical cell studies as described in Ref. 15 or calculated if the necessary thermodynamic data are available. The ranking of the oxides $Al_2O_3, Cr_2O_3, MoO_3, V_2O_5, SiO_2, WO_3$ and TiO_2 based on the thermodynamic calculations are listed in Table V.

When mixtures of V_2O_5 or MoO_3 and Na_2SO_4 are applied onto nickel base superalloys or onto NiAl + V or NiAl + Mo alloys, sulfidation inhibition is not observed and the apparent corrosivity of the fused salt is enhanced.

It has been proposed by Goebel, et al (13) that the additions of MoO_3 or V_2O_5 reduce the oxide ion content of the fused melt to a low enough level so that the activity of oxygen ions in the melt is less than that required for the protective oxide scale to be stable in the melt. The oxide

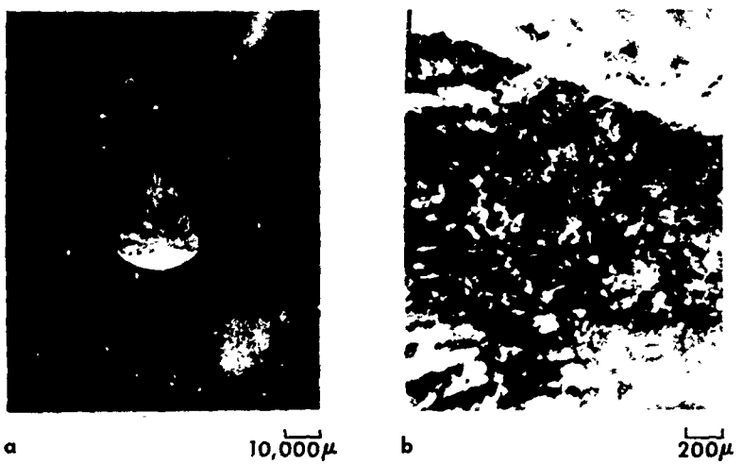

Figure 11. Microstructure of Na_2SO_4-V_2O_5 melt.

ALLOY	B-1900
SALT	1 MG/CM^2 Na_2SO_4 1 MG/CM^2 M_xO_y
TEMP	900°C

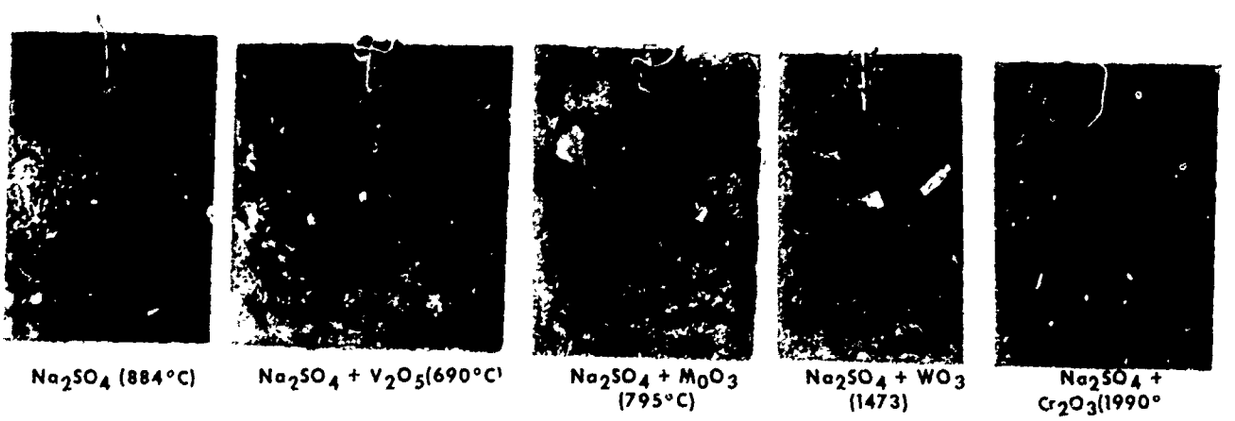

Figure 12. Relationship between MxOy melting point and sulfidation inhibition.

Table V
Relative Ranking Order of Oxides which Lower $O^{=}$ Content of Na_2SO_4

All Calculations are at 1200°K

Oxide	Reaction	P_{SO_2} for P_{O_2} equal to 0.2 atm Ref.[1]
Al_2O_3	$Na_2SO_4 + Al_2O_3 \rightleftharpoons 2\,NaAlO_2 + SO_2 + 1/2\,O_2$	$10^{-7.22}$
Cr_2O_3	$2\,Na_2SO_4 + Cr_2O_3 + 1/2\,O_2 \rightleftharpoons 2\,Na_2CrO_4 + 2\,SO_2$	$10^{-6.12}$
SiO_2	$Na_2SO_4 + 2\,SiO_2 \rightleftharpoons Na_2Si_2O_5 + SO_2 + 1/2\,O_2$	$10^{-3.36}$
MoO_3	$Na_2SO_4 + MoO_3 \rightleftharpoons Na_2MoO_4 + SO_2 + 1/2\,O_2$	$10^{-3.29}$
WO_3	$Na_2SO_4 + WO_3 \rightleftharpoons Na_2WO_4 + SO_2 + 1/2\,O_2$	$10^{-2.28}$
V_2O_5	$Na_2SO_4 + V_2O_5 \rightleftharpoons 2\,NaVO_3 + SO_2 + 1/2\,O_2$	$10^{-2.28}$
TiO_2	$Na_2SO_4 + 3\,TiO_2 \rightleftharpoons Na_2Ti_3O_7 + SO_2 + 1/2\,O_2$	$10^{+13.73}$

[1]References appear in Appendix

scale would then be thermodynamically unstable and decompose by ionic dissolution into the melt, thereby allowing the salt to come in contact with and react with the metal alloy substrate.

The stability of Na_2SO_4 as a function of the partial pressures of O_2 and SO_2 at 1200K, constructed from the data referenced in Appendix I is shown in Fig. 13. Oxides such as Al_2O_3, Cr_2O_3, MoO_3 and V_2O_5 can react with Na_2SO_4 to form alkali compounds such as $NaAlO_2$, etc. or acidic compounds such as $Al_2(SO_4)_3$. The stability fields of AlO_2^- - Al_2O_3, $CrO_4^=$ - Cr_2O_3, $MoO_4^=$ - MoO_3, VO_3^- - V_2O_5, and Al_2O_3 - $Al_2(SO_4)_3$ are also shown in Fig. 13. If the metallic ion is defined as the basic salt, then the field of stability of the basic salt lies to the left of the reaction line. The acidic salts (only $Al_2(SO_4)_3$ is shown) lies to the right of the oxide-sulfate line as shown for the Al_2O_3 - $Al_2(SO_4)_3$ reaction line.

As shown in Fig. 13, for all P_{O_2} pressures greater than 10^{-5} atm, Cr_2O_3 will preferentially react with $[O^=]$ to form chromates thereby inhibiting the formation of alkali aluminates. In a similar fashion V_2O_5 and MoO_3 should preferentially react with oxide ions to the exclusion of Al_2O_3 as well as NiO. The phase boundary line for $NaNiO_2$ is not shown since the necessary free energy of formation data is not available. However, it is expected that the reaction line for $NaNiC_2$/NiO lies to the left of that shown for $NaAlO_2/Al_2O_3$.

It is possible to dissolve an Al_2O_3 scale if the sulfur potential in the fused melt is sufficiently increased such that sulfate formation occurs, i.e.

$$Al_2O_3 + SO_2 + \frac{3}{2}O_2 \rightarrow Al_2(SO_4)_3. \qquad (1)$$

In terms of oxide ion concentration, if the oxide ion content of the melt can be reduced to a sufficiently low level, Al_2O_3 can become thermodynamically unstable and ionically dissolve to give Al^{+3} and $O^=$.

Al_2O_3 dissolution occurs if the presence of $SO_{2(g)}$ produced by the reaction

$$V_2O_{5(\ell)} + SO_4^= \rightarrow 2\,VO_3^- + \frac{1}{2}O_2 + SO_{2(g)}, \qquad (2)$$

is greater than the pressure required for reaction (1). The calculated partial pressures of SO_2 corresponding to a wide range of oxygen conditions are presented in Table VI and indicate that magnitude of P_{SO_2} necessary for ionic dissolution of Al_2O_3 to occur.

These results indicate that even at the very low oxygen pressures, the equilibrium pressure of $SO_{2(g)}$ in the melt of Na_2SO_4 which contains V_2O_5 will not be high enough to promote the ionic dissociation of Al_2O_3.

The aforementioned calculations are valid only if the activity of $SO_4^=$ in the melt does not vary significantly from unity.

If it is assumed that the activity of $SO_4^=$ departs appreciably from unity, then the oxide ion content of the melt can be further decreased from the calculated value. However, this infers the V_2O_5 very rapidly reacts with Na_2SO_4 liberating SO_2 from the melt. But this is not in agreement

Table VI
Calculated P_{SO_2} Pressures Over MxOy-Na_2SO_4 Melts at Various P_{O_2} Pressures

Compound	Reaction	P_{SO_2} for P_{O_2} Equal to	
		0.2 atm	$10^{-13.75}$ atm
$Al_2(SO_4)_3$	$Al_2(SO_4)_3 \rightarrow Al_2O_3 + SO_2 + 1/2\ O_2$	104	3.49×10^8
V_2O_5	$V_2O_5 + Na_2SO_4 \rightarrow 2\ NaVO_3 + SO_2 + 1/2\ O_2$	9.13×10^{-4}	3.2×10^3

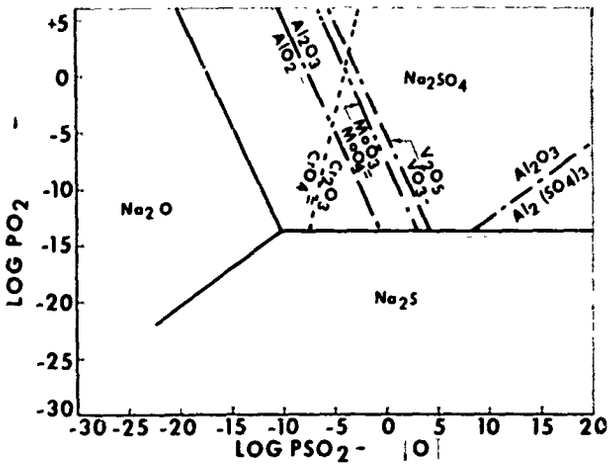

Figure 13. Stability fields for Na_2SO_4, Na_2O and Na_2S at 1200°K.

with the results of the melt experiments described previously in which a mixture of Na_2SO_4 and V_2O_5 were liquefied in a quartz tube. Based upon the results of the melt experiments, after 1 hr at 900°C, the 10 m/o V_2O_5 in the Na_2SO_4 melt had not completely reacted. Of particular importance is the uneven distribution of V_2O_5 observed in the interstices of the cellular microstructure (see Fig. 11). The concentration of this phase is more pronounced at the bottom of the melt than at the top as if the more dense V_2O_5 liquid tended to separate from the less dense Na_2SO_4 liquid. Thus, it is not surprising that when an Al_2O_3 specimen was immersed in a Na_2SO_4-V_2O_5 mixture in which no special precautions were taken to separate the V_2O_5 from the Na_2SO_4, some dissolution of the Al_2O_3 was observed. However, when the V_2O_5 was physically separated from the Na_2SO_4, and although mixing of the two compounds did occur (and subsequent lowering of the oxide content of the Na_2SO_4), no measurable weight losses of the Al_2O_3 specimen were observed.

This does not imply that ionic dissolution of protective oxide scales in acidic Na_2SO_4 solution cannot occur; only that, based upon the experimental results reported herein, the addition of V_2O_5 to Na_2SO_4 did not result in complete reaction of the metal oxide with the fused salt and as such unreacted V_2O_5 was always present. Since V_2O_5 readily reacts with alumina, it is not surprising that when mixtures of Na_2SO_4-V_2O_5 are applied onto nickel base superalloys, no sulfidation inhibition is noted since the V_2O_5 can react with the normally protective alumina rich scale and allow the Na_2SO_4 to contact the sulfidation prone alloys.

The addition of WO_3 to a Na_2SO_4 coated superalloy specimen did not result in sulfidation attack. Sodium sulfate, Na_2SO_4 + MoO_3 and Na_2SO_4 + V_2O_5 coated specimens underwent severe sulfidation attack when exposed at 900°C. However, the specimens coated with Na_2SO_4 + Cr_2O_3 or Na_2SO_4 + WO_3 exposed at 900°C did not exhibit sulfidation attack.

Tungsten trioxide is like Cr_2O_3, MoO_3 and V_2O_5, in that it can react with and decrease the oxide ion concentration of Na_2SO_4. In this respect WO_3 is an acidic oxide. Based upon the available thermodynamic data the relative position of WO_3 is between MoO_3 and V_2O_5 as shown in Table V. Thus, WO_3 is more acidic than Cr_2O_3 and MoO_3. However, whereas the addition of MoO_3 to Na_2SO_4 coated superalloys resulted in sulfidation attack, the addition of WO_3 to the Na_2SO_4 proved to be beneficial. In terms of relative melting points, the oxides of both molybdenum and vanadium are molten at the test temperature whereas the oxides of chromium and tungsten are solids.

Oxides such as V_2O_5 and MoO_3 were shown to be sulfidation inhibitors for alloys which do not form alumina-rich scales. This behavior is most likely related to the formation of refractory and protective vanadates and molybdates, ($Ni_3(VO_4)_2$ 1220°C and $NiMoO_4$ 1350°C) the latter shown to be protective by Imai (14). The compound $AlVO_4$ is not refractory and reportedly melts at 650°C.

The addition of SiO_2 to Na_2SO_4 coated B-1900 specimens prevented sulfidation attack from occurring provided that the specimen was not thermally shocked. When thermally shocked, the specimen rapidly oxidized. Visual examination of Na_2SO_4 + SiO_2 coated B-1900 alloy specimens removed after exposure for more than 10 hrs at 1000°C revealed the presence of a glassy scale on the surface. The "glass" was insoluble in water. Based upon the Al_2O_3-SiO_2-Na_2O phase diagram (12), it is believed that the glassy scale is a sodium-aluminum silicate, the soda obtained from the Na_2SO_4, the silica applied with the Na_2SO_4 and the alumina from the oxide scale formed on the superalloy

surface. When thermally shocked, the glassy phase most probably cracks; the cracking due to the large stresses which result from the differences in coefficients of thermal expansion between the glass and the substrate. When reinserted into the furnace, the liquid Na_2SO_4 is in direct contact with the substrate, hence sulfidation attack follows.

The initial reaction product between SiO_2 and Na_2SO_4 is, based upon the results of the Na_2SO_4 coated Si_3N_4 specimens, $Na_2Si_2O_5$. Based upon the available thermodynamic data, SiO_2 is an acidic oxide lying slightly above MoO_3 in its ability to reduce the oxide ion concentration of Na_2SO_4, (Table V).

Although no direct experiments were performed with Na_2SO_4 and TiO_2, thermodynamically the oxide TiO_2 is extremely acidic, i.e. the partial pressures of SO_2 over TiO_2-Na_2SO_4 mixtures is greater than 1 atm, (Table V). Since the partial pressure of SO_2 over MoO_3 or V_2O_5-Na_2SO_4 mixtures is less than one atm, it is concluded that TiO_2 is more acidic with respect to Na_2SO_4 than either MoO_3 or V_2O_5. However, titanium has generally been regarded as either innocuous or a beneficial alloying element with respect to sulfidation attack. In fact the newer high strength nickel base superalloys such as In 792, which exhibit superior sulfidation resistance than the alloys such as Inco 713 and B-1900 contain appreciably more titanium and significantly less molybdenum. It should also be noted that the alkali titanates are solids in the temperature range of interest. The formation of an adherent alkali titanate can prevent complete reaction between TiO_2 and Na_2SO_4 from occurring, i.e. just as an adherent Al_2O_3 film prevents oxidation of aluminum and its alloys. The product of the reaction between Cr_2O_3 and Na_2SO_4 is Na_2CrO_4 which is a liquid completely miscible in Na_2SO_4.

The addition of molybdenum or vanadium to NiAl markedly increased the rate of oxidation of this refractory intermetallic compound. The increase in rate is due to the presence of the corrosive liquid formed during oxidation of the insoluble second phase (molybdenum or vanadium). When vanadium was present, the liquid phase V_2O_5 was formed. When molybdenum was the alloying element, the corrosive liquid MoO_3 was formed but since this oxide is quite volatile, significant losses of MoO_3 occurred. It was observed during oxidation of NiAl-10 w/o Mo specimens that material evaporating from the surface of the specimen had condensed on the cooler platinum chain used to support the specimen in the furnace. This material was soluble in water and the only metallic ion identified by qualitative chemical analyses was molybdenum.

When Na_2SO_4 was applied onto the molybdenum alloyed NiAl specimens, no sulfidation inhibition was observed but the rate of oxidation was significantly faster than that observed for Na_2SO_4 coated NiAl. When the salts present on the surface of the salt-coated NiAl + 10 w/o Mo specimen were chemically analyzed it was found that the quantity of sodium applied was in good agreement with that found and likewise with respect to sulfate. However, in addition to sodium and sulfate, soluble molybdenum was also found. Since the ratio of sodium to sulfate has not changed and since MoO_3 is sparingly soluble in water, it is concluded that the fused salt present on the surface of the alloyed aluminide specimen consisted of a mixture of Na_2SO_4 and MoO_3.

CONCLUSIONS

1. Sulfidation attack can occur when an alkali salt condenses onto turbine components
2. Initially the fused salt is insulated from the alloy substrate by a protective oxide scale.
3. Oxide ions present in the melt react with the normally protective oxide scale; the product of the reaction is nonprotective with respect to the alloy substrate.
4. As a result of sulfide formation, the oxide ion content of the fused melt is increased to a sufficiently high level so that reformation of a protective oxide cannot occur.
5. The initiation of sulfidation attack can be prevented by reducing the oxide ion content of the fused melt below that necessary for reaction between oxide ions and the alumina rich protective oxide scale.
6. Oxides such as Cr_2O_3, SnO_2, SiO_2, MoO_3, V_2O_5, WO_3, and TiO_2 can react with and reduce the oxide ion content of Na_2SO_4.
7. During oxidation of superalloys, molybdenum trioxide which forms when molybdenum rich precipitates are exposed to free surfaces, rapidly evaporates.
8. When covered by a film of Na_2SO_4, the rate of evaporation of MoO_3 is significantly decreased. Mixtures of Na_2SO_4 and MoO_3 occur on the surface of the superalloy.
9. Oxides such as MoO_3 and V_2O_5 are liquids at current metal gas turbine temperatures and are corrosive liquids readily capable of fluxing the alumina rich protective oxide scale formed on superalloys.
10. Oxides such as SiO_2 can react with oxide ions to form alkali silicates. However, alkali silicates can react with many oxides to form "glasses." The formation of these "glasses" can increase the rate of oxidation of the substrate by consumption of the normally protective oxide scale. If as a result of differences in coefficients of thermal expansion, the glass is cracked, any Na_2SO_4 present on the surface will react with the substrate and sulfidation attack will occur.
11. Oxides such as TiO_2 are very reactive with respect to reducing the oxide ion content of Na_2SO_4. However the formation of adherent alkali titanates may prevent the reaction between Na_2SO_4 and TiO_2 from going to completion.
12. Sulfidation attack can be prevented by lowering the oxide ion content of the fused melt. However, the sulfidation inhibitor must not in itself be corrosive, e.g. V_2O_5 and MoO_3. In addition the products of the reaction between the sulfidation inhibitor and the fused melt should not be corrosive, e.g. SiO_2 alkali silicates. Oxides such as Cr_2O_3 appear particularly beneficial in that it (a) reduces the oxide ion content of Na_2SO_4, (b) is innocuous with respect to Al_2O_3, and (c) the product of the reaction

between Cr_2O_3 and Na_2SO_4 is completely miscible in the fused melt. In this respect Cr_2O_3 might be more effective than TiO_2 which although capable of readily reducing the oxide ion content of Na_2SO_4, can form an alkali compound which separates the TiO_2 from the Na_2SO_4.

ACKNOWLEDGMENT

The work reported herein was sponsored by the Office of Naval Research, Department of the Navy (Contract N00014-70-C-0234 NR 036-089/1-12-70(471)). The authors wish to thank Dr. Phillip Clarkin of ONR for his interest and stimulating discussions.

REFERENCES

1. M. A. DeCrescente and N. S. Bornstein, *Corrosion* (1968) Vol. 24, pp. 127-33.
2. E. L. Simons, G. V. Browning and H. A. Liebhefsky, *Corrosion* (1955) Vol. 11, No. 12, p. 505.
3. G. J. Danek, Jr., *Naval Engineers Journal* (Dec. 1965) p. 859.
4. A. U. Seybolt, *Trans. TMS-AIME* (1968) Vol. 242, pp. 1955-61.
5. J. M. Quets and W. H. Dresher, *M. Mater.* (1969) Vol. 4, pp. 583-99.
6. N. S. Bornstein and M. A. DeCrescente, *Trans. TMS-AIME* (1969) Vol. 245, pp. 1947-52.
7. N. S. Bornstein and M. A. DeCrescente, Final Report Conducted for U.S. Naval Ship Research Development Laboratory, Contract N00600-68-C-0639 (Apr. 1969) Annapolis, Md.
8. N. S. Bornstein and M. A. DeCrescente, *Trans. TMS-AIME* (1971) Vol. 2, pp. 1971-83.
9. N. S. Bornstein, M. A. DeCrescente and H. A. Roth, "Effect of Vanadium and Sodium Compounds on Accelerated Oxidation of Nickel Base Alloys," Annual Report Conducted for Office of Naval Research, Contract N00014-70-C-0234-NR 036-089/1-12-70(471), June 1972.
10. J. A. Goebel and F. S. Pettit, *Trans. TMS-AIME* (1970) Vol. 1, pp. 1943-54.
11. U.S. Bureau of Mines Report of Investigation 7371 (Apr. 1970).
12. Phase Diagrams for Ceramists Published by American Ceramic Society Inc., (1964 & 1969).
13. J. A. Goebel, F. S. Pettit and G. W. Goward, Personal Communication.
14. Yunoshin Imai and Yoshizumi Nishi, Sci. Rept. Res. Inst. Tohoku Univ. Ser. A 14, No. 6 (1962) pp. 347-62.
15. C. T. Brown, N. S. Bornstein and M. A. DeCrescente, "High Temperature Metallic Corrosion of Sulfur and Its Compounds," Edited by Z. A. Foroulis, Published by Corrosion Division, The Electrochemical Society, Inc. (1970) p. 170.

APPENDIX
All Calculations at 1200°K

1. Na_2SO_4-Na_2O

$$Na_2SO_4 \rightleftharpoons Na_2O + SO_2 + 1/2\ O_2$$

$$\Delta F_{Rx} = +95.2 \text{ Kcal}$$

$$a_{Na_2O} = a_{Na_2SO_4} \simeq 1$$

$$P_{SO_2} P_{O_2}^{1/2} = 10^{-17.25}$$

2. Na_2SO_4-Na_2S

$$Na_2SO_4 \rightleftharpoons Na_2S + 2\ O_2$$

$$\Delta F_{Rx} = +151.6 \text{ Kcal}$$

$$a_{Na_2SO_4} = a_{Na_2S} \simeq 1$$

$$P_{O_2} = 10^{-13.75}$$

3. Na_2O-Na_2S

$$Na_2S + 3/2\ O_2 \rightleftharpoons Na_2O + 5\ O_2$$

$$\Delta F_{Rx} = -56.4 \text{ Kcal}$$

$$P_{SO_2} P_{O_2}^{-3/2} = 10^{+10.02}$$

4. Na_2SO_4-$Al_2(SO_4)_3$

$$3\ Na_2SO_4 + Al_2O_3 + 3\ SO_2 \rightleftharpoons Al_2(SO_4)_3 + 3\ Na_2S + 9/2\ O_2$$

$$\Delta F_{Rx} = +482.5 \text{ Kcal}$$

$$P_{O_2}^{9/2} P_{SO_2}^{-3} = 10^{-87.2}$$

5. Na_2SO_4-$NaAlO_2$

$$Na_2SO_4 + Al_2O_3 \rightleftharpoons 2\ NaAlO_2 + SO_2 + 1/2\ O_2$$

$$\Delta F_{Rx} = +41.8 \text{ Kcal}$$

$$P_{SO_2} P_{O_2}^{1/2} = 10^{-7.57}$$

6. Na_2SO_4-V_2O_5

$$V_2O_5 + Na_2SO_4 \rightleftharpoons 2\ NaVO_3 + SO_2 + 1/2\ O_2$$

$$\Delta F_{Rx} = +14.5 \text{ Kcal}$$

$$P_{SO_2} P_{O_2}^{1/2} = 10^{-2.62}$$

7. Na_2SO_4-MoO_3

$$MoO_3 + Na_2SO_4 \rightleftharpoons Na_2MoO_4 + SO_2 + 1/2\ O_2$$

$$\Delta F_{Rx} = +20.1 \text{ Kcal}$$

$$P_{SO_2} P_{O_2}^{1/2} = 10^{-3.62}$$

8. Na_2SO_4-Cr_2O_3

$$2\ Na_2SO_4 + Cr_2O_3 + 1/2\ O_2 \rightleftharpoons 2\ Na_2CrO_4 + SO_2$$

$$\Delta F_{Rx} = +45.3 \text{ Kcal}$$

$$P_{SO_2} P_{O_2}^{-1/2} = 10^{-8.21}$$

References

Na_2SO_4, Na_2MoO_4, Na_2CrO_4: W. J. Cooper and D. A. Scarpullo, Final Report, SC-RR-64-67, Calleny Chemical Co. to Sandia Corp. (Jan. 1964).

TiO_2, Na_2O, Na_2S, Cr_2O_3, WO_3: Thermochemistry for Steelmaking, Addison-Wesley (1960).

SO_2, Na_2WO_4: Janaf Thermomechanical Tables. The Dow Chemical Co., Midland, Michigan.

$NaAlO_2$: J. P. Coughlin, J. Am. Chem. Soc., 79, 2397 (1957).

$Al_2(SO_4)_3$: High Temperature Properties and Decomposition of Inorganic Salts–Part I, U.S. Dept. of Commerce, National Bureau of Standards, NSRDS-NBS-7 (1966).

V_2O_5, $NaVO_3$: A. D. Mah, Report of Investigations 6727, Bureau of Mines, U.S. Dept. of Interior (1966).

Na_2CrO_4: L. A. Zharkova and Y. Gerasimov, Zhur. Fiz. Khim, 35, 2291-6 (1961).

SiO_2, $Na_2Si_2O_5$: M. A. Matveev, B. N. Frenkel and G. M. Matveev, Izv. Akad. Nauk. SSSR, Neorg. Mater., Vol. 1, No. 8, 1426-36 (1965).

$Na_2Ti_3O_7$: A. M. Bobrova, A. A. Fotiev and M. Kh. Karapet'yants, Russian Journal of Physical Chem., Vol. 40, No. 8, 986 (1966).

The Mechanism of Hot Corrosion in Marine Gas Turbines

J. F. G. Condé
Admiralty Materials Laboratory
Holton Heath, Poole
Dorset, UK

SUMMARY

The origins of corrosive contaminants are discussed and the conditions existing in the gas turbine are examined. The chemistry of contaminants in the combustion environment is introduced and evidence is cited to show that in the short residence times available, gas phase sulphation of chloride is not significant. The mechanism of salt deposition in the gas turbine on nozzles and blades is considered briefly and the role of the obvious contaminants, sulphur, sodium and chloride is examined in relation to sulphidation and accelerated oxidation. A model is suggested in which periodically extremely local non-equilibrium conditions arise on the surfaces of nozzles and turbine blades due to impaction of sea-salt particles. It is suggested that such conditions may permit chloride to destroy the integrity of protective scale layers under low oxygen pressure conditions existing beneath liquid sulphate deposits. Additional reactions between scale constituents and sulphate lead to sulphidation accompanied by accelerated oxidation but the precise mechanism of this latter is not defined although several possible explanations exist. It is suggested that carbon and water vapour are additional contaminants which should be considered in the corrosion process. Finally certain areas are indicated where definitive information is lacking and further data are required. It is proposed that in the future attention should be paid to the influence of vanadium on hot corrosion if there is economic pressure or logistic argument to employ other than low vanadium distillate fuel in the gas turbine for marine or land based applications.

INTRODUCTION

Hot corrosion of metals is characterised by sulphidation of surface layers accompanied by accelerated oxidation and is associated with contaminants present in combustion environments and a film of condensed alkali metal sulphates on the surface of hot components (see Fig. 1). The phenomenon has been recognised in gas turbines since about 1950 and is most commonly found in marine gas turbines employed for the propulsive machinery and auxiliaries in ships but aircraft flying low over the sea or in a marine environment may also be affected.

During the past 10 years hot corrosion has been the subject of extensive investigation and there are several review articles (1-5) as well as numerous papers dealing with operating and test bed experience on engines, test data on materials, theoretical aspects and basic investigations aimed at establishing the mechanism. This paper seeks to review briefly what is known of the mechanism of hot corrosion and with the aid of some recent data to propose a model of the process.

GENERAL CONSIDERATIONS

Aviation kerosine is employed in the aero gas turbine and the cheaper dieso fuel or gas oil in marine engines. Specification limits for sulphur in gas oil are normally about 1% by weight and typical analyses are around 0.45%. Fuels for marine gas turbines are usually contaminated with seawater which contains not only sodium chloride but also significant amounts of sulphur in the form of sulphate (ca. 2,650 ppm).

Sea-salt or seawater aerosol will be present in the air and the concentration at turbine intakes in ships may range from 0.01 ppm in good weather to several ppm in bad weather. The concentration and particle size will be dependent on factors such as ships speed, height of intakes, etc. as well as weather conditions. Aircraft flying low over the sea may experience salt levels of up to 0.1 ppm at 100 ft.

Sea-salt contamination levels of fuel and air can be reduced significantly by filtration and practical levels achieved in RN ships are about 0.3 ppm sodium (0.76 ppm NaCl) in the fuel and 0.01 NaCl in the air. Filtration of air cannot be applied in aircraft engines but aviation fuel must be water-free for safety and NaCl is not soluble in kerosine.

Fuels for marine gas turbines may also contain vanadium depending on the grade of fuel employed but current RN fuels contain less than 0.01 ppm.

In general, air/fuel ratios in the gas turbine are about 50/1 by weight. The fuel will only burn efficiently at a ratio of about 15/1 and usually about 25 to 28% of the air is used for combustion. The balance of the air provides cooling for flame tubes and dilution to reduce the temperature of the combustion gases which initially may be 1800 to 2000°C. In advanced engines a few percent of the air may be used for nozzle and blade cooling. Aerosol salt in the air will be subjected to varying temperature histories and residence times will show a distribution about the

WROUGHT ALLOY

Pack-Aluminised Nimonic 115. 1st Stage. Turbine Blade run for 951 h with last 409 h 0.01 ppm salt in air and 0.6 ppm sodium in fuel. Peak temperature 870°C. X 375

CAST ALLOY

Pack-Aluminised IN 738 test specimen after 200 h, 750°C, 1.0 ppm seasalt, in AML Low Pressure combustion test rig. X 375

Figure 1. Typical hot corrosion effects.

mean (6). The quenching effect of cooling air may lead to certain chemical species surviving at levels in excess of equilibrium at the subsequent lower temperature levels.

Recent measurements made on a G6 compressor (7) under simulated salt ingestion conditions with a mean aerosol concentration at the inlet of 0.027 ppm NaCl have indicated that with an initially clean compressor up to 90% of the salt intake was removed by the compressor. It follows that if effective compressor cleaning is not carried out regularly pieces of salt may break away from deposits on compressor blades, casings, etc. and pass into the engine. "Break-through" of salt solution from wet filters may also give rise to particulate salt which may escape capture in the compressor and pass into the hot areas of the engine. The dubious practice of "hot washing" of compressors which is sometimes adopted may also transfer salt from the compressor into the turbine.

COMBUSTION CHEMISTRY

Whilst thermodynamic considerations and thermochemical calculations can lead to a much better insight into the chemistry of the combustion environment, in practice the kinetics of the various chemical reactions taking place in the environment may be overriding. This is particularly relevant to gas/liquid/solid equilibria in the gas turbine where residence times in the combustion system may be only 5 milliseconds. Thus the short residence combustion chemistry of the environment is of crucial importance.

The major chemical reagent responsible for hot corrosion is generally assumed to be sodium sulphate (Na_2SO_4) and a secondary or unimportant role is often attributed to sodium chloride (NaCl). The thermodynamics of formation and reactivity of sodium sulphate have been well covered in the literature (8). It is assumed that sodium chloride reacts with SO_2, SO_3 and water vapour formed by combustion of sulphur present in the fuel. This conversion or sulphation reaction may be represented:

$$2\,NaCl + SO_2 + \frac{1}{2}O_2 + H_2O \rightarrow Na_2SO_4 + 2\,HCl \quad (1)$$

$$2\,NaCl + SO_3 + H_2O \rightarrow Na_2SO_4 + 2\,HCl \quad (2)$$

Further sulphate may arise from sea-salt as stated earlier.

It should be noted that conditions may favour the formation of SO_3 due to the high pressure in the combustion zone and possible catalytic activity on the hot metal walls of the combustion chamber (6). A high excess air level may also favour formation of SO_3.

The proportion of sea-salt exposed to initial combustion will be completely dissociated (6) and at high temperatures (1800-2000°C) the reaction to sodium hydroxide may be favoured:

$$NaCl\ (vapour) + H_2O \rightarrow NaOH\ (vapour) + HCl \quad (3)$$

This reaction is likely to go to completion at low concentrations of chloride. However it may be that dissociation of NaCl is suppressed by the presence of SO_2 (6,9) due to the reaction between atomic hydrogen and SO_2 being favoured thus disturbing the dissociation reaction to the left, i.e.

$$NaCl + H \rightleftharpoons Na + HCl \quad (4)$$

At lower temperatures NaOH may be converted to Na_2SO_4:

$$2\,NaOH\,(vapour) + SO_2 + \frac{1}{2}O_2 \rightarrow$$

$$Na_2SO_4\,(vapour) + H_2O \qquad (5)$$

The kinetics of the reactions leading to formation of Na_2SO_4 have been studied using a controlled mixing history combustor (6) which permits the progress of the reactions to be followed in relation to residence time by the technique of isokinetic sampling. Residence times of up to 16 milliseconds have been examined. The rig is operated at atmospheric pressure but the contaminant level is raised over the practical levels in order to keep the product (ppm X vapour pressure) constant. The gas velocity is 152 ms (500 fs).

The results obtained up to the present are indicated in Fig. 2 which shows the effect of NaCl concentration in the air, sulphur content of the fuel and gas temperature, on sulphation rate. Gas phase sulphation is clearly very limited in residence times as low as those in the gas turbine. The presence of sulphate in sea-salt is likely to reduce gas phase sulphation still further. The small effect of increased gas temperature is attributable to NaCl being thermodynamically favoured and the equilibrium sulphate concentration is lower, although the rate of sulphation is increasing with temperature. The SO_2 level increases over a finite period and sulphation rate increases with time. The effect of salt concentration is in agreement with predictions from thermodynamic equilibria which indicate that the sulphate/chloride equilibrium is not influenced by the initial salt concentration provided that this is low compared with the partial pressures of the combustion products. It should be noted that even at 0.1% sulphur in the fuel it is present in amounts far in excess of stoichiometric in relation to NaCl at the concentration levels considered.

In support of the combustor studies and based on equations 3 and 5 above for which the free energy change relationships are known, the equilibrium partial pressures of Na_2SO_4, NaCl, NaOH and HCl have been computed (6) for a range of temperatures and gas compositions. These calculations indicate that if steady state low concentration conditions exist around the nozzles and blades and there is time for equilibrium to be achieved then at temperatures below about 925°C Na_2SO_4 and HCl will be the major constituents. At higher temperatures NaOH, HCl and NaCl are favoured. Salt concentration has little effect on the equilibrium level of Na_2SO_4 and hence the Na_2SO_4 concentration is a function of temperature. At 1225°C the equilibrium concentration of Na_2SO_4 is about 8.5% and hence in the combustion zone, even if residence times were sufficiently great, the amount of sulphate already present in sea-salt represents a super-equilibrium concentration.

During start-up of the gas turbine incomplete combustion is a common phenomenon and particulate carbon or soot may form. It has been found (10) that particles up to 1000Å in size may occur. In addition pyrolysis of fuel may occur at the burner leading to build-up of pyrolytic carbon deposits on burner components. Such deposits may break away during operation of the engine and particles of pyrolytic carbon of much higher density than porous soot particles may pass through the system.

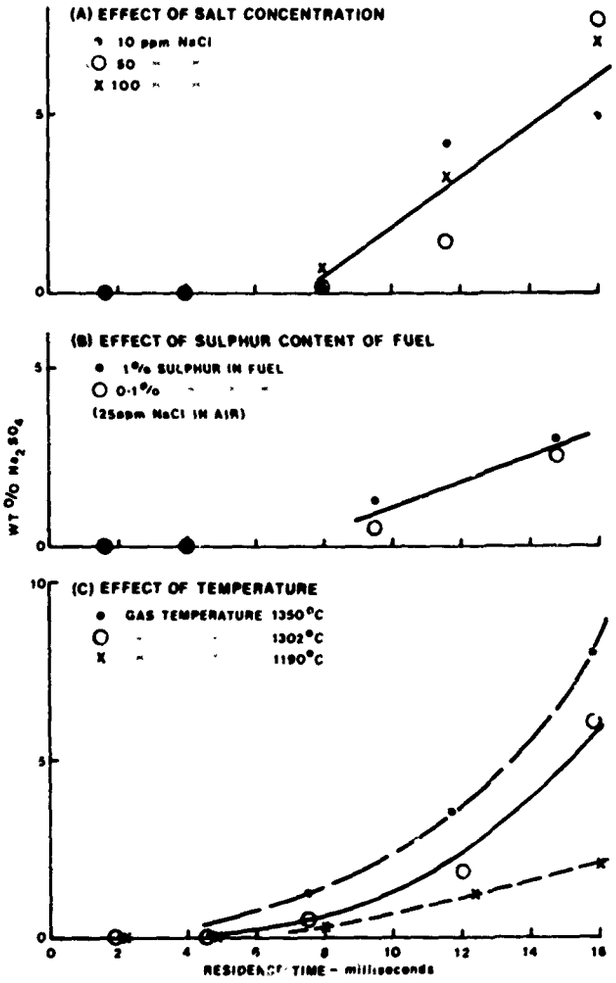

Figure 2. Gas phase sulphation of sodium chloride (Ref. 6)

SALT DEPOSITION PROCESSES

The mechanisms by which solid or liquid particles or vapour carried in a gas stream may be deposited onto surfaces are reasonably well understood (11). Provided that the sizes of the particles, their diffusion coefficients and the velocity field of the gas can be established then it is in principle possible to predict deposition in a system.

Large particles of sea-salt formed from salt solution droplets in the air entering the compressor or similar particles breaking away from filter or compressor deposits may be sufficiently large, even after partial evaporation, to deposit on nozzles and/or blades by impaction. Somewhat smaller particles may evaporate to a greater extent but not necessarily completely and may reach the nozzles/blades by one

of several diffusion processes. Smaller particles will vaporise completely and the vapour may diffuse to nozzle and blade surfaces and condense there if the surface temperature is below the dewpoint of the vapour. Evaporation times for NaCl and Na_2SO_4 particles in the size range 0.01 to 10 micrometres at an ambient pressure of 10 atmospheres have been calculated (11) and are shown in Fig. 3. It will be noted that at the same temperature a given size of Na_2SO_4 particle may survive about 10 times as long as the same size particla of NaCl.

Vapour pressure data for both NaCl and Na_2SO_4 are by no means definitive since considerable discrepancies exist between data from various sources. Such data have been presented in both the open and unpublished literature (8,11). Data on partial pressure and concentration in relation to dewpoint temperature have been collated (11) and are shown in Tables 1 and 2 together with the original source. It will be noted that the vapour pressure of Na_2SO_4 is lower than that of NaCl and hence the sulphate can survive as liquid on hot surfaces at higher temperatures than can the chloride. Total system pressure in relation to salt concentration will have a significant effect and in general terms, below dewpoint temperatures where condensation is possible, the increase in amount of condensed salt will be directly proportional to the pressure rise (8,11) as may be seen by comparing the data in Tables 1 and 2. The system pressure in current marine gas turbines may be up to 10 atmospheres and higher pressure ratios obtain in more advanced aero-engines.

Sea-salt is a complex mixture with a melting point of about 757°C (18) compared with 801°C for NaCl and 890°C for Na_2SO_4. The vapour pressure in complex mixtures will be lower than the respective vapour pressures of the pure individual salts and hence "sea-salt vapour" might be expected to condense at somewhat higher temperatures than either NaCl or Na_2SO_4 separately. Even if sodium sulphate condenses and not NaCl then some chloride may be absorbed from the vapour phase by the Na_2SO_4. It has been observed that Na_2SO_4-NaCl mixtures are very nearly ideal (19) and hence the concentration of NaCl in the condensed sulphate phase (20) at any particular temperature will be proportional to the concentration of NaCl in the gas at that temperature.

In corrosion rig experiments (8) it has been noted that deposits may form under conditions where theory would predict no condensation. This has also been found in more recent combustion rig studies in the United Kingdom (21) where at a sea-salt concentration level of about 0.1 ppm deposits are formed on test blades at temperatures as high as 900°C and slightly above one atmosphere system pressure.

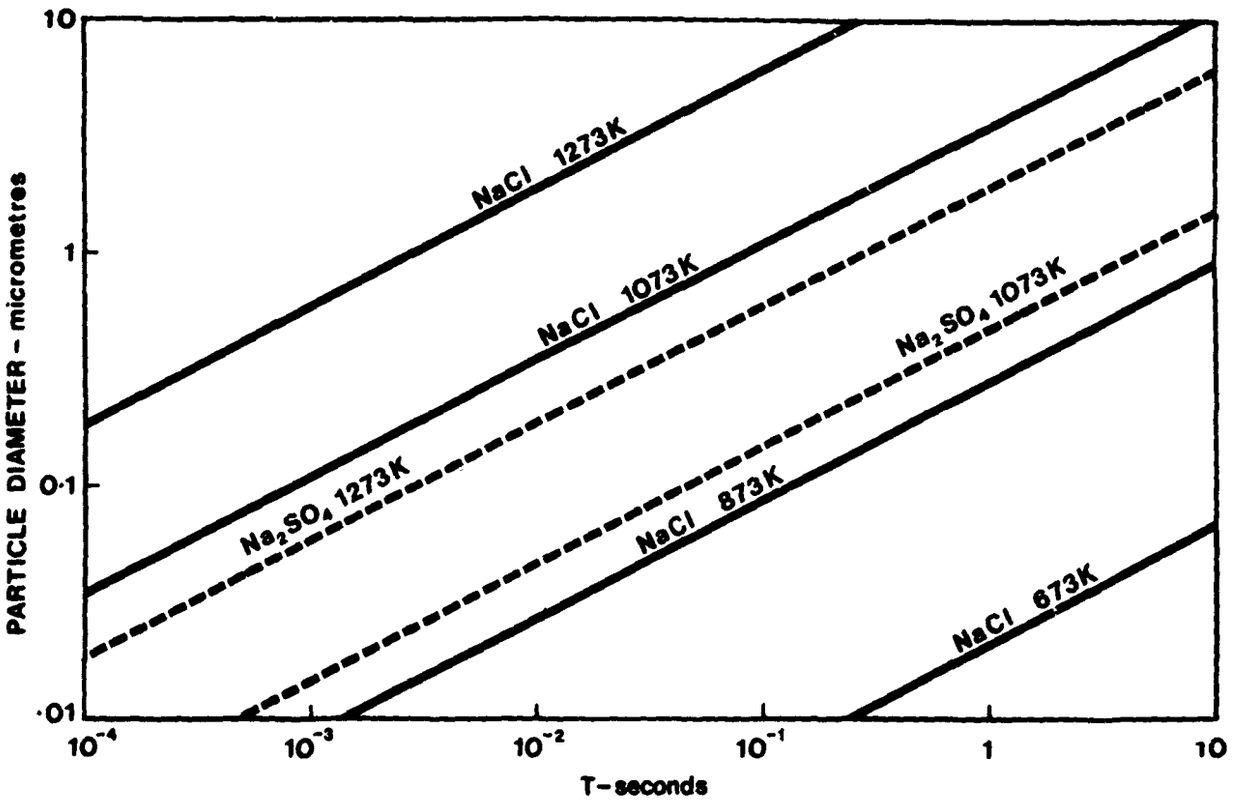

Figure 3. Evaporation times for NaCl and Na_2SO_4 droplets (Ref. 7).

This may be due to local temperature/pressure gradients or impaction of particles arising from deposits formed in the system.

It has been observed (15) that supercooling of NaCl deposits may occur where vapour condenses on surfaces and hence deposits may remain liquid at temperatures lower than the nominal melting point of the salt or mixture. Supercooling of 190°C has been found with NaCl.

MECHANISM OF HOT CORROSION

Complete elucidation of the mechanism of hot corrosion requires understanding of processes occurring in the gas phase, the condensed sulphur containing deposit on hot surfaces, the complex layer of corrosion products on the metal under the deposit and the metal itself. The alloy chemistry of the superalloys employed in gas turbines is complex and significant detailed differences in corrosion behaviour and also in the mechanism of the process are to be expected on the basis of the synergistic effects of alloying elements.

As shown earlier, consideration of the fluid dynamic situation in the engine, particularly residence times of contaminants in the combustion zone in relation to the kinetics of certain of the postulated chemical reactions, leads to the conclusion that thermodynamic equilibrium is unlikely. The gas phase situation must be considered as one of non-equilibrium. Processes occurring within deposits formed on nozzles or blades by condensation or impaction where residence times may be extended may be subject to transient perturbations of equilibrium. The probability that sizeable sea-salt particles breaking away from deposits on filters, compressor blades or casings, even after some attrition or evaporation by their subsequent passage through the engine, will impact onto surfaces must lead to local transient conditions far removed from equilibrium. It would appear that it is the fine structure of deposits which is important rather than the overall average composition.

It has often been assumed that chloride does not play a significant part in the hot corrosion process largely because chloride has seldom been detected in post mortem examinations of deposits on corroded components. In addition certain experimental data obtained at 950°C and above have tended to support this contention. The kinetics of the sulphation reaction (conversion of NaCl to Na_2SO_4) and the volatility of chlorides are such that it is not surprising that chloride is not found in deposits. At temperatures above 900°C where volatility of chloride is high and, in general, with most superalloys, oxidation predominates, the influence of chloride may be less significant than in the range 700 to 900°C where the greatest rates of sulphidation/oxidation are normally found.

In a recent review paper (22) the author has attempted to examine the roles of sulphur, sodium and chloride in hot corrosion and for a more detailed account the reference should be consulted. The present paper is intended only to highlight significant new data which have a bearing on the mechanism and to present these in the context of existing information.

The short residence combustion chemistry indicates that sodium chloride as vapour, liquid or solid can exist in the high temperature nozzle or blade area. This existence will be transitory since under the highly oxidising conditions alkali chlorides will be thermodynamically unstable at prevailing temperature levels and will be rapidly converted to sulphate. Reaction of chloride to form volatile heavy metal

Table I
NaCl Dewpoint Temperature Data

NaCl Concentration		Dewpoint Temperature °C		
mm Hg	ppm	(12)	(13)	(14, 15)
0.25	660	775	749	760
0.11	290	747	705	793
0.005	145	718	676	707
3.8×10^{-4}	1	567	–	–
3.8×10^{-5}	0.1	517	–	–
3.8×10^{-6}	0.01	456	–	–

Table II
Na_2SO_4 Dewpoint Temperature Data

Na_2SO_4 Concentration		Dewpoint Temperature °C		
mm Hg	ppm	(16)	(17)	Derived from (14, 15)
1.53×10^{-2}	100	883	884	827
1.53×10^{-3}	10	727	814	687
1.53×10^{-4}	1	612	758	612
1.53×10^{-5}	0.1	514	707	492
1.53×10^{-6}	0.01	437	654	422

chlorides is only feasible under conditions of low oxygen partial pressure (23):

$$2\,NaCl + SO_2 + \frac{1}{2}O_2 + MO \rightarrow$$

(liquid or solid)

$$MCl_2 + Na_2SO_4$$

(volatile) (liquid or solid) (6)

Direct attack by vapour phase chloride (i.e. NaCl or HCl) is not likely due to the high level of excess oxygen.

Where a liquid deposit of sodium sulphate plus other contaminants exists on surfaces then an impacting particle of sea-salt, which may be part liquid/part solid, may penetrate the liquid film and come to rest in contact with the deposit/scale interface. The viscosity of the deposit may be such that the particle is held by surface tension forces or the surface roughness be such that mechanical adhesion operates (as for example in a pit). Conditions at the deposit/scale interface may be sufficiently reducing that, very locally, appreciable equilibrium pressures of heavy metal chlorides are generated. Scales on superalloys may contain chromium, nickel, cobalt, titanium and aluminum all of which form volatile chlorides which may rapidly diffuse away from the initial point of formation. Clearly formation of volatile metal chlorides is in competition with other processes such as melting and diffusion or convective mixing, evaporation and sulphation which may dissipate a local high sodium chloride concentration.

The dramatic and destructive effects of solid, liquid and gaseous sodium chloride on the integrity of scales formed on superalloys is now well demonstrated (21,25,26,27). The effects of sodium chloride and sea-salt in contrast with sodium sulphate have been studied at AML on a number of superalloys over a range of temperature from 750 to 950°C employing specimens heated in air with crystals of the salts on the surface. The effects found on the surface of Nimonic 90 (18/21% Cr; 15/21% Co; 5% Fe; 1.8/3.0% Ti; 0.8/2.0% Al; Bal. Ni) at 850°C are shown in the series of scanning electron micrographs in Fig. 4. Spalling of the oxide occurred on cooling specimens coated with NaCl or sea-salt but the oxide remained much more adherent with Na_2SO_4. A significant feature of this study has been that resistance to chloride apparently decreases with increasing chromium content in distinction to attack in the presence of sodium sulphate where the reverse applies and higher chromium alloys are more resistant. Reactions with sodium chloride may be:

$$2\,NaCl + NiO = NiCl_2 + Na_2O \quad (7)$$

$$4\,NaCl + Cr_2O_3 = 2\,CrCl_2 + 2\,Na_2O + \frac{1}{2}O_2 \quad (8)$$

However it has been suggested (28) that for the heavy metal chlorides to be stable Na_2O must be removed by volatilisation or formation of NaOH by reaction with water vapour or some alternative mechanism. The water vapour concentration in the combustion products will be about 5% and hence NaOH formation is, in principle, feasible. Additions of Cr_2O_3 apparently inhibit both attack by chloride and sulphate (21, 29). The overall reaction with chloride may be:

$$2\,Cr_2O_3 + 5O_2 + 8\,NaCl = 4\,Na_2CrO_4 + 4\,Cl_2 \quad (9)$$

$$24\,NaCl + 10\,Cr_2O_3 + 9O_2 = 12\,Na_2CrO_4 + 8\,CrCl_3 \quad (10)$$

(volatile)

The effect of extraneous Cr_2O_3 in the inhibition of chloride attack may be to provide a source of heavy metal chloride other than the protective oxide scale. The mechanism in the case of sulphate attack is somewhat different (29) as discussed later.

A further possible effect of chloride may be to reduce the melting point of deposits (cf. melting point of sea-salt) leading to corrosion at lower temperatures. Recently, NaCl has been shown to increase the wetting properties of fused Na_2SO_4 deposits (30) enabling films to spread more extensively. Reactivity of oxides with chloride will be related to the work necessary to remove ions from oxides (31) and this may be significant in hot corrosion since this parameter increases in the order chromium, aluminum, titanium, tantalum, molybdenum, tungsten.

Sodium sulphate is generally recognised as the source of sulphur leading to internal sulphidation in hot corrosion and since reduction of the sulphur content of fuel (32,33) to as low as 0.0002% does not prevent sulphide formation it is likely that sea-salt can provide sufficient sulphur. The morphology of sulphide found in hot corroded materials is indicative of a low partial pressure process and this is in keeping with thermodynamic reasoning (34). Beneath a Na_2SO_4 deposit the oxygen potential will be low and the sulphur potential may be sufficient to form metal sulphides.

The thermochemical and thermodynamic bases of attack by fused sulphates or simultaneous attack by two oxidants have been well documented in the literature (28,34,35,36). Where the two oxidants are oxygen and sulphur then provided that transport of sulphur can occur through the oxide layer (formed due to the greater affinity of the metal for oxygen compared with sulphur) sulphide may form in the metal beneath the scale where oxygen activity is low. Diffusion of sulphur through Cr_2O_3 has been demonstrated (37) and hence concurrent oxidation/sulphidation reactions are feasible.

It has been inferred from thermodynamic reasoning that once sulphides have formed in an alloy they will persist and migrate inwards under oxidising conditions (34) and this has recently been demonstrated on pre-sulphidised samples of an 85% Ni; 15% Cr alloy (38). The self regenerating

X 100

(a) NaCl – 750°C

X 500

(b) NaCl – 850°C

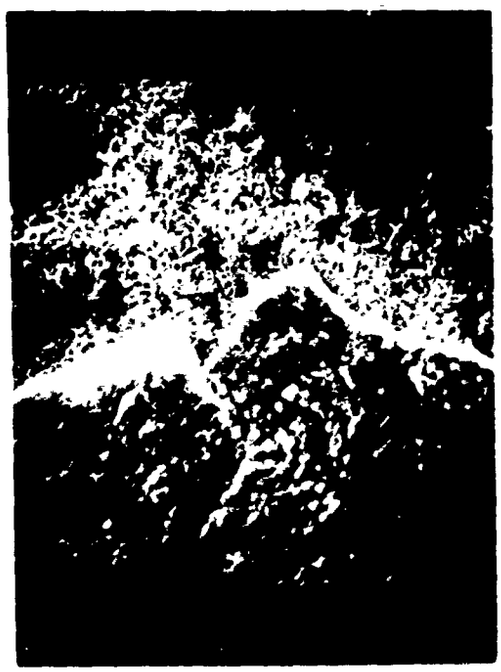

X 500

(c) Seasalt – 850°C

X 500

(d) Na_2SO_4 – 850°C

Figure 4. Scanning electro micrographs of surfaces of nimonic 90 heated for 6.5 h. in contact with NaCl, sea-salt and Na_2SO_4 in air.

mechanisms of sulphide propagation were thought to be:

$$2\,Cr_3S_4 + 9\underline{O} \rightarrow 3\,Cr_3O_3 + 8\underline{S} \qquad (11)$$

$$8S + 6\,\underline{Cr} \rightarrow 2\,Cr_3S_4 \qquad (12)$$

Nickel sulphide, if present, was considered to react:

$$Ni_3S_2 + 2\underline{O} \rightarrow Ni\underline{O} + 2\underline{S} \qquad (13)$$

The sulphur diffusing to form further chromium sulphide.

The accelerated oxidation occurring during hot corrosion has been attributed in some part to the local depletion of chromium occurring adjacent to sulphide particles (37) but not all investigators are agreed on this inference. It has also been suggested (29,39) that it is only when sulphides are formed in the external scale layer that accelerated oxidation occurs. However, in general, the sulphide-induced accelerated oxidation mechanism is favoured only for low aluminum nickel base alloys which do not form Al_2O_3 scales.

Evidence that accelerated oxidation is not related either to a depleted zone or to preferential oxidation of sulphides has been provided by other investigators (40,41) who demonstrated that the effect could be due to reactions between sodium oxide and the substrate alloy.

On the basis of thermochemistry it has been suggested (28) that certain alloying elements present in superalloys are able to promote the corrosion reaction by the ability of their oxides to combine with Na_2O to form chromates or aluminates. The incubation period in hot corrosion is consistent with the need for elements which promote hot corrosion to be in the oxide form, i.e. a period of initial oxidation. It has also been argued that similar elements can act to retard corrosion by formation of stable sulphides which may be oxidised subsequently to release sulphur to form further sulphides. The relative balance between inhibition and acceleration must be dependent on alloy chemistry.

There now appears to be some agreement that formation of Na_2O is probably the essential step in the accelerated oxidation process. However the suggestion that formation of mixed oxides such as chromate or aluminate, with attendant effects on the co-stability of oxides and sulphides, is a necessary condition for sulphide formation has been challenged (29). It has been proposed (29) that oxidation of nickel to NiO reduces the oxygen activity to a level where sulphides can form and that removal of sulphur from Na_2SO_4 increases the oxide ion concentration by decreasing the SO_3 pressure:

$$SO_4^{2} = O^{2-} + SO_3 = O^{2-} + \frac{1}{2}S_2 + \frac{3}{2}O_2 \qquad (14)$$

The sulphur activity of the Na_2SO_4 will reduce as oxide ion production occurs. This mechanism was tested (29) by oxidising nickel in Na_2SO_4 with and without additions of Cr_2O_3 which would be expected to accept oxide ions and decrease the activity:

$$Cr_2O_3 + \frac{3}{2}O_2 + 2O^{2-} = 2\,CrO_4^{2} \qquad (15)$$

With Cr_2O_3 the oxidation rate was reduced. It is further postulated that NiO is insoluble in Na_2SO_4 unless Na_2O is present when Na_2NiO_2 is formed which decomposes at the molten salt/gas interface to NiO and Na_2O. This process inhibits the formation of a protective scale layer and oxidation is rapid. The presence of Cr_2O_3 decreases the Na_2O activity and prevents dissolution of the protective NiO scale.

There has been a great deal of emphasis in studies on the mechanism of hot corrosion on the effects of sodium chloride and sodium sulphate but little attention has been paid to water vapour and carbon which are present in the gas turbine environment. Whilst water vapour is always present carbon may only arise intermittently. The presence of water vapour is an essential prerequisite of many of the reactions which are postulated and will not be discussed further. Carbon may play a crucial role in certain stages of hot corrosion. If carbon particles impact onto salt-coated surfaces then even though they may have an extremely transient existence in the highly oxidising environment they may lead, locally, to reducing conditions, particularly if they are immersed in the liquid salt film. Whilst the effect may not be a major factor it will certainly make some contribution particularly when considered in conjunction with chloride.

A further area which is of interest is the influence of low levels of vanadium in the presence of sea-salt contamination. The influence of vanadium content has been studied extensively in the past in connection with burning low-cost residual fuels in the gas turbine and its corrosive effects are well documented. However most of these data refer to vanadium levels of 7 ppm or greater. More recently experimental data on the effects of 2 and 10 ppm vanadium in fuel with and without sodium salt contamination have been published (42). The effect of the two contaminants together was greater than either separately and both nickel and cobalt base superalloys showed characteristic sulphidation effects. Clearly the mechanism by which low levels of vanadium enhance hot corrosion damage requires further investigation.

DISCUSSIONS AND CONCLUSIONS

The mechanism of hot corrosion is clearly complex and whilst the overall products can be identified unstable intermediate products may not be found in post-mortem examinations. On the basis of the available evidence it seems likely that a variety of mechanisms may operate separately or together and the rate controlling process(es) must depend on the constitution of alloy, the precise nature of the environment and the particular temperature.

Some progress has been made towards elucidation of the processes occurring in the environment; in particular the effect of short residence times on the persistence of chloride has been established. There can be no doubt that chloride exists in those areas of the turbine where hot corrosion is found. The processes of condensation and/or impaction require further investigation but in general terms it must be assumed that chloride plays a crucial role in the mechanism of hot corrosion. Quite apart from providing a source of sodium for the formation of sodium sulphate it seems highly probable that the major role of chloride is in initially destroying the integrity of protective scale layers. Thermal cycling is a normal phenomenon in the gas turbine and thermal shock combined with chloride effects can be assumed to result in inhibition of the formation of protective layers. Although chloride must have a transient existence if deposited on nozzles or blades its intermittent or continuous replenishment may also provide secondary effects in promoting reduction in the melting point of deposited salts and also in increasing wetting properties. These effects may result in hot corrosion at lower temperatures and over more extensive areas of components. This combined with the volatility of deposits may control the lower and upper temperatures at which the sulphidation/accelerated oxidation effect is found.

The manner in which Cr_2O_3 inhibits the effect of chloride requires further examination particularly in the light of the apparently contradictory finding that alloys of higher chromium content are more rapidly attacked by chloride.

Whilst initially the role of sulphur is to form alkali sulphate deposits by sulphation of sea-salt, it ultimately results in the formation of stable sulphides under scale layers in positions of low oxygen activity. Once sulphides are formed it seems certain that even under conditions where the matrix of the alloy is being progressively oxidised, the sulphur released by oxidation of the sulphide will be conserved and migrate inwards to form further sulphide.

The influence of sulphide formation in inducing accelerated oxidation by impoverishment of the matrix in elements promoting oxidation resistance is arguable. In certain types of alloy the presence of sulphide in oxide layers can be associated with enhancing oxidation rates by providing rapid diffusion paths for oxygen.

There is growing evidence that the most important factor in the accelerated oxidation effect is sodium oxide although there are conflicting opinions as to the precise mechanism by which sodium oxide produces this effect. On the one hand formation of mixed oxides such as chromates or aluminates is cited; on the other there is evidence that it is the oxide ion activity which is rate controlling and that oxides, such as Cr_2O_3, which can accept oxide ions produce an inhibiting effect.

Existing information on the mechanism of hot corrosion provides some rational basis on which to explain the improvement in hot corrosion resistance shown by certain of the recently developed alloys of higher chromium content. Such information may also provide useful pointers to further progress in development of alloys and protective coatings or diffusion-bonded claddings. However, whilst the available thermochemical and experimental data enable the behaviour of certain alloying elements to be explained with some reliability, there are clearly gaps in existing knowledge on the synergistic effects of alloying elements which make the prediction of alloy response uncertain.

Final elucidation of the complex mechanism(s) of hot corrosion must rely on more precise determination of the thermochemical data which are lacking, further elucidation of the part processes leading to sulphidation and accelerated oxidation, and more detailed information on the environment and deposition processes within the gas turbine. In addition to sodium chloride and sodium sulphate there are clearly other chemical species present in the environment which play an important role and in particular the influence of carbon and water vapour requires further investigation. The role of vanadium will need to be investigated if economics or logistics dictate the use of fuels having higher contents of vanadium than the current low levels.

ACKNOWLEDGMENTS

Acknowledgment is made to Director, AML for permission to present this paper and appreciation is expressed to all of those who have provided information, advice and assistance. Thanks are also due to the authors of the many literature sources which have been employed and have provided valuable information.

REFERENCES

1. C. J. Danek, "State of the Art Survey on Hot Corrosion in Marine Gas Turbines," unpublished US Report, 1965.
2. P. Hancock, "Corrosion of Alloys at High Temperatures in Atmospheres Consisting of Fuel Combustion Products and Associated Impurities–A Critical Review," London, HMSO, 1968.
3. J. F. G. Condé, "The Control of Corrosion in Marinised Gas Turbines," Third Inter-Naval Corrosion Conference, April 14-18, 1969, London.
4. "Hot Corrosion in Gas Turbines," NMAB 260, May 1970.
5. A. J. Stapley, "Mechanisms of Corrosion in Marine Gas Turbines," to be published, *Brit. Corr. J.*, 1972.
6. V. I. Hanby and J. M. Beer, "Salt Deposition and Corrosion in Marine Gas Turbines," unpublished work under UK MOD Contract, 1969-1972.
7. J. A. C. Samms, unpublished report, UK MOD Contract, March 1971.
8. M. A. DeCrescente and N. S. Bornstein, "Formation and Reactivity Thermodynamics of Sodium Sulphate with Gas Turbine Alloys," *Corrosion* Vol. 24, No. 5, May 1969, p. 127-133.
9. A. S. Kallend, *Trans. Faraday Soc.* Vol. 63, No. 538, October 1967.
10. J. J. MacFarlane, unpublished report, NGTE.
11. J. A. C. Samms, unpublished work under UK MOD Contract, September 1969.

12. B. H. Zim and J. E. Mayer, *J. Chem. Phys.* Vol. 12, No. 362, 1944.
13. H. C. Duffin, unpublished work, NGTE, 1960.
14. R. J. Bishop, K. R. Cliffe and T. H. Langford, private communication, BCURA, 1969.
15. R. J. Bishop and K. R. Cliffe, "Condensation of Sodium Chloride from a Moving Gas Stream," *J. Inst. Fuel,* July 1969, p. 283-285.
16. H. Liander and G. Olsson, *IVA Stockholm,* Vol. 4, 1937.
17. C. Kroger and J. Stratmann, *Glastechn. Ber.* Vol. 34, 1961.
18. J. Billingham, Fulmer Research Institute Ltd, unpublished work under UK MOD Contract, 1969-1972.
19. G. Bertozzi and G. Soldani, "Surface Tension of Molten Salts: Alkali Sulphate and Chloride-Sulphate–Binary Systems," *J. Phys. Chem.* Vol. 71, 1967, p. 1536-1538.
20. W. D. Halstead and E. Raask, "The Behavior of Sulphur and Chlorine Compounds in Pulverized-Coal-Fired Boilers," *J. Inst. Fuel,* Sept. 1969, p. 344-349.
21. J. F. G. Condé, G. C. Booth, A. Taylor and B. Wareham, unpublished work, MOD, Admiralty Materials Laboratory.
22. J. F. G. Condé, "What are Separate and Interacting Roles of Sulphur Sodium and Chloride in Hot Corrosion?" AGARD Conference, High Temperature Corrosion of Aerospace Alloys, Denmark, April 1972.
23. A. J. B. Cutler, W. D. Halstead, J. W. Laxton and C. G. Stevens, "The Role of Chloride in the Corrosion Caused by Flue Gases and Their Deposits," *J. of Engng. for Power,* July 1971, p. 307-312.
24. P. S. Gray, in discussion of paper by H. Lewis and R. A. Smith, 1st Int. Congress on Metallic Corrosion, London, April 10-15, 1961.
25. P. Hancock, unpublished work under UK MOD Contract, Cranfield Institute of Technology, 1971-72.
26. A. U. Seybolt, "Oxidation of Ni-20 Cr Alloy and Stainless Steels in the Presence of Chlorides," *Oxidation of Metals,* Vol. 2, No. 2, 1970, p. 119-143.
27. A. U. Seybolt, "Internal Oxidation in Heat-Resisting Stainless Steels Caused by the Presence of Halides," *Oxidation of Metals,* Vol. 2, No. 2, 1970, p. 161-171.
28. J. M. Quets and W. H. Dresher, "Thermochemistry of the Hot Corrosion of Superalloys," *J. of Materials,* Vol. 4, No. 3, Sept. 1969, p. 583-589.
29. J. A. Goebel and F. S. Pettit, "Na_2SO_4-Induced Accelerated Oxidation (Hot Corrosion) of Nickel," *Met. Trans.* Vol. 1, July 1970, p. 1943-1954.
30. I. A. Menzies, unpublished work, Loughborough University, 1971.
31. A. K. Uijh, "A Possible Interpretation of the Influence of Chloride Ions on the Anodic Behaviour of Some Metals," *Corrosion Science,* Vol. 11, p. 161-167, 1971.
32. R. M. Schirmer and H. T. Quigg, "The Effect of JP-5 Sulphur Content on Hot Corrosion of Superalloys in Marine Environment," ASTM STP 421, p. 270-296, 1967.
33. P. A. Bergman, "Hot Corrosion of Gas Turbine Alloys," *Corrosion,* March 1967, p. 72-81.
34. F. S. Pettit, J. A. Goebel and G. W. Goward, "Thermodynamic Analysis of the Simultaneous Attack of Some Metals and Alloys by Two Oxidants," *Corrosion Science,* Vol. 9, 1969, p. 903-913.
35. G. Bombara, G. Baudo and A. Tamba, "Thermodynamics of Corrosion in Fused Sulphates," *Corrosion Science,* Vol. 8, 1968, p. 393-404.
36. E. A. Gulbransen and S. A. Jonsson, "High Temperature Metallic Corrosion of Sulphur and its Compounds," 1970, p. 3-51.
37. A. U. Seybolt, "Contribution to the Study of Hot Corrosion," *Trans. Met. Soc. AIME,* Vol. 242, Sept. 1968, p. 1955-1961.
38. C. J. Spengler and R. Viswanathan, "Effect of Sequential Sulphidation and Oxidation on the Propagation of Sulphur in an 85 Ni-15 Cr Alloy," *Met. Trans.* Vol. 3, Jan. 1972, p. 161-166.
39. J. A. Goebel and F. S. Pettit, "The Influence of Sulphides on the Oxidation Behaviour of Nickel-Base Alloys," *Met. Trans.* Vol. 1, 1970. p. 3421-3429.
40. N. S. Bornstein and M. A. DeCrescente, "The Role of Sodium and Sulphur in the Accelerated Oxidation Phenomenon–Sulphidation," *Corrosion,* Vol. 26, No. 7, July 1970, p. 209-214.
41. N. S. Bornstein and M. A. DeCrescente, "The Role of Sodium in the Accelerated Oxidation Phenomenon Termed Sulphidation," *Met. Trans.* Vol. 2, Oct. 1971, p. 2873-2883.
42. S. Y. Lee, S. M. DeCorso and W. E. Young, "Laboratory Procedures for Evaluating High Temperature Corrosion Resistance of Gas Turbine Alloys," *J. of Engng. for Power,* July 1971, p. 313-318.

Discussion:

MECHANISM OF HOT CORROSION

H. S. Spacil
General Electric Corporate Research and Development
Schenectady, New York

The use of phase stability diagrams, or isothermal Pourbaix-type diagrams, can be helpful in visualizing chemical interactions occurring during corrosion. For more complex systems, involving more than four reactive components and which may be difficult to depict in a two-dimensional plane, consideration of the simultaneous values of chemical potentials existing throughout the system can be useful. A basic assumption here is that local thermodynamic equilibrium exists throughout each phase, and that deviations from LTE occur only at phase boundaries where interface reactions may be rate-limiting.

Four examples will be examined in this discussion, pertaining to the Na-base salt condensates formed from combustion products.

1. Na_2SO_4 Condensation: A general criterion for the condensation of Na_2SO_4, when coupled with consistent thermodynamic data on gaseous Na_2SO_4, indicates when condensation may be expected under any particular service or test conditions.

2. Condensate/Carbon Interactions in Gas Turbines: Solid carbon, which occurs in gas turbines, can react locally with Na_2SO_4 to decrease the oxygen potential and increase the sulfur potential. The salt compositions resulting from this reaction can be calculated, leading to a maximum sulfur potential which is high enough to cause formation of the liquid Ni-S eutectic liquid in the presence of Ni.

3. Non-Equilibrium NaCl-Na_2SO_4 Mixtures: The reaction of ingested NaCl with combustion products can be used to calculate the salt compositions and chemical potentials expected. The results show that HCl and Cl_2 are the principal volatile products, that salt mixtures containing about 90% NaCl should have a finite life, and that the maximum chlorine potential should exist at the salt/gas interface.

4. Oxide-Na_2SO_4 Interactions: Mixtures of metal oxides, such as Cr_2O_3 and Al_2O_3, with Na_2SO_4 are indeterminate systems in that the extent of reaction between these species depends on the rate at which gases are either supplied to or removed from the reaction site. Thus, incorporation of the oxide into the salt melt will vary with the relative amounts of oxide and melt, gas composition and flow, etc. For any expected level of dissolved oxide, the chemical potentials and composition can be calculated for all points between the alloy melt and melt/gas interfaces. In this area especially, accurate thermodynamic data are lacking, and many assumptions may be necessary.

Discussion:

MECHANISM OF HOT CORROSION

F. S. Pettit
Pratt and Whitney Aircraft, Division of United Aircraft Corporation
East Hartford, Connecticut

"Accelerated Corrosion in Gas Turbine Engines," N. S. Bornstein, M. A. DeCrescents and H. A. Roth

This paper by Bornstein, DeCrescente and Roth emphasizes an important feature of the accelerated oxidation of materials induced by Na_2SO_4, in particular, reactions between normally protective oxide scales and Na_2SO_4 melts as well as Na_2SO_4 melts modified by oxides of certain elements in the alloy undergoing attack. In view of their work, it has become apparent that Na_2SO_4-induced accelerated oxidation of some metals and alloys (e.g. nickel, Ni-Al alloys) can occur because protective oxide scales are not stable on such materials in the presence of Na_2SO_4 melts containing relatively high oxide ion activities. In addition, the beneficial effect produced by chromium in inhibiting this type of attack has also become obvious since these authors have shown Cr_2O_3 can decrease the oxide ion content of Na_2SO_4.

At present, however, it may be an over-generalization to propose that the Na_2SO_4-induced accelerated oxidation of all alloys is caused by reactions between protective oxide scales and oxide ion-enriched Na_2SO_4 melts. Concomitant with reactions between oxide scales and oxide ion-enriched Na_2SO_4, ancillary processes consisting of the introduction of sulfur into the alloy and depletion of the alloy of those elements necessary for the formation of a protective oxide scale are also frequently taking place. It therefore is possible that, even though the increased oxidation is initially caused by reaction between protective oxide scales and the oxide ion-enriched Na_2SO_4, in some alloys these ancillary processes may also cause increased oxidation concurrently or at a later stage in the process when reaction between the oxide scale and the Na_2SO_4 melt is no longer possible. A more important reason for exercising restraint in generalizing the basic fluxing concept (i.e. reactions between protective oxide scales and oxide ion-enriched Na_2SO_4) is that, as shown in this paper, MoO_3 and V_2O_5 in Na_2SO_4 can produce a significant increase in the Na_2SO_4-induced accelerated oxidation of some alloys. Since the present authors have shown that such oxides decrease the oxide ion content of Na_2SO_4, it is not obvious that such detrimental effects are caused by oxide ion-enriched Na_2SO_4 melts.

Additional experimental work as well as theoretical considerations concerned with Na_2SO_4 melts modified by various oxide additions is required before the effects of oxides such as MoO_3 and V_2O_5 on the Na_2SO_4-induced accelerated oxidation of alloys can be completely described. Thermodynamic calculations, such as those performed by the authors, are not sufficient. For example, in using Eqs. 1 and 2 to compare the SO_2 pressures required to form $Al_2(SO_4)_3$ and that established by saturating Na_2SO_4 with V_2O_5, it is implied that solid Al_2O_3 can coexist with liquid V_2O_5. Such a condition is not stable since the Al_2O_3 will react with V_2O_5. In certain cases, a more rigorous approach may consist of considering reactions between protective oxides and modified Na_2SO_4 melts. For example, in the case of MoO_3, one would consider the MoO_3-modified Na_2SO_4 to be composed of a solution of two solvents, in particular, Na_2SO_4 and Na_2MoO_4. For such considerations the use of three-dimensional diagrams such as that presented in Fig. 1 are helpful. The oxide phases which may be stable in such a melt are not significantly influenced by the oxygen pressure and before attempting to construct boundaries in diagrams of the type presented in Fig. 1 it is possible to consider melts at constant oxygen pressure. In Fig. 2, the phases or aluminum that may be stable in a MoO_3-modified Na_2SO_4 melt at constant oxygen pressure are illustrated. Such a diagram can in turn be used to determine the SO_3 pressure at which Al_2O_3 will donate oxide ions to a Na_2SO_4 melt containing a specified amount of MoO_3. As illustrated in Fig. 3, the boundary at which Al_2O_3 reacts with a MoO_3-modified melt can be displaced to much lower SO_3 pressures than that which is obtained by neglecting the formation of a solution of Na_2SO_4 and MoO_3.

"The Mechanism of Hot Corrosion in Marine Gas Turbines," J. F. G. Condé.

The paper by Condé presents a very complete review of mechanisms that can be used to describe the hot corrosion of metals and alloys. The emphasis placed on the origins of corrosive contaminants in gas turbines is very appropriate. The thermodynamic calculations that have been performed to attempt to define conditions in gas turbines are valuable but obviously are at most gross approximations. In view of the short residence times in the

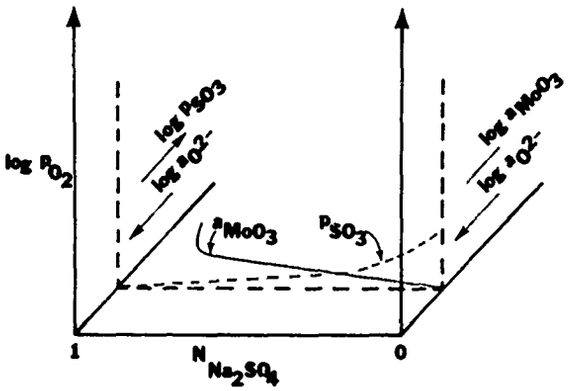

Figure 1. Schematic diagram showing the variables that must be considered when examining effects produced by solutions of Na_2SO_4-Na_2MoO_4. In the pure Na_2SO_4 plane (i.e., $N_{Na_2SO_4}$ = 1) oxygen, SO_3 and oxide ion activities are variables whereas in the Na_2MoO_4 plane (i.e., $N_{Na_2SO_4}$ = 0) oxygen, oxide ion and MoO_3 activities are variables. In the solution region there are four variables. In this diagram the thick dashed line indicates an isoactivity line for oxide ions, the thin dashed line is an isobar of SO_3 and the solid line an isoactivity line for MoO_3.

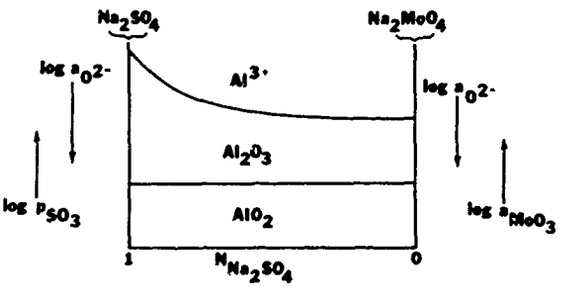

Figure 2. Schematic diagram showing the phases of aluminum which are stable in Na_2SO_4-Na_2MoO_4 solutions at a constant oxygen pressure.

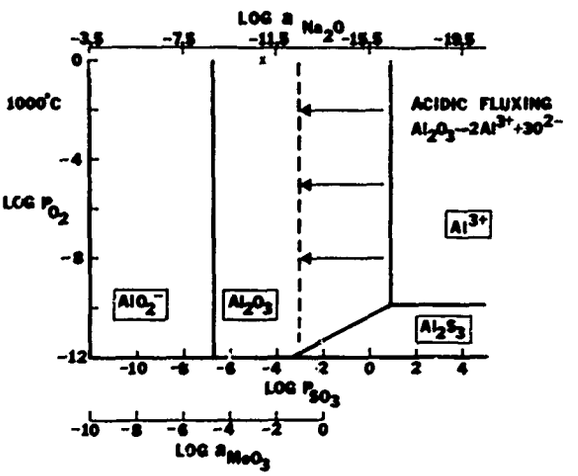

Figure 3. Stability diagram showing the displacement of the boundary (arrows) at which Al_2O_3 reacts with a modified Na_2SO_4 melt (acidic fluxing) for the case where Na_2SO_4 contains MoO_3 in solution such that the MoO_3 activity is 0.1 at a mole fraction of Na_2SO_4 of 0.99.

combustion system, the amount and compositions of the salts deposited at temperature on turbine hardware are unknown parameters which can be obtained only from additional experimental studies.

This paper also rightly directs attention to the possible effects produced by carbon, water vapor and NaCl on the hot corrosion process. Such effects have been neglected in numerous studies and certainly require consideration. It seems reasonable to assume that impacting carbon particles will cause the local oxygen activity to be reduced in the vicinity of salt deposits on turbine components and conditions suitable for the introduction of sulfur into the alloy with attendant increases in the oxide ion content of Na_2SO_4 will be developed. Both of these conditions can be expected to cause increased oxidation of some alloys. The influence of NaCl on Na_2SO_4-induced accelerated oxidation alloys is not clear. As mentioned by Condé, NaCl may cause the generation of heavy metal chlorides. Another possibility is that NaCl in Na_2SO_4 may influence the solubility of certain protective oxide scales in such melts and thereby have an important effect on the fluxing of protective oxide scales by liquid salt deposits. While carbon, NaCl and water vapor may influence the Na_2SO_4-induced hot corrosion of alloys, it is important to determine whether

such effects are of primary or secondary importance to the hot corrosion process. It is apparent from laboratory studies that a deposit of Na_2SO_4 is a sufficient condition to cause the hot corrosion of many alloys and coatings in the absence of NaCl, carbon or water vapor. For example, the lives of aluminide coatings on B-1900 have been found to be less in a laboratory test using Na_2SO_4 deposits than in a burner rig test at the same temperature with ingested sea salt. Such results indicate that effects produced by NaCl, carbon or water vapor may be of secondary importance to the hot corrosion of materials in the presence of Na_2SO_4.

Session II

GAS TURBINE MATERIALS AND COATINGS

Session Chairman:

George Wacker
Naval Ship R&D Center, Annapolis, Maryland

WEDNESDAY, OCTOBER 25, 1972

THURSDAY, OCTOBER 26, 1972

Superalloys Development for Gas Turbines Operating in the Marine Environment

C. C. Clark and W. R. Hulsizer
The International Nickel Company Inc.
New York, New York

SUMMARY

This presentation is a summary of recent developments and behavioral investigations in progress at the International Nickel Laboratories in Sterling Forest, New York, and Birmingham, England. It is not intended to present a wealth of background information but only significant points which hopefully will stimulate a meaningful discussion. The many gas turbine alloys that have been developed in Inco's laboratories but have already reached commercial use will not be discussed except for several that are primarily of interest in Europe.

TURBINE BLADE ALLOY DEVELOPMENTS

In 1964 the Naval Ships Systems Command established a program with the following objectives:

1. Develop a turbine blade alloy combining the hot corrosion resistance of Udimet* 500 in 1% sulfur diesel fuel combustion products with the strength and ductility of alloy 713C at 1600°F (100 hr rupture life at 43,000 psi).
2. Develop a cobalt-base turbine nozzle alloy with the 1900°F strength of WI-52 (100 hr rupture life at 10,000 psi) but with improved hot-corrosion resistance.

These targets were accepted by the metals industry and a number of alloys soon appeared which met the blade target. These included the now familiar IN-738. In 1970 the National Materials Advisory Board Committee on "Atmospheric Deterioration of Superalloys" (1) considered a number of alloy or process approaches which might result in alloys meeting the following objectives:

- Sulfidation and oxidation resistance ≥ Udimet 500
- Temperature-strength capability for blades ≥ IN-100
- Temperature-strength capability for vanes ≥ WI-52

Meeting these objectives through alloy modification or development proved to be difficult as predicted. IN-792 meets the strength goals for the blade alloy but falls somewhat short of the desired corrosion resistance. Nevertheless, the alloy is receiving wide attention for turbine blades and promises to become a widely used material.

A wrought alloy was developed by Inco's Birmingham Laboratory in the late 1960's which meets the guide vane target of corrosion resistance but lacks the desired WI-52 strength capability. Perhaps that is why it has received little attention to date in the U.S.A. The alloy is designated IN-597 (2). Its chemical composition is:

C:	.05	Cb:	1.0
Cr:	24.5	Mo:	1.5
Co:	20.0	Zr:	.05
Ti:	3.0	B:	.012
Al:	1.5	Ni:	Bal

Its high chromium content makes the alloy highly resistant to sulfidation in a crucible test in which a 75% Na_2SO_4-25% NaCl mixture is continuously deposited at 1650°F, Fig. 1. The alloy is only roughly equivalent to Udimet 500 in temperature capability and, hence, falls short of the WI-52 temperature strength goal.

The development of this alloy has led to work on a cast 23% chromium alloy which has strength nearly as good as IN-738 at 1600°F, Fig. 2. Although only in its early stages of development, the alloy does not yet meet WI-52 properties at higher temperatures. Progress to date is encouraging, however, and a useful guide vane and/or turbine blade alloy may result.

The subcommittee which considered approaches to meeting the target requirements was not very hopeful that straight alloy modifications would meet the target properties. So far this prediction has proven correct. We at Inco think that in the nickel base system, at least, it will be very difficult to meet these targets. It appears, however, that there is a possibility for developing an alloy about 50°F stronger than IN-792. Even though its corrosion resistance is expected to be much better than that of IN-100, it will fall short of the corrosion resistance of Udimet 500.

MECHANICAL ALLOYING

Increasing demand by turbine designers and operators for improved efficiency and durability over many thousands of hours means that materials are being utilized to their utmost capability. Their survival at the very high turbine inlet temperatures used in today's turbines is dependent upon

*Trademark of Special Metals, Inc.

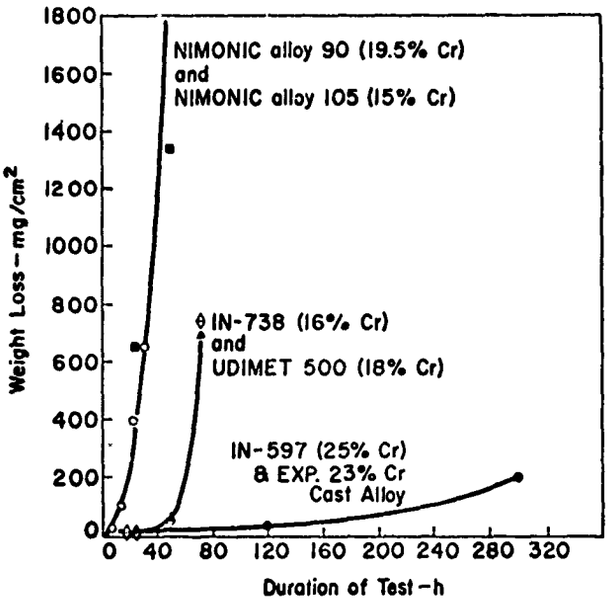

Figure 1.

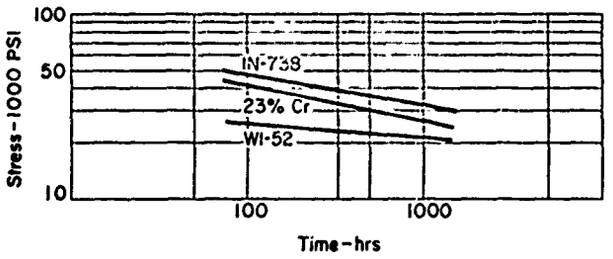

Figure 2. Rupture strength of experimental 23% Cr Alloy at 1600° F compared with IN-738 and WI-52

design innovations such as convection and film cooling and their surface stability is frequently provided by coatings.

We at Inco believe that the development of the mechanical alloying process (3) offers opportunities for the metallurgist to meet these requirements by increasing temperature capability and stability and at the same time to increase surface stability. The first mechanical alloyed material is IN-853. The commercial development of this alloy is in its early stages and is being offered as Inconel* alloy MA-753. Figures 3 and 4 compare its strength with several established turbine blade and guide vane alloys and t. ₂General Electric Company's Co74XV goals (4). We consider that IN-853 is a forerunner of a family of dispersion strengthened alloys. For example, good progress is being made toward the development of highly oxidation-resistant sheet material and the feasibility of an alloy with significantly better intermediate temperature strength than IN-853 is also becoming apparent.

*Trademark The International Nickel Company, Inc.

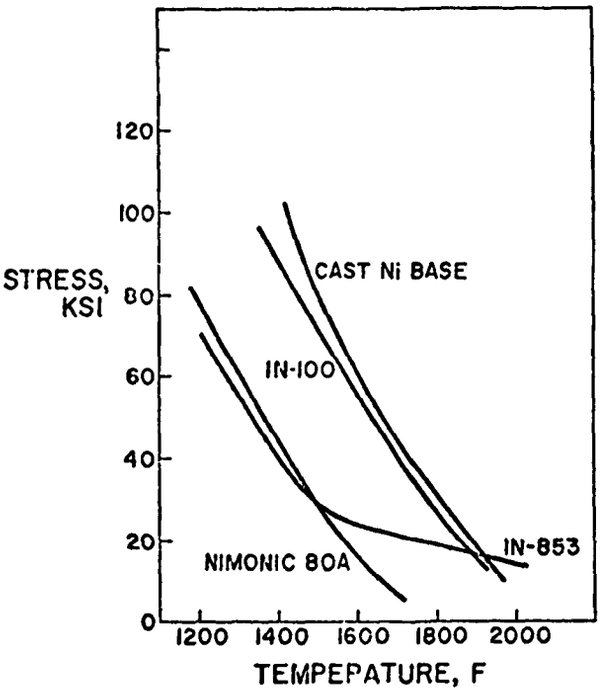

Figure 3. Turbine blade alloys, 100 hour creep rupture.

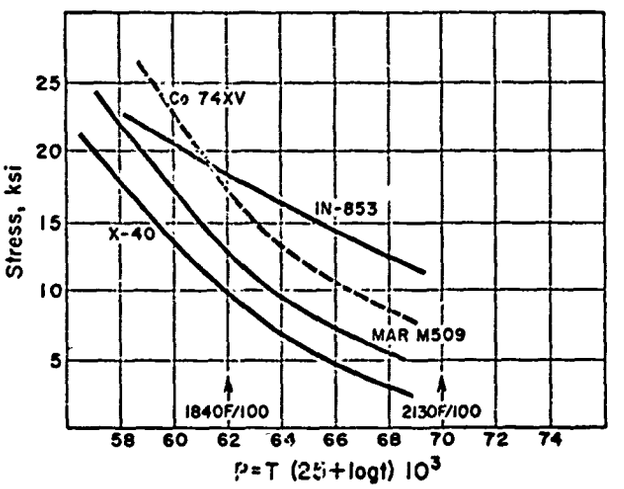

Figure 4. General Electric Company turbine vane alloy requirements.

Alloys of this type differ from conventional superalloys and will have to be handled somewhat differently in design. For example, as temperature increases the slope of the creep rupture strength for superalloys becomes steeper indicating an instability of the hardening mechanism, namely, gamma prime. The slope of the creep rupture curve for IN-853, however, becomes flatter as temperature increases thereby indicating good long-time temperature stability (5), Fig. 5. The strengthening effect of the yttria dispersoid becomes evident at 1500°F which coincides with the knee of the stress rupture curve in Fig. 3. Subsequent alloys are expected to behave similarly.

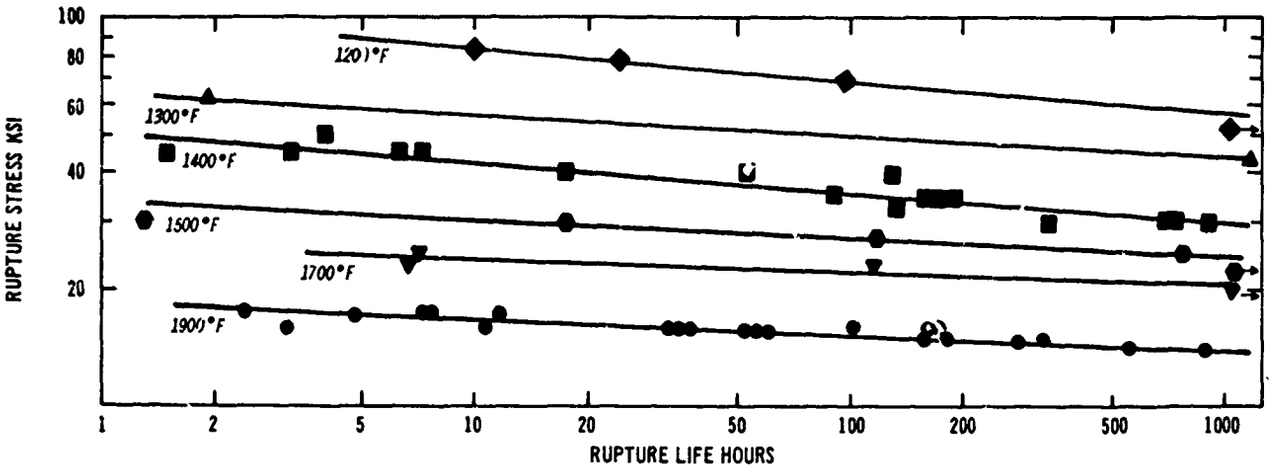

Figure 5. Stress rupture test lives of IN-853.

Another benefit of dispersion strengthened alloys is that the dispersoid itself has been shown to improve corrosion behavior. This is evident in Fig. 6, which compares the structures of IN-853 and Nimonic* alloy 80A after exposure in a laboratory sulfidation test. An important difference in composition is the presence of about 1.2% Y_2O_3 in IN-853. The attack was light and general along the surface of the IN-853 while in Nimonic alloy 80A a significant amount of intergranular attack occurred in addition to general corrosion. The beneficial effect is believed to result from the high affinity of yttrium for sulfur in forming an oxysulfide and thereby inhibiting diffusion of sulfur into the metal.

OXIDATION OBSERVATIONS

While attempting to explain variable results in a simple laboratory oxidation test, McCarron and Schultz (6) "confirmed" the effects of water vapor on scaling resistance of Fe-Ni-Cr alloys. This prompted the study of the specific effects on a series of high temperature alloys ranging from Type 304 stainless steel to IN-738, (Table 1).

Cyclic (24 hr or 100 hr) oxidation tests were conducted at 2012°F in a slow moving atmosphere containing 0.1, 5 and 10% water vapor for 400 to 1000 hours. Oxidation was measured by weight loss, both undescaled after each cycle and descaled at the end of each test.

The alloys studied fall into three distinct categories: an iron-nickel-chromium series without additional significant alloying additions, two matrix stiffened alloys for sheet metal components, and six superalloys typical of currently used turbine blade alloys.

Results of the tests on the Fe-Ni-Cr alloys are typified by the results for Type 304 stainless steel and alloy 600 shown in Figs. 7 and 8. Water vapor had a significant effect on the cyclic oxidation behavior of all except Nichrome* V, which is iron-free. The severity of the effect increased as the level of water vapor increased. It is also clear from this series of tests, which is summarized in Fig. 9, that water vapor has an increasingly severe effect on scaling behavior as the iron content is increased. When tested under isothermal or static conditions no significant effect of water vapor was observed.

Two matrix stiffened alloys, Hastelloy** alloy X and IN-586, an alloy developed by Inco's Birmingham, England Research Laboratory, were also tested. The results summarized in Figs. 10 and 11 show that there was little degradation in resistance when water vapor was increased from 0.1% to 5% H_2O, but the resistance of both alloys deteriorated in 10% H_2O. The slightly better resistance of IN-586 in this test can be as easily attributed to its lower iron content as to the presence of 0.04% cerium.

The last six alloys are typical of those currently used for cast turbine blades. They were only tested in air containing 0.1 and 3.0% water vapor. The results are summarized in Figs. 12-17. IN-100 exhibited little sensitivity to increased water vapor while Mar-M*** alloy 421 showed markedly increased scaling in the presence of air + 3% H_2O. While these represent the two extremes, all alloys showed increased scaling as water vapor was increased.

The original paper (6) reports results of x-ray diffraction and microprobe studies and contains an extensive discussion about the possible mechanisms responsible for the behavior of the alloys when exposed to high temperature air containing water vapor. In general these can be summarized as follows:

1. In Fe-Ni-Cr alloys an inner Cr_2O_3 layer exists between the substrate and an outer (FeNi) Cr_2O_4 scale. The inner Cr_2O_3 layer gradually disappears with time when the alloy is tested in humidified air and the thicker (FeNi) Cr_3O_4 spalls more easily.

*Trademark The International Nickel Company, Inc.

*Trademark of Driver-Harris

**Trademark of Cabot Corporation

***Trademark of Martin Marietta Corporation

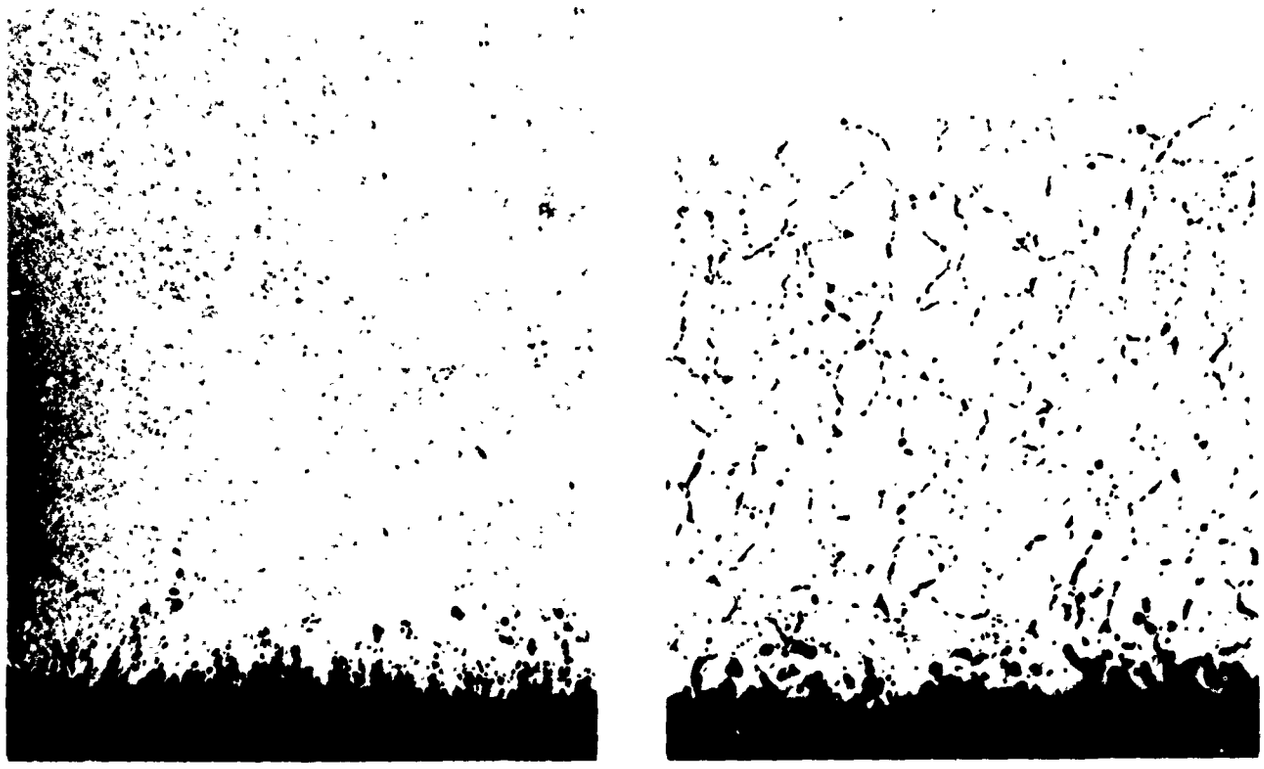

NIMONIC 80 A

IN 853

Figure 6. Effect of Y_2O_3 in 1700°F sulfidation test. 250X (Approx.)

Table I
Composition of Alloys – McCarron-Schultz Oxidation Study

Alloy	Fe	Ni	Cr	Co	Al	Ti	Mo	W	Cb	Ta
304 SS	Bal.	9.0	18.3	–	–	–	–	–	–	–
310 SS	Bal.	19.4	23.9	–	–	–	–	–	–	–
Incoloy alloy 800	Bal.	30.1	20.8	–	–	–	–	–	–	–
Inconel alloy 600	7.3	Bal.	16.0	–	–	–	–	–	–	–
Nichrome V	0.5	Bal.	20.6	–	–	–	–	–	–	–
Hastelloy alloy X	19.5	Bal.	21.6	–	–	–	8.6	0.5	–	–
IN-586*	–	Bal.	24.0	–	–	–	9.3	–	–	–
IN-100**	–	Bal.	10.1	14.4	5.5	4.7	3.0	–	–	–
Alloy 713C	–	Bal.	13.0	–	6.3	0.9	4.0	–	2.1	–
Udimet 700	–	Bal.	14.3	14.6	4.0	3.0	3.7	–	–	–
IN-738	–	Bal.	15.0	8.9	3.5	3.5	1.5	2.6	0.9	1.3
Mar-M alloy 421	–	Bal.	15.1	9.8	5.4	2.7	1.6	3.7	2.1	0.3
Udimet 500	–	Bal.	18.9	18.4	3.2	3.0	3.5	–	0.1	0.1

*Also contains 0.04 Ce
**Also contains 1.0 V

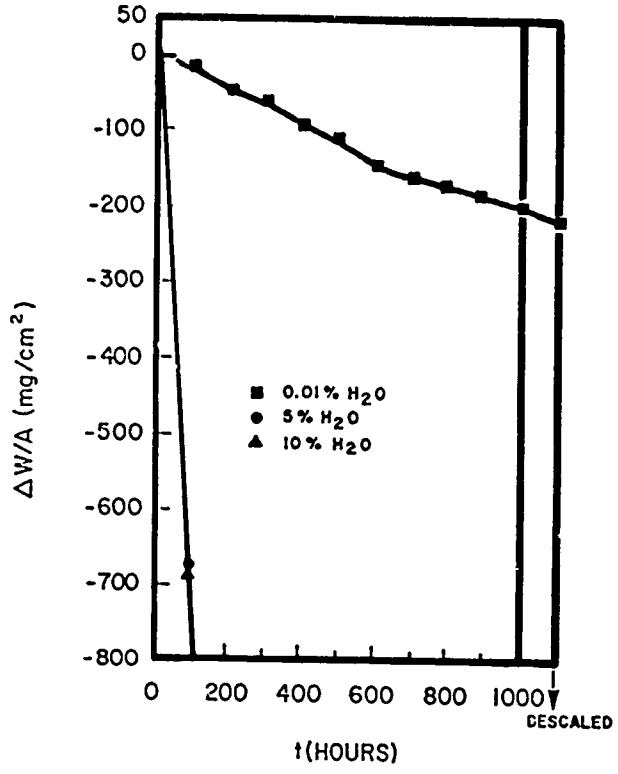

Figure 7. Effect of water vapor on the cyclic oxidation resistance of 304 SS at 1100°C in air. (Cycled every 100 hours.)

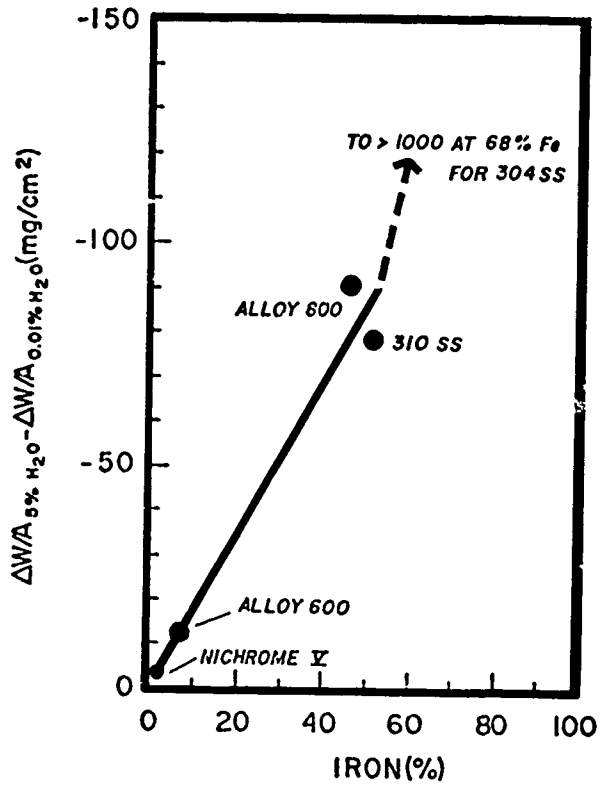

Figure 9. Relationship between iron content and water vapor effect for Fe-Ni-Cr alloys after 1000 hours of cyclic oxidation at 1100°C.

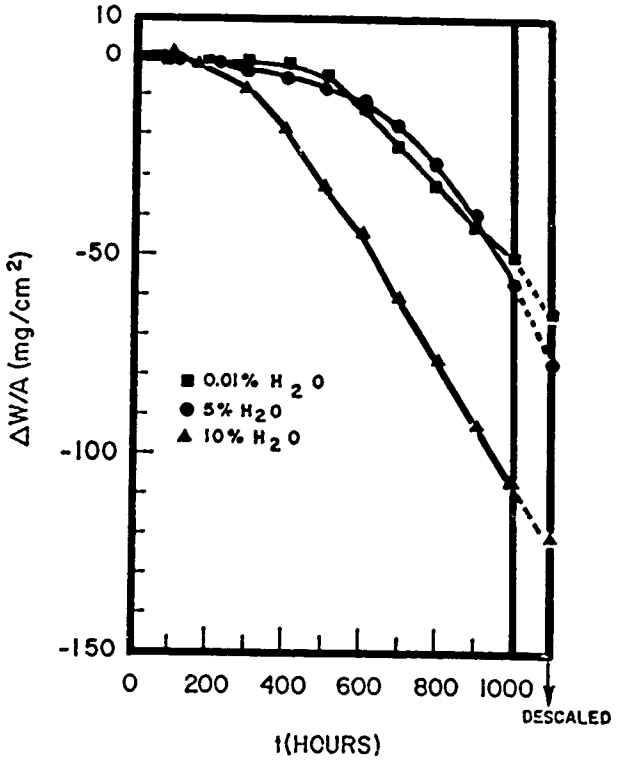

Figure 8. Effect of water vapor on the cyclic oxidation resistance of alloy 600 at 1100°C in air. (Cycled every 100 hours.)

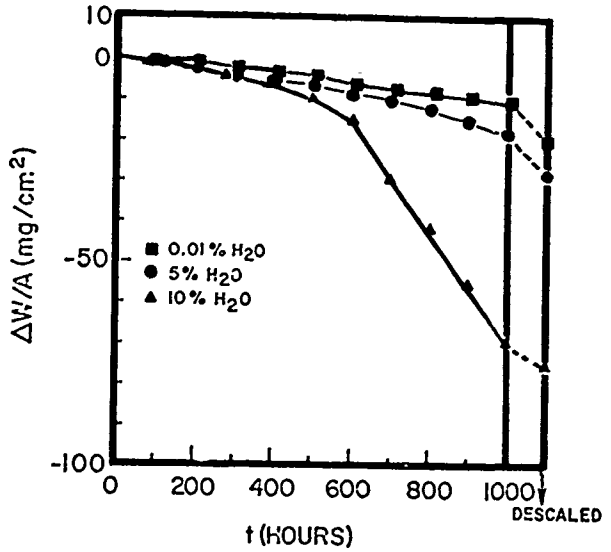

Figure 10. Effect of water vapor on the cyclic oxidation resistance of Hastelloy alloy X at 1100°C in air. (Cycled every 100 hours.)

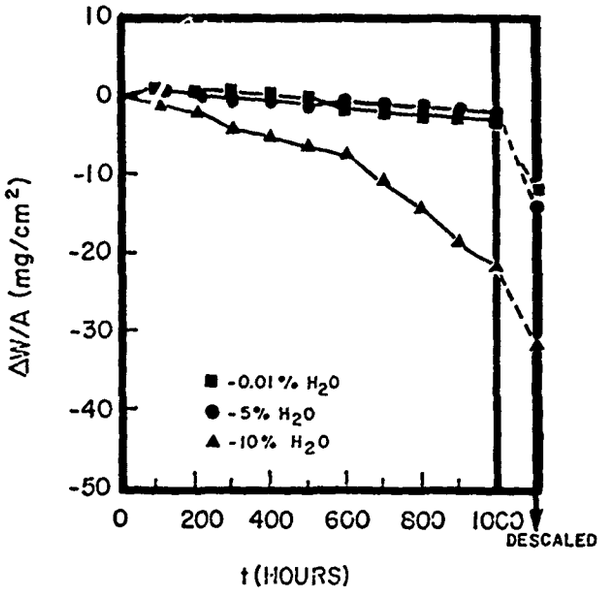

Figure 11. Effect of water vapor on the cyclic oxidation resistance of IN-586 at 1100°C in air. (Cycled every 100 hours.)

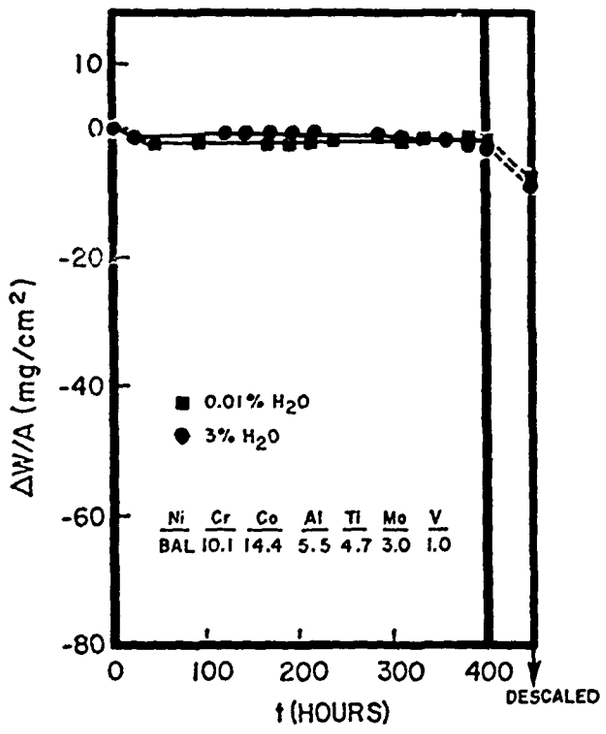

Figure 12. Effect of water vapor on the cyclic oxidation resistance of IN-100 at 1100°C in air. (Cycled 24 to 100 hours.)

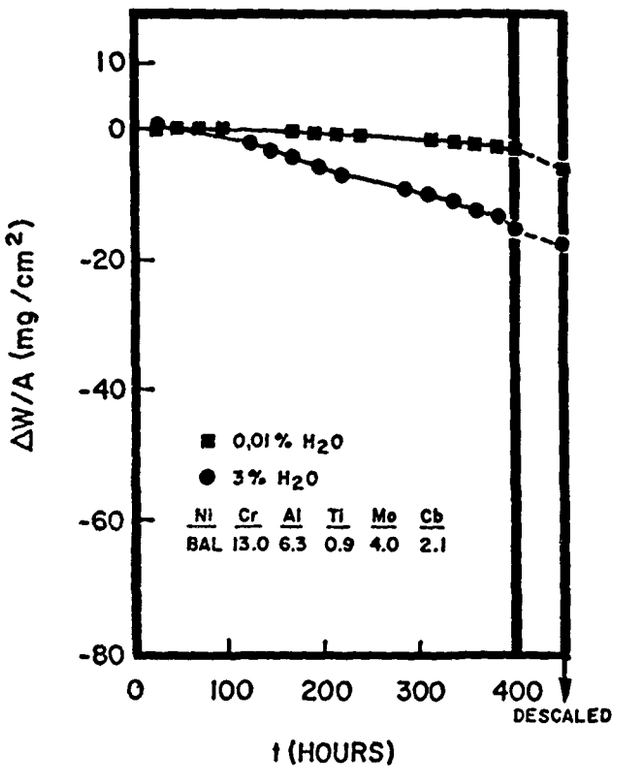

Figure 13. Effect of water vapor on the cyclic oxidation resistance of alloy 713C at 1100°C in air. (Cycled 24 to 100 hours.)

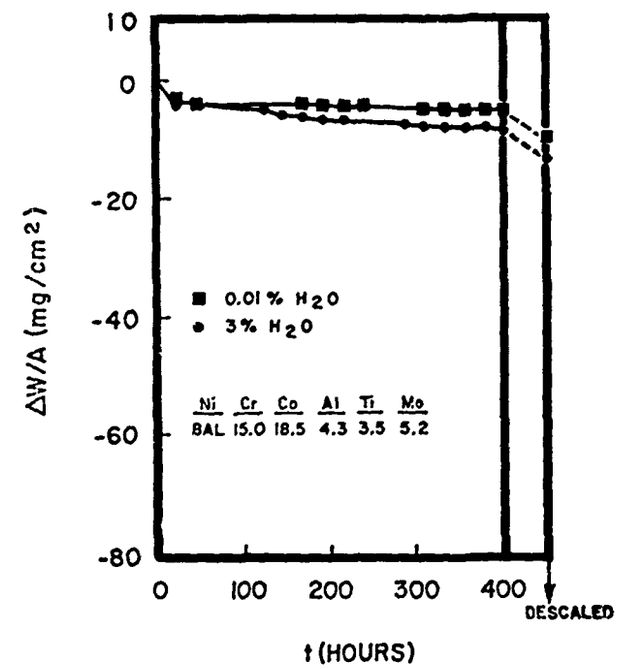

Figure 14. Effect of water vapor on the cyclic oxidation resistance of Udimet 700 at 1100°C in air. (Cycled 24 to 100 hours.)

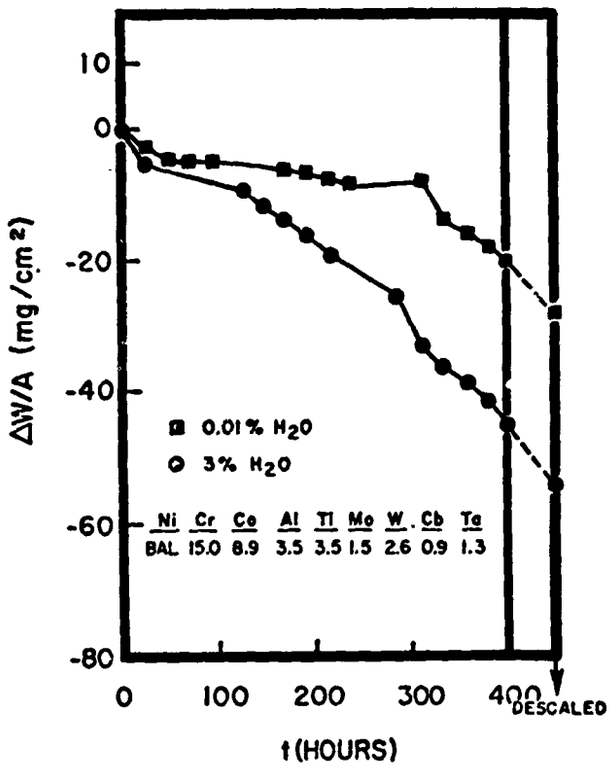

Figure 15. Effect of water vapor on the cyclic oxidation resistance of IN-738 at 1100°C in air. (Cycled 24 to 100 hours.)

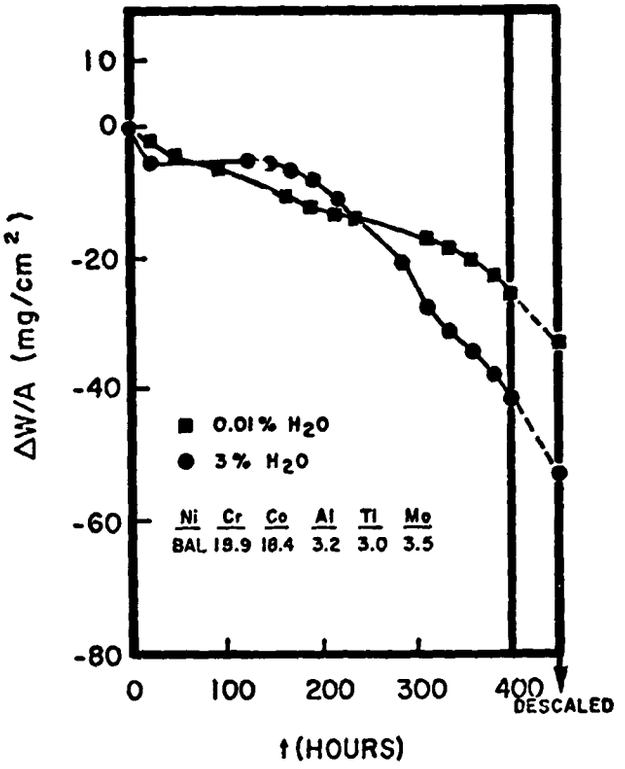

Figure 17. Effect of water vapor on the cyclic oxidation resistance of Udimet 500 at 1100°C in air. (Cycled 24 to 100 hours.)

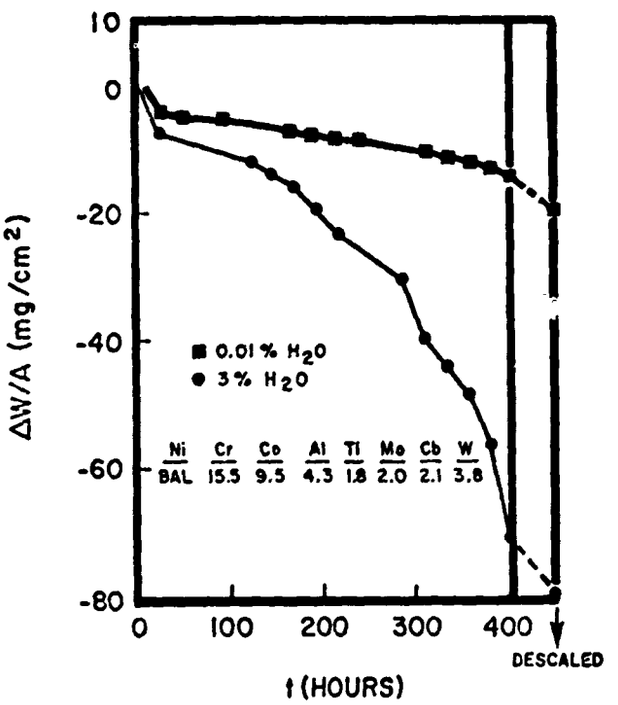

Figure 16. Effect of water vapor on the cyclic oxidation resistance of Mar-M alloy 421 at 1100°C in air. (Cycled 24 to 100 hours.)

2. The more complex scales which form on the superalloys are more difficult to interpret. In the higher aluminum-lower chromium alloys, a heavy continuous Al_2O_3 layer forms and is maintained while subsequent layers of $NiAl_2O_4$, $Ni(AlCr)_2O_4$, $NiCr_2O_4$ and NiO overgrow the Al_2O_3 in that order. In the higher chromium-lower aluminum alloys, the Al_2O_3 layer is eventually replaced by an inner layer of Cr_2O_3 containing aluminum or $Ni(AlCr)_2O_4$ while the outer layers tend to be $NiCr_2O_4$ and NiO in that order. The high chromium-low aluminum IN-100 and Udimet 700 are less sensitive to the effect of water vapor than high chromium-low aluminum Udimet 500.

3. A high refractory metal content appears to be a factor because the other three alloys, alloy 713C, IN-738, and Mar-M alloy 421, which showed the greatest drop when tested in wet air, contained 6.1, 6.5 and 7.7% of Mo + W + Cb + Ta respectively. Mar-M alloy 421 showed by far the greatest effect of water vapor.

It is obvious that the McCarron-Schultz paper raises more questions than it answers because all testing was done at one temperature and true dynamic effects that are encountered in gas turbines were not studied. It is equally obvious, however, that oxidation and the way it is influenced by water vapor must be considered in the application or development of future turbine materials. Since the end product of sulfidation is oxidation, it is logical to expect that water vapor also influences the behavior of turbine

materials in sulfidation inducing environments. We have not tested the high chromium alloys discussed earlier in an air environment with water vapor present.

INFLUENCE OF HAFNIUM ON OXIDATION

While not reported in the McCarron-Schultz paper, some oxidation data on IN-792 with 0 to 1.4% hafnium are shown in Fig. 18. Hafnium has been reported to improve the oxidation resistance of IN-792 but these tests conducted in air plus 5% water vapor suggest that hafnium is deleterious and that water vapor is a factor which must be taken into consideration in future tests on hafnium containing alloys.

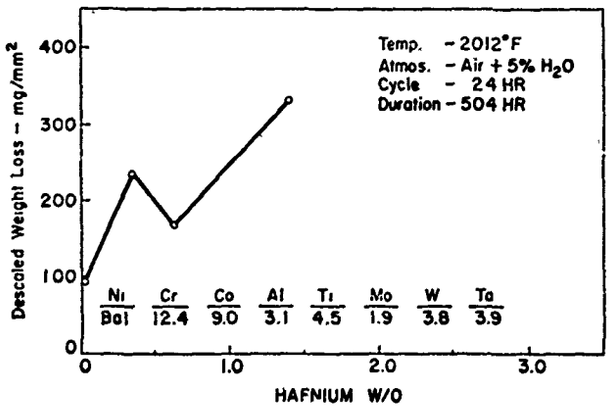

Figure 18. Effect of hafnium on the static-cyclic oxidation resistance of IN-792.

SUMMARY

This paper has summarized several developments from our laboratories which are or should become significant contributions to the behavior of materials in turbine environments. Some results raise more questions than they answer and, obviously, more work remains to be done to further define causes and effects.

Gas turbine material developers still require better input from the field about the behavior of established alloys and the need for improved ones. One of the recommendations made by the Committee on Atmospheric Deterioration of Superalloys (1) was: "Establish meaningful targets for mechanical and environmental performance of advanced gas turbines. Represented viewpoints should include turbine producers and users as well as materials developers and designers." As one of the major gas turbine users, the Navy should be in a good position to do this.

REFERENCES

1. Publication NMAB-260.
2. N. Stephenson and D. H. Maxwell, "High Temperature Alloys for Industrial Gas Turbines," presented at Inco Power Conference, Lausanne, Switzerland, May 1972.
3. J. S. Benjamin, "Dispersion Strengthened Superalloys by Mechanical Alloying," *Metallurgical Transactions,* Volume 1, October 1970.
4. E. W. Ross, E. D. Sayre, G. D. Oxx and J. W. Semmel, "Advanced Alloy Goals for 1972-1976," G.E. Report TM 68-835, January 15, 1969.
5. J. S. Benjamin and R. L. Cairns, "Elevated Temperature Mechanical Properties of a Dispersion Strengthened Superalloy." International Powder Metallurgy Conference, New York, N.Y., July 1970. Proceedings published by Plenum Press, New York.
6. R. L. McCarron and J. W. Schultz, "The Effects of Water Vapor on the Oxidation Behavior of Some Heat Resistant Alloys." Submitted for publication in Proceedings, Symposium on High Temperature Gas-Metal Reactions in Mixed Environments, May 1972, Boston, Mass.

Hot Corrosion of Coated Superalloys in a Gas Turbine Environment

A. R. Stetson and V. S. Moore
Solar Division of International Harvester Company
San Diego, California

ABSTRACT

The final results of a hot corrosion rig test evaluation of 45 coating-alloy combinations are presented. Alloys included were B1900, Inco 713C, IN-100, Rene' 41, SEL-15, U-700, U-710, MAR-M246, WI-52 and X-40. Rig tests were performed for up to 150 hours at 1650°F and 1800°F on nickel-base alloys and 1800°F and 2000°F on cobalt-base alloys in a high-velocity environment obtained from the combustion of JP-5 fuel and air and ingestion of 35 parts sea salt per one million parts air.

The coatings tested (1) were commercially available, (2) were essentially βNiAl or βCoAl with numerous secondary phases, and (3) were formed from the combination of the reaction of aluminum with the substrate and with elements codeposited with aluminum. One exception was a coating on B1900 which appeared to be a silicide.

Under the conditions of the test, protection could be afforded by at least one of the coatings on the nickel-base alloys for 150 hours at 1650°F and 100 hours at 1800°F. At 1800°F the relatively thin coatings on cobalt-base alloys exhibited poorer protection than coated nickel-base alloys at this temperature. At 2000°F the coatings on WI-52 could not afford protection beyond 60 hours. Performance was only slightly better on the higher chromium X-40 alloy. The life of coatings closely correlated with thickness on both nickel- and cobalt-base alloys and was strongly influenced by the chromium content of the substrate. Minor additives to the aluminides, notably silicon, also significantly enhanced the performance of the aluminide coatings on nickel-base alloys.

The effects of coatings, processing conditions, and long-term, high-temperature exposures on the mechanical properties of the nickel- and cobalt-base alloys were also evaluated. Data are presented on (1) the low-cycle fatigue life of the ten alloys uncoated as-received, uncoated and coated after 500 hours exposure at high temperature, and (2) the elevated temperature stress rupture properties of the coated alloys after long-term exposures and after coating stripping and recoating operations to simulate repair of used blades and vanes.

INTRODUCTION

Currently a large variety of alloys and diffusion formed aluminide coatings are used for the protection of gas turbine blades and vanes in operational aircraft gas turbine engines. Data are generally lacking which compare (1) the efficiency of the various available alloy-coating combinations in resisting a hot corrosion environment (operation in a marine environment), (2) the influence of coatings on critical mechanical properties, and (3) the influence of recoating the components after extended service. The need for such data is critical when turbine manufacturers and users must select base alloys and coatings, establish quality control specifications, and determine post-service reprocessing economics.

In this paper, results will be presented on an evaluation of the performance of ten common alloys with respect to hot corrosion, low-cycle fatigue and stress rupture. Each of the alloys was also tested after being coated with any of 3 to 5 commercially available coatings from the generic group–PWA 47, ALPAK, CODEP, UC, MDC, HI-15 and Chromalloy 870.

EXPERIMENTAL PROCEDURES

ALLOYS AND TEST SPECIMENS

Compositions of the 10 nickel- and cobalt-base alloys are shown in Table I. The alloys are coded for convenience in presentation and may be divided into classes as noted below:

B1900 MAR-M246 IN-100 SEL-15	Low chromium
Inco 713C Udimet 700	Medium chromium
Udimet 710 Rene' 41	High chromium
WI-52 X-40	Cobalt-base, high chromium

For hot corrosion rig testing, these alloys were cast into the simulated airfoil configuration shown in Fig. 1. For low-cycle fatigue and for stress rupture, eight of the alloys were cast into standard R3 tensile bars with a 0.250-inch diameter reduced section (per Federal Test Standard 151A, Method 211.1, for stress rupture testing). The diameter of each bar was reduced from 0.250 to 0.185 inch to promote

Table I
Compositions of Alloys

Cast Alloys	Code	Composition (Weight Percent)													
									Others						
		Ni	Co	Cr	Al	Ti	Mo	W	Ta	Cb	V	C	Zr	B	Fe
B1900	B	Bal	10.30	8.50	5.85	1.02	5.95	-	4.23	0.1	-	.093	.09	.011	.21
713C	C	Bal	0.22	13.80	5.85	0.78	4.55	-	-	2.27	-	.135	.10	.010	.12
IN-100	I	Bal	15.40	10.50	5.49	4.34	3.17	-	-	-	.76	.16	.16	.013	.12
MAR-M246	M	Bal	10.10	8.69	5.47	1.52	2.69	10.00	1.39	-	-	.144	.05	.011	.08
Rene' 41	R	Bal	11.30	19.20	1.56	3.30	9.79	-	-	-	-	.078	-	.006	.35
SEL-15	S	Bal	13.70	10.70	5.51	2.18	6.18	1.9	-	0.45	-	.057	.10	.014	.15
U-700	U	Bal	14.90	14.30	4.25	3.42	4.10	-	-	-	-	.06	.04	.015	.22
U-710	D	Bal	14.60	17.90	2.50	4.84	3.10	-	-	-	-	.07	-	.020	.10
WI-52	W	0.47	Bal	20.70	-	-	-	10.90	-	1.81	-	.488	-	-	2.09
X-40	X	10.70	Bal	25.80	-	-	-	7.54	-	-	-	.487	.06	.003	.21
Wrought Alloys															
U-700	U	Bal	18.70	15.10	4.49	3.44	4.95	-	-	-	-	.06	.05	.014	.15
Rene' 41	R	Bal	11.05	18.90	1.53	3.13	9.73	-	-	-	-	.08	-	.005	1.17

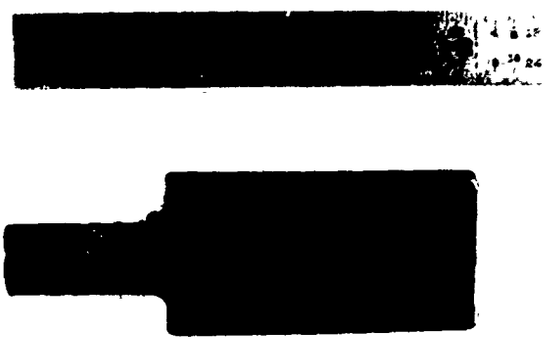

Figure 1. Simulated airfoil specimen.

failure in the test section and reduce the frequency of failures in the threaded ends of the bars during low-cycle fatigue testing. Rene' 41 and U limet 700 were obtained as wrought bar stock and were machined to the above dimensions before being heat-treated according to standard techniques.

Prior to testing, the reduced section of each stress rupture or fatigue test bar was polished to a surface finish of less than 10 μ inch (rms) for uncoated specimens and less than 25 μ inch (rms) for coated specimens.

COATINGS

At the time of performance of this program, the coatings included were primarily those in use by the Navy in aircraft gas turbines. The instructions issued to coating vendors were (1) to apply a coating between 0.002 and 0.0035 inch in thickness on nickel-base alloys or 0.0015 and 0.0025 inch on cobalt-base alloys, and (2) to apply a coating that would provide the best compromise between hot corrosion resistance and retention of uncoated alloy mechanical properties. Coding of the coatings was again by letter and is defined below:

A ALPAK (Allison Division, GM)
B HI-15 (Alloy Surfaces)
C UC (Chromizing Corp., Chromalloy Am. Corp.)
D CODEP B (General Electric Corp.)
F CODEP C2 (General Electric Corp.)
G MDC-1 (Misco Div., Howmet Corp.)
H MDC-9 (Misco Div., Howmet Corp.)
I MDC-701 (Misco Div., Howmet Corp.)
J PWA-47 (Pratt & Whitney)
K 870 (Chromizing Corp., Chromalloy Am. Corp.)

Individual specimens were identified by the alloy code letter, the coating code letter, and a number.

The metallurgically determined coating thickness for all coating-alloy combinations is shown in Fig. 2. Weight gain

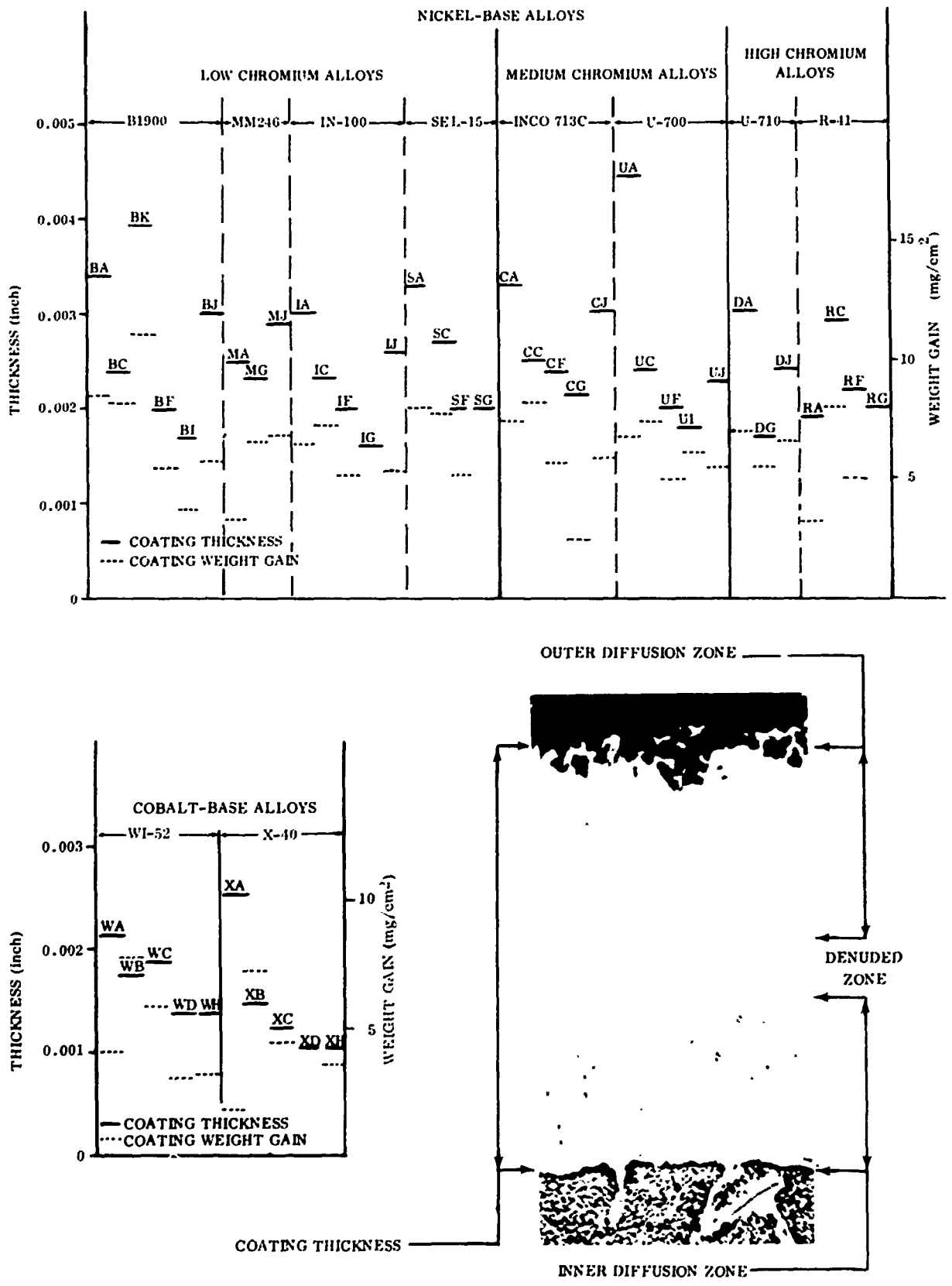

Figure 2. Coating thickness and weight on nickel- and cobalt-base alloys.

during coating is also shown in this figure. Correlation between coating thickness and specimen weight gain is not necessarily good because weights were determined at Solar before and after coating and do not take into account the effects of any surface preparation processes utilized by coating vendors. The photomicrograph inset in Fig. 2B indicates the dimension measured metallographically as coating thickness. It includes essentially all of the coating thickness above the undisturbed substrate alloy structure. Intergranular penetration, if any, was not counted as part of a coating. Thus the interdiffusion zone which is high in chromium, refractory metals, interstitial elements, etc. was included in the coating thickness together with the surface aluminide or "silicide."

With nickel-base alloys, the majority of coatings were found to be within the requested thickness specification. Only the BK and UA alloy-coating systems were thicker and the BI, IG, UI and DG combinations thinner than the requested range, i.e., 6 combinations out of 34 for nickel-base alloys. Coatings on cobalt-base alloys were relatively thin. Fifty percent of these had a thickness of less than 0.0015 inch.

Two major types of coatings were applied by vendors to the various nickel-base alloys. These two types and their variations are described below:

Type 1(a) High Aluminum Activity–These coatings are applied from a source very rich in aluminum, i.e., with high chemical activity of aluminum. The coating is formed by the predominant inward diffusion of aluminum. The microstructure is characterized by the precipitation of chromium-rich phases (Cr_2Al and Cr_3Al_2) and carbides in the outer areas of the coatings due to their insolubility in β-NiAl. The β-NiAl contains 25 to 33 weight percent of Al and the ratio between total coating thickness (t_c) and the interdiffusion layer thickness (t_d) is usually greater than 2.5. No continuous γ' layer (Ni_3Al) is present at the interdiffusion zone/substrate interface.

Type 1(b) High Aluminum Activity–These coatings are applied similarly to Type 1(a) but are the end result of a decrease in Al activity during the process cycle. Chromium-rich outer layer precipitates are retained, but the high aluminum β-NiAl phase is not present. The β-NiAl phase contains 18 to 24 percent Al and the diffusional stability of the coatings is superior to the Type 1(a) coatings. No γ' is usually present in the as-coated condition.

Type 2 Low Aluminum Activity–These coatings are applied from a low chemical activity source with the coating formed by the predominant outward diffusion of nickel. The t_c/t_d ratio is less than 2.5 and the outer coating is free of carbides and chromium containing precipitates. Concentration of aluminum in the β-NiAl phase is 18 to 24 percent.

Most commercially available coatings are modifications of Type 1 or 2. Some variations were observed and included: (1) coatings containing major quantities of elements added in addition to Al, e.g , a very high silicon content such as in coating K (up to 15 percent silicon), (2) additions of inert materials such as the aluminum oxide found in coating G, and (3) the high titanium and Al_2O_3 phases found in coating F. Minor elemental or compound additions may be present in a coating without changing its major class.

Typical examples of the coating types found on the nickel-base alloys and included in this evaluation program are shown in Fig. 3. The classification of each tested coating is listed in Table II.

No attempt will be made in this paper to classify coatings on cobalt-base alloys because insufficient data were available to set up any semblance of a classification system. All of the coatings tested bore some resemblance to Type 2 coatings primarily because of the high carbon, chromium and tungsten content diffusion zones. Presence of these elements at the coating-alloy interface may tend to force coating formation to occur by the outward movement of cobalt rather than the inward movement of aluminum.

Typical microstructures of aluminide coatings on cobalt-base alloys are shown in Fig. 4. A typical coating on WI-52 alloy has a carbide interface and shows significant internal oxidation within the interdiffusion zone. Coatings on the X-40 alloy also have a carbide interface, but have a less complex diffusion zone and show little or no internal oxidation.

Hardness values of the aluminide coatings generally range between 500 and 850 KHN (50 gram load) as was noted in Fig. 3. The high silicon K-coating and the high titanium phase in the F-coating can have hardnesses of between 1300 and 2100 KHN. In general, coatings on cobalt-base alloys were similar in hardness to aluminides on nickel-base alloys, i.e., 500 to 850 KHN.

HOT CORROSION TESTING

Equipment Description

The two Solar gas turbine environmental simulators used throughout the program are shown in Figs. 5 and 6. A straight-through, can-type combustor is used with atomization from a single fuel nozzle. A water-cooled, one-inch diameter stainless steel nozzle is used for long-time trouble-free operation.

The control console for the simulators is shown in Fig. 5 Duplicate controls and measuring equipment are provided for independent operation of each simulator. Specifically, sea water flow, fuel flow, air flow, and temperature (from thermocouples) are monitored and controlled from this console.

Figure 6 shows a close-up of the two simulators. In this setup, note that the two combustors are mounted vertically while the specimen holder rotation motor, drive shaft, and the slip-ring assembly are mounted horizontally. The pneumatic piston that cycles the specimens in and out of the hot gas stream is mounted horizontally underneath the table top.

During the rig tests, eight specimens were mounted in a holder which was rotated at 1725 rpm. The holder was

positioned so that the leading edge of each specimen was one inch from the exit of the nozzle.

Temperature Calibrations

Specimen metal temperature was continually monitored, recorded and controlled throughout the test duration by means of a thermocouple inserted into a small hole inside a test specimen. This hole was electrical discharge machined through the base of the blade and was two inches deep so as to locate the thermocouple tip at the center of the test section. One specimen in each group of blades (in the holder) was instrumented in this manner with a 0.040-inch diameter-Inconel-sheathed, insulated, chromel-alumel thermocouple. Output of the thermocouple was fed to a slip-ring assembly and then to a potentiometer-type strip chart temperature recorder and three mode controller. Control of the specimen metal temperature was automatic and was accomplished by regulating the fuel flow to the combustor nozzle. Air flow was held constant by means of dome loading, diaphragm-type, high-capacity air regulators.

Small thermocouples were imbedded in the airfoil section at known locations in order to determine the temperature gradient and the temperature distribution along the length and width of the airfoil-type specimens. The results of these blade temperature measurements are shown in Fig. 7. In Fig. 7A the data from the internal thermocouples show that the center of the hot zone on the airfoil surface was 3/4 inch down from the blade tip. The thermocouple control temperature was established as 1510°F for operation of this turbine simulator at 1650°F. (Note: The peak temperature was determined to be 1670°F after initiation of the tests.)

Figure 7B shows the specimen temperature distribution for the 1800°F hot corrosion tests. A thermocouple control temperature of 1650°F produced a peak metal temperature of 1800°F in this turbine simulator test rig.

The internal blade temperature distribution for tests at the 2000°F temperature level is shown in Fig. 7C. For these tests, the peak temperature determined during calibration tests was 2035°F. A thermocouple control temperature of 1840°F was established.

Procedures

Hot corrosion tests were performed under the following conditions:

- Standard grade JP-5 fuel was used (sulfur content 0.04 to 0.12 percent).
- A synthetic sea water was made (Fed. Test Method Std. No. 151, Method 812) and 35 parts sea salt per 10^6 parts air were injected into the combustion gases.
- Duplicate specimens of the nickel-base alloys were tested at 1650°F and 1800°F.
- Cobalt-base alloys were tested at 1800 and 2000°F.
- Nozzle exit gas velocity was maintained at Mach 0.85 (<2000 ft/sec) for all tests.

One hour thermal cycles were used for a total of 150 hours maximum at temperature for each test. Coated specimens were removed at the end of each 30-hour exposure (30 cycles) for visual examination, cleaning and weighing. This interval was shortened to 10 to 20 hours for most of the uncoated alloys due to early failures. Specimens were cleaned by soaking in distilled water (160-200°F) for 15 minutes and hand scrubbed with a fine wire stainless steel brush. This cleaning method was not detrimental to the coatings and easily removed the accumulated salt deposit.

The various substrate-coating combinations were sectioned and examined metallographically before and after hot corrosion rig testing. In all cases, the specimens were sectioned through the hottest area on the blade. Standard metallographic techniques were used. An electrolytic etchant (2% aqueous solution of CrO_3) was used throughout the program.

Criteria of Failure

All hot corrosion tests were terminated at 150 hours exposure, or at the first visual observation of substrate corrosion.

Curves of cumulative weight change as a function of exposure time were plotted for each test. These graphs were used to continuously record specimen performance during the test. Generally, the weight change curves provide a good indication of coating performance during testing. Major inflections in the curves (large weight gains and losses) usually indicated onset of coating failure and substrate corrosion.

STRESS RUPTURE TESTING

Two batches of specimens of two selected coatings on the eight nickel-base and the two cobalt-base alloys were subjected to isothermal furnace exposure for 500 hours duration in air atmosphere. The coated nickel-base alloys were exposed at 1800°F; the cobalt-base alloys at 2000°F. Following this 500-hour exposure, specimens from one batch (duplicate specimens of all coating-alloy combinations) were returned to the appropriate coating vendor for stripping and recoating with the same coating system. After recoating, the specimens were subjected to the 100-hour stress rupture tests together with the uncoated alloys being used to generate baseline data. Tests were performed at 1650°F for the nickel-base alloys and 1800°F for the cobalt-base alloys. The stress level for each alloy, at each temperature level, was selected to produce rupture in approximately 100 hours maximum.

SEL-15 - Coating A
Type 1(a)

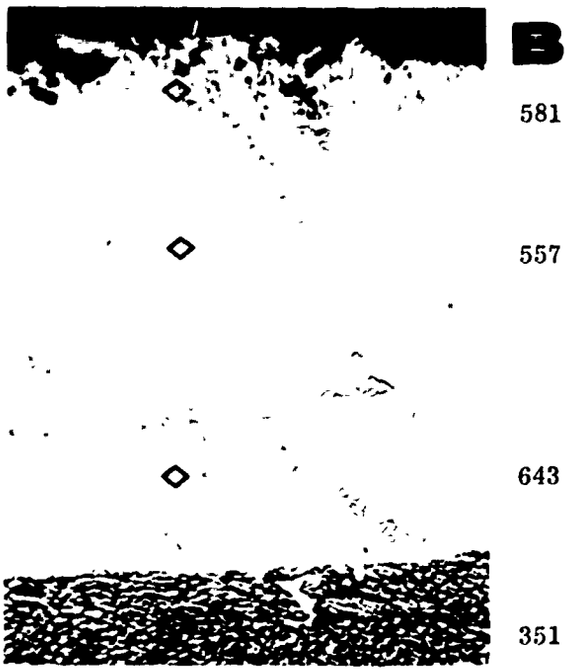

Inco 713C - Coating J
Type 1(b)

Magnification: 1000X (Approx.)

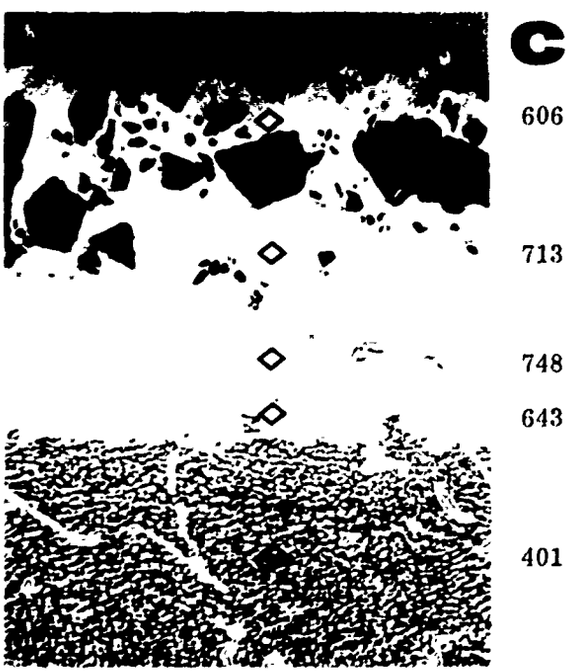

Inco 713C - Coating G
Type 2 (with Al_2O_3 inclusions)

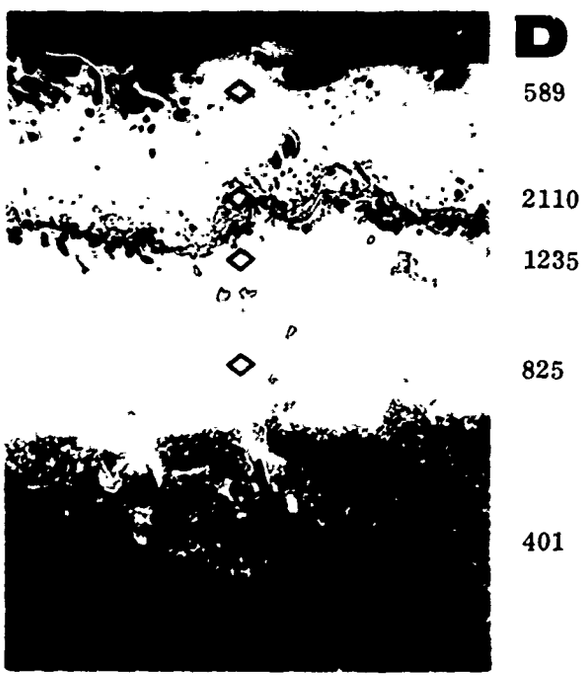

Rene' 41 - Coating F
Type 2 (with Al_2O_3 and Ti-rich phase)

Figure 3A. Coating types 1(a), 1(b), 2 and special (sheet 1 of 2)

LOW-CY LE FATIGUE TESTING

The fatigue tests were performed using a tension-tension test. An MTS closed-loop electrohydraulic fatigue testing machine was used with a sine wave load program. All tests were run at a constant stress ratio (R) of 0.15 ($R = \sigma$ min./σ max.) and at a frequency of 20 cycles per second.

The tests were run in such a manner that the effects of exposure in an oxidizing environment were assessed, as well as the ability of the coatings to provide protection to the alloys for a minimum of 500 hours. Duplicate specimens of all uncoated alloys and of the 20 coating-alloy combinations were tested as follows:

- The stress for failure in 5,000 to 50,000 cycles was determined at 1400°F in an oxidizing environment.
- Coated and uncoated specimens of each alloy were subjected to isothermal furnace exposure for 500 hours at the following temperatures:
  Nickel-base alloys–1800°F
  Cobalt-base alloys–2000°F
  (Uncoated alloys were exposed in an inert environment and coated alloys in air).
- Following the furnace exposures, specimens were fatigue tested to failure at 1400°F.
- The test stresses were calculated based on original cross-sectional areas of the bars measured before coating, and also on the unaffected cross-sectional areas of the coated specimens after the high temperature exposures.

The 1400°F temperature was selected because many of the nickel-base alloys experience a ductility minimum in the 1200 to 1600°F temperature range. Thus, the combination of a hard, relatively brittle coating and a substrate of minimum ductility would be expected to exhibit the maximum interaction in this temperature range. Any notches formed by the cracking of the coating could be expected to markedly decrease the low-cycle fatigue life.

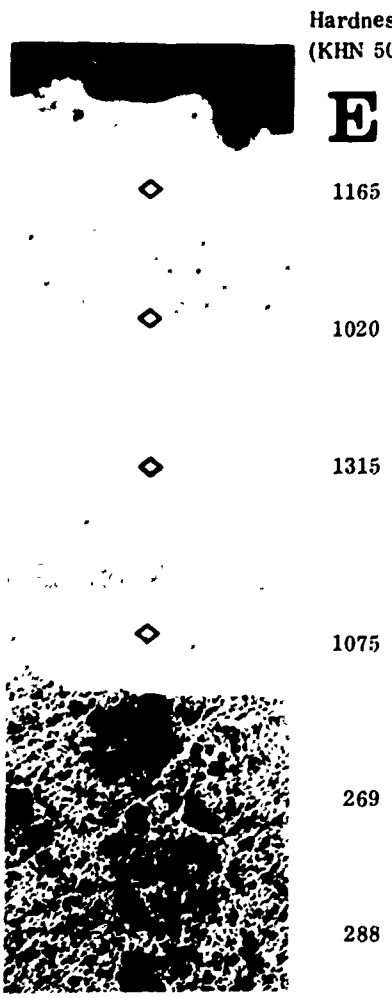

B1900 - Coating K
Special - High Silicon (to 15%)

Magnification: 1000X

Figure 3. Coating types special (sheet 2 of 2).

Table II
Classification of Coatings on Nickel-Base Alloys

Coating Designation	Type	Comments
A	1(a)	Appears to be simple high Al activity coating.
C	1(b)	Not clearly Type 1(b) because significant γ' formed at the substrate diffusion layer interface.
F	2	Major oxide inclusions
G	2	Major oxide inclusions
I	1(a)	Structure less well defined than "A" but ratio $t_c/t_d = 3$.
J	1(b)	Minor silicon addition–less than 1 percent.
K	Special	High silicon addition–up to 15 percent.

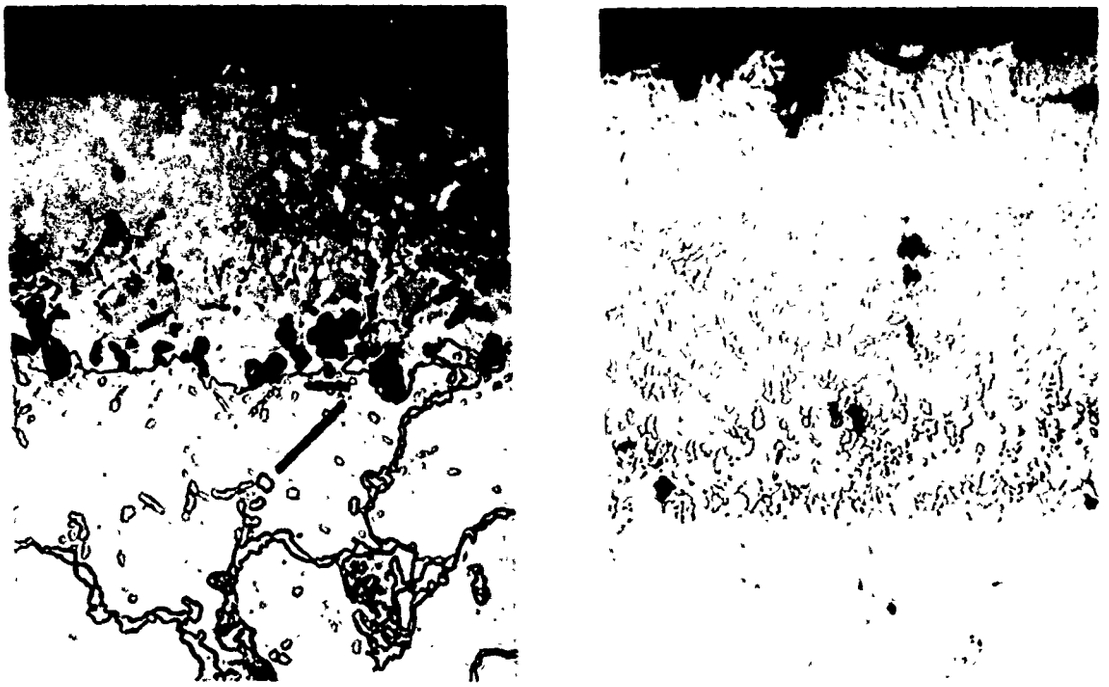

Coating C on WI-52 | Coating A on X-40

Magnification: 1000X (Approx.)

Figure 4. Typical aluminide coatings on cobalt-base alloys.

EXPERIMENTAL RESULTS

HOT CORROSION

For clarity of presentation, the hot corrosion experimental results will be subdivided into four topical areas–uncoated nickel- and cobalt-base alloys; coated low-chromium, nickel-base alloys; coated medium-chromium, nickel-base alloys; coated high-chromium, nickel-base alloys; and coated cobalt-base alloys.

Uncoated Nickel-Base Alloys

Figure 8 shows the time to gross failure of the uncoated nickel-base alloys at 1650 and 1800°F in hot corrosion rig testing. Time to failure is plotted against alloy chromium content and effective chromium content (Cr + 1/2Al - 1/2Mo). This latter parameter was selected rather than the Lewis and Smith (1) parameter–Cr + 1.1(Ti) + 0.7(Al) or the Rentz (2) parameter–Cr - 3.8(Al-5) + 2.0W - 12.5C - 1.4(Mo-1) because of the better fit to the data at 1650°F. None of the parameters show a good linear fit to the data at the 1800°F test temperature.

At 1650°F the low-chromium alloys B1900, IN-100, MAR-M246 and SEL-15 had a test life of approximately 10 hours. Significant distinctions were difficult to note between these alloys. Attack was general, with the SEL-15 and B1900 alloys being representative of this class of alloys (Fig. 9). SEL-15 shows the majority of attack in areas in which the temperature is between 1450 and 1625°F and a minimum of attack at temperatures between 1625 and 1650°F; whereas the B1900 alloy shows maximum attack in the 1550° to 1650°F range.

The medium-chromium alloys, Inco 713C and U-700, performed fairly well in the 1650°F test, withstanding 50 to 110 hours of exposure before localized attack resulted in removal from test. The location and type of attack noted is shown in Fig. 10 and generally occurred in the high temperature area of the test paddle. The higher chromium contents of these alloys appear to afford nearly complete protection to the test environment at temperatures below 1550°F for the periods noted in Fig. 8A.

The high-chromium alloys–Rene' 41 and U-710–withstood the full test period of 150 hours at 1650°F. The surface finish of U-710 was essentially unaffected; whereas localized attack in the 1650°F area of the paddle was apparent with R-41 at the conclusion of the test. The molybdenum concentration in the alloy is probably responsible for a performance poorer than that of U-710. The effective chromium calculations of this paper and of Rentz would

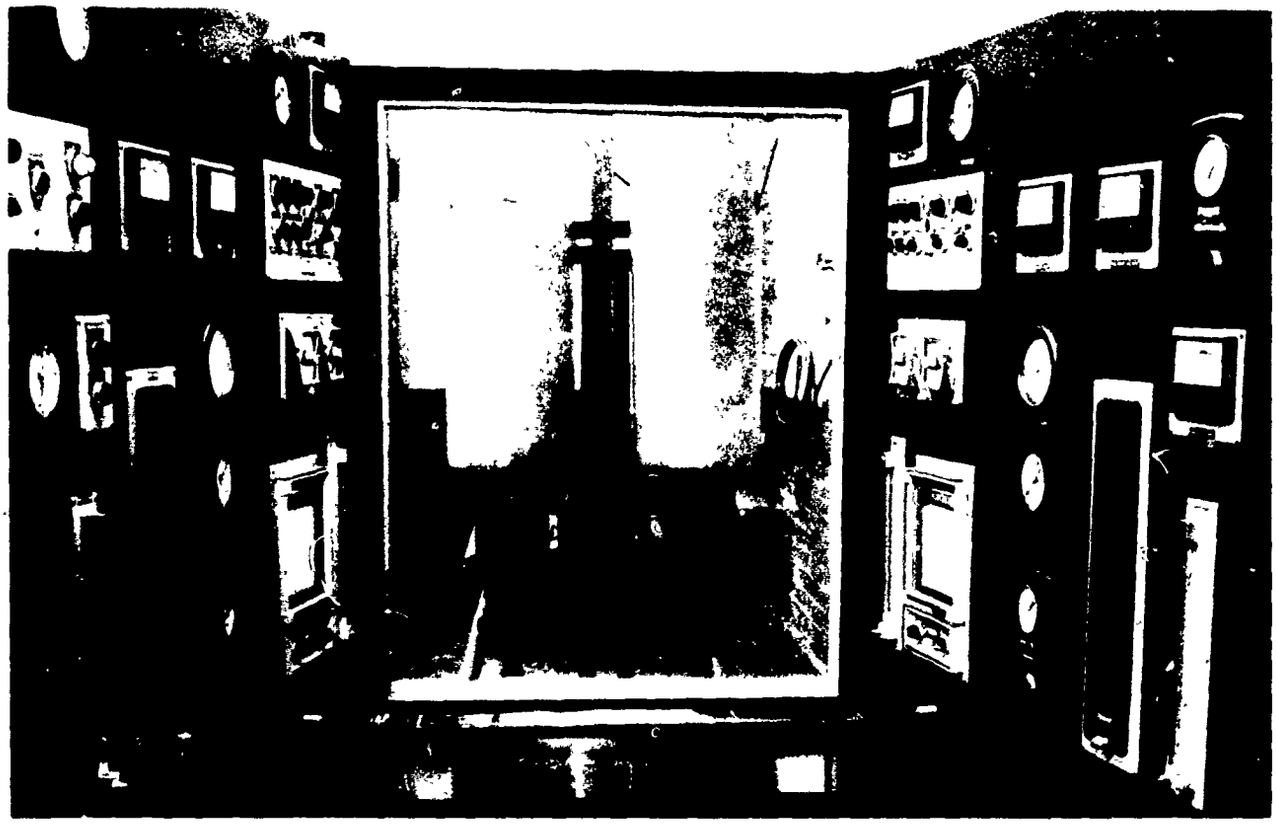

Figure 5. Control console for gas turbine environmental simulators.

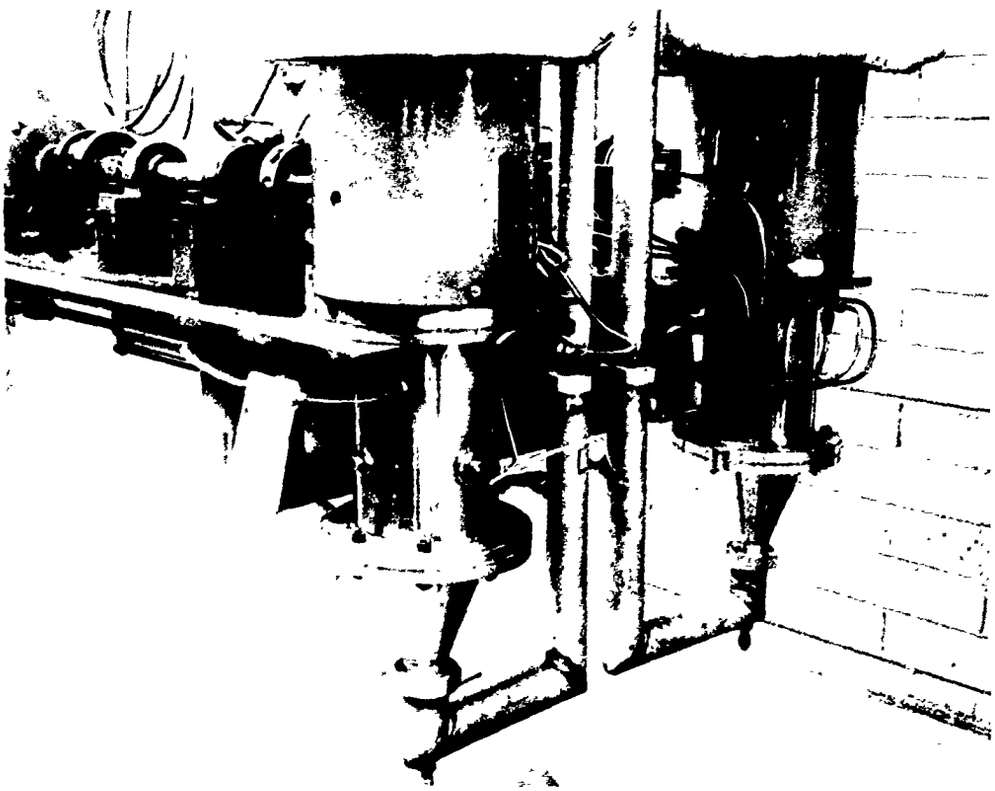

Figure 6. Gas turbine environmental simulators.

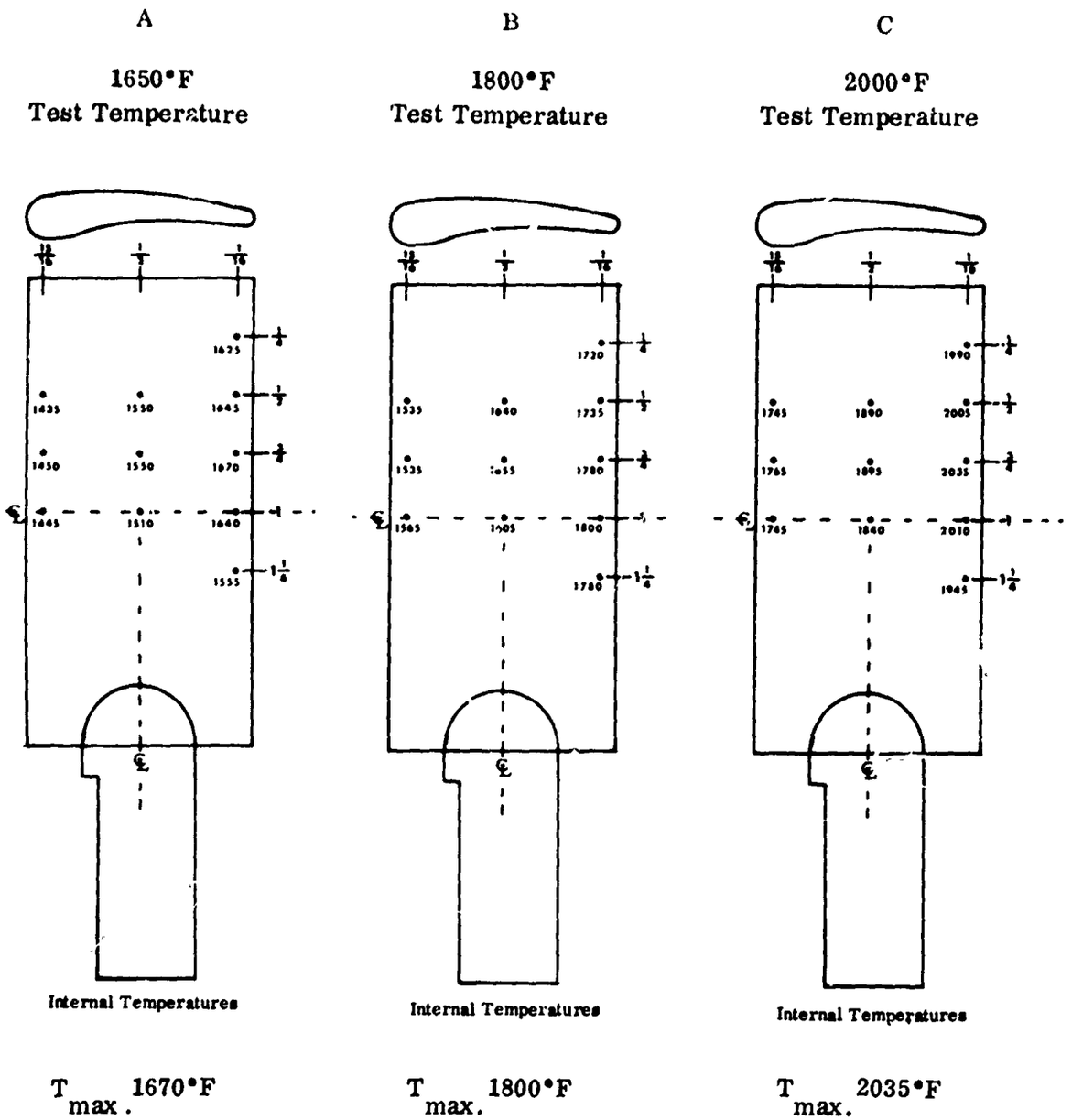

Figure 7. Specimen temperature distribution for hot corrosion test.

indicate a significant negative effect of the nearly 10 percent molybdenum content of Rene' 41.

In the 1800°F test the low-chromium alloys and Inco 713C had less than 5 hours life as shown in Fig. 8B. The difference in performance of U-700 and Inco 713C is very marked under this test condition with the former alloy withstanding the entire 150 hours and the latter withstanding less than 5 hours. An effective chromium content calculated with the Lewis and Smith equation, which heavily weights the presence of titanium, would predict the noted distinction between these two alloys; however, this same equation would not predict the fact that the U-710 alloy and Rene' 41 would exhibit poorer performance than U-700. U-710 withstood the test but exhibited significantly more surface attack than U-700, although attack was minor in depth, resembling oxidation rather than the catastrophic local attack characteristic of hot corrosion.

A constrast between the best performing alloy, U-700, and one of the poorest performing alloys, SEL-15, after 1800°F hot corrosion rig testing is presented in Fig. 11 and serves to illustrate the extremely important role coatings must play in order to effectively use low-chromium, high-strength alloys in a salt-containing environment.

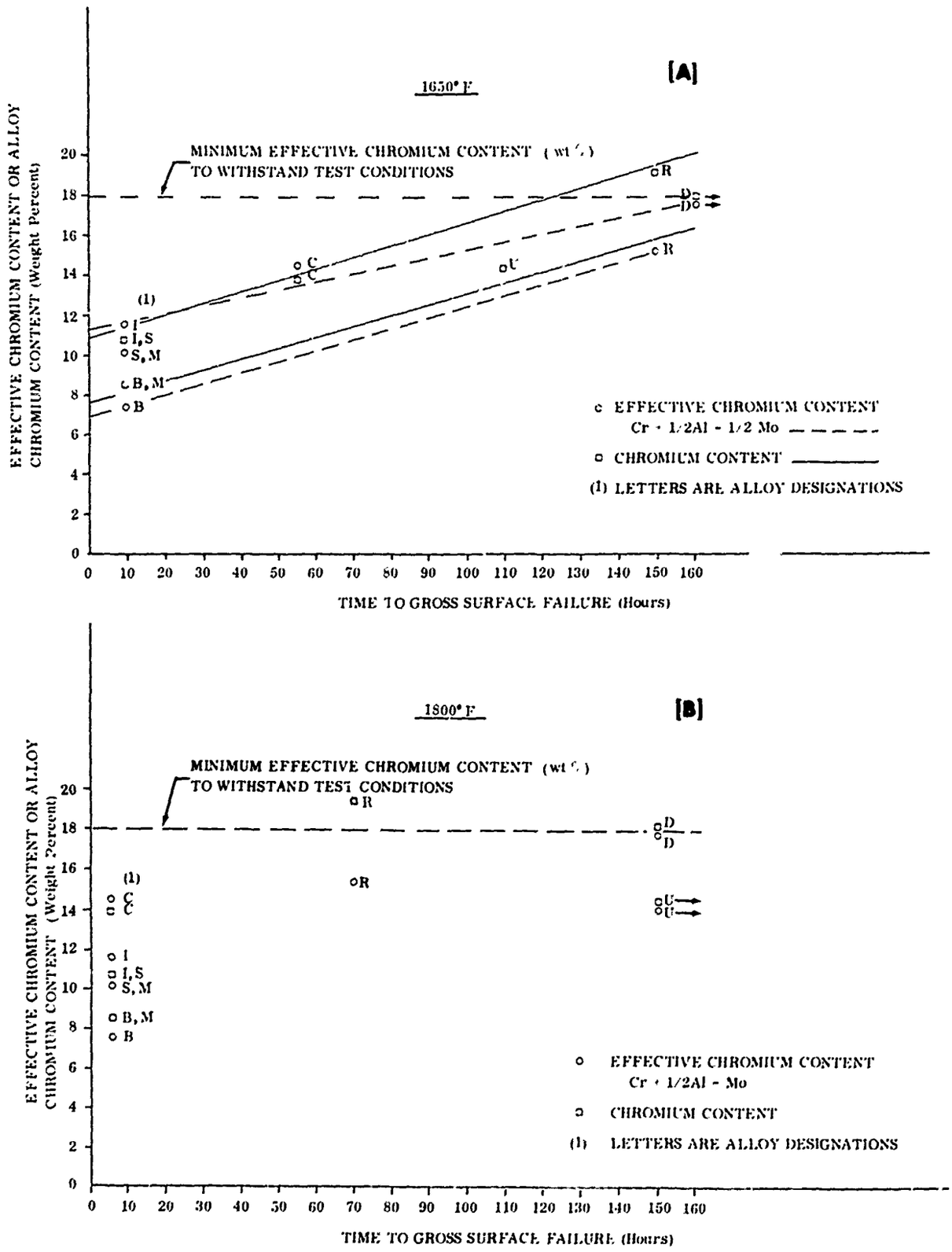

Figure 8. Hot corrosion rig test results for uncoated nickel-base alloys.

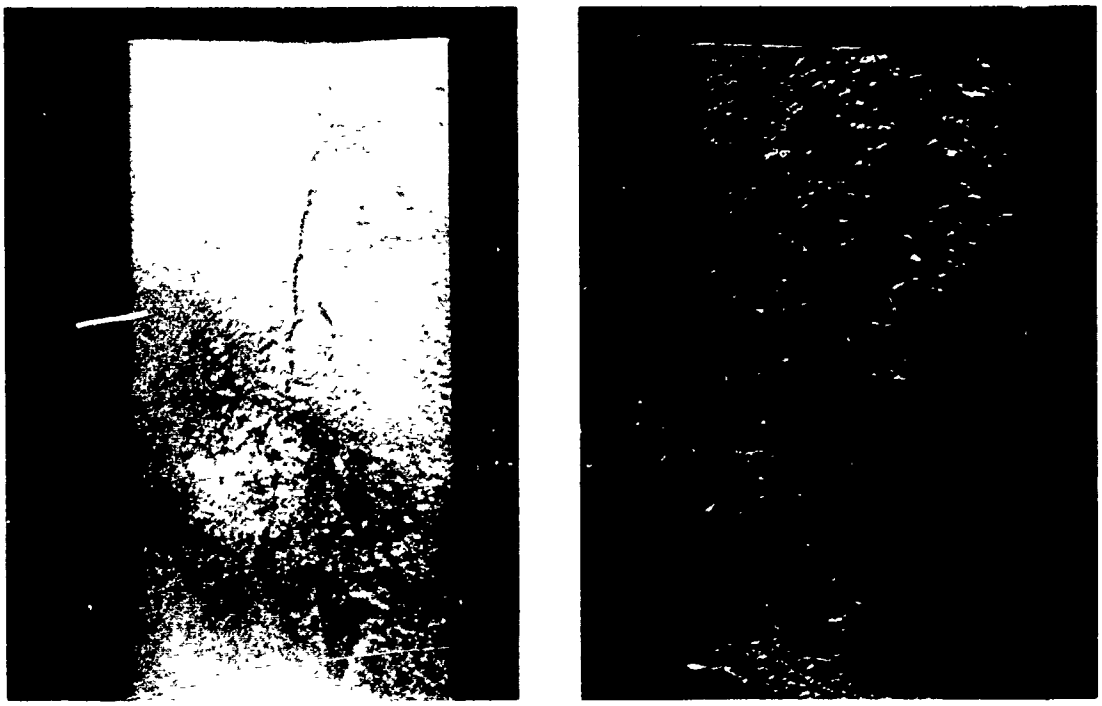

B1900 – 10 Hours

SEL-15 – 10 Hours

Figure 9. Typical surface attack on low-chromium, nickel-base superalloys during 1650°F hot corrosion rig testing (specimens glass bead blasted).

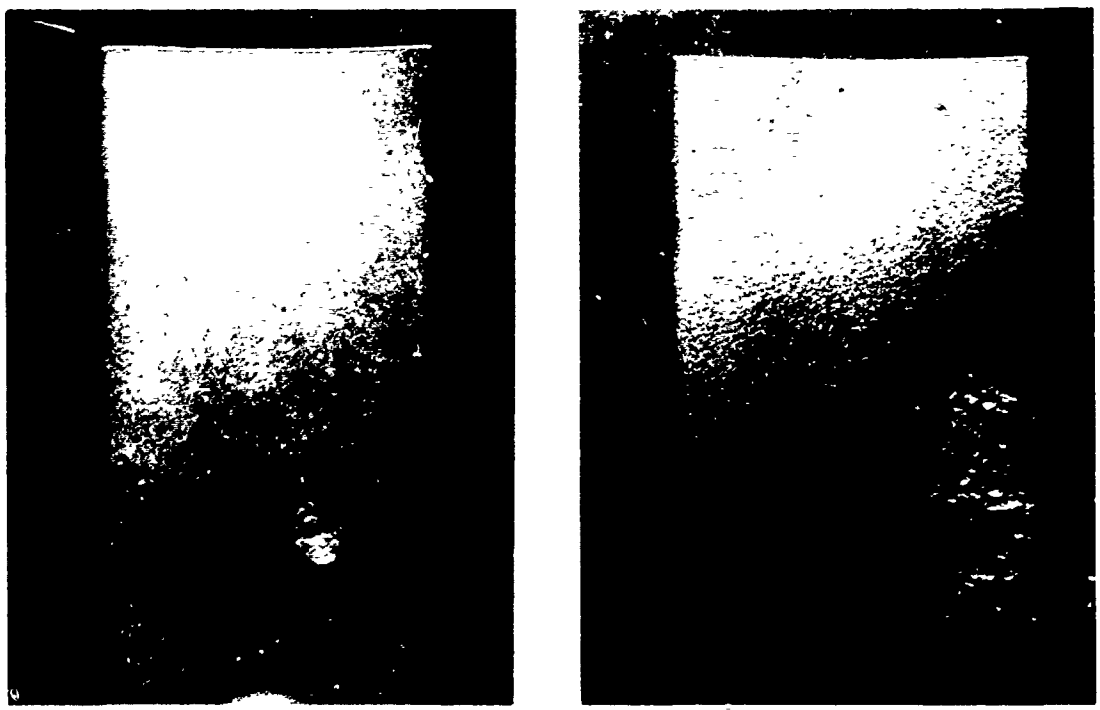

U-700 – 110 Hours

Inco 713C – 60 Hours

Figure 10. Typical surface attack on medium-chromium, nickel-base superalloys during 1650°F hot corrosion rig testing (specimens glass bead blasted).

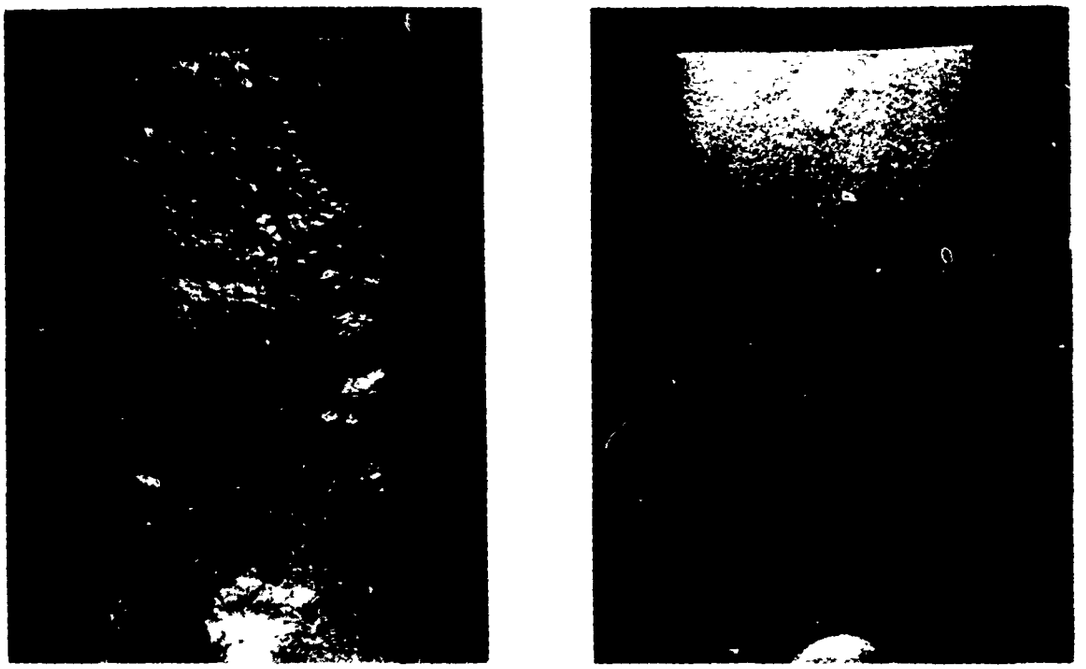

SEL-15 – 20 Hours

U-700 – 150 Hours

Figure 11. Typical surface attack on nickel-base alloys after 1800°F hot corrosion rig testing (specimens glass bead blasted).

Uncoated Cobalt-Base Alloys

The baseline temperatures (1800 and 2000°F) at which uncoated cobalt-base alloys (X-40 and WI-52) were hot corrosion rig tested produced extremely rapid corrosion. Tests were terminated on both alloys after 17 hours at 1800°F and a loss of 0.3 to 0.5 gram per paddle. At 2000°F, the WI-52 alloy was catastrophically attacked, losing 1.3 grams per paddle in 10 hours. A similar weight loss required 30 hours for the X-40 alloy. The attack on the cobalt-base alloys was relatively general in nature as if occurring primarily by oxidation-erosion rather than by the very selective attack seen on the low-chromium, nickel-base alloy.

Uncoated Alloy Performance

At the comparable 1800°F test temperature the cobalt-base alloys were superior in hot corrosion resistance to B1900, IN-100, MAR-M246, SEL-15 and Inco 713C and markedly inferior to Rene' 41, U-700 and U-710 as can be seen in Fig. 12. From the test results on the uncoated alloys it should be clear that the evaluation of the effectiveness of coatings in resisting hot corrosion will be more easily determined on the alloys B1900, IN-100, MAR-M246, SEL-15 and Inco 713C than on the other nickel-base alloys which can withstand a high percentage of the test duration of 150 hours without a protective coating as noted in Fig. 12. The cobalt-base alloys, which exhibit little resistance to attack at the two test temperatures when uncoated, form an excellent base for coating evaluation.

HOT CORROSION OF COATED NICKEL-BASE ALLOYS

Low-Chromium Content Alloys

Figure 13 illustrates the hot corrosion rig lives of all of the coatings on the low-chromium alloys as a function of original coating thickness. With few exceptions, the thicker coatings provided the superior protection to the substrates. A coating at least 0.003 inch in thickness is required to withstand this very severe 150-hour test. The thicker coatings generally have the Type 1(a) or 1(b) (e.g., A and J) high aluminum activity structures in order to generate the thickness of coating by relatively rapid inward diffusion of aluminum; consequently, there are the variables of thickness, structure, and chemical composition that can be responsible for performance rather than thickness alone. It should be noted that a thin coating, e.g., the I coating on B1900, which is rated as Type 1(a) (see Table II), performed very poorly in test indicating the almost complete dependence of these β-NiAl type coatings on thickness to afford long-time protection.

Generally the Type 2 coatings (F and G) performed poorly as did the over-diffused Type 1(b) coating (C).

Failure of these coatings was usually in less than 10 to 40 hours. An interesting exception was the "G" coating which exhibited good and bad performance even though the thickness was less than 0.002 inch. This coating contains large quantities of angular aluminum oxide particles (see Fig. 3A), some of which are 50 percent or more in cross section of the total outer β-NiAl layer. It must be concluded that these oxide particles significantly contribute to the coating performance in a hot corrosion environment.

Within the test temperature range, the severity of attack did not consistently increase with temperature as can be seen from the following tabulation of the better performing alloy-coating combinations:

Alloy-Coating Code	Life (hours) 1650°F	Life (hours) 1800°F
BA	60	150
BJ	120	150+
BK	120	150
IA	150+	120
IJ	150+	90
IG	60	120
MA	150+	150+
MJ	150+	150+
MG	20	150
SA	150+	150+
SG	35	120

The Type 1(a) and (b) coatings (A and J) performed in a random manner in the two temperature environments, sometime failing in a shorter time at the lower temperature and longer time at the higher temperature. The thin, particle-containing, Type 2 coating (Coating G) on three different alloys exhibited shorter lives at 1650°F than at 1800°F indicating a strong temperature dependency of the mechanism of protection of this coating.

Particle inclusions cannot be rated as generally enhancing the performance of coatings. The F coating (Type 2) had significant numbers of aluminum oxide inclusions as well as the complex high-titanium phases (see Fig. 3A), was consistently thicker than the G coating, and yet its performance was consistently poorer on the low chromium alloys.

Composition of the substrates, particularly with the Type 1 coatings, is significant in the final composition of the outer layer of the coatings. Coatings formed by the inward diffusion of aluminum tend to precipitate phases that are only slightly soluble in β-NiAl, e.g., Cr, Mo, W, in the outer region of the coating as well as in the interdiffusion zone (see Fig. 3A). These precipitates, primarily carbides, chromium aluminides (Cr_2Al + Cr_3Al_2) and alloys of chromium can be concurrently oxidized with the β-NiAl thus changing the character of the oxides. The test results on the four low-chromium alloys indicate that an alloy low in molybdenum and high in tungsten (MM246) can be more consistently protected than an alloy such as B1900

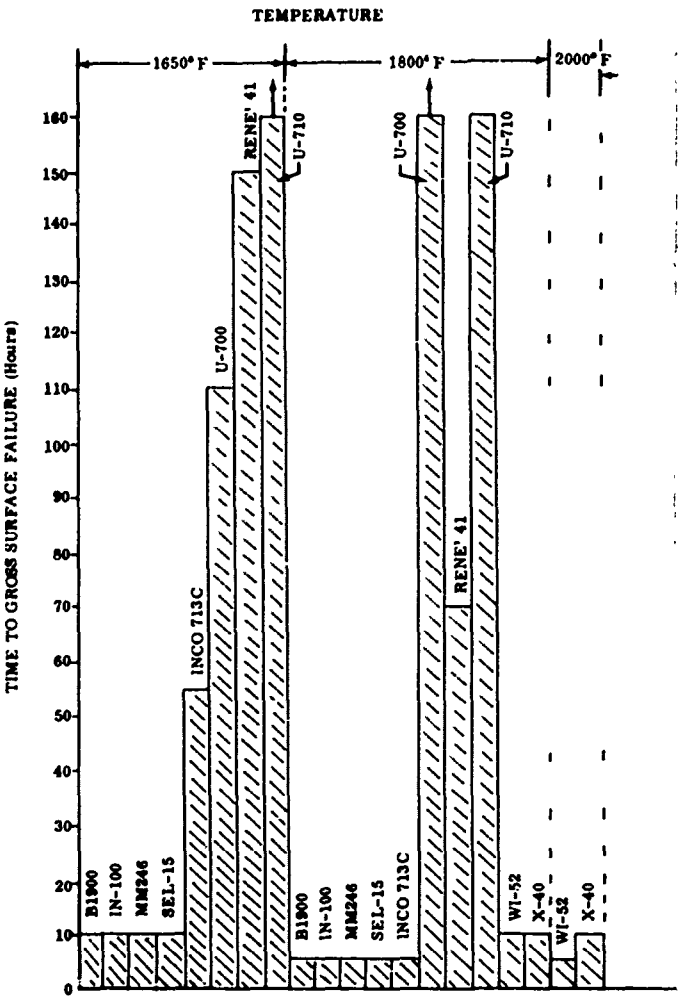

Figure 12. Summary of hot corrosion rig tests on uncoated nickel- and cobalt-base alloys.

containing large quantities of molybdenum with no tungsten. The complexity of the superalloys, however, makes any generalization on compositional effects extremely questionable.

Little has been noted about the K coating, which EMP data show to contain up to 15 percent silicon. The performance of the coating was quite good. The coating, which, by X-ray diffraction contained Cr_3Si as well as β-NiAl and Cr_3Al_2, and some unidentified other phases, probably silicides, appeared to be low in expansion and was high in hardness. Cyclic thermal exposure produced progressive spalling of the coating indicating a near total lack of ductility. It was the only coating on nickel-base alloys with a severe spalling problem. The basic composition of the K coating appeared to be extremely resistant to the test conditions; stresses developed from differential thermal expansion between coating and substrate were far more deleterious to the coating than any observable effect of hot corrosion.

Microstructures illustrating the changes occurring in the better performing coatings on low-chromium, nickel-base

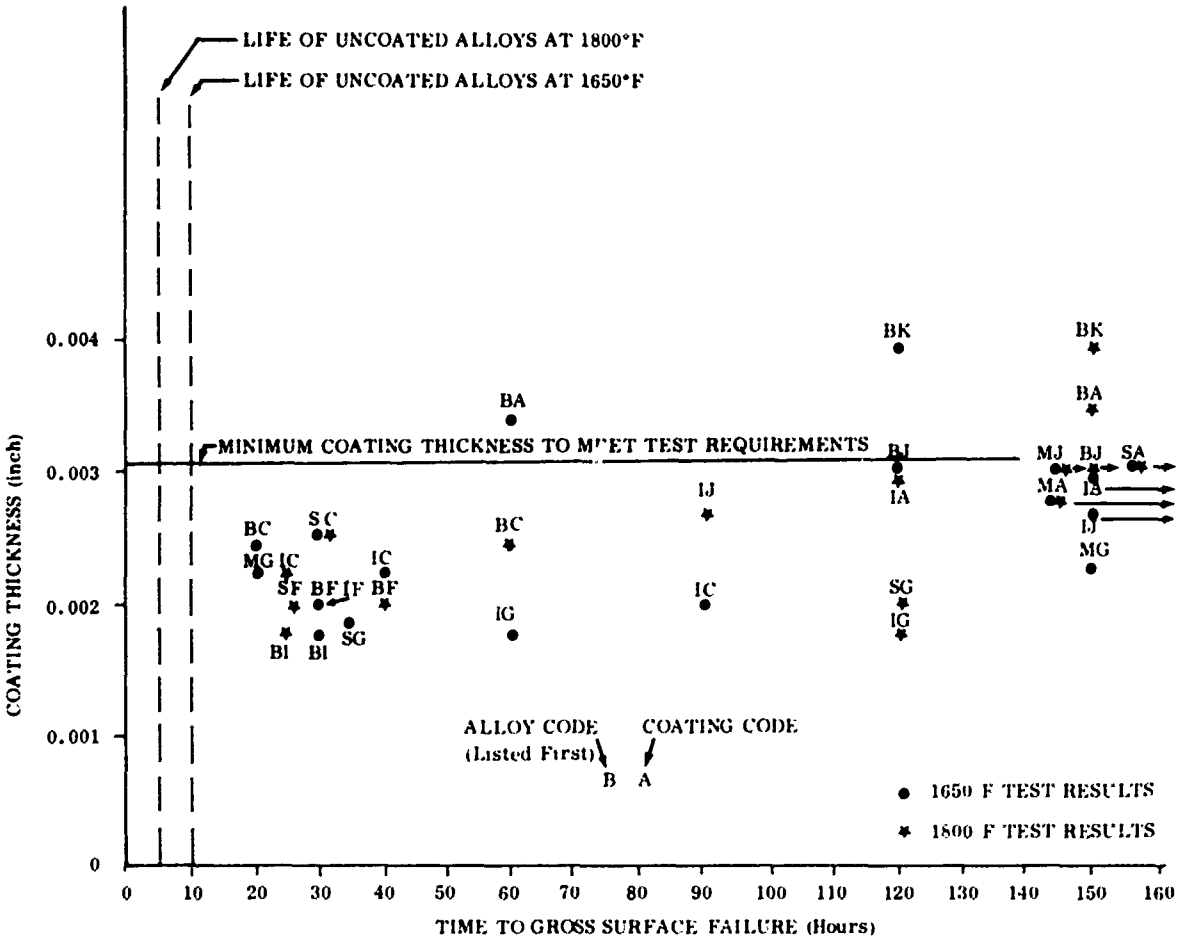

Figure 13. Summary of hot corrosion rig test results on coated low-chromium content nickel-base superalloys.

alloys are shown in Figs. 14 and 15 for the as-coated, 1650°F tested and 1800°F tested A and J coatings on IN-100 alloy. Both coatings as applied have the typical Type 1 structure, i.e., an outer layer containing a light etching chromium-rich phase and carbides, a denuded zone of relatively pure β-NiAl, and th iplex interdiffusion zone that is high in carbides, chrom nd refractory elements which have low solubility and low usion rates into β-NiAl. Both coatings have a continuous γ-Ni solid solution phase between the substrate and the interdiffusion zone as-coated which is due to the high coating application temperature and to the instability of γ′ in the presence of high percentages of Cr and Mo. Exposure at 1650°F for 150 hours converts the γ phase to a complex γ′ and sigma phase and results in slight interphase and internal oxidation. The A coating, which has an Al content of approximately 30 percent increases in thickness by 0 0005 inch during this exposure; whereas the lower Al content J coating (20-24 percent) is more diffusionally stable. At 1800°F the high alumi A coating shows much more resistance to the environment than the lower aluminum coating. The J coating is completely penetrated in only 90 hours while only slight selective attack occurs on the A coating in 120 hours.

The glass bead blasted surface finish of selected specimens after test is shown in Fig. 16 and illustrates attack of coatings with excellent hot corrosion resistance and from those showing almost no improvement over the substrate alloys.

Medium-Chromium Content Alloys

Figure 17 presents the hot corrosion rig lives of the various coatings on the medium-chromium, nickel-base alloys (Inco 713C and U-700) plotted against original coating thickness. The data show that coatings can shorten the time to gross failure over the uncoated alloys. This early attack was not observed with any of the very short-lived low-chromium, nickel-base alloys. Coatings C, F, and I decreased the time to significant attack on the U-700 alloy at 1800°F and the A and J coatings showed little or no increase in the time to gross attack on this alloy. The type of attack was similar to that observed on the low-chromium alloys although slightly less severe. The deep localized attack of both low- and medium-chromium alloys in hot corrosion rig testing indicates a strong galvanic influence of the

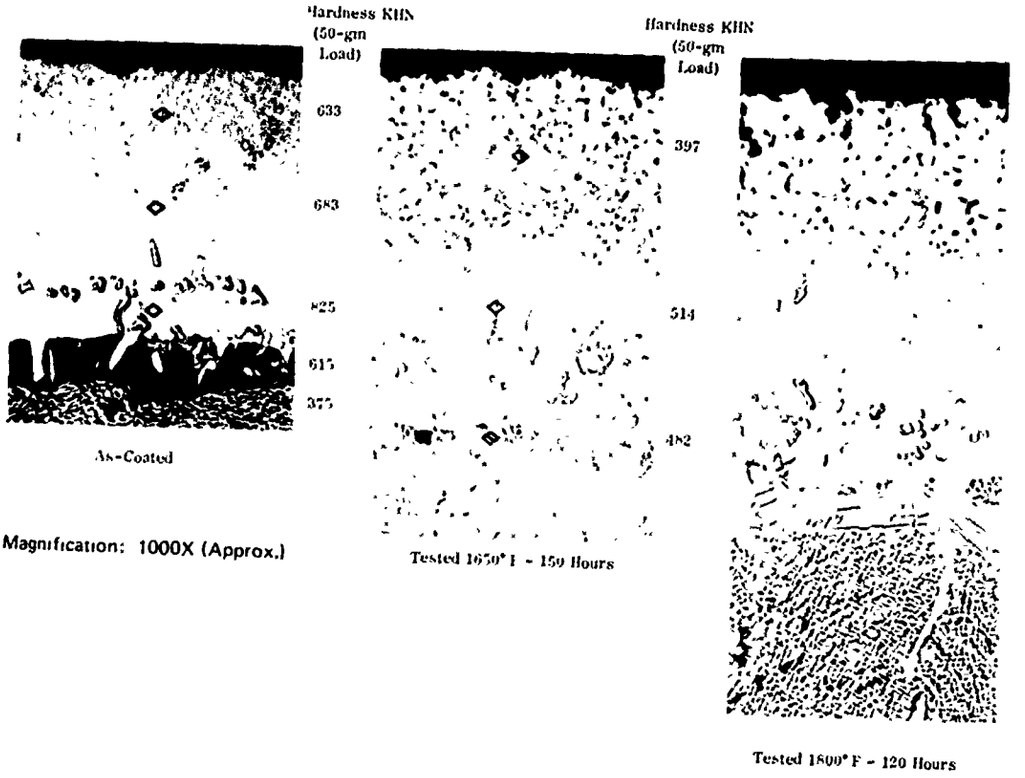

Figure 14. Coating A on IN-100 alloy before and after hot corrosion testing.

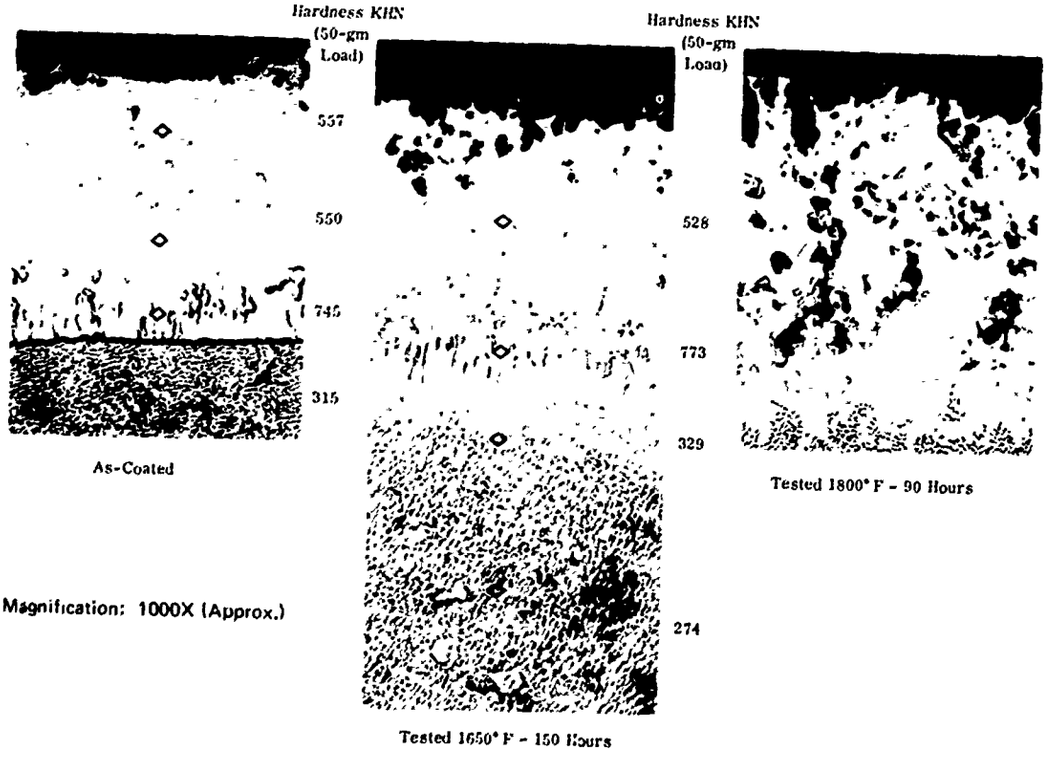

Figure 15. Coating J on IN-100 alloy before and after hot corrosion testing.

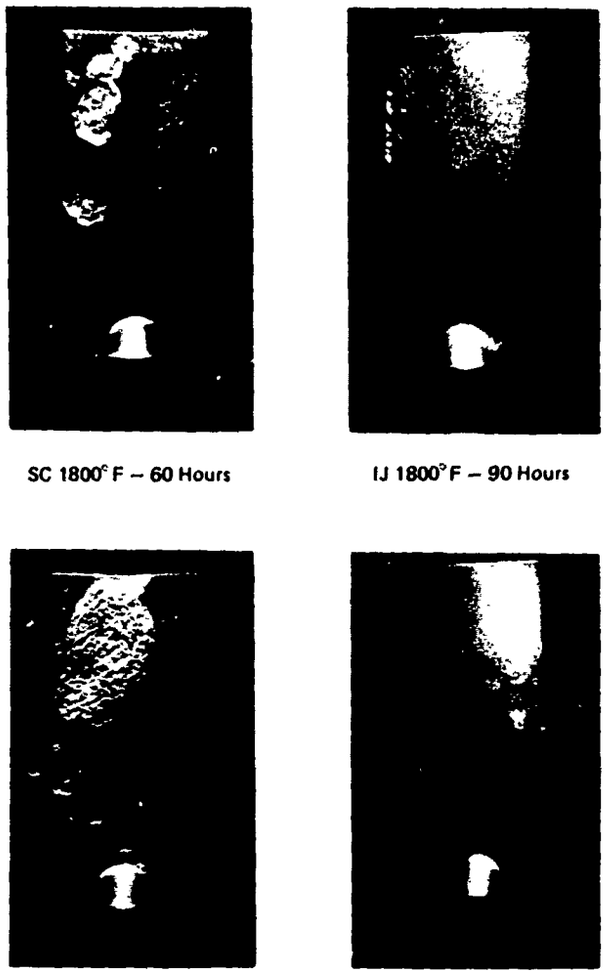

Figure 16. Surface appearance of coated low-chromium, nickel-base alloys after hot corrosion rig testing (specimens glass bead blasted).

attack. The substrate appears anodic to the coatings and, consequently, at a breakthrough in the coating the attack is accelerated over that of the uncoated alloy. This effect is more readily apparent with the U-700 alloy because of relatively good performance in hot corrosion rig testing in the uncoated condition.

From the test data (Fig. 17) the influence of coating thickness is not clearly as apparent as with the low-chromium alloys. Good and bad performance was noted with thick and thin coating. The type of coating does, however, appear to strongly influence performance. Type I coatings (A, I and J) show excellent protection to both Inco 713C and U-700 at 1650°F; however, at 1800°F none of these coatings performed as well as the uncoated alloy in inhibited localized attack. The thicker A and J coatings were, however, superior to the thin I coating at 1800°F. The unusual performance in the test was exhibited by a Type 2 coating containing large alumina particles (G). This coating, at only 0.0021 inch in thickness, afforded complete protection to Inco 713C for the 150-hour test duration at both maximum test temperatures. Other coatings affording equivalent protection to G coating on Inco 713C were thicker by 50 percent or more.

Microstructure of the G coating on Inco 713C is shown in Fig. 18. Structures previously shown for the A and J coatings are similar to the structure on low-chromium alloys. There were only minor differences in microstructure of coatings on the two medium-chromium alloys, the principal difference being the increase in sigma phase needles or platelets in the U-700 alloy at the coating substrate interface during testing. Very little change was noted in the structure of the G coating after 1650°F exposure. Both as-coated and 1650°F tested structures were primarily β-NiAl with included Al_2O_3 particles. The chromium and refractory metal-rich interface was present as was the interface of γ' characteristic of Type 2 coatings. Sigma phase was not present. Principal change was in the increase in thickness of the γ' layer and a decrease in hardness of the β-NiAl indicating a decrease in aluminum content. After the 1800°F exposure the matrix of the coating was γ' with retained islands of β. Sigma phase was beginning to form at the coating substrate interface. From the microstructure it would appear that little retained protection would be afforded by the coating after the 1800°F exposure. The J coating on Inco 713C retained β-NiAl structure and the potential for significantly longer protection than the G coating after 1800°F-150-hour testing.

The surface appearance of representative coated U-700 alloy specimens after test is shown in Fig. 19. U-700 alloy specimens only are used to illustrate the potential for more severe pitting attack than is experienced by the uncoated alloy. Overall, this pitting attack is more severe at 1650°F than at 1800°F which contrasts with the generally increased coating loss at 1800°F and may indicate an attack mechanism change on this alloy between the two test temperatures.

High-Chromium Content Alloys

Figure 20 presents the hot corrosion rig lives of the various coatings on the high-chromium, nickel-base alloys (R-41 and U-710). The uncoated lives of these alloys were so long that little improvement could be expected to be observable by macro-examination of the specimen. All coatings increased the life of Rene' 41 at 1800°F and did not decrease the life at 1650°F. On U-710, the very thin G coating appeared to afford no enhancement of protection to the alloy and perhaps produced a slight increase in the rate of pitting type of attack on the alloy. This effect was not nearly as pronounced as with the C, F and I coatings on U-700 Alloy.

The microstructures of the A and J coatings on U-710 are typical of the better performing coatings on the high-chromium, nickel-base alloys and are shown in Fig. 21 in

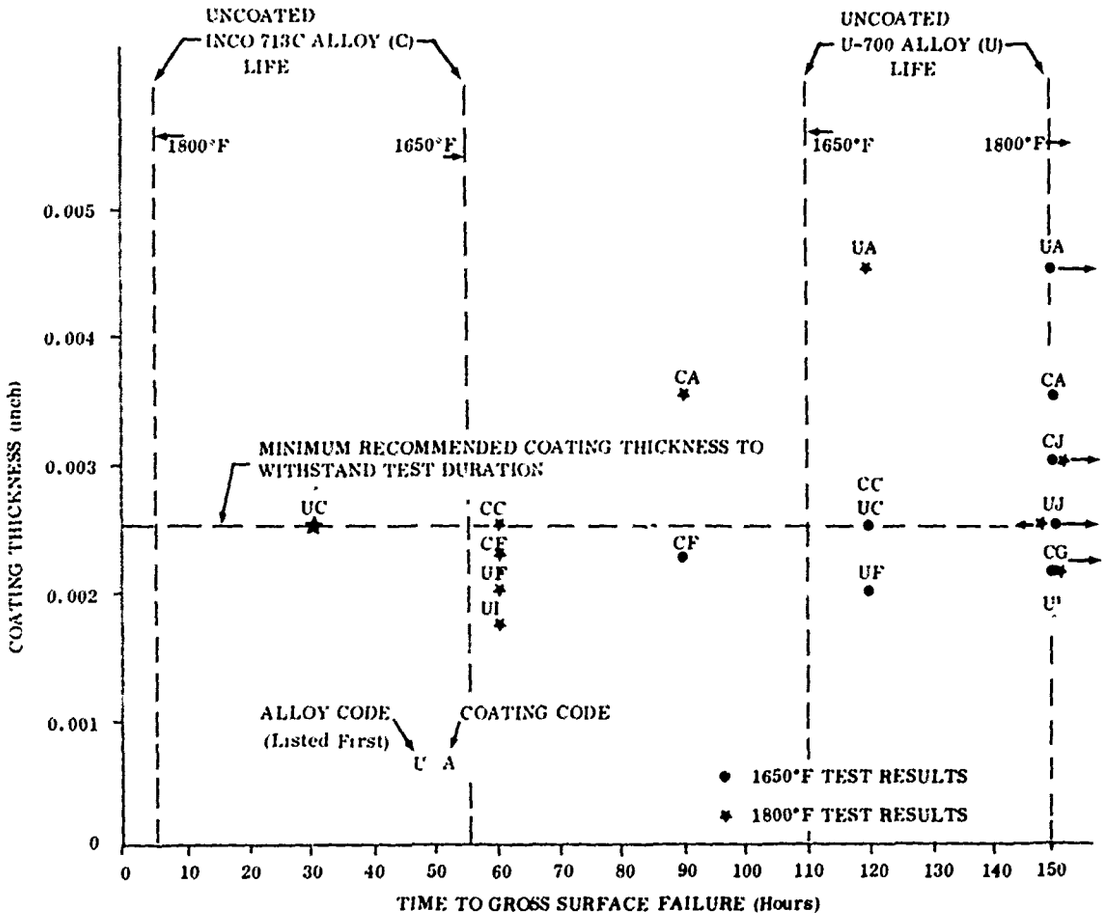

Figure 17. Summary of hot corrosion rig test results on coated medium-chromium content nickel-base superalloys.

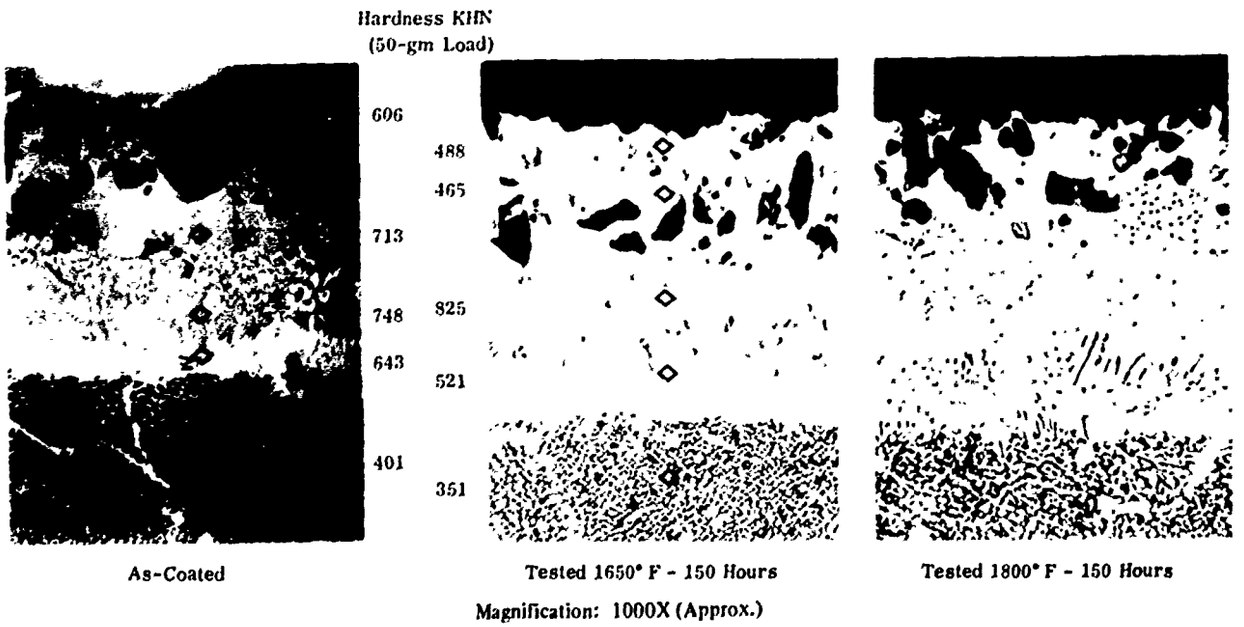

Figure 18. Microstructure of coating G on Inco 713C before and after hot corrosion rig testing.

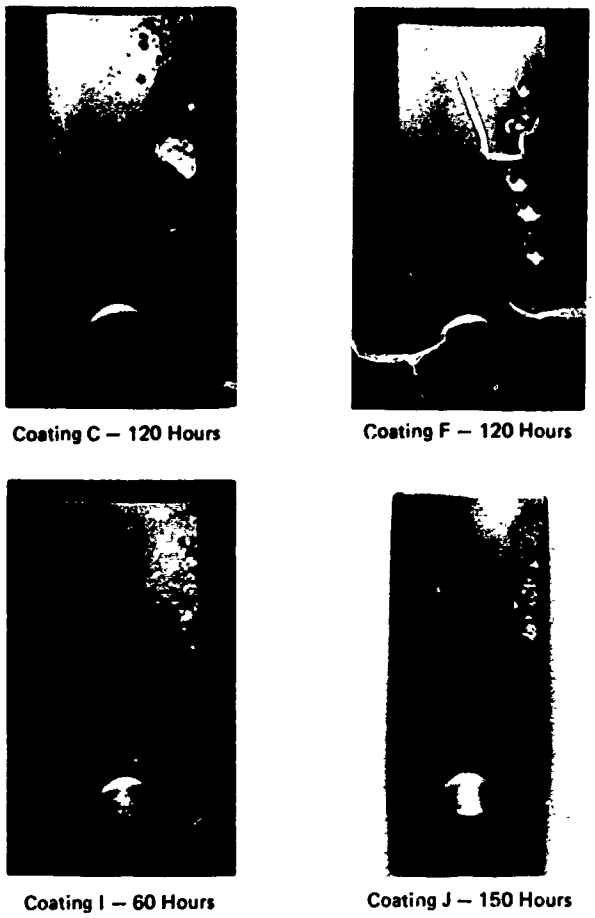

Coating C – 120 Hours | Coating F – 120 Hours

Coating I – 60 Hours | Coating J – 150 Hours

Figure 19. Surface appearance of coated Udimet 700 alloy after hot corrosion rig testing (specimens glass bead blasted).

the as-coated and tested conditions. Both coatings show large amounts of the light etching chromium-rich phase in the outer region of the as-applied coating with the A coating containing the higher concentration. Aluminum concentration, judged by EMP analyses and etching, was also higher in the A than in the J coating. The γ interface layer, as previously noted, of both the A and J coatings on IN-100 alloy (Figs. 14 and 15) was present on the A coating only as-coated which is an indication of a higher application temperature for this coating than for the J coating. Coating thicknesses were similar for the two coatings–0.0025 to 0.0028 inch. After 150-hour exposure at 1650°F, the A coating increased in thickness to approximately 0.004 inch and the J coating showed no thickness change. The interface area of both coating-alloy combinations developed a significant γ' layer without growth of acicular sigma phase. Surface attack appeared minor. After the exposure to 1800°F for 150 hours, the A coating showed some deepening surface attack, but protection was complete and a continuous β-NiAl layer of over 0.002 inch in thickness was maintained. The J coating was essentially consumed in the 1800°F exposure, retaining no continuous β-NiAl and only a 0.0015-inch layer of γ'. The A coating was markedly superior to the J coating on U-710 alloy. A comparison between the A and J coatings cannot be made on Rene' 41 because the J coating was not applied to this alloy. Protection afforded by the A coating on Rene' 41 was equivalent at 1650°F, but performance at 1800°F was similar to the J coating on the U-710 alloy. The high-molybdenum content of the Rene' 41 alloy may noticeably decrease coating life above 1650°F. A negative point for the high-aluminum content type 1(a) coating is poor diffusional stability. Up to 50 percent thickness growth is noted in the coating after 150 hours at 1650°F on both Rene' 41 and U-710 alloys.

HOT CORROSION RIG TEST OF COATED COBALT-BASE ALLOYS

Figure 22 illustrates the life of coated cobalt-base alloys versus original coating thickness. Within the thickness range investigated, there was not a strong correlation between coating thickness and resistance to hot corrosion at either 1800° or 2000°F.

All coatings on WI-52 and X-40 alloys protected the substrate from attack for 120 hours or longer at 1800°F. Coating C on WI-52 provided the longest protection and was also nearly the thickest coating. The H coating, which was 25 percent thinner than the C coating, provided nearly equivalent protection. On X-40, the thickest and thinnest coatings, A and D respectively, provided the better performance, again pointing out the lack of correlation between coating thickness and test life.

Testing at 2000°F produced failure in all coatings between 50 and 70 hours on both substrates. This life correlates well with the simple oxidation lives of coated alloys at this temperature in rig tests (3) and does not indicate major acceleration of attack by salt corrosion. Although these coated cobalt-base alloys have seen extensive use in first stage turbine nozzle vanes, the life expectancy of coatings and alloys is extremely short at the 2000°F temperature and only moderate at 1800°F with or without salt addition. This is in marked contrast to many nickel-base superalloys that have excellent oxidation lives in these temperature ranges without salt being present.

Typical appearances of (coated WI-52 and X-40) specimens after exposure to 1800°F and 2000°F are shown in Figs. 23 and 24. As can be seen, failure is never catastrophic and is localized in or near the hottest area on the test specimen.

The microstructures of the best performing coatings on WI-52 and X-40 after 150 hours exposure at 1800°F are shown in Fig. 25. The C coating on WI-52 was almost unaffected by the exposure. No γCo was evidenced at the surface; there was little evidence of an increased amount of internal oxidation; and slight diffusion of Al into the substrate was noted. The A coating on X-40 showed little

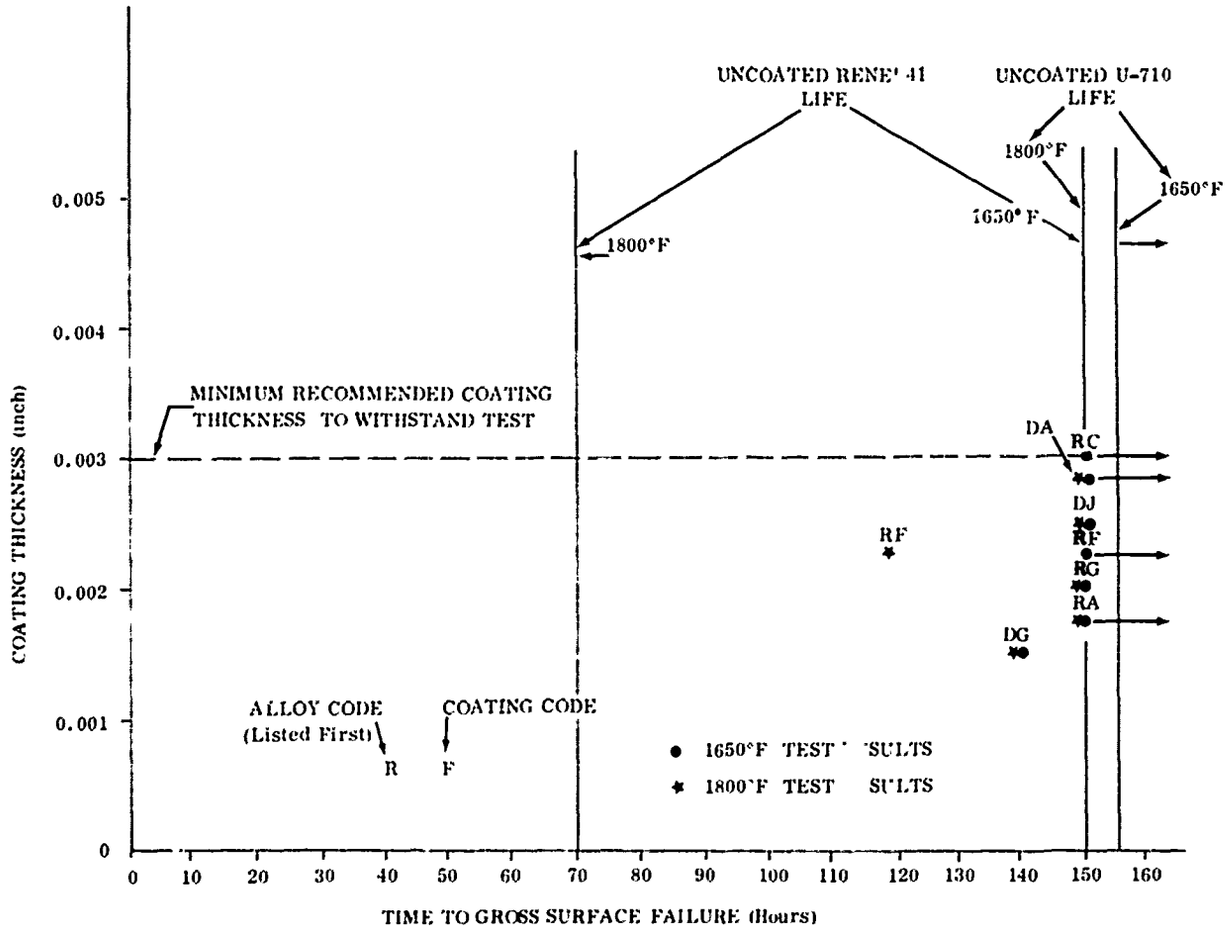

Figure 20. Summary of hot corrosion rig test results on coated high-chromium content nickel-base alloys.

evidence of change in coating thickness, but significant internal oxidation had occurred and γCo was beginning to form on the surface and was widely distributed throughout the coating. The C coating on WI-52 was by far the most stable coating evaluated on cobalt-base alloys at a test temperature of 1800°F. All other coatings showed significant consumption in the test, e.g., D and H on WI-52 and B and H on X-40 were over 80 percent consumed in 150 hours at 1800°F.

LOW-CYCLE FATIGUE TESTS

Uncoated Nickel-Base Alloys

The two wrought alloys, U-700 and Rene' 41, exhibited the highest fatigue strength for a 10^4 cycle life in the as-heat-treated condition (Fig. 26). The U-700 alloy was slightly superior to the Rene' 41 alloy (133.0 ksi to 124 ksi).

Of the four as-cast, low-chromium alloys, the MAR-M 246 alloy exhibited a fatigue strength of 123 ksi, approximately the same as the wrought Rene' 41 alloy. All other low-chromium alloys (IN-100, SEL-15 and B1900) were lower in strength, with the B1900 alloy showing a strength of 107.5 ksi or 13 percent less than the MAR-M246 alloy.

All uncoated alloys were thermally exposed in a dry argon atmosphere for 500 hours at 1800°F. After exposure, the test sections of all specimens were machined from the initial 0.250-inch diameter to the 0.185-inch diameter required for consistent failure in the gage section of the specimens.

The test data indicate a reduction in the fatigue life following the prolonged exposure for all the uncoated alloys except 713C. The 713C alloy showed good metallurgical stability with the fatigue strength slightly higher after the long term exposure. Only a small decrease in strength was exhibited by the IN-100 (-1%), SEL-15 (-3%). All others showed a loss in strength in excess of 3 percent indicating a potential problem for long-term, high-temperature operation with these alloys. The largest reduction in fatigue strength, as would be expected, occurred with the two wrought alloys, U-700 and Rene' 41, 16 and 14 percent, respectively.

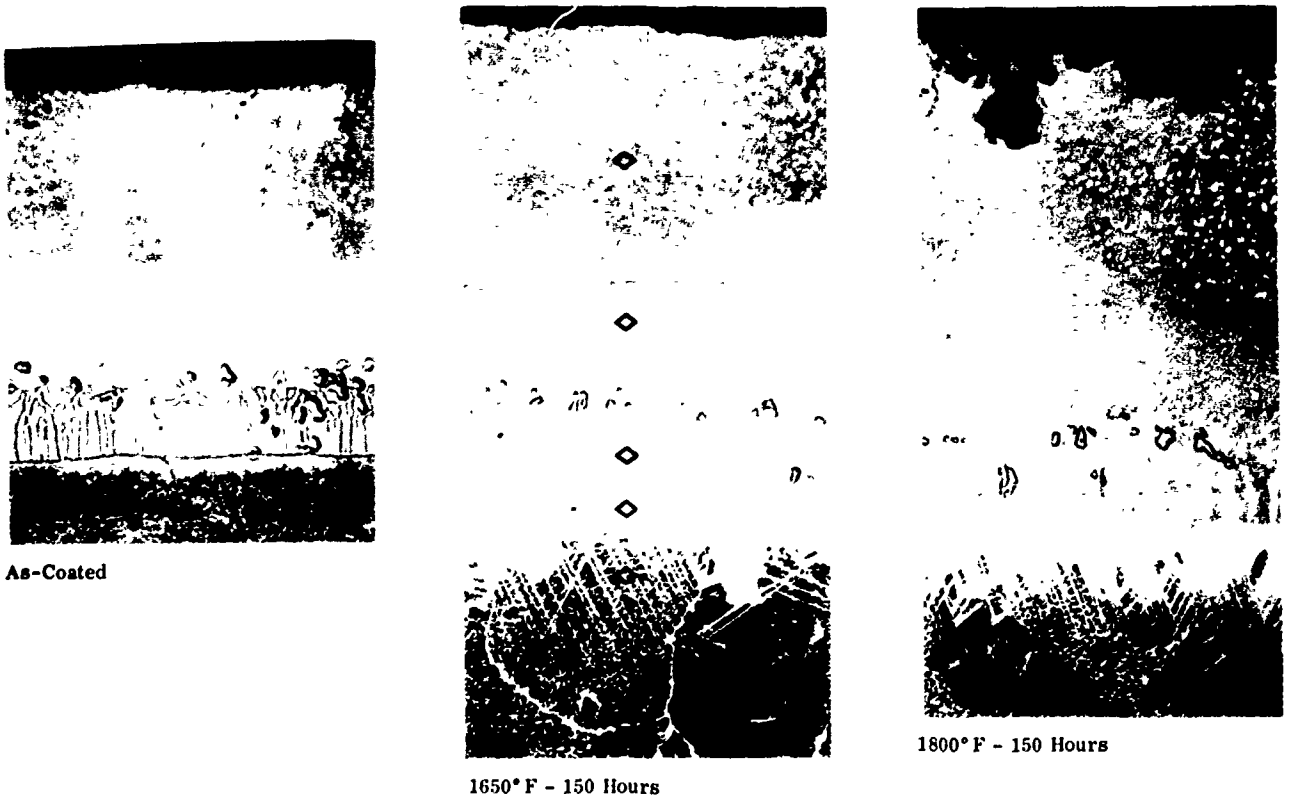

As-Coated

1650° F - 150 Hours

1800° F - 150 Hours

COATING A

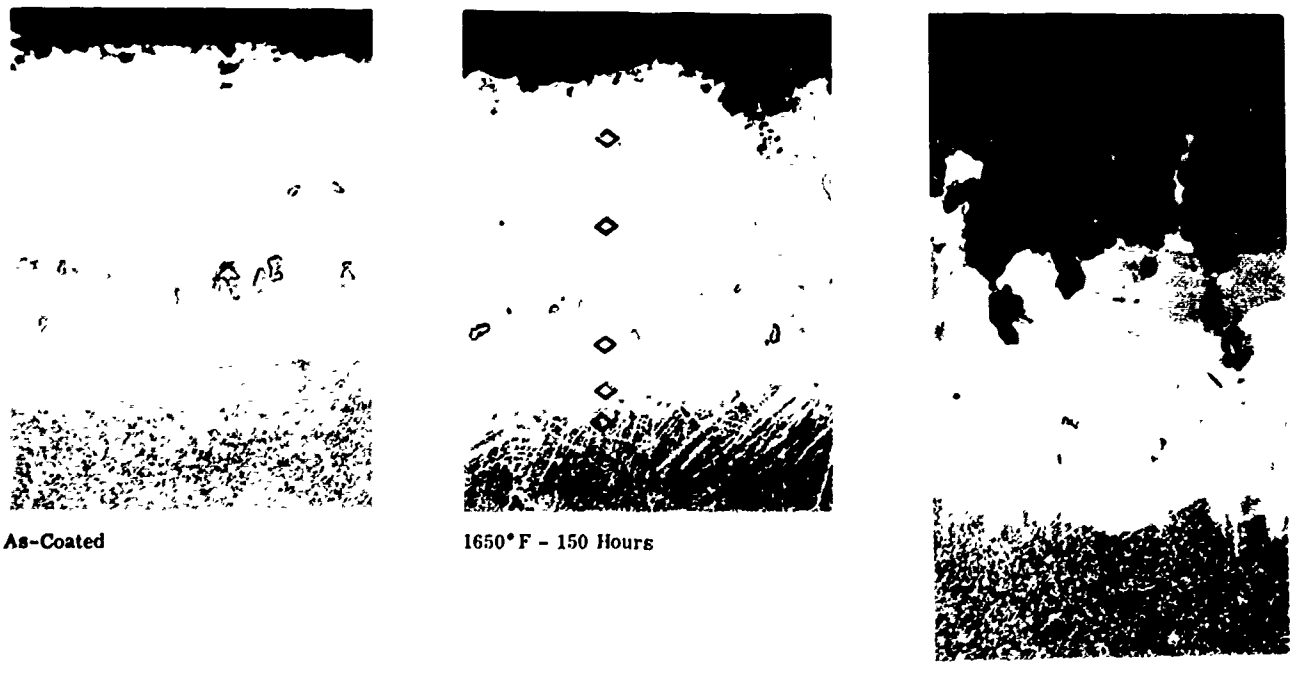

As-Coated

1650° F - 150 Hours

1800° F - 150 Hours

COATING J

Magnification: 1000X (Approx.)

Figure 21. Microstructure of coatings A and J on U-710 alloy before and after hot corrosion testing.

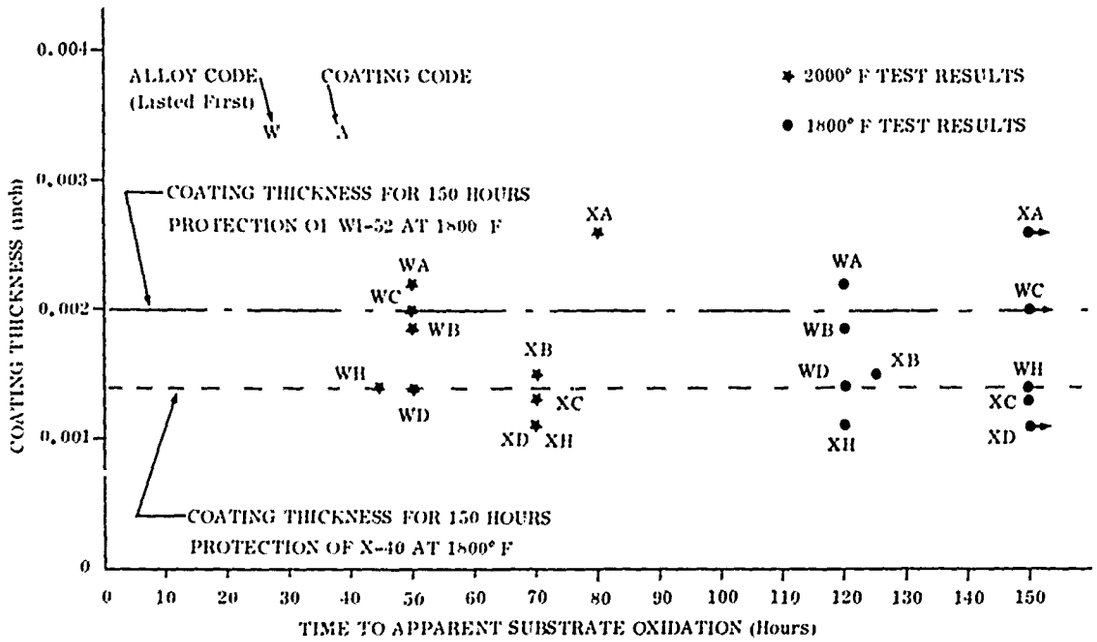

Figure 22. Summary of hot corrosion rig test results on coated cobalt-base alloys.

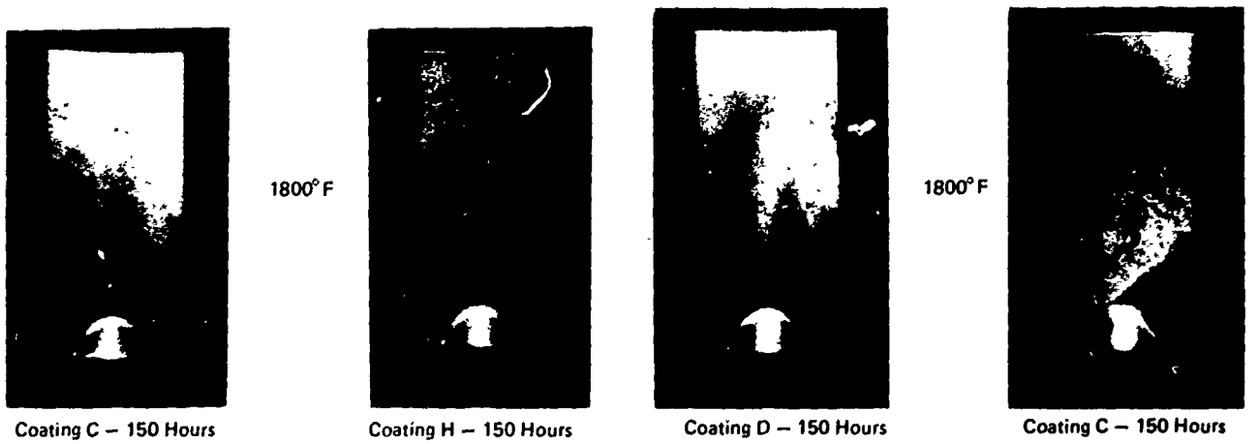

Coating C – 150 Hours | Coating H – 150 Hours | Coating D – 150 Hours | Coating C – 150 Hours

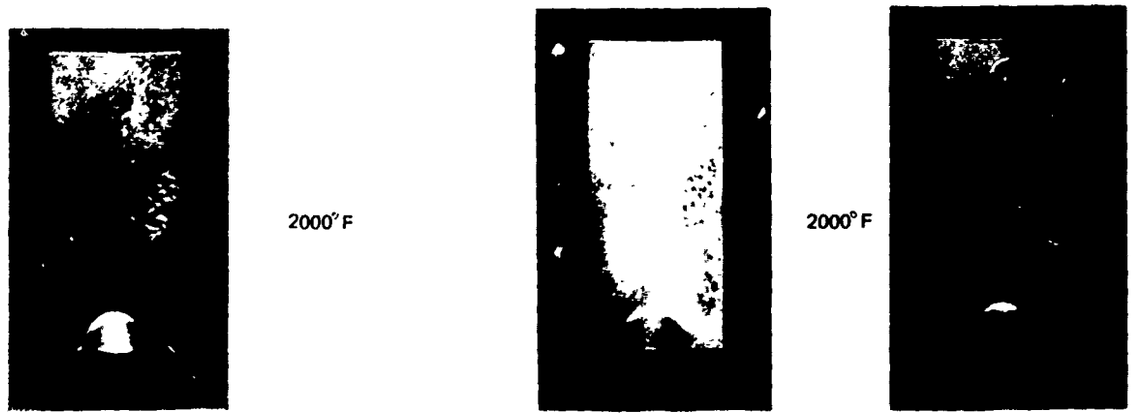

Coating C – 60 Hours | Coating D – 90 Hours | Coating B – 90 Hours

Figure 23. Typical surface attack on coated WI-52 alloy after hot corrosion rig resting.

Figure 24. Typical surface attack on coated X-40 alloy after hot corrosion rig testing.

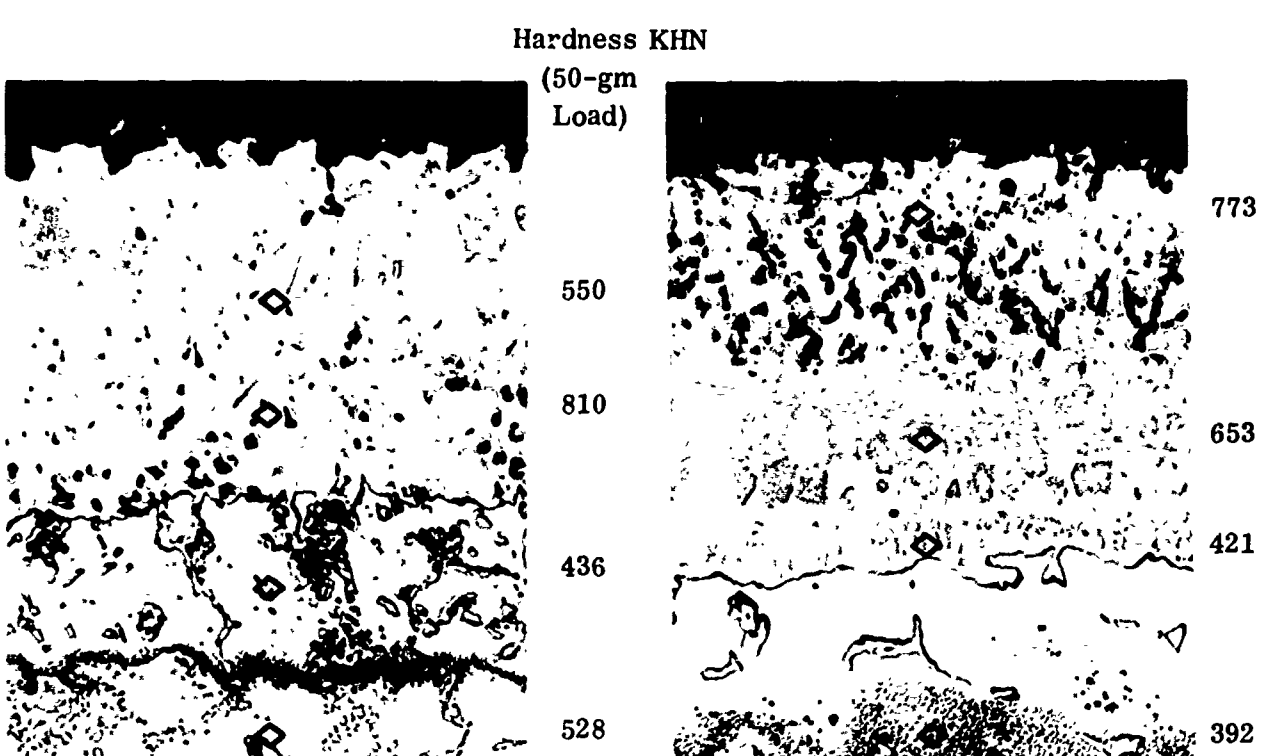

Figure 25. Typical microstructure of superior coatings on cobalt-base alloys after exposure for 150 hours.

Coated Nickel-Base Alloys

Another reduction in fatigue strength was apparent for most of the nickel-base alloys after coating and then exposing the specimens in an air environment at 1800°F for 500 hours.

The J coating (Type 1(b)) on B1900 and MAR-M246 did not cause any significant reduction in the low-cycle fatigue strength of these alloys. This coating, which was applied to six of the eight nickel-base alloys, appeared to have the least influence on the fatigue properties of any of the coatings evaluated. Loss in strength ranged from zero (on B1900) to a maximum of 15 percent on the U-710 alloy. The type 1(a) A coating with a high-aluminum activity was applied to seven of the alloys and caused the largest drop in fatigue strength of the coatings evaluated. This is undoubtedly due to the diffusional instability of this coating system. Rapid diffusion of aluminum into the substrate was noted for this coating system during hot corrosion testing at 1650 and 1800°F.

Best metallurgical stability was exhibited by the MAR-M246 and B1900 alloys. The A and J coatings (Type 1(a) and Type 1(b) coatings) on these two alloys reduced the 10^4 cycle fatigue strength by 3 percent of the MAR-M246 alloy (average loss of both coatings) and 2 percent of the B1900 alloy, respectively. However, *total* loss in strength of these two alloys after coating and prolonged exposures at 1800°F was generally in excess of 10 percent.

The two wrought alloys, Rene' 41 and U-700, showed the largest average loss in strength due to the coating and prolonged exposure. The two coatings on Rene' 41 dropped the strength 27 and 45 percent, whereas on U-700, the coatings reduced the strength by 12 and 33 percent. Again, the Type 1(a) coating caused the largest drop in fatigue strength.

Uncoated Cobalt-Base Alloys

The fatigue strength of the two cobalt-base alloys was considerably lower than the nickel-base alloys (Fig. 27). The maximum stress level for a 10^4 cycle life was 69.5 ksi for the WI-52 alloy and 59.5 ksi (15 percent less) for the X-40 alloy.

Both of the cobalt-base alloys showed a decrease in fatigue strength following the exposure at 2000°F for 500 hours duration. The X-40 alloy exhibited a small decrease in strength (approx. 3%); whereas the WI-52 alloy showed a loss of ~8 percent, dropping from 69.5 ksi to 64.0 ksi for a 10^4 cycle life.

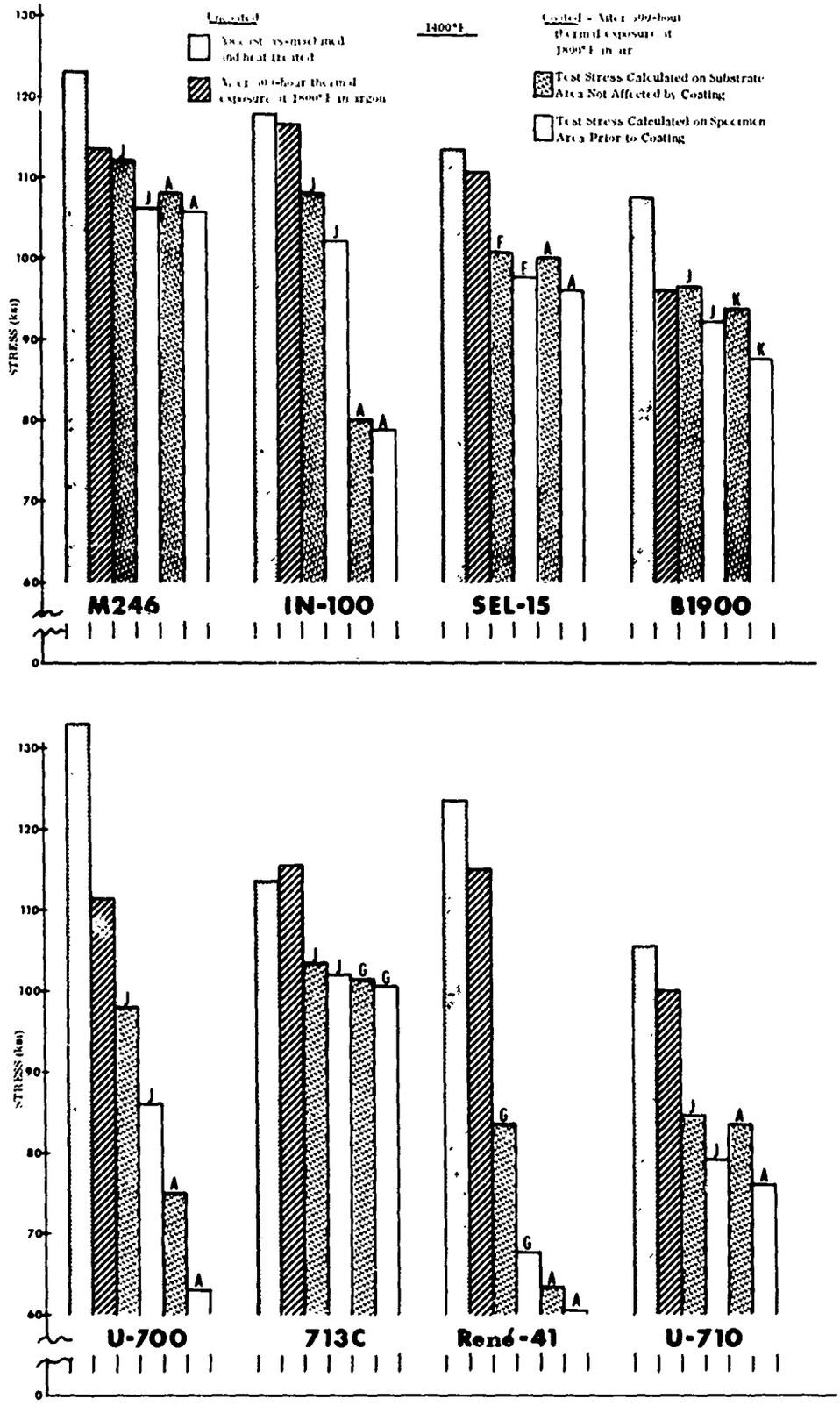

Figure 26. Comparison of failure stresses at 10^4 cycles for nickel-base alloys.

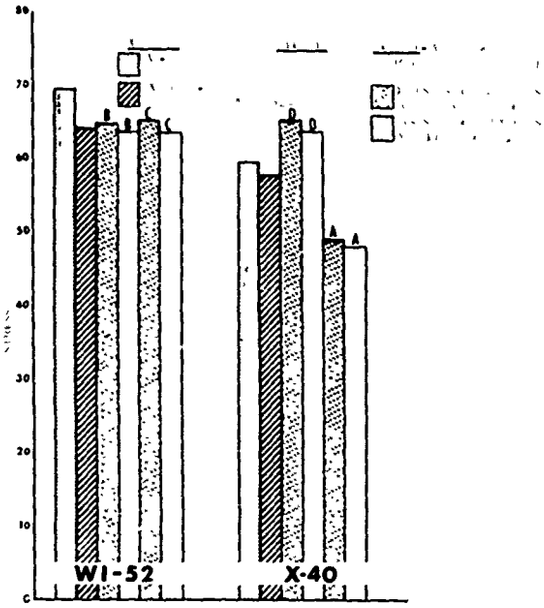

Figure 27. Comparison of failure stresses at 10^4 cycles for cobalt-base alloys.

Coated Cobalt-Base Alloys

The WI-52 alloy did not show any drop in fatigue strength due to the coating and prolonged exposure at 2000°F. Both the B and C coated WI-52 alloy specimens exhibited a 10^4 cycle fatigue strength of 64 ksi, approximately the same strength as the uncoated exposed specimens. The X-40 alloy with the A coating showed a 15 percent decrease in strength after coating and exposing at 2000°F. The strength dropped from 57.8 ksi (uncoated-exposed) to 49.0 (coated-exposed). The D coating on X-40 exhibited a 12 percent increase in strength due to the coating-exposure cycle.

STRESS RUPTURE TESTS

Uncoated Nickel-Base Alloys

The stress rupture data for the uncoated nickel-base alloys were in good agreement with the published literature values. Most of the test points were on, or quite close to, the standard curves with very little scatter between the duplicate test specimens.

Coated Nickel-Base Alloys—Thermally exposed

The results of the stress rupture tests on the nickel-base alloys are shown in Fig. 28. These data are presented as a ratio of the hours to rupture for the coated alloys to baseline alloys after (1) thermal exposure for 500 hours, and (2) thermal exposure for 500 hours followed by stripping and recoating. For most uncoated nickel-base alloys, a decrease in time to rupture was noted after the 1800°F, 500-hour exposure.

At a test temperature of 1650°F, the U-710, MAR-M246, SEL-15 and IN-100 alloys showed a definite decrease in life for both coating systems. The decrease in rupture life was greatest for the U-710 and MAR-M246 alloys (approximately 30% of baseline). The U-700 and B1900 alloys exhibited a decrease in rupture life with only one of the two applied coating systems and an increase with the other coating, but this apparent increase in strength may be due to scatter in the test data. Neither of the two coatings on Rene' 41 caused a reduction in stress rupture life at 1650°F. The stress rupture tests were terminated after exposures ranging up to 329 hours at 1650°F. Only one G coated Rene' 41 specimen failed after 206 hours exposure at 1650°F. Total elongation was approximately 30 percent, which was in good agreement with the results of the tests on the uncoated, unexposed alloy.

The B1900 alloy showed a severe drop of 85 percent in stress rupture life after coating with the K coating (special high-silicon type) and exposing for 500 hours. The average life dropped from 61 to 9 hours when tested at 1650°F.

Coated Nickel-Base Alloys—Exposed, Stripped and Recoated

All coating vendors were able to strip the coating, either partially or completely, and recoat satisfactorily with the original coating system. The stripping and recoating operations on the nickel-base alloys after the 500-hour thermal exposure did not appear to have any appreciable *added* detrimental effects on the stress rupture lives (Fig. 28). Some coating-alloy combinations exhibited an increase in the stress rupture life after the stripping and recoating (IN-100, U-710, MAR-M246), and others showed a decrease in the stress rupture life after this recoating operation. No real trend, however, was apparent to show that the one additional thermal cycle from recoating was significantly harmful to the alloys.

Coated Cobalt-Base Alloys—Thermally Exposed

The uncoated WI-52 and X-40 cobalt-base alloys exhibited a slightly higher stress rupture strength than literature data in the as-received condition at the 1800°F test temperature.

The cobalt-base alloys both exhibited a decrease in stress rupture life after coating and exposing in air for 500 hours at 2000°F (Fig. 29). When stress-rupture tested at 1800°F, both coatings on WI-52 alloy decreased the time to rupture by more than 65 percent. The decrease in stress rupture life was not as great, however, for the two coatings on X-40 alloy; average time to rupture was decreased by only 13 percent.

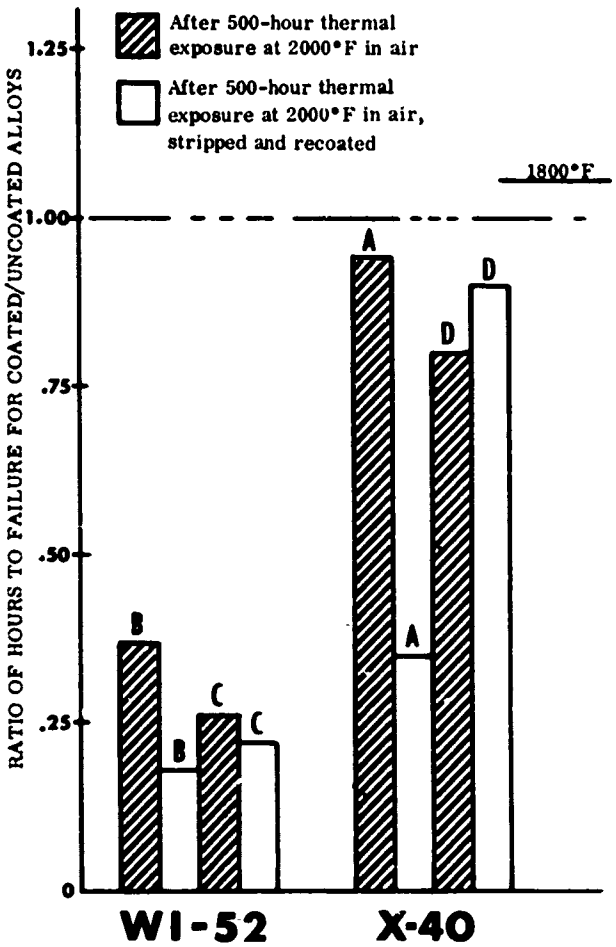

Figure 29. Comparison of stress rupture life for coated cobalt-base alloys at 1800°F.

Coated Cobalt-Base Alloys—Exposed, Stripped and Recoated

The two cobalt-base alloys both exhibited an additional *small* decrease in the rupture life at 1800°F when stripped and recoated after prior 2000°F exposure. For example, the average time to rupture for the exposed, stripped and recoated B and C coatings on WI-52 alloy was about 19 hours compared to approximately 30 hours average life for the specimens coated and exposed only.

DISCUSSION AND SUMMARY

HOT CORROSION

In this program, nickel-base alloys were grouped into low-chromium, medium-chromium, and high-chromium alloys. With few exceptions the test results on uncoated alloys indicated that the higher chromium alloys were most resistant to the high velocity, hot corrosion environment. At 1650°F, B1900, SEL-15, IN-100 and MAR-M246 underwent catastrophic attack in less than 10 hours; whereas the shortest life time to initial attack of the medium- and high-chromium alloys (medium Cr IN-713C and U-700 and high Cr Rene' 41 and U-710) was 55 hours for IN-713C. The high-chromium alloy withstood at least 150 test hours without significant surface attack.

At a T_{max} of 1800°F, uncoated alloy performance changed slightly. IN-713C performed similarly to the low-chromium alloys which all failed within 5 hours; the medium-chromium U-700 performed better than U-710, although both withstood the test duration of 150 hours. U-700 withstood only 110 hours of testing at 1650°F. The hot corrosion resistance of the high-molybdenum R41 alloy was markedly poorer at the 1800°F temperature, failing in 70 hours as compared to 150 hours at 1650°F. Ranking of all uncoated alloys is shown in Fig. 12. Cobalt-base alloys are also shown in this figure, and uncoated performance is poor at the two test temperatures, ranking these alloys with the low-chromium, nickel-base alloys at the 1800°F test temperature. Attack on the cobalt-base alloy tended, however, to be more general and less catastrophic than with the nickel-base alloys.

Application of coatings to all of the alloys was by commercial organization, and all coatings evaluated were of the diffusion type, that is, coatings formed by the deposition of an element, primarily aluminum, that required interdiffusion with the substrate to form the coating. Three general types and one special type of coatings could be distinguished on nickel-base alloys by microstructure, electron microprobe analyses, and X-ray diffraction (Table II), i.e., Type 1a, 1b and 2. The following coatings are in these various types:

Type 1a:	Coatings A and I
Type 1b:	Coatings C and J
Type 2:	Coatings F and G
Special:	Coating K, high silicon

Coatings on cobalt-base alloys appeared to be of Type 2. Coatings are much more complex than can be accounted for by the Table II classification. For example, many contain elemental additives that perhaps contribute to performance (Si in the J coating, oxide in the G and F coatings, differing Al contents in the Type 1 subgroups, viz., 30% Al in A and 20-24% in J). The types noted as well as coating thickness, however, provide a basis for discussion.

Restricting the initial discussion to low-chromium-nickel-base alloys and IN-713C, the combination of a greater thickness and a Type 1a or b coating affords the most consistent protection to the large number of alloys tested. For protection at 1650°F and 1800°F, the coating thickness should be at least 0.003 inch. Type 2 coatings and excessively diffused Type 1b coatings (e.g., coating C) performed generally poorly in test, exhibiting only 20 to 60 hours of protection compared to 150 plus hours for the better Type 1a and 1b coatings near 0.003 inch in thickness. Direct comparison between Type 1 and Type 2 coatings is not possible

because the Type 2 coatings formed from low-chromium activity sources cannot or are not deposited to the 0.003-inch thickness of the satisfactorily performing Type 1 coatings. Thin Type 1(a) and (b) coatings also perform poorly, e.g., coating I.

The Type 2G coating which contains a high percentage of large aluminum oxide particles showed inconsistent performance on various alloy systems. The G coating on IN-713C, MAR-M246 (1650°F) and SEL-15 and IN 100 (1800°F) afforded protection well above other coatings at a comparable thickness. The inconsistency of performance of the G coating is one of its prime limitations as compared to the performance of the Type 1a and 1b, A and J coatings.

Oxide additions are not necessarily associated with improved performance. The F coating with both an aluminum oxide and a high-titanium oxide addition performed consistently poorly in test on the low-chromium alloys.

The effectiveness of coatings in resisting hot corrosion on the high-chromium, nickel-base alloys and medium-chromium, U-700, alloy was more difficult to interpret because the substrate performed very well in test when uncoated. The high-molybdenum content R41 alloy showed the shortest life in test—120 hours at 1800°F—but this was significantly longer than the uncoated life—70 hours. The combination of a substrate with good hot corrosion resistance with a coating would certainly be expected to provide the most consistent resistance to hot corrosion. This was generally observed in the test results. A significant need for the coatings on high-chromium alloys was not established in the hot corrosion tests. The data did show Type 1 coatings to be generally more protective than Type 2 coatings and high percentage aluminum coatings, e.g., A, to retain more coating after 150 hours of exposure than the lower aluminum content J coating.

As an overall generalization, the Type 1b, J coating, which contains up to 1% silicon, and the Type 1a, A coating, were the most protective coatings on all nickel-base alloys. The thin Type 1 and 2 coatings (I, F and C) generally afforded relatively poor protection. The Type 2, G coating, with high Al_2O_3 content was intermediate in performance and, particularly, afforded good protection to Inco 713C alloy.

The high silicon coating K, applied to B1900 alloy only, is of special note. This coating, containing up to 15% silicon, essentially provided complete protection to the substrate for the 150-hour duration of the test at 1650 and 1800°F when continuous. The extreme hardness and brittleness of the coating and mismatch in thermal expansion resulted in shear fracture within the coating that produced an occasional test failure. The addition of silicon in the coating and in a lesser percentage in the J coating appeared to enhance the effectiveness of the aluminide coating in resisting hot corrosion.

The test temperatures for coated cobalt-base alloys, WI-52 and X-40, were 1800 and 2000°F for up to 150 hours. None of the coatings tested, which all appeared quite similar and primarily CoAl, would provide more than 80 hours of protection to either alloy at 2000°F. Generally at the 2000°F test level, all coated X-40 specimens outperformed coated WI-52 specimens. At 1800°F, the C coating only appeared to be capable of affording protection for more than 150 hours to WI-52 with the H coating a close second; on X-40 at 1800°F, the A and D coatings (thickest and thinnest coatings, respectively) protected the alloy for more than 150 hours with the C coating affording protection for up to 150 hours. Protection afforded by all coatings evaluated (on X-40 and WI-52 alloys) at 1800°F (A, B, C, D, and H) afforded protection for at least 120 hours; thus the grouping of coating performance was in a very narrow band. No effect of coating thickness could be noted.

Comparing the performance of the better coatings on nickel-base alloys with coatings on cobalt-base alloys in hot corrosion indicates better general performance for the coated nickel-base alloys but more catastrophic failure when the coating is penetrated. Coatings were generally thicker and more ductile on nickel-base alloys, probably accounting for the majority of improved performances.

By visual examination of specimens, most coated nickel- or cobalt-base alloys failed in localized areas rather than by uniform corrosion. Some of this effect can be attributed to temperature variations and some appear related to the presence of the coating. For instance, uncoated U-700 alloy corroded slowly and quite uniformly at 1650 and 1800°F. Virtually no hot corrosion was noticeable after 150 hours at 1800°F. Both cobalt-base alloys appeared to corrode rapidly but relatively uniformly at 1800 and 2000°F. All coatings tested on U-700 actually reduced the capability of the alloy to withstand the test conditions at 1800°F. Severe localized failures were observed after as few as 30 hours of testing. Coatings C and F also promoted deep pitting of U-700 when tested at 1650°F. Visual evaluation of the coated cobalt-base alloys indicated localized areas of damage. The indication that some coatings promoted corrosion of nickel- or cobalt-base alloys is quite clear. These data point toward the operation of an electrochemical mechanism of corrosion which results from the presence of two or more dissimilar metals in electrical contact and covered with a strong, molten electrolyte.

Early work by von Doering (4) measured the potential difference between a platinum electrode and various pure metals, alloys and intermetallic compounds when immersed in Na_2SO_4. All investigated materials were anodic (active) with respect to platinum. Following is the approximate electrochemical series determined for various materials in 1650°F Na_2SO_4.

Material	Potential (volts)	
Cr	+0.31	↑
70Ni-30Cr	+0.29	Noble
80Ni-20Cr	+0.29	
Inco 713C, Ni_3S_2	+0.01	

Ni	0	0
TiC	–0.19	
90Ni-10Cr	–0.30	
Co	–0.33	
Ni_3Al	–0.39	Active
Ti	–0.39	
Inco 713C (after 20 hours in melt)	–0.4	
NiAl	+0.79	
Ni_2Al_3	+0.81	

The series has been adjusted relative to nickel and shows chromium and high-chromium alloys to be noble with respect to nickel. It is known that nickel reduces sulfate ions to yield nickel sulfides (5) and it is, therefore, probable that the above activity series is actually relative to Ni_3S_2. This is supported by the nearly equal potentials observed for Ni and Ni_3S.

Reference to the above potential data helps to explain both the initial protection afforded a nickel-base alloy by NiAl coatings and the eventual contribution of those coatings to very rapid substrate corrosion. Initially, NiAl was observed to be anodic and presumably protective with respect to the Inco 713C alloy. After a period of exposure sufficient to (1) partially degrade a NiAl coating to Ni_3Al, to (2) possibly penetrate the coating at a defect site, and to (3) possibly permit chromium depletion of the substrate at a coating failure site, it is seen that the substrate (713C alloy) may become anodic with respect to interfacial carbides (TiC) and the Ni_3Al. As shown by Berkowitz (6), exposure in molten Na_2SO_4 for different times is sufficient to develop slightly different surface compositions on a Nichrome alloy. Potential differences could then be measured between two such specimens while immersed in molten Na_2SO_4. A change in relative potential between residual coating and substrate plus the very high exchange current densities (i.e., amps/cm^2) possible in molten salt systems at high temperatures are just the conditions necessary to promote severe pitting. Such conditions apparently arise as a result of (1) coating degradation by oxidation, (2) coating-substrate interdiffusion, and (3) physical damage which exposes a fresh metal surface.

In other related work, DeCrescente and Bornstein (7) have shown that the addition of oxides such as Cr_2O_3, Sm_2O_3 and SnO to molten Na_2SO_4 can lower the oxide ion concentration in the melt. Reaction such as

$$2Cr_2O_3 + 3O_2 \rightarrow 4CrO_3$$

$$CrO_3 + O^{=} \rightarrow CrO_4$$

may explain this observation. Presumably, this lowers the oxygen activity below that necessary to support the rapid oxidation associated with hot corrosion. These authors further showed that oxides could be used to inhibit the hot corrosion of laboratory test coupons. Unpublished work at Solar has shown that addition of oxides to fuels burned in gas turbine simulators does in fact inhibit hot corrosion of low-chromium alloys. The most effective inhibitor has been Cr_2O_3.

Oxidation of the nickel alloys with low- to medium-chromium contents tends to yield NiO, spinels and Al_2O_3. The high chromium-containing nickel alloys generally contain relatively low quantities of Al and yield outer layers of Cr_2O_3 when oxidized (8). These alloys, therefore, generate an oxidation product which can aid in lowering the oxygen activity of a thin surface salt layer. Such action, while not indefinitely sustainable, could inhibit hot corrosion and may partially explain why high-chromium alloys resist hot corrosion.

MECHANICAL PROPERTIES

The results obtained on mechanical properties (low-cycle fatigue and stress rupture) were quite limited and were performed on two coating systems per alloy. Exposure after coating was for 500 hours at 1800°F and 2000°F for nickel- and cobalt-base alloys, respectively. Stress to produce failure in 10^4 cycles at 1400°F was determined on all alloys and stress to produce rupture in 100 hours was measured at 1650°F on nickel-base alloys and 1800°F on cobalt-base alloys.

Based on equivalently exposed alloys and the unaffected cross section after coating exposure, alloys vary considerably in their tolerance for coatings without loss in low-cycle fatigue performance. Coating type also influenced cycles to failure. The combination of the J coating (Type 1b) with MAR-M246 and B1900 alloys exhibited no drop in stress to 10^4 cycles after 500 hours' exposure. Coatings such as A (Type 1a) which interdiffuse rapidly with the substrate produced major losses in fatigue strength. The higher chromium alloys, U-700, R41 and U-710, all exhibit major losses in low-cycle fatigue strength, e.g., 45 percent on R-41 and 32 percent on U-700. Coatings on cobalt-base alloys tended to influence cycles to fatigue fracture less than the coatings on nickel-base alloys. Losses all appear to be the result of loss in substrate cross-sectional area rather than any contribution of coating properties. Stable coating systems such as J, developed for B1900, show that an optimized system can minimize degradation by low-cycle fatigue after exposure.

The data obtained in this program indicate that several coating-alloy combinations–BJ, CG, UA, RA and RG–have no brittle or no adverse effect on the 1650°F, 100-hour rupture strength after exposure to 1800°F for 500 hours. Other coating combinations can produce an 80 percent loss in strength–DA and BK. The data also indicate that coating vendors have little capability to strip and recoat alloys and retain original substrate rupture properties. Losses in properties are significantly greater than would be anticipated from a strip and recoat operation.

Retention of stress rupture life of coated cobalt alloys showed a marked difference in alloy systems. The coated WI-52 alloy lost 65 plus percent of the life upon coating and exposure to 2000°F for 500 hours, regardless of coating. The coated X-40 alloy showed a maximum of 20 percent loss in rupture life. Recoating the X-40 alloy with the D coating did not result in additional loss in rupture life.

ACKNOWLEDGMENT

This program was performed under the sponsorship of the Naval Air Systems Command with Mr. Samuel Goldberg acting as NASC Project Manager. The NASC contract was N00019-68-C-0532. The final report was entitled "Hot Corrosion of Coated Superalloys in a Gas Turbine Environment," RDR 1626-5 (December 1970).

REFERENCES

1. H. Lewis and R. A. Smith, "Corrosion of High Temperature Nickel-Base Alloys by Sulphate-Chloride Mixture." Proceedings of the First International Congress on Metallic Corrosion, London, 1961, pp. 326-336.
2. W. A. Rentz, "Sulfidation (Hot Corrosion) Symposium on High Temperature Alloys." Ninety-fifth AIME Annual Meeting, New York, Feb. 1966.
3. V. S. Moore, W. D. Brentnall and A. R. Stetson, "Evaluation of Coatings for Cobalt- and Nickel-Base Superalloys." NASA CR-72714, Vol. II (July 1970), NASA Contract NAS3-9401.
4. Harvey von E. Doering, "Behavior of Nickel-Base Superalloys in Molten Salts." Naval Ship Research and Development Center, Marine Engineering Laboratory, Report 2468, Sept. 1967.
5. C. H. Liu, *J. Phys. Chem.: 66,* 164 (1962).
6. Joan B. Berkowitz and David W. Lee, "Effect of Applied Electric Fields on the Mechanisms of Oxidation of Metals and Alloys." Naval Air Systems Command, First Quarterly Report, Contract No. N00019-72-C-0217.
7. N. S. Bornstein and M. A. DeCrescente, *Metallurgical Trans.: 2,* 2875 (1971).
8. C. S. Giggins and F. S. Petit, *J. Electrochem. Soc.: 118,* 1782 (1971).

Turbine Corrosion and Protection in Marine Environments

Irwin I. Bessen and Robert E. Fryxell
General Electric Company, Aircraft Engine Group
Cincinnati, Ohio

ABSTRACT

The rate of hot corrosion attack in aircraft and shipboard gas turbines is influenced by specific environmental factors which vary with different engine applications. For any given application, the corrosion rate also varies within the engine from stage to stage. Conditions leading to salt condensation have been better defined, and allow a better understanding of observations which show more condensation than one would expect from previously published work. Also, the presence of reducing conditions–which may occur locally in an engine–was found to be deleterious. To withstand corrosive attack, resistant superalloys–particularly Rene' 80 and cobalt alloys–provide inherent protection, while coatings extend the part life. The simple and inexpensive Codep-B coating has afforded good protection in aircraft applications and on some stages in LM2500 shipboard engines. In the most severe LM2500 local environment, the General Electric BC21 coating on Rene' 80 greatly extends part life. Further improvements are foreseen for extremely long life and for lower cost processes. An example that characterizes the corrosion mode in a long-lived, LM2500 BC21-coated turbine bucket is cited.

INTRODUCTION

A full understanding of hot corrosion in marine jet engines and shipboard gas turbines is elusive because of the large number of variables entering the problem, and the difficulty in controlling or measuring these variables in engine experiments. Yet, the motivation for pressing ahead with corrosion studies is the important payoff in reliability and TBO (time between overhauls) afforded by protection schemes. This paper seeks to present some current views, work in progress, and directions for further work in corrosion and protection.

Two methodologies have been used by investigators: (a) laboratory experiments based on suspected corrosion mechanisms to see what reactions can possibly take place and with what kinetics, and (b) measurements of engine component performance in given environments or applications, followed by bench experiments that help explain what happened in the engine. The latter approach with cognizance of the former is considered to be more relevant and useful. This work leans heavily on engine observations and comparisons, even though it is difficult to design engine experiments that follow the many variables with rigor.

The strongest influence on hot corrosion in engines is the environment in the immediate neighborhood of a given part. It is characterized by gas chemistry, temperature, velocity and pressure, part surface temperature and chemistry, and perhaps other factors such as particles in the gas stream. The change in corrosion behavior from point to point in a given engine is striking because of environmental changes. A turbine bucket in a given application can be severely attacked, while the adjacent nozzle of the same alloy and coating, barely two inches away, will show no corrosion. Also, turbine buckets have corroded only in spots, remaining virtually untouched in other areas of the same airfoil after thousands of operating hours. The notion that all components in an engine are subject uniformly to the effects of Na_2SO_4 is not accurate.

There are good examples of the locational variations in corrosion severity. Figure 1 shows uncorroded stage-2 high-pressure turbine buckets after running 3600 hours on a shipboard LM2500 test engine. The buckets are Rene' 80 coated with General Electric's Codep aluminide coating. The stage-2 nozzle vanes of a similar alloy, Rene' 77, with a Codep coating also appeared free of corrosion. Stage-1 buckets of aluminide coated Rene' 77, however, corroded in shipboard engines, as shown in Fig. 2. On the basis of evaluations to be discussed, the stage-1 bucket environment was found to be more severe in several respects.

Thus, the well known and available aluminide coatings suffice on many components, but in some cases something better is needed. Figure 3 shows the stage-1 and stage-2 buckets of another shipboard LM2500 test engine. No corrosion is apparent after 2600 hours. The buckets are Rene' 80. The coatings are General Electric's BC21 on stage 1 and Codep on stage 2. BC21 is substantially more corrosion resistant than the aluminides.

Coated alloys used in different engine applications sometimes show similar corrosion severity. Thus, an aluminide-coated Rene' 80 stage-2 bucket in an LM2500 engine can look very similar to one in a J79 engine with similar running time. The environmental severities are probably similar or sufficiently mild in relation to the protection capability so as to avoid major distress. In general, most aircraft and shipboard type engine components using a resistive superalloy and the aluminide coatings fall in this category.

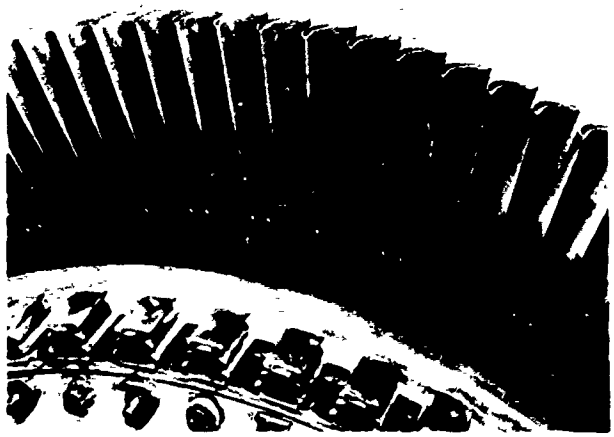

Figure 1. LM2500 stage-2 turbine buckets after 3600 hours of shipboard operation.

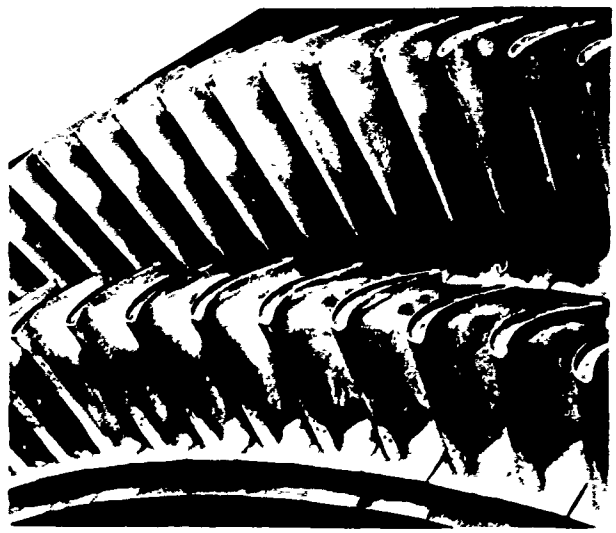

Figure 3. Stage 1 and stage 2 buckets on LM2500 rotor uncorroded after 2600 hours of shipboard exposure. Coatings are the General Electric Company's Codep on stage 2 and BC21 on stage 1.

Figure 2. Aluminide coated Rene' 77 bucket after 1900 hours of shipboard exposure.

One big environmental factor in a comparison of engine applications is the salt ingestion level. Newhart (1) lists salt ingestion measurements in engine tests and around naval vessels. They range from 4 to 1000 ppb (parts per billion). Some engines employ demisters that lower salt ingestion level. Also, the engines condense out considerable quantities of salt in the compressor. It is not known whether the compressor deposits reach a steady state thickness with time or continue to collect salt. Measurements of salt entering the turbine are lacking.

A second environmental factor important in a comparison of engines is power cycling. Turbine temperatures which cycle can provide part-time conditions favorable for Na_2SO_4 condensation or evaporation. Measurements of salt deposits in turbines should take into account the kind of operating condition for the period of time just preceding shutdown and measurement.

A third environmental factor is the occasional appearance of sooty surfaces. This may be related to power cycling through operational regimes conducive to the generation of reducing conditions. Figure 4 shows carbon deposits in the cool root and platform region of an LM2500 stage-1 bucket, and corrosion in areas where reducing conditions may exist at least on a temporal basis. The effects of reducing environments were studied in the laboratory and will be discussed below.

DEPOSITION OF Na_2SO_4

The major source of sodium in a marine environment is sea water ingested with intake air or present in contaminated fuel tanks. This sodium is predominantly present as chloride and only to a minor extent exists as sulfate. The sulfate ion

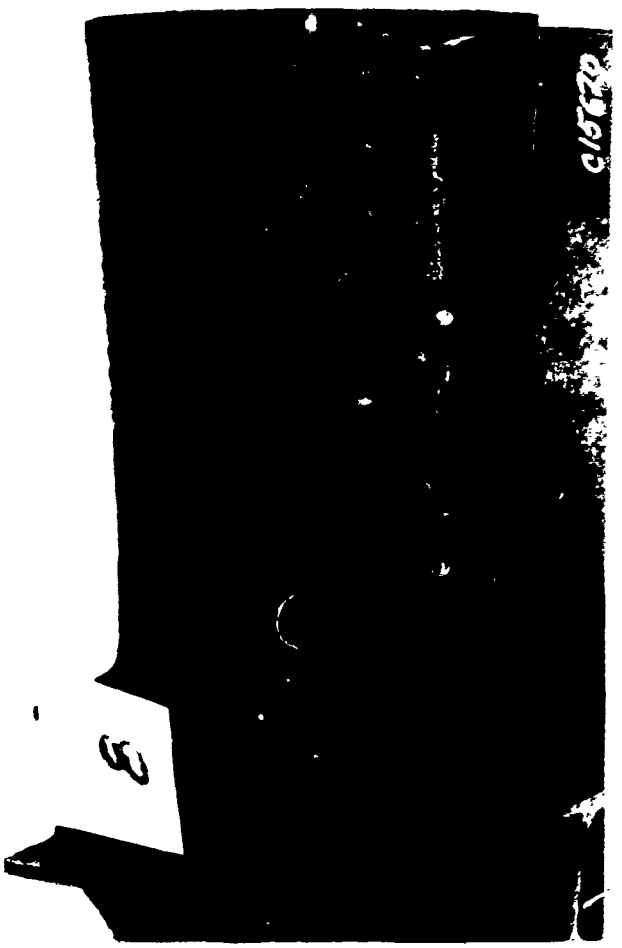

Figure 4. Carbon deposits sometimes appear in cool local areas as at the root of this aluminide-coated, Rene' 77, turbine bucket airfoil. These may indicate reducing conditions in the vicinity.

in sea water is equivalent to about 12 percent of the sodium. A much higher source of sulfur is the fuel which on combustion yields a mixture of SO_2 and SO_3. It is commonly held that a substantial amount of sodium sulfate, Na_2SO_4, is formed during combustion by reaction of sodium chloride and the SO_2 and SO_3 derived from the fuel. DeCrescente and Bornstein (2) have presented convincing thermodynamics that this reaction can go essentially to completion.

One reason for the interest in this reaction is the great disparity between observations (both in engines and in burner rigs) and predictions of Na_2SO_4 deposition. That is, deposits are observed under temperature and salt concentration conditions considerably removed from threshold levels based on available vapor pressure data. The present authors agree with Tschinkel (3) that the published vapor pressure data are probably not reliable. Liander and Olsson (4) made measurements only above 2000°F and Kröger and Stratmann (5) below 1550°F. The latter used a Knudsen technique and the results are possibly biased by some thermal decomposition which will take place in vacuum. The Liander and Olsson data may suffer by a long extrapolation into the temperature range of interest in high-pressure turbines. In any event, the vapor pressure data are much higher than is compatible with experience.

To help remedy this discordant situation, the vapor pressure of Na_2SO_4 has been measured, as part of the present study, in the temperature range of 1750°F to 2200°F. These measurements, obtained by the transpiration method, will be reported in detail elsewhere (6). Briefly, the new results are about a factor of 20 below the Liander and Olsson results at 2200°F and more than a factor of 100 below at 1750°F.

The consequences of the new measurements are displayed in Fig. 5 in terms of condensation temperature versus ppm sea salt in the combustion products for 1 and 15 atmospheres and for the two limiting cases of none and of complete conversion of NaCl to Na_2SO_4. Each curve is shown as a band which represents a tentatively assigned ±20°F uncertainty. Also shown in Fig. 5 is a curve for 15 atmospheres based on the Liander and Olsson data and assuming complete conversion of NaCl. For all curves below the melting point of Na_2SO_4 (1620°F), the parent Arrhenius plot of vapor pressure recognized the increase in slope of 5.8 kcal/mole, the heat of fusion.

The curves based on the new vapor pressure measurements are strikingly different from predictions based on previously published results. Clearly, these new curves are more consistent with a variety of engine and burner rig observations, some examples of which will be discussed later.

In fact, the reasonableness of these curves even for the case of no conversion of NaCl to Na_2SO_4 (i.e., 12 percent of the total sodium present as Na_2SO_4) revives the question whether the conversion does actually take place to a significant degree in an engine. In this regard, it should be pointed out that the conversion reaction

$$2NaCl + SO_3 + H_2O \rightarrow Na_2SO_4 + 2HCl$$

involves a four-body collision which is certainly a very low efficiency process at the concentrations involved, particularly in a dynamic system where the reaction has only a few milliseconds in which to take place. Hedley (7) studied the SO_2/SO_3 equilibrium in a similar dynamic system and found that even for this much simpler two-body collision case, only 1-2 percent of the equilibrium amount of SO_3 was formed!

The "true" condensation behavior may well lie between the two extremes of total and of no conversion of NaCl to Na_2SO_4, and certainly is dependent on kinetic factors related to design and operating parameters of any particular engine. Certain other factors should also be pointed out: The salt level monitored for an engine represents the intake air and/or the fuel. In principle, salt in the intake air may deposit along all channels within the engine and thus the measured level may not relate to that in the turbine which is the region of greatest interest here. It is a matter of record that significant amounts of NaCl are frequently found in engine compressors; however, information is not available

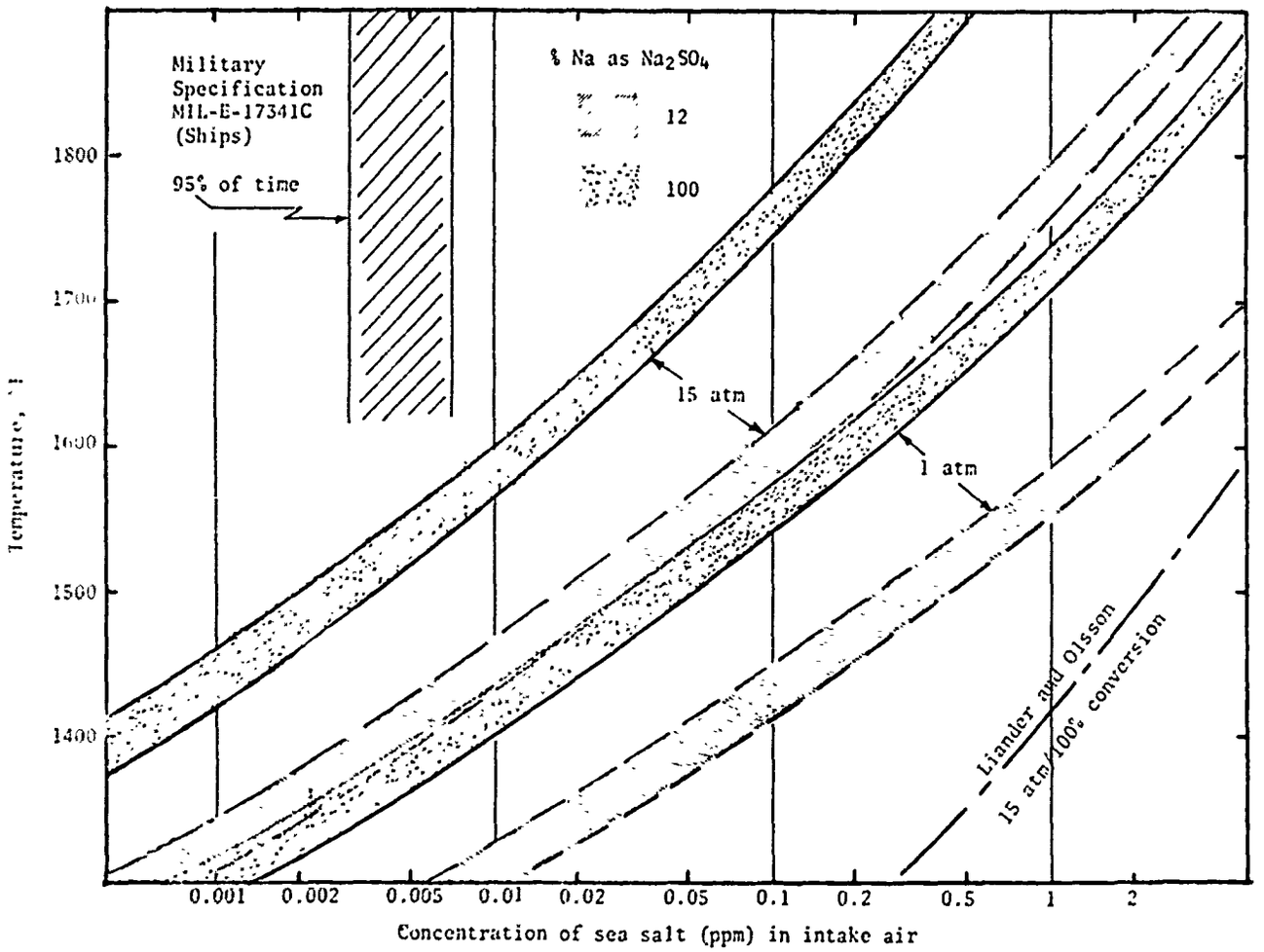

Figure 5. Condensation temperatures for Na_2SO_4 as function of concentration and pressure.

at present whether these deposits contain Na_2SO_4. If large fractions of NaCl are deposited upstream to the turbine, this represents an additional reason why the no-conversion curves in Fig. 5 may well be closer to the truth.

Although there are these limitations to the application of the curves in Fig. 5, the salt ingestion level shown (Military Specification MIL-E-17341C[8]) is of interest. The listing by Newhart (1), however, reports much higher levels of salt which can be ingested at ship deck elevations. Also, it must be emphasized that salt deposits found on turbine parts may, in some instances, represent deposition during a final low power cycle or slow cooldown. That is, correlation of predictions from Fig. 5, observed deposition, and corrosion must factor in as much information as possible about operating parameters.

EFFECTS OF REDUCING ENVIRONMENTS

The corrosion described earlier for the LM2500 stage-1 buckets is sometimes more severe than might be expected for coated alloys on the basis of their general performance in burner rig tests. It was suspected that the carbon deposits observed in some instances were either the cause of the enhanced corrosion rates by inducing local reducing conditions on the component surfaces, or the indicator of a reducing condition in the vicinity.

Such aggravated Na_2SO_4 attack has been noted qualitatively for a variety of alloys under laboratory conditions (9-14) and has also been reported for actual turbines by Morgan and Lamport (15). As part of the present evaluation, studies have been carried out to determine the magnitude of the aggravated attack for the alloys and coatings of interest to the LM2500. These have been either crucible tests in which a pin specimen has been partially submerged in molten salt (1650°F) or tests in which specimens were dip coated at 1650°F and then exposed at 1400°F or 1500°F (solid state).

Three test conditions have been compared:

1. Na_2SO_4 in air (oxidizing)
2. Na_2SO_4 in argon (intermediate)
3. Na_2SO_4 plus carbon in argon (reducing).

Exposure was in a slowly moving gaseous atmosphere. Argon was used as the environment for the reducing condition to prevent loss of carbon as CO_2. Several features of the liquid state tests (1650°F) should be pointed out:

1. The molten salt wet the specimen surfaces and formed a film over the entire nonsubmerged portion. The salt film thickness was in the range 1 to 3 mg/cm^2, not unlike the thicknesses observed on some engine components.

2. Descaled specimens after test showed nominally the same degree of attack for the submerged portion and that above, and showed no differences at the "water line" where excess carbon powder was concentrated.

3. The carbon solubility is far less than the one weight percent used in the typical experiment. This has important implications in an engine. Only very small amounts of carbon, relative to deposited Na_2SO_4, are required to achieve saturation (i.e., unit thermodynamic activity) and hence maximum effect on the rate of corrosion.

For these reasons, the laboratory studies are believed sufficiently representative of engine conditions to yield valid information about the general magnitude of corrosion aggravation caused by a reducing environment.

Typical results for several nickel-base alloys are given in Table I. Clearly, there is a large increase in the rate of corrosive attack in the absence of air (argon atmosphere) which is further increased if carbon is also present. Similar increases in corrosion rate have been observed for aluminide-coated Rene' 77. In one instance, 1500°F for 285 hours, the nominal 2-mil coating was essentially intact in an argon atmosphere test, but about half-penetrated in a matching test with carbon present. On the other hand, the BC21 type coatings survived a variety of tests with carbon present, the advantage over aluminide being of the order of a factor of 6 (per crucible tests.)

The nature of the influence of a reducing environment, be it deletion of air or addition of carbon, is largely an increase in sulfidation rate; i.e., a consequence of the increased sulfur activity accompanying the decreased oxygen activity. Evidence of greatly increased sulfur activity was obtained by analyses of salt slags. In argon-only tests, small amounts of Na_2S were detected; in argon/carbon tests amounts as high as 1.8 mole percent were observed, in accord with the known ability of carbon to reduce alkali sulfates. A secondary effect of Na_2S, a consequence of its strong alkalinity, is that it can function as a flux for acidic-type oxides such as Al_2O_3.*

*In addition, evidence for Na_2O formation was obtained in these tests, based on reactions of the type

$$Na_2SO_4 + 9/2\ Ni \rightarrow Na_2O + 3NiO + 1/2\ Ni_3S_2$$

This compound was actually measured as Na_2CO_3 formed either during air tests or in post-test handling of the slag by reaction with CO_2 in the air. Similar conversion from Na_2O to Na_2CO_3 undoubtedly takes place in an operating engine where the CO_2 level is considerably higher than in ambient air.

In some peripheral experiments, an interesting observation was made in the lower temperature tests where the salt is solid. If carbon powder was uniformly dispersed in the dip-coated salt, the enhanced attack also was uniform. If however, the carbon was in the form of a rod strapped to the specimen, the enhanced attack was localized at the point of contact. This is of importance in the interpretation of engine performance. If operating conditions are such that carbon and Na_2SO_4 deposit simultaneously, or carbon first, enhanced corrosion rates may be expected at any given temperature. On the other hand, if a coherent film of Na_2SO_4 deposits first, and carbon later, the enhancement caused by carbon may be far less at temperatures where the salt is solid (melting point 1620°F). Above the melting point, however, there is sufficient mobility of carbon within the salt such that corrosion rates will be independent of the sequence of deposition.

One other peripheral experiment should be mentioned in which carbon powder was added to Na_2SO_4 and exposed with a test specimen in air at 1650°F. The carbon burned off in less than two hours, and was replenished periodically. The total corrosion (mils penetration) for Rene' 80 and U500 specimens was at least a factor of 10 greater than for the corresponding case without carbon. This demonstrates that corrosion rates are increased by local reducing conditions even in a nominally oxidizing environment. It must be emphasized that in an engine, chemical equilibrium in the combustion products is not necessarily attained. As noted above, carbon deposits have been observed on components when it was certain that excess air was present during operation. It is similarly possible that combustion equilibrium may not be attained even if particulate carbon is absent. Carbon monoxide and possibly other reducing gases may be present which could create a reducing condition on the metal surface analogous to the argon atmosphere tests typified in Table I. Whether chemical reduction actually occurs depends on the kinetics of reaction between the reducing gases and corrodants on the metal surface relative to other possible reactions. These possibilities can be collectively described as a series of "shades of gray" in which there is a continuous range of oxidizing → reducing conditions which undoubtedly involve a complex interaction of combustion temperature, type of fuel, air/fuel ratio, aerodynamic and design differences. Further progress in understanding will involve detailed studies of combustion chemistry both in actual engines and in the burner rigs used to evaluate materials.

EFFECTS OF SUBSTRATE ALLOY

The development of high strength superalloys has, in recent years, given more emphasis to improved environmental resistance as part of the overall goal to be achieved. This has been difficult in view of the need to reduce chromium levels for increased strength. Nevertheless, the

Table I
Effect of Reducing Environment in Na_2SO_4 Hot Corrosion

Alloy	Temperature °F	Hours	Maximum Affected Depth, mils		
			Air	Argon	Argon + Carbon
U500	1400	500		0.4	6.9
Rene' 77	1400	500		0.5	7.8
U500	1500	500		2.4	>5.4
Rene' 77	1500	285		1.0	>7.0
Rene' 80	1500	500		2.2	>4.7
U500	1650	100	0.7	>20.0	53.
Rene' 77	1650	72	32.		66.
Rene' 80	1650	100	2.1	>15.	36.
Inco 738	1650	100	1.0		19.

See Appendix for alloy compositions.

reliance on the superalloy itself for inherent corrosion protection has been considered necessary because coatings can be penetrated by FOD (foreign object damage) and, after a time, by the environment itself. The substrate alloy in combination with a coating can be considered as having a composite behavior in a corrosive environment, with the coating serving to provide extended life.

Extensive corrosion testing on four high-strength, nickel-base alloys was conducted in environments considered relevant to an LM2500 shipboard application. The alloys were Rene' 77, Rene' 80, U500 and IN738. Crucible tests of these alloys in air and argon were described above and the corrosion penetrations listed in Table I. Rene' 77 showed appreciably more corrosive attack than the other alloys. The corrosion was considerably greater in the reducing environment, which had a greater relative effect on the more resistant alloys.

Tunnel tests (described in Ref. 16) of Rene' 77 and Rene' 80 conducted at 1600°F, using 5 ppm sea salt injected with the air and JP5 referee fuel, confirmed the ranking of the crucible tests. Figure 6 shows graphically the data points for the period of time each alloy was exposed.

Shipboard engine tests confirmed the difference between Rene' 77 and Rene' 80 with coatings applied. LM2500 buckets of each alloy were coated with General Electric's BC21 coating and placed in the same engine. Coatings from 0.001-0.0035 inch acted to prevent penetration of the base metal for periods of time depending on thickness. The duration and severity of the test was such as to cause penetration into the substrate only in one small area of the bucket, while in other areas the coating was unattacked. The unattacked surface provided the reference for the original coating thickness.

Figure 7 shows the base metal penetration for this 3600-hour test as a function of coating thickness. After the thinnest coating on the Rene' 80 buckets was penetrated, the penetration into the base metal was such as to reach about a 10-mil depth in the test time remaining; however, the Rene' 77 was penetrated 20-30 mils in the shorter time remaining after penetration of a thicker coating. This analysis assumes a relationship between exposure time and coating thickness penetration which probably exists. Thus, engine experience has confirmed the alloy rankings by tunnel tests, and also the importance of having good resistance in the superalloy under a coating.

A similar difference in alloy behavior has been seen in a helicopter engine. The T58 ingests large and variable quantities of salt (and particulates) in Navy service. In a 146-hour Navy engine test with about 250 ppb sea salt ingestion using JP5 referee fuel, an aluminide-coated IN713 nozzle showed some corrosion blistering and attack to the base metal. A cobalt-base X40 vane included in the test was not corroded. Aluminide-coated buckets of SEL and Rene' 80 alloys were compared, and the latter was found slightly more resistant. The behavior corroborated separate

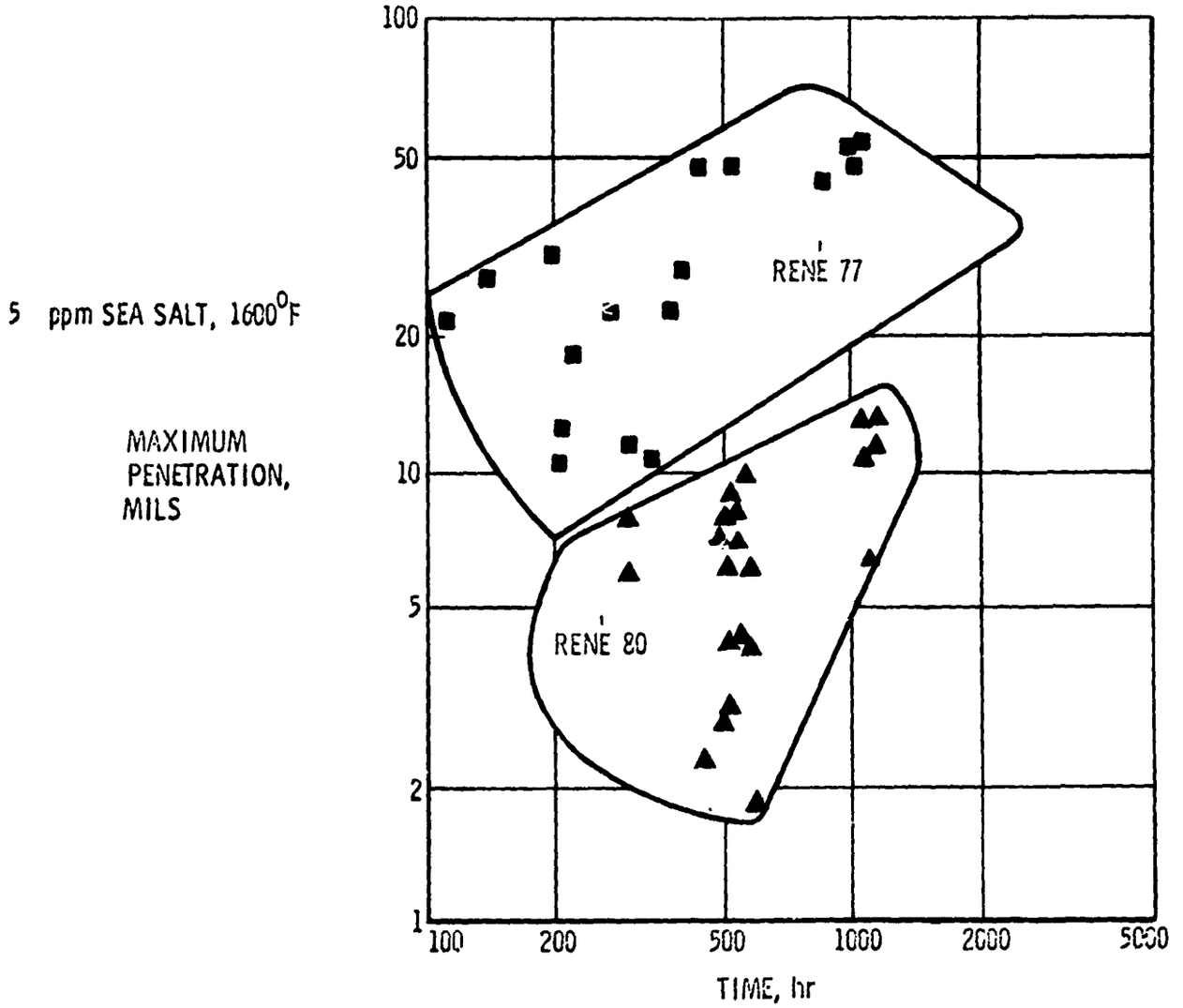

Figure 6. Flame Tunnel Data.

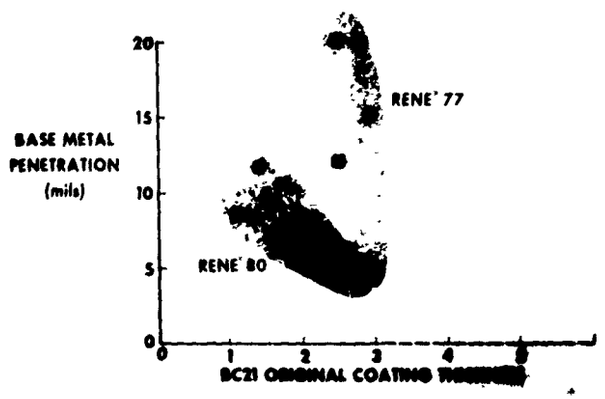

Figure 7. Comparison of BC21 on Rene' 77 and Rene' 80 in long-time corrosion penetration test.

laboratory tunnel-ranking tests of the alloys and aluminide-coated alloys.

PROTECTION FROM COATINGS

Extended life is available through coatings. The most common type is the simple aluminide coating formed by diffusion of aluminum, or aluminum plus other minor additions, with the substrate superalloy. Its corrosion features are, in part, determined by substrate chemistry, and its structure generally consists of a β-NiAl or β-CoAl as an additive layer over a diffusion zone. The β-NiAl seldom shows the presence of sulfides but prolonged oxidation depletes the Al level, forming patches of Ni_3Al which are rapidly corroded. Thus, life extension depends on the concentration of Al in the original coating, the rate at which it is lost to the scale, and the removal rate of the scale.

The addition of Al_2O_3 particles in General Electric's Codep (aluminide) coating (Fig. 8) has been found to delay the onset of corrosion in certain cases relative to the Codep coating without Al_2O_3 particles. Its effect with Rene' 80 is quite pronounced in a 1700°F, 5-ppm-salt tunnel test. The average time to the first sign of corrosive attack was extended from 265 hours to 385 hours in this test. There are several theories of why the alumina particles are beneficial, but the proofs have been evasive. They probably act to cause better retention of surface oxide films. Codep coatings containing the Al_2O_3 particles have shown excellent performance in fighter aircraft and helicopter engines.

In LM2500 shipboard engine tests, Codep-coated X40 and Rene' 77, and another aluminide coating on Rene' 77 showed variable results depending on environmental severity. The aluminide performed well on the stage-1 X40 vanes, although the metal temperature is moderately high. The part is upstream in the turbine gas and has the best location for condensing out quantities of salt. Because of power cycling, the quantities of salt condensed during cruise are not known, but, in any case, the good performance is not surprising in view of the greater resistance of the higher Cr-containing cobalt alloy with the aluminide. Coated Rene' 77 used in the stage-2 vane was also protected. It showed little corrosion in tests at 3600 hours.

The corrosive attack on the Rene' 77 stage-1 bucket was severe when coated with aluminide (Figs. 2 and 4). The environmental factors that produced this condition will be discussed below; however, the coating penetration was influenced by the type of fuel used. Coating penetration (1.7-mil coating) with marine diesel fuel was estimated at 900 hours and with Navy distillate fuel, 400 hours.

To accommodate the more severe environmental attack at the stage-1 turbine buckets, Rene' 80 was introduced in place of Rene' 77, and the General Electric BC21 coating was developed. Aside from being resistant to Na_2SO_4 with either fuel, the coating has a very close thermal expansion match to Rene' 80. In engine tests aboard ship, the BC21-coated Rene' 80 buckets resist attack and penetration for thousands of hours.

An interesting feature of the BC21-coated buckets was the mode of attack when it occurred. In severe environments, attack with less resistant coatings festered so grossly that it was difficult to see patterns and differences which could be interpreted from a mechanistic viewpoint. With the more resistant BC21 coating, it took much longer for changes to develop, and in the time of a given engine test program, only spotty areas showed corrosive attack at all. These areas could be studied with greater definition.

Figure 8. Structure of a Codep coating with Al_2O_3 particles embedded (500X).

The corrosion pattern was interesting from two points of view: the differences in envrionment from area to area of the airfoil, and the mechanism of coating degradation. Figure 9 shows the appearance of an early BC21-coated Rene' 77 bucket exposed long enough in a severe test to corrode the base metal. Also shown diagrammatically are the variations in the gas stream. The corroded area on the concave face corresponds to a cool region of metal temperature resulting from the configuration of internal, labyrinthal cooling chambers. The corresponding area on the convex face has a similar cold spot, but no corrosion appears. The gas stream undergoes a 4-atmosphere drop in pressure from concave to convex side of the bucket and there are gas temperature variations as indicated.

Prior to dissection, the surfaces were analyzed for water-soluble compounds. The concave face had 4-10 times the SO_4 ion concentration than the convex face. The lower half of the concave face had twice the SO_4 concentration as the upper half, while the leading edge half and trailing edge half showed about equal concentrations. Also, the area of the corroded cold spot showed about the same concentration as the concave area surrounding the cold spot. Borescope pictures taken throughout the test period showed that the oval spot near the trailing edge and airfoil tip developed first.

Figure 10 shows the degree of corrosive attack around the airfoil in terms of an arbitrary rating index. In the worst areas the base metal has been penetrated. In the best areas, it is difficult to see that the coating has changed as a result of exposure. The thickness appears to have been undiminished. The coating surrounding the penetrated regions was particularly interesting because the microstructure indicated something of the corrosion mechanism.

The BC21 coating has two phases, an Al-rich, Cr-lean insular phase in an Al-lean, Cr-rich matrix phase. The low solubility of Cr in the insular phase has forced the Cr to an unusually high level in the matrix. Before corrosion occurs in a given region, the insular phase disappears and the Cr level of the remaining single-phase region drops. It appears as though the degradation mechanism involves a depletion of Al to a surface oxide until the Al-rich phase is dissipated and disappears. This dilutes the Cr level in the matrix; however, with full dilution to the nominal Cr level, the coating still appears to resist corrosion.

The process described was studied by exposing coated Rene' 77 and Rene' 80 pins, and also cast coating alloy pins in Na_2SO_4 crucible tests at 1650°F. The dissipation of the insular phase was reproduced (Figs. 11a and 11b). The roles of Al and Cr were partially clarified by observations of Al and Cr oxides, and Cr and other sulfides in the corroded

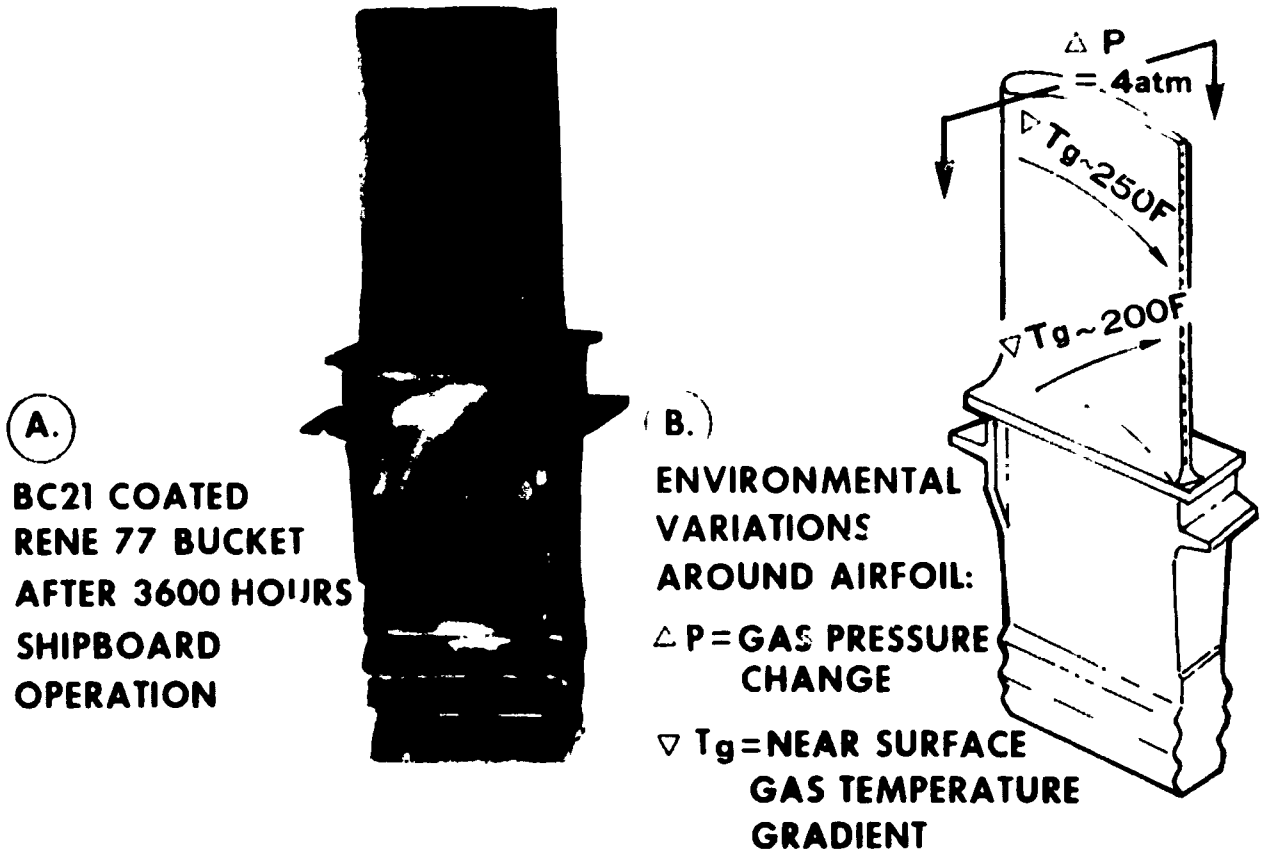

Figure 9.

surface regions. As shown, the reducing environment produced substantially greater corrosion.

TECHNICAL DISCUSSION

The occurrence and distribution of hot corrosion within an engine depend on a variety of factors which influence kinetics. These include:

Temperatures, metal and gas
Gas pressure
Oxygen partial pressure; fuel combustion efficiency
Type of fuel
Quantity of condensed Na_2SO_4
Residence time of deposited salt on metal surface.

All of these have been considered in the preceding text; however, in attempting to apply combinations of these variables to the explanation of any specific instance of materials performance, certain limitations should be pointed out.

Fuel combustion efficiency: Only limited information is available concerning the chemical composition of combustion products. This clearly is a function of engine design, fuel/air ratio, type of fuel and power setting. The only certain observation is that the presence of particulate carbon deposited on metal surfaces indicates or can cause a reducing condition which is deleterious if salts have also deposited; however, the absence of carbon deposits should not be construed as evidence for oxidizing conditions on a local scale.

Deposition of Na_2SO_4: The uncertainties in using predicted condensation conditions have been reviewed above. Nevertheless the new data presented herein fulfill three useful functions:

1. They remove, to a large extent, the disagreement between engine experience and prior predictions.

2. In a marine environment, hot corrosion must be accepted as an inevitable possibility, to be minimized by design and/or materials/coatings improvements. Thus, the new data provide useful input for tradeoff studies between design and materials applications.

3. They permit plausible explanations for a variety of specific examples of materials performance in a marine environment.

The first-stage, high-pressure turbine blades in the LM2500 engine provide an interesting example. Although

the actual average salt ingestion level in the shipboard tests is not available, the condensation requirements shown in Fig. 5 are consistent with the observation that the central portion of the airfoil concave surface may, at steady-state operating conditions, allow Na_2SO_4 deposition. On the other hand, regions nearer the edges are at higher temperature, and the convex surface sees a lower gas pressure. Hence, deposition may not occur in those areas at steady state and this is consistent with observations of no corrosion in these areas. It is postulated that salt measured in these regions deposited primarily during a final idling and shutdown cycle. Stated another way, interpretation of corrosion behavior requires not only information of the *amount* of deposited salt, but its *residence time* on a given surface.

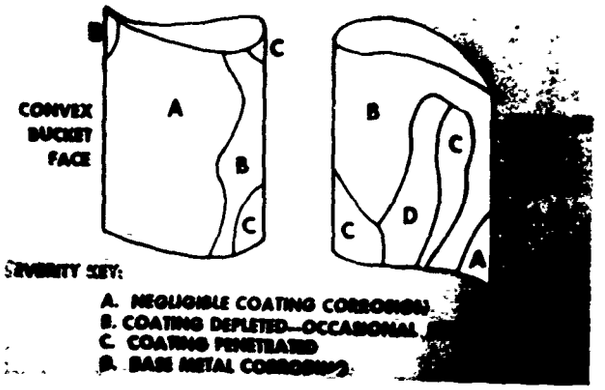

Figure 10. Degrees of corrosive attack after long-time engine operation—BC21 coating on Rene' 77.

Further, a steady-state film thickness probably forms when deposition occur at cruise conditions, with loss rates by evaporation balancing the continuing input.

First-stage vanes in the LM2500 generally show at least as much deposited salt (but little corrosion) in spite of temperatures somewhat higher than the first-stage blades. Since they are a bit upstream, this may be the result of higher pressure, higher salt concentration, or alternatively may be a consequence of slow cooling through the idle and shutdown procedure. Second-stage blades, on the other hand, generally show little or no salt deposits. These components are slightly downstream and thus are at a lower pressure, and are exposed to less salt by the amounts deposited under cruise conditions on upstream components. This latter factor, however, is invalid if the notion of steady-state salt-film thickness is correct.

An alternate view of the LM2500 first-stage blade corrosion pattern derives from Fig. 9b, where the corrosion pattern is related to gas and metal conditions on an airfoil area basis. Information has appeared in the literature (17) that if internally cooled metal components are subjected to a corrosive environment, the rate is not that corresponding to the metal temperature, but more nearly corresponds to the temperature of the gaseous environment. An analysis was made of the LM2500/stage-1 bucket by mapping both gas temperatures and metal temperatures over the airfoil surface. The closest fit to the corrosion pattern was the gas-metal temperature difference, a ΔT effect. The areas where the gas temperature was high and the metal temperature was low were corroded most.

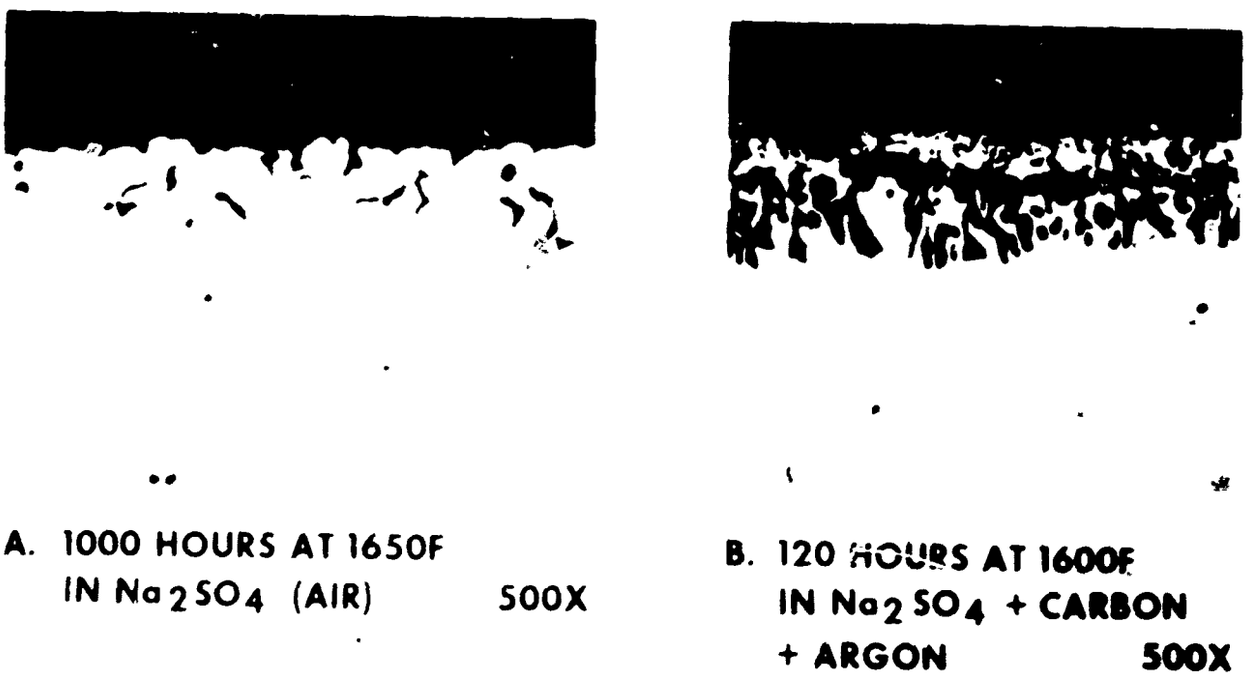

Figure 11. Cast coating alloys exposed in crucible corrosion test.

A choice cannot be made between these two alternative interpretations at this time. In any event, the situation can and has been alleviated with improved materials.

The performance of BC21-coated Rene' 80 in this tough environment relates in part to the reservoirs of Al and Cr in the coating that participate in the protective mechanism. The rates by which the coating oxides are removed and the Cr depleted by S are more favorable than for most other coatings examined. At low temperatures, say 1200°F and below, it is estimated that reaction rates will become sufficiently low so that corrosion there will be inconsequential. At higher temperatures, Fig. 5 indicates that a temperature will be reached above which the Na_2SO_4 would not condense or would evaporate. It is only in a narrow band of operating conditions that the corrosion rates are significant, and the BC21 coating is adequately protective in this range.

Good performance is also attributed, in part, to the close match in thermal expansion coefficient between BC21 and Rene' 80. Cyclic thermal strains across the substrate-coating interface become minimized and are considered to reduce coating crack tendencies, particularly in cycling to temperatures below 1200°F where the coating has little ductility.

In applications less severe because of lower salt ingestion, or because operation is mainly above the appropriate condensation curve of Fig. 5, or because operation is mainly below temperatures at which corrosion reaction rates are significant, the aluminide coatings provide fully adequate protection. These conditions exist in most components, even in the shipboard engines like the LM2500, and also in aircraft engines.

DIRECTIONS FOR FURTHER WORK

Before identifying the need new or continued technical programs, the following is a summary of the current status of coatings. It is presented in terms of families of coatings and alloys, although others of the same generic class of materials should fit the pattern too.

Table II
Current Status of Coating Types

Status	Codep	BC21
Protection–mild or moderate environment	Good	Good
Protection–severe environment	Limited	Good
Cost	Low	Medium
Widespread production capability	Yes	No
Investment for overhaul shops	Modest	High

With this chart in mind, the following are indicated as directions for further technical effort:

1. A coating significantly superior to BC21 for future shipboard applications demanding longer TBO. Applications with TBO exceeding 15,000 hours represents a next target. With severe environments anticipated for some components and with distillate fuels, an improved coating may be needed.

2. A lower cost and more efficient process than that utilized for BC21 and/or an improved coating.

3. Laboratory studies of gas-metal and salt-scale-metal reactions. These studies would develop the understanding in support of improved coating design.

4. Measurements of salt ingested into turbines, and combustion reactions in turbines in a given application under power cycling. Salt measurements would better define the environmental regimes that could be plotted in Fig. 5 for assessment of when condensation will occur or how to avoid it. The combustion reactions would relate to the effects of reducing environments on hot corrosion.

CONCLUSIONS

Corrosion patterns appearing in engines can be explained on the basis of operating conditions and local component environments. The explanations are aided by new information that Na_2SO_4 condenses at higher temperatures and lower concentrations than had been hitherto recognized. Reducing conditions in engines are identified by the occasional appearance of carbon deposits, but better measurements are needed to define the effects precisely.

Engines show varying levels of corrosive attack. For mild conditions aluminide coatings, such as Codep, afford suitable protection and component life in aircraft and shipboard engines. For severe conditions, the BC21-coated Rene' 80 combination resists attack for the thousands of hours required of naval vessel TBO. With increased TBO and performance anticipated for future applications, a coating with greater resistance than BC21 is desired.

ACKNOWLEDGMENT

The helpful contributions and discussions of R. V. Hillery and R. C. Schwab of the Material and Process Technology Laboratories are gratefully acknowledged.

REFERENCES

1. J. E. Newhart, "The Detection of Hot Corrosion-Sulfidation in Navy Aircraft Turbine Engines," presented at the American Society of Nondestructive Testing, Detroit, Michigan, October 1971.
2. M. A. DeCrescente, and N. S. Bornstein, "Formation and Reactivity Thermodynamics of Sodium Sulfate With Gas Turbine Alloys," *Corrosion*, **24**, 127 (1968).

3. J. G. Tschinkel, "Formation of Sodium Sulfate in Gas Turbine Combustors," *Corrosion*, **28**, 161 (1972).
4. H. Liander and G. Olsson, IVA, Tidskrift for Teknisk Vetenskaplig Forskring, p. 145 (1937).
5. C. Kröger and J. Stratmann, Glasstech, Berichte, 34, No. 6, 311 (1961).
6. R. J. Perkins, C. A. Trythall, and R. E. Fryxell, "The Vapor Pressure of Sodium Sulfate from 1750F to 2200F," to be published.
7. A. B. Hedley, "A Study of SO_3 Formation in Pilot Scale Furnace," Proceedings Conference on Corrosion by Fuel Impurities, Wood Engineering Laboratories, Southhampton, England. Butterworth, pp. 204-215 (1963).
8. Military Specification, "Engines, Gas Turbine, Propulsion, and Auxiliary Naval Shipboard," MIL-E-17341C (Ships).
9. E. L. Simons, G. V. Browning, and H. A. Liebhafsky, *Corrosion*, 11 505t (1955).
10. G. Llewellyn, "Protection of Nickel-Base Alloys Against Sulfur Corrosion by Pack Aluminizing," in "Hot Corrosion Problems Associated with Gas Turbines," ASTM Special Technical Publication No. 421, Philadelphia, June 1966, page 3.
11. A. V. Dean, "Investigation Into the Resistance of Various Nickel and Cobalt-Base Alloys to Sea Salt Corrosion at Elevated Temperatures," NGTE Report, January 1964.
12. W. L. Wheatfall, H. Doering, and G. J. Danek, Jr., "Behavior of Superalloy Oxide Films in Molten Salts," in "Hot Corrosion Problems Associated with Gas Turbines," loc. cit., page 206-222.
13. A. U. Seybolt, "Na_2SO_4–Superalloys Corrosion Mechanism," General Electric Company, Research and Development Center, Report No. 70-C-189, June 1970.
14. B. O. Buckland, C. M. Gardiner, and D. G. Sanders, "Residual Fuel-Oil Ash Corrosion," ASME Paper A-52-161, New York, 1952.
15. S. G. Morgan and A. W. Lamport, "Gas Turbines in the Royal Navy, 1965-1969," ASME Paper 70-GT-10, Gas Turbine Conference, Brussels, May 1970.
16. H. E. Doering and P. A. Bergman, "Construction and Operation of a Hot Corrosion Test Facility," *Materials Research and Standards*, Vol. 9, No. 9, September 1969.
17. S. Y. Lee and W. E. Young, "Corrosion Testing of High Temperature Gas Turbine Alloys," *Combustion and Heat Transfer in Gas Turbine Systems*, Pergamon Press, 1971, pages 253-290.

Appendix

CHEMICAL COMPOSITIONS OF SUBSTRATE ALLOYS (Minor elements excluded)

Element	Rene' 77 w/o	Rene' 80 w/o	IN738 w/o	U500 w/o	X40 w/o
Co	15.0	9.5	8.5	18.5	Bal.
Cr	14.6	14.0	16.0	18.5	25.0
Al	4.3	3.0	3.4	3.0	–
Ti	3.35	5.0	3.4	3.0	–
Mo	4.2	4.0	1.75	4.0	–
W	–	4.0	2.6	–	7.5
Ta	–	–	1.75	–	–
Ni	Bal.	Bal.	Bal.	Bal.	10.5
Fe	–	–	–	2.0	2.0

Materials and Coatings for Gas Turbine Hot-Section Components

G. W. Goward
Pratt and Whitney Aircraft
East Hartford, Connecticut

INTRODUCTION

Reasons for the occurrence of hot corrosion degradation of gas turbine hardware under marine operating conditions have been covered in detail in other presentations at this conference. Briefly, then, hot corrosion is caused by the fluxing of normally protective oxide scales by molten salts, principally sodium sulfate, of either high or low oxide ion activity as exemplified in Fig. 1 for aluminum oxide. As originally proposed by Bornstein and DeCrescente (1) oxides such as aluminum oxide can dissolve in sodium sulfate of sufficiently high oxide ion activity. The underlying metal then undergoes accelerated oxidation because of either thinning or complete absence of a protective oxide (2). It is further proposed (1-3) that the oxide ion activity is increased because of removal of sulfur from the sodium sulfate to form sulfides in the surface of the underlying metal. Formation of sulfides requires a low oxygen activity which is the condition at the oxide-metal interface; the process therefore requires transport of sulfur through the oxide scale.

Pettit, Goebel and Goward (3) and others propose that some normally protective oxides can also be fluxed or dissolved by molten media having sufficiently low oxide ion activity or in equivalent terminology, high acidity. Oxides of elements such as molybdenum, tungsten and vanadium, which are strong oxide ion acceptors, or strongly acidic oxides, constitute the origins of this high acidity. These elements, particularly molybdenum and tungsten, are normal constituents of superalloys used in gas turbines and vanadium is a natural contaminant in several types of fuels.

Chromium, either in the base material or externally applied, inhibits what has now been defined as basic hot corrosion. As suggested by Bornstein and DeCrescente (1) this seems to be because it is an acceptor of oxide ions and thus reduces the basicity of high oxide ion containing melts. Whether or not chromium inhibits so called acidic hot corrosion is still open to question. The reported moderately good resistance to Na_2SO_4-V_2O_5 attack of nickel base alloys with high chromium contents suggests that chromium may also inhibit this type of corrosion to some extent.

BASE METALS AND THEIR PROBLEMS

Early nickel base superalloys such as Nimonic 80A and Waspalloy contained substantial amounts of chromium and therefore derived oxidation resistance by the formation of chromium-rich protective oxides. These high chromium contents also conferred a reasonable degree of hot corrosion resistance, at least of the basic fluxing type, upon these alloys. However, as illustrated in Fig. 2, strength increases required for modern aircraft gas turbines caused decreases in chromium contents and increases in the contents of aluminum and acidic oxide forming elements such as molybdenum and tungsten. Only recently, in the face of increasingly severe hot corrosion problems has this trend been reversed with the development of more hot corrosion resistant alloys such as INCO 738 and 792. In general, cobalt-base alloys, usually used for turbine vanes, have retained the high chromium content and correspondingly high resistance to hot corrosion, although information presented later in this paper will suggest that, at least for basic fluxing hot corrosion, the resistance of these alloys may originate in the cobalt base as well as in the high chromium content.

PROTECTION WITH COATINGS

While coatings would be required to extend the life of superalloy airfoils from simple oxidation processes at the operating temperatures of modern naval aircraft, the requirement is much more compelling in the face of the possible extent of hot corrosion degradation of airfoils operating in an environment contaminated with sea salt and/or other contaminants such as vanadium and lead. For these reasons Pratt and Whitney Aircraft first used coatings for the protection of WI52 first stage vanes from oxidation attack, and then in sequence on Udimet 700 and B-1900 first stage blades. Higher operating temperatures in commercial and military engines and the extra severity of salt and fuel contaminant corrosion provided the impetus for the development of the CoCrAlY series of coatings first put in service in 1970.

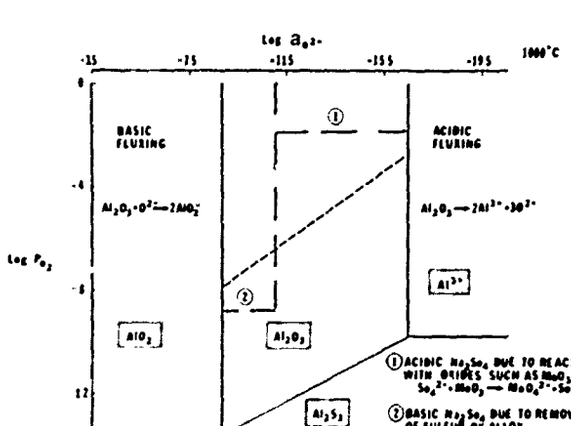

Figure 1. Illustration of fluxing or dissolution of Al_2O_3 by basic (high oxide ion concentration) and acidic (low oxide ion concentration) Na_2SO_4. Region of stability of Al_2O_3 in "neutral" Na_2SO_4 is also indicated.

THE NATURE AND PERFORMANCE OF DIFFUSION COATINGS

The first practical coating for nickel and cobalt-base superalloys were based on the intermetallic compounds NiAl and CoAl, respectively, produced by elevated temperature diffusional interaction of aluminum with the substrate alloys.

The large number of patents issued on this type of coating and the number of proprietary coatings marketed and used, particularly on nickel-base alloys, suggests a large number of variations on this theme. It has been proposed, however, by Goward et al (4,5) that there are only two basic types of the so-called diffusion aluminide coatings possible

BLADE ALLOY COMPOSITIONS

	Al	Cr	Ti	Mo	Ta	Co	C	Ni
WASPALOY	1.3	19	3.0	4.3		13	.08	BAL
UDIMET 700	4.3	15	3.5	5.2		19	.08	BAL
B-1900	6.0	8.0	1.0	6.0	4.0	10	.10	BAL
NASA IVA	5.5	6.0	1.0	2.0	9.0	7.5	.13	BAL
INCO 738	3.4	16	3.4	1.7	1.7	8.5	.17	BAL

Figure 2. Historical progression of nickel base blade alloy compositions. The trend toward decreasing hot corrosion resistance is reversed with INCO 738.

on at least nickel and probably also on cobalt-base alloys. These archetypes are shown in Fig. 3 and are designated as inward diffusion and outward diffusion types. As explained elsewhere (4,5) the two basic structures are produced by the virtually unidirectional motion of nickel or aluminum which occurs in the intermetallic compounds involved in the initial formation of the coatings. This postulate seems to hold true regardless of the type of processing used to synthesize the coating and whether or not the coatings are modified with other elements such as chromium, in single step or two step processes.

It is generally agreed that these coatings derive their protectivity from the formation of protective Al_2O_3 scales (4,6) and the coatings can therefore be considered to be aluminum reservoirs. Degradation of these coatings involves, in relatively clean environments, loss of aluminum through repetitive formation and thermal cyclic spalling of Al_2O_3 and subsequently less protective oxides. While these coatings, typified by a slurry aluminum-silicon system in wide use at Pratt and Whitney for a decade, also provide

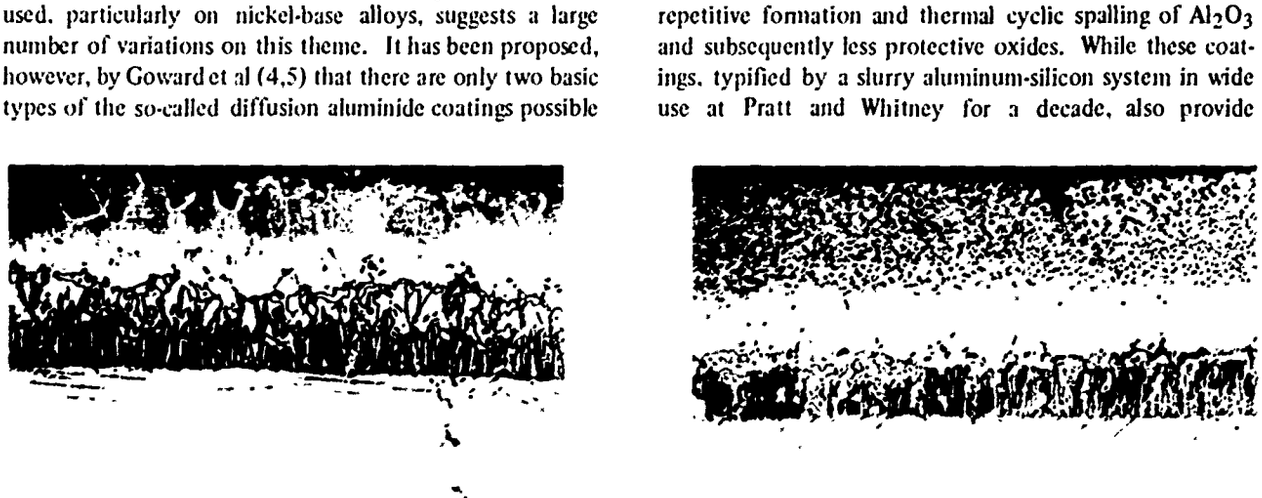

Figure 3. Archetypical diffusion aluminide coatings formed by outward diffusion of nickel (left) and inward diffusion of aluminum (right). (500X)

economicaliy useful protection from hot corrosion in contamir.ated environments, sodium sulfate, for example does accelerate degradation of the coatings and substantially shortens their useful lives. The mechanism of hot corrosion degradation is presumed to be similar in principle to that previously described, i.e., initiated by oxide fluxing, although mechanistic studies on these more complex systems are still to be performed.

Insofar as effects of diffusion coatings on superalloy mechanical properties are concerned, the situation can be briefly summed up as follows:

1. Properly matched to the alloy heat treatment, diffusion coatings cause no debit in creep properties other than those accountable for by loss in load bearing area; beneficial effects of coatings on creep properties have been observed as shown in Fig. 4.

2. The relatively inflexible brittle-ductile transition temperature of these coatings governs their effect on thermally induced fatigue–if blade design allows thermal strains to peak above the transition temperature (Fig. 5) coatings can improve thermal fatigue life; if the opposite occurs. i.e. strain peaking in the brittle region, blade life can be shortened.

3. Properly designed coatings can increase high frequency fatigue strength over some range of temperature (Fig. 6) (7); debits in HFF strength when encountered are usually tolerable.

LIMITATIONS OF CLASSICAL DIFFUSION COATINGS

Under severe hot corrosion conditions, for example for aircraft engines operating in a marine environment or for engines adapted to ship propulsion, the hot corrosion lives of these coatings are frequently unacceptably short. Although additions of certain elements, such as chromium, appear to improve hot corrosion protectivity, the benefits to be gained have generally not proved to be cost effective over the required range of conditions.

After several years of relatively unproductive testing of modified diffusion coatings, in 1965 Pratt and Whitney initiated a program to develop a so-called overlay coating of composition specifically designed to combat hot corrosion degradation.

DEVELOPMENT OF CoCrAlY OVERLAY COATINGS

The initial product of this development program, an iron-chromium-aluminum-yttrium coating proved to have significantly greater hot corrosion resistance than the P & WA slurry diffusion coating, particularly at intermediate temperatures. This coating was however, less diffusionally stable than desired in the 1900-2000°F range. A search for a better balance between intermediate temperature corrosion performance and higher temperature diffusional stability with attendant desirable oxidation properties, led to the development of the CoCrAlY series of coatings. This development was aided in part by a NASA contract (8).

The rationale behind the development improved performance of this coating will now be discussed in some detail. It is obvious that all of the following points were not known during the early development stages but they do now tend to fall into place and serve a useful purpose of describing the properties of the coating system and perhaps suggesting a line of reasoning for future development programs.

	1400°F			1800°F		
	HOURS TO RUPTURE	HOURS TO 1% CREEP	% ELONG	HOURS TO RUPTURE	HOURS TO 1% CREEP	% ELONG
UNCOATED						
ALLOY 1	38-207	—	04-08	20-68	18-60	13-15
ALLOY 2	162-222	68-12	39-70	104-119	27-29	100
COATED						
ALLOY 1	483-548	245-325	18-21	67-137	38-65	29-46
ALLOY 2	365-464	22-24	89-100	78-99	21-22	100
STRESSES (ksi)						
ALLOY 1		80			25	
ALLOY 2		100			30	

Figure 4. Effects of diffusion coatings on creep rupture properties of typical nickel base alloys. All results are corrected for loss of load bearing area consumed by coating formation.

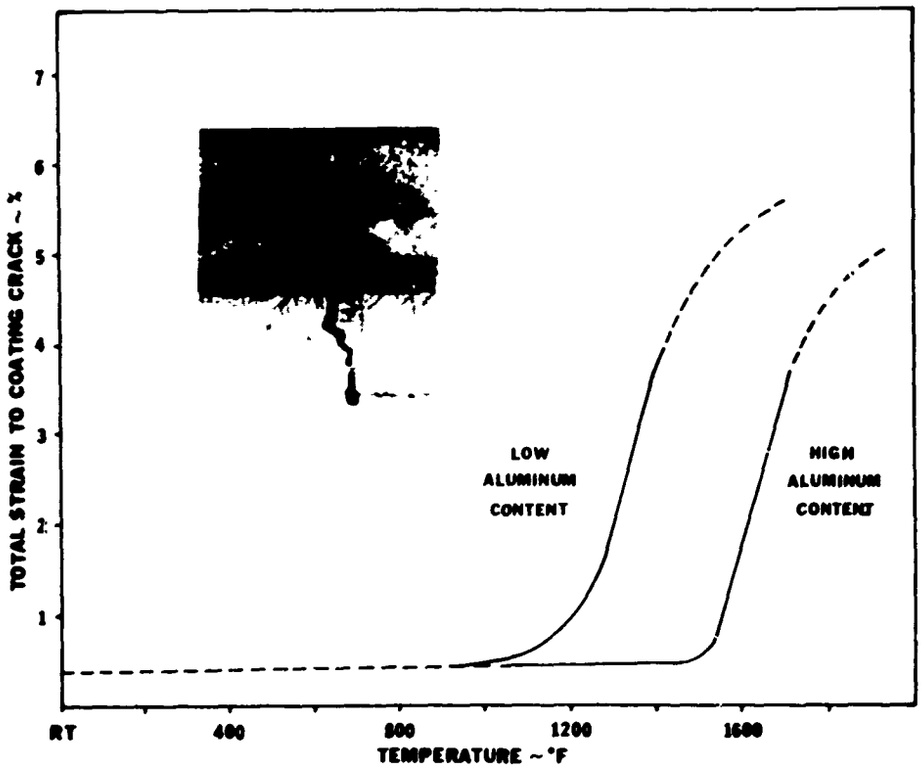

Figure 5. Brittle-ductile transition behavior of a diffusion aluminide coating. Inset illustrates transgranular cracking mode at low temperatures.

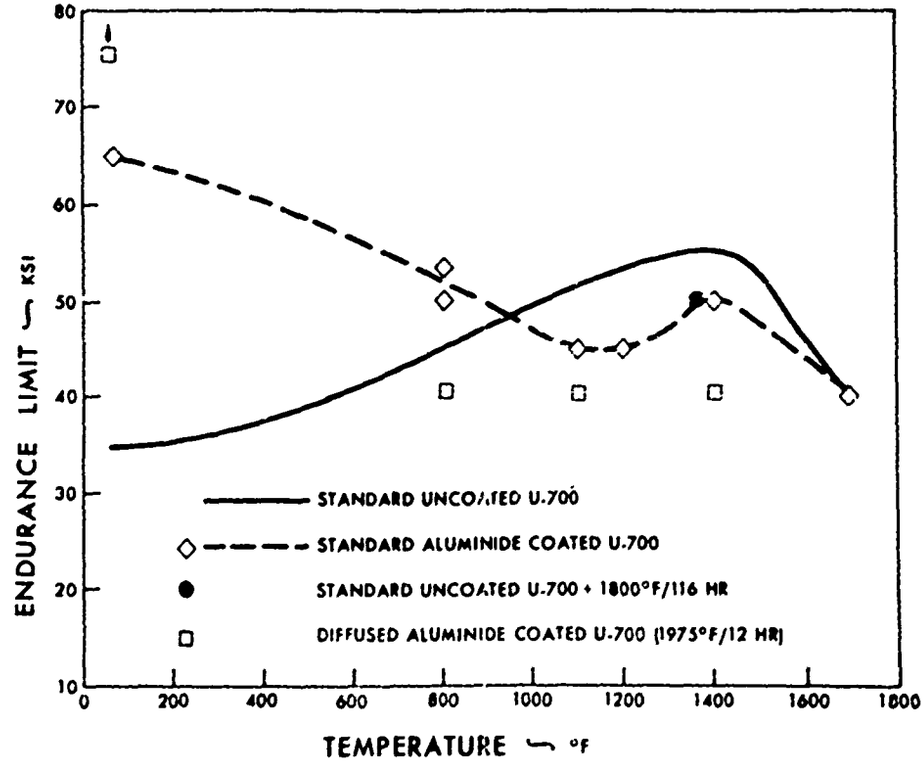

Figure 6. Effects of a diffusion coating on high frequency fatigue strength of a nickel-base alloy.

HOT CORROSION RESISTANCE OF COBALT vs. NICKEL-BASE ALLOYS

Figures 7 through 10 illustrate an apparent fundamental property of Co-Cr-Al in comparison to Ni-Cr-Al alloys. Cobalt and nickel-base alloys of identical composition were rig hot corrosion tested, in the uncoated and diffusion coated condition. The photomicrographs clearly show that the cobalt-base alloy, and the coating thereon, are substantially more corrosion resistant than the nickel-base analogues. This simple experiment confirmed previous general observations that CoAl based coatings on cobalt-base vane alloys are more resistant to sea salt induced hot corrosion than are NiAl coatings on nickel-base alloys. The experiment also indicates that differences in chromium content are not the reason for the performance difference. While there is as yet no mechanistic explanation for this advantage of cobalt over nickel-base alloys, it is clear that of the two elements, cobalt is the best choice as the base for a hot corrosion resistant coating. Further studies on this subject are in progress under an Air Force (ARL)–Pratt and Whitney Contract.

ROLE OF ALUMINUM AND CHROMIUM

At this time it is generally agreed that Al_2O_3 is still the best protective oxide available for high temperature (>1800°F) coatings. Figure 11 shows parabolic rate constants for oxide growth derived from isothermal oxidation studies and illustrates that the choice of Al_2O_3 is soundly based. Reason suggests that from a protectivity standpoint, a coating should have the highest possible aluminum content.

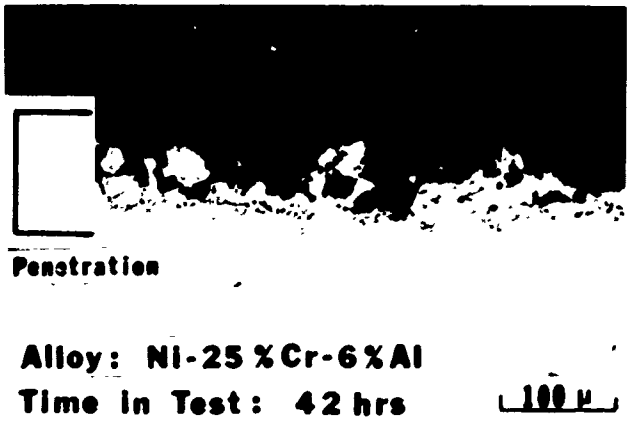

Figure 7. Surface degradation of Ni-25Cr-6Al alloy after 42 hours in cyclic 1800°F, 3.5 ppm sea salt sulfidation test.

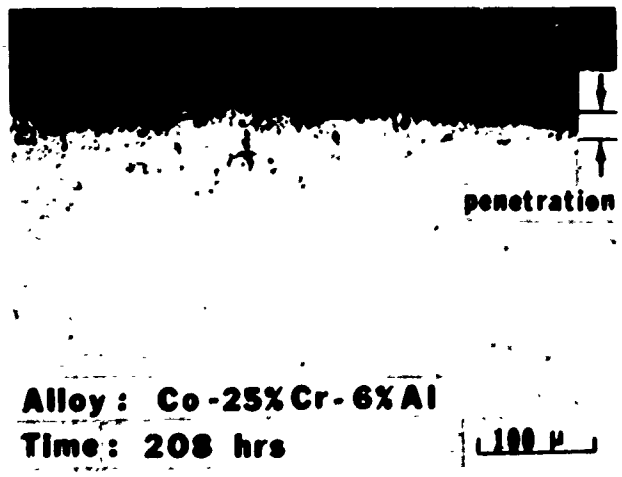

Figure 8. Surface degradation of Co-25Cr-6Al alloy after 208 hours in cyclic 1800°F, 3.5 ppm sea salt sulfidation test. Note substantially less attack than for the corresponding nickel-base alloy in Figure 7.

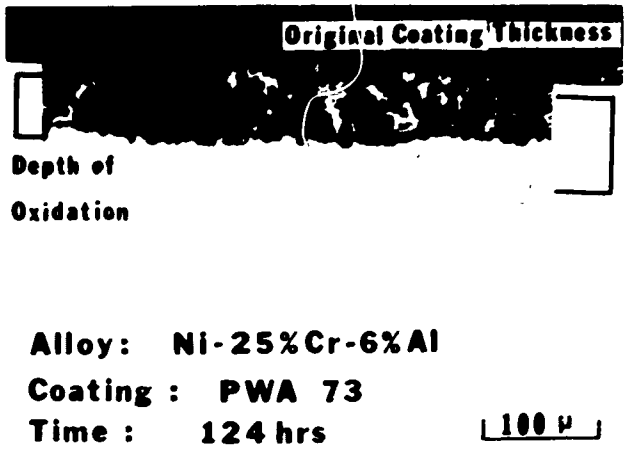

Figure 9. Extent of degradation of aluminide coating on Ni-25Cr-6Al alloy after 124 hours in cyclic 1800°F, 3.5 ppm sea salt sulfidation test.

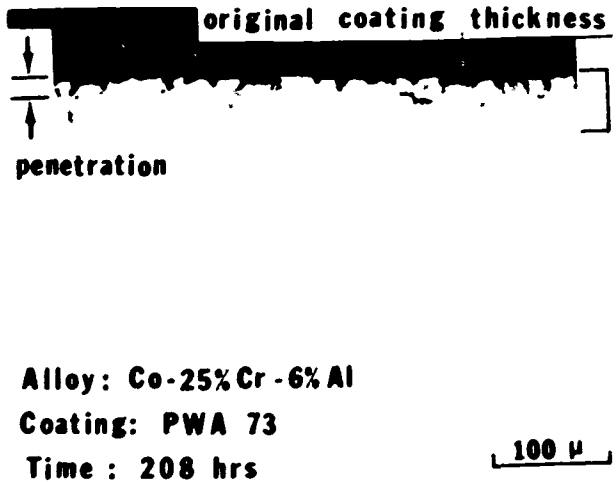

Figure 10. Extent of degradation of aluminide coating on Co-25Cr-6Al alloy after 208 hours in cyclic 1800°F, 3.5 ppm sea salt sulfidation test.

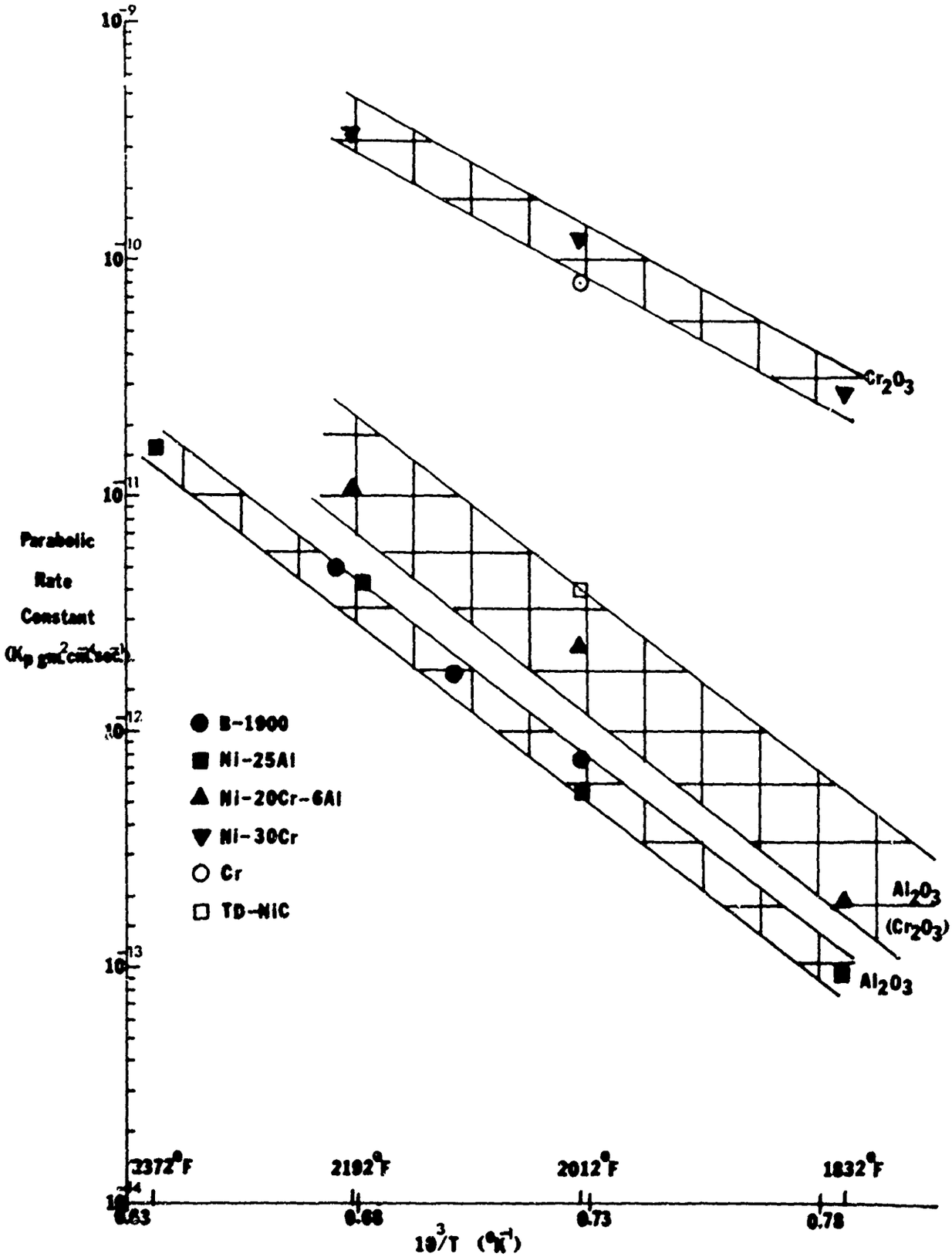

Figure 11. Parabolic rate constants for isothermal growth of Cr_2O_3 and Al_2O_3 protective scales.

From this standpoint a choice of chemistry corresponding to the CoAl intermetallic phase would be indicated, but overlay coating processing limitations and mechanical property effects (to be discussed in a later section of this paper) negate this choice and dictate lower aluminum contents.

Figure 12 shows the results of limited work on the determinations of oxides formed on Co-Cr-Al alloys. This data indicates that chromium promotes alumina formation at aluminum contents lower than those at which this oxide will form on binary Co-Al alloys, probably by mechanisms similar to those described by Pettit and Giggins (9) for Ni-Cr-Al alloys.

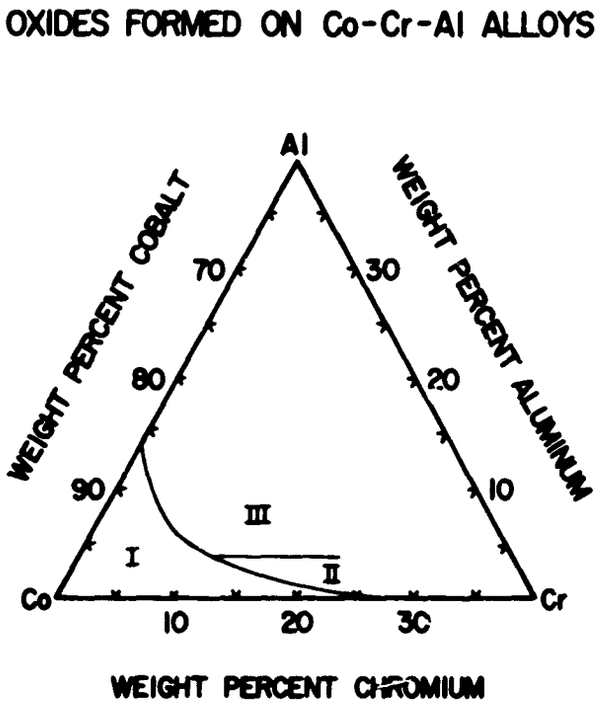

Figure 12. Oxides formed on Co-Cr-Al alloys by isothermal oxidation at 2000°F. Region I–CoO + internal Al_2O_3 and Cr_2O_3; Region II–Cr_2O_3 + internal Al_2O_3; Region III–external Al_2O_3.

Thus, coatings practically useful from the standpoints of processing and mechanical properties can be designed in the nominal range of 10 to 15% aluminum by appropriate additions of chromium. From a great deal of previous work in many laboratories, it is immediately assumed that chromium should also provide additional hot corrosion resistance. Definitive work which allows first principle selections of chromium contents has not yet been performed and so the selection of exact chromium contents has been based largely on empirical development. Adding to these considerations was the prior existence of low aluminum Co-Cr-Al-Y structural alloys of significant hot corrosion resistance developed by Garrett Airesearch (8).

ADHERENCE OF PROTECTIVE Al_2O_3

Collins and Wukusik (11) and others have demonstrated the advantages in cyclic oxidation resistance to be gained by promoting improved oxide (Al_2O_3) adherence by the addition of reactive metals such as yttrium to alumina forming alloys. The beneficial effect is illustrated in Fig. 13; it is reasonably clear that such effects should minimize coating degradation by aluminum depletion caused by oxide spalling under practical gas turbine conditions. Further, since it is believed that hot corrosion via basic fluxing of Al_2O_3 must involve sulfur transport through the oxide scale, it can be theorized that thicker, adherent scales should be more resistant to this type of hot corrosion than the thinner scales which must reform after spalling on coatings which do not form adherent oxides. Stringer (12) has proposed and Tien and Pettit (13), more recently, have demonstrated fairly conclusively that prevention of vacancy condensation at the oxide-metal interface on FeCrAlY alloys is at least one of the major reasons for the oxide adherence effect promoted by reactive elements such as yttrium. Further research is in progress, under an Air Force (ARL)–Pratt and Whitney contract to further elucidate the adherence effect on Co-Cr-Al-(Y) and Ni-Cr-Al-(Y) type alloys.

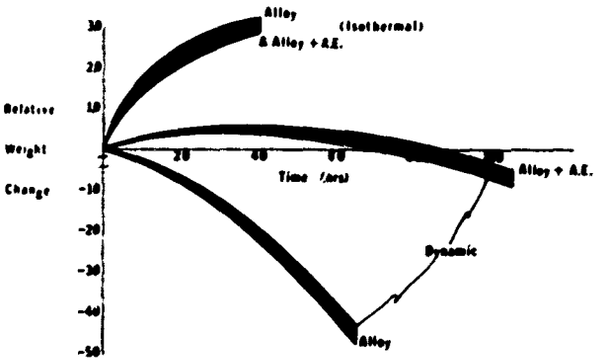

Figure 13. Generalized illustration of effect of active element (A.E.) addition, e.g. yttrium, on adherence of Al_2O_3 scales.

MECHANICAL PROPERTY EFFECTS

Certain design of modern air-cooled hardware can impose peak tensile thermal strains at relatively low temperatures where coatings based on intermetallic matrices such as CoAl and NiAl exhibit brittle behavior. Cyclic tensile strains near to or in excess of the fracture strains of such coatings cause coating cracking in a very few cycles or in the extreme case, one cycle. As would be expected and as will be shown, ductility and/or brittle-ductile transition temperature is a strong function of aluminum content and therefore design of overlay coatings for certain critical application becomes a trade-off between aluminum content, which equates to durability, and ductility which contributes to thermal fatigue resistance.

PROCESSING

After consideration and preliminary testing of a number of possible processing techniques such as foil cladding, plasma spraying and slurry sintering or fusion, induction heated crucible evaporation, and electron beam evaporation, the latter technique was finally developed as the most successful method of coating application. The process is illustrated schematically in Fig. 14. Briefly, a CoCrAlY ingot of composition predetermined to yield the desired coating chemistry, is fed upward into a water cooled copper hearth where it is melted by an impinging electron beam. When pool equilibrium has been reached with respect to the varying vapor pressures of the component elements, clusters of blades or vanes are inserted through a load lock over the molten pool. Coating is deposited on the slowly rotated parts held at elevated temperature by a radiant heater. The parts are withdrawn and subjected to post-coating processing, including heat treatment to produce the structure shown in Fig. 15.

PROPERTIES OF CoCrAlY COATINGS

HOT CORROSION RESISTANCE

A general comparison of the hot corrosion resistance (sea salt contamination) of CoCrAlY coatings and a diffusion coating (JoCoat) is given in Fig. 16. As expected, durability, which must sometimes be traded off with ductility (fatigue), is strongly affected by aluminum content. Also, in rig testing, and tentatively confirmed in engine tests, the relative durability increases markedly with decreasing temperature. Field evaluation has confirmed the advantages shown by the rig tests (Fig. 17) although it will require several more years to determine relative performances under a variety of conditions.

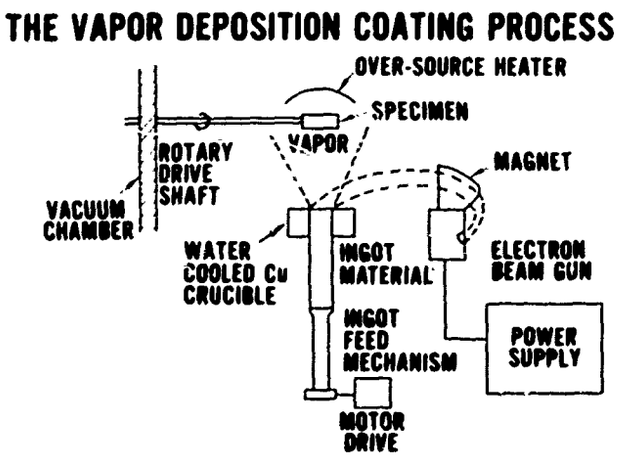

Figure 14. Schematic illustration of the electron beam vapor deposition coating process.

Figure 15. Typical fully processed CoCrAlY coating illustrating two phase structure–β (CoAl) (dark phase) and γ (Co solid solution) light phase. (500X)

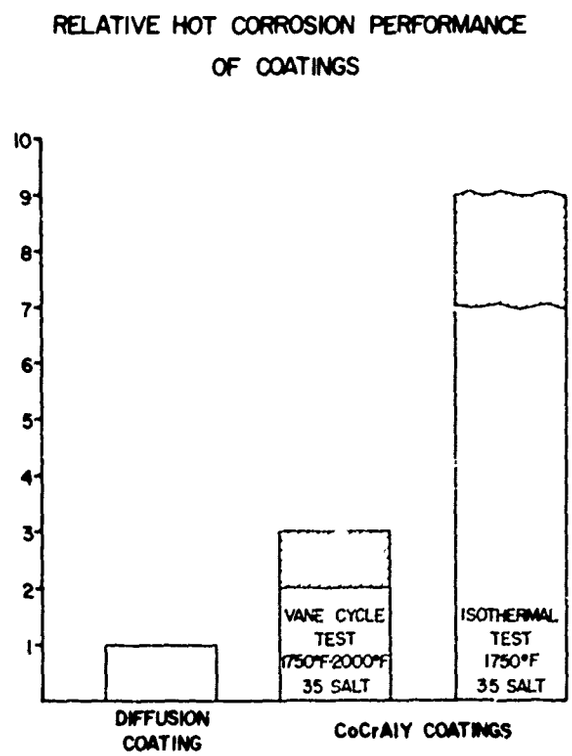

Figure 16. Relative hot corrosion resistances of CoCrAlY and diffusion aluminide coatings. As indicated, relative lifetimes depend on test conditions with performance of CoCrAlY increasing at lower temperatures and lower salt contamination levels.

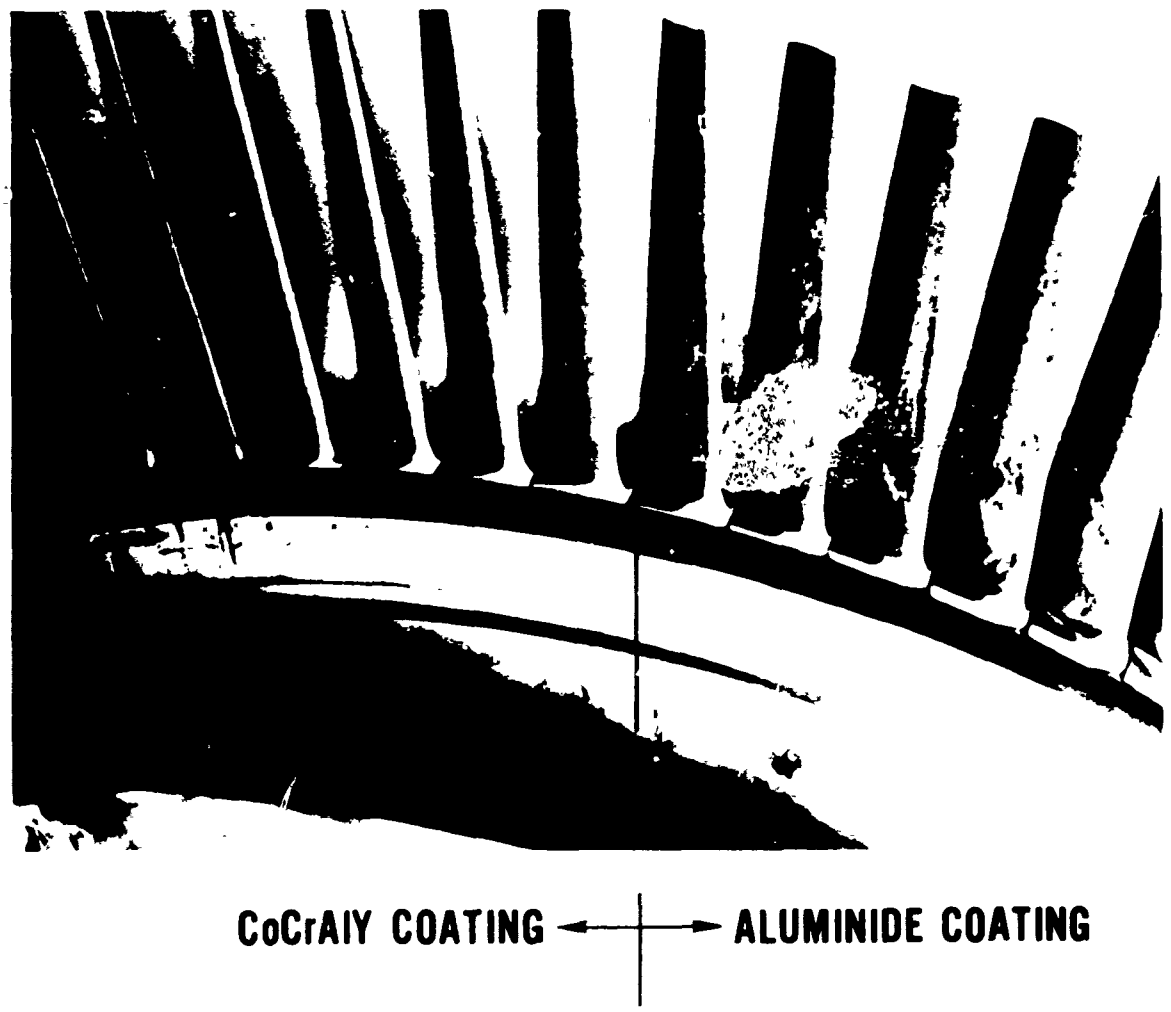

Figure 17. Results of initial field service evaluation of CoCrAlY coatings on FT4 first turbine blades.

On the debit side, limited laboratory and rig testing, and field experience indicate that the protective life of CoCrAlY, as with other types of coatings, is shortened by Na_2SO_4-V_2O_5 attack. Figure 18 shows the pitting type of attack observed on parts run in a marine engine burning fuel contaminated with vanadium. Localized penetration of the coating is imminent and has occurred on other parts observed from this field test.

MECHANICAL PROPERTIES

Since CoCrAlY must be applied to a number of different blade designs ranging from simple solid configurations to impingement or film cooled hollow configurations, a range of ductility/durability trade-offs were necessary to provide the required flexibility for these applications. Figure 19 shows the range of properties available over a relatively narrow range of aluminum contents. Low cycle thermal fatigue (thermal-mechanical, strain controlled test) properties, based on cycles to crack initiation are illustrated in Fig. 20. This crack/fatigue resistance has also been demonstrated in a number of purposely severe engine tests.

When properly matched to the base alloy heat treatment, the only effect which virgin CoCrAlY coatings can have on blade creep properties arises from the additional non-load bearing weight of the coating on the blade. The importance of the effect depends on the specific blade design and its particular life limiting property--obviously for a creep limited blade, the effect can be quite important as illustrated in Fig. 21. Consideration of this effect early in the blade design system is obviously of importance.

In addition, loss of substrate load bearing area by coating/substrate interdiffusion can become important at higher temperatures, in excess of 2000-2100°F, for example. This effect is currently of little importance at the relatively low temperatures encountered in marine turbine applications.

Figure 18. Localized pitting attack of CoCrAlY coating run in a marine engine environment. Attack is believed to be caused by Na_2SO_4-V_2O_5 deposits. (500X)

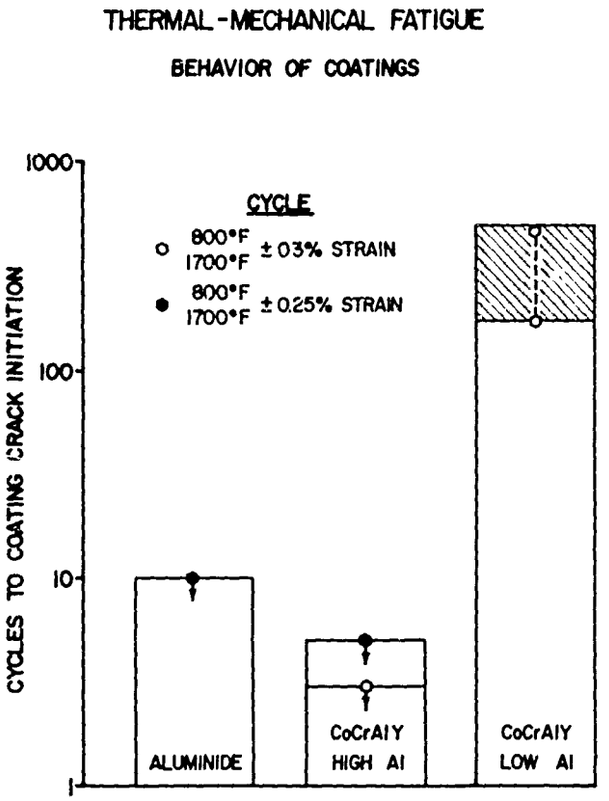

Figure 20. Effects of coating composition on low cycle fatigue cracking of coatings. Strain was purposely high in this test to illustrate beneficial effects of a more ductile CoCrAlY composition.

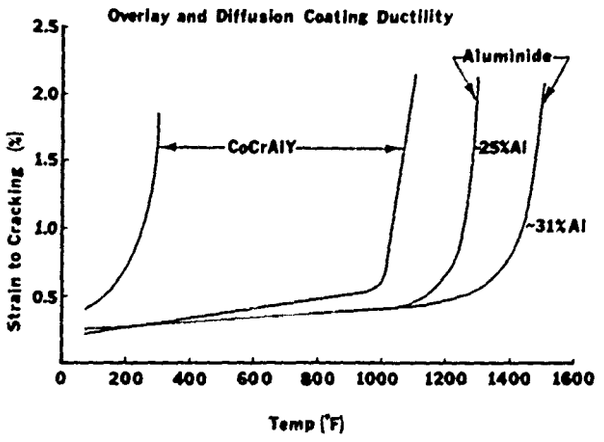

Figure 19. Relative brittle-ductile transition behavior of CoCrAlY and diffusion aluminide coatings. Range indicated for CoCrAlY reflects the variation of ductility with aluminum content.

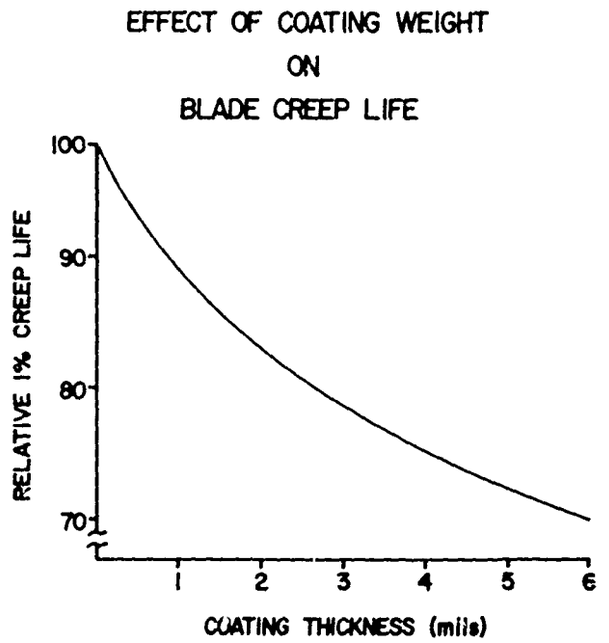

Figure 21. Typical effect of coating thickness (weight) on blade creep life. The effect is of importance only for creep limited blade designs.

PROCESSING

The electron beam evaporation process has proved more than adequate for production purposes and CoCrAlY coatings are being produced for several different engine types, including those used for marine and power generation purposes.

The line-of-sight properties of the vapor cloud have been at least partly compensated for by the use of complex rather simple rotational modes over the molten pool. By these techniques adequate coating coverage of shrouds and platforms of blades and vanes can be obtained. As expected, recessed areas, such as deep holes and internal cooling passages cannot be coated by the current process. Where required, resort is made to the use of pack cementation coatings for the protection of such surfaces.

At aluminum contents such that the coating consists of single phase CoAl (or NiAl for nickel based coatings) the total process tends to produce coatings of undesirable structure shown in Fig. 22. Thus the chemistry limitations of the current process; chemistries adjusted to provide two phase β (CoAl) + γ Co solid solution provide the most satisfactory structures. This has not proved to be a serious limitation for it has been shown that for most applications, single phased CoAl coatings are usually too brittle and are thus not sufficiently resistant to transient thermal strains.

By virtue of the particular vapor deposition conditions used for practical production of hardware, the coating structures are usually columnar in nature but to date no serious deleterious effects have been observed because of this structure.

Figure 22. Example of undesirable CoCrAlY coating structure produced from abnormally high aluminum content. (500X)

For most critical applications where the diffusion coatings cause specific airfoils to be coating limited, the overall cost effectiveness of the electron beam vapor deposited coatings is judged to be satisfactory. Nevertheless, these coatings are quite expensive and every effort is being made through improved process development to reduce processing costs. As is to be expected, increasing volume of production is a substantial aid in this respect.

THE FUTURE

While there is a current tendency to hold the line or even decrease metal operating temperatures in ship propulsion turbines to reduce hot corrosion problems, there are certainly strong reasons to require higher temperatures in the near future. Metal temperatures can also be expected to increase in aircraft gas turbines. Both types of engines will continue to encounter environments which cause life limiting hot corrosion problems, with ship propulsion turbines presenting the most severe problems because of the use of contaminated fuel and the possibility of more continuous ingestion of sea salt. While significant relief apparently can and will be gained by the use of fuel washing, fuel additives and air filtration, the demand for more corrosion resistant coatings will continue.

Depending on accurate long term projections for the availability of various types of fuels, more or less attention will have to be given to development of resistance to hot corrosion caused by various combinations of sulfates and vanadium and lead oxides.

It seems clear that overlay coatings in some form, with their relative independence of substrate properties and flexibility in turns of compositional variations will continue to be a profitable route to pursue. Systems deserving further investigation include:

1. High chromium nickel-base alloys;
2. Platinum metal modifications of current coating systems;
3. Overlay coatings containing dispersed oxide particles;
4. Ceramic coatings including the insulative type.

The last item may be looked upon as a forerunner to the use of corrosion resistant ceramic airfoils, a concept which appears to be limited mainly by design problems at this time.

Process development for overlay coatings with a view to cost reduction and increased flexibility with respect to both compositional variations and coverage of complex surfaces should be vigorously pursued.

The use of fuel additives to inhibit hot corrosion is receiving renewed interest and as understanding of hot corrosion mechanisms advances, both in the engine and in the laboratory, it is likely that this will prove to be a valuable approach at increasingly high temperatures, particularly with respect to ship propulsion turbines.

Basic research required to support development work in the above areas should include:

1. Further refinement of theories of hot corrosion mechanisms;
2. Understanding of engine conditions which lead to hot corrosion;
3. Further understanding of active element and particle effects with respect to oxide adherence and structure;
4. Continued search for oxides or other compounds which inhibit hot corrosion.

No one approach will solve the hot corrosion problem. Various combinations of improved coatings and alloys, fuel purification and additives, air filtration and periodic turbine cleaning (washing) will provide significant increases in turbine durability in the future.

REFERENCES

1. M. A. DeCrescente, and N. S. Bornstein, *Met. Trans.*, 2 2875 (1971).
2. J. A. Goebel, and F. S. Pettit, *Met. Trans.*, 1 3421 (1970).
3. J. A. Goebel, F. S. Pettit, and G. W. Goward, *Met. Trans.*, Accepted for Publication.
4. G. W. Goward, D. H. Boone, and C. S. Giggins, *Trans. ASM*, 60 228 (1967).
5. G. W. Goward and D. H. Boone, *Oxidation of Metals*, 3 475 (1971).
6. T. K. Redden, *Trans. TMS-AIME*, 242 (1695 (1968).
7. G. F. Paskiet, and D. H. Boone, *J. Inst. Met.*, 100 58 (1972).
8. F. P. Talboom, R. C. Elam, and L. W. Wilson, "Evaluation of Advanced Superalloy Protection Systems," NASA CR-72813, December 2, 1970.
9. C. S. Giggins, and F. S. Pettit, *J. Electrochem. Soc.*, 118 1782 (1971).
10. U.S. Patent 3, 399, 058, August 1968.
11. C. S. Wukusick, and J. F. Collins, *Mater. Res. Std.*, 4 637 (1964).
12. J. Stringer, *Met. Rev.*, 11 113 (1966).
13. J. K. Tien, and F. S. Pettit, *Met. Trans.*, 3 1587 (1972).

Life Prediction of Turbine Components: On-Going Studies at the NASA Lewis Research Center

David A. Spera and Salvatore J. Grisaffe
NASA–Lewis Research Center
Cleveland, Ohio

SUMMARY

The purpose of this report is to present an overview of the many studies at the NASA-Lewis Research Center which together form the turbine component life-prediction program. This program has three phases: (1) development of life prediction methods for each of the major potential failure modes through a wide range of materials studies, (2) evaluation and improvement of these methods through a variety of burner rig studies on simulated components, and (3) application of a unified life-prediction method to prototype turbine components in research engines and advanced rigs.

In different temperature ranges, different properties become dominant in determining engine component life. The resistance of materials to fatigue, creep, and oxidation are being determined through closely controlled laboratory tests. In addition to conventional testing machines, specialized equipment has been developed to obtain material properties under simulated engine environments. For example, automatic cycling furnaces are used to determine changes in weight, surface chemistry, microstructure, and oxide scale. Fluidized beds are used to study thermal-fatigue cracking in various alloys and coatings and to evaluate fatigue-life theories.

Because the engine environment is much more aggressive than that in furnaces or fluidized beds, it can cause important changes in material behavior. Tests in high-velocity burner rigs have shown drastic increases in weight loss, consumption of coatings, and creep rates. Large decreases have been found in rupture and fatigue lives. Thus, rig and furnace test data must be integrated before the lives of engine components can be predicted.

Computer codes are now being developed that consider fatigue, creep, and oxidation life prediction in a unified manner. The first two of these failure modes are now included in a computer code called THERMFI. With this code, thermal-fatigue life can be calculated for known temperature and deformation cycles using conventional mechanical properties. THERMFI has been verified with a wide variety of laboratory and rig tests. Studies are in progress to extend this code to include failure by coating consumption during long hold times at elevated temperature.

INTRODUCTION

The Lewis Research Center is the principal NASA laboratory for research and development of aerospace propulsion systems. A major goal of Lewis is to advance the technology of aircraft gas turbine engines, from component details to complete systems. One highly complex area of special importance is the prediction and improvement of the life of turbine blades and vanes. The purpose of this report is to present an overview of the many studies at Lewis that together form the turbine component life-prediction program.

The program has three phases: (1) development of life prediction methods for major potential failure modes through a wide range of materials studies, (2) evaluation and improvement of these methods through a variety of burner rig studies on simulated components, and (3) application of a unified life prediction method to prototype turbine components in research engines and advanced rigs. These three phases form a cooperative, interdisciplinary program involving mission analysis, fluid and solid mechanics, thermodynamics, metallurgy, and statistics.

Predicting the lives of turbine components is complicated by the complex geometry of the parts themselves. Typical air-cooled components are shown in Fig. 1. These are small, intricate, thin-walled structures acting both as highly loaded airfoils and high-flux heat exchangers. They must perform this dual role at extreme metal temperatures, in an oxidizing atmosphere, and, in the case of blades, while moving at speeds approaching sonic velocities. Moreover, they are routinely subjected to vibration and to severe transient loading during frequent starts and stops. Finally, a failure in one of these critical components can quickly escalate to loss of performance and, potentially, to the loss of an engine.

Figure 2 shows the complex internal geometries required for advanced cooling methods (1,2), that make the modern cooled turbine airfoil a costly as well as a critical component. Thus, the ability to predict and eventually improve the life of a turbine blade or vane can result in higher performance, lower engine and maintenance costs, and increased safety.

In general, the scope of this review will be limited to those studies at Lewis that include both turbine components and life prediction. A number of other Lewis publications provide comprehensive reviews of related areas: references 1 to 3 review efforts on aircraft gas turbines; references 4 to 8 review efforts to understand and develop better turbine materials; and references 9 to 11 deal with the areas of stress analysis and fatigue.

TURBINE COMPONENT LIFE-PREDICTION PROGRAM

POTENTIAL FAILURE MODES

The major potential failure modes for turbine components are presented schematically in Fig. 3. Stresses high enough to produce premature fracture or buckling are generally avoided by a preliminary elastic stress analysis. The long-term failure mechanisms are those that dictate life. At temperatures below approximately 800°C mechanical fatigue is often the dominant failure mode. The engine environment usually exerts only a second-order influence in this temperature range. At the higher temperatures, above about 1000°C, creep, oxidation, and thermal fatigue (acting alone or together) usually cause failure. Environmental effects are dominant in this temperature range. In the intermediate temperature range, 800° to 1000°C, any of the several failure modes shown in the figure can be dominant, depending on the structure, the material, and the engine cycle. This temperature range is particularly critical for sulfidation, a failure mode of importance for marine gas turbines.

Protective coatings can alter the mode of failure and extend the life of the component until the coating itself is depleted by oxidation or cracked by fatigue. Generally, mechanical fatigue and creep form an upper bound on life, for a given application. Although Fig. 3 is merely a schematic representation of possible interactions of the major failure modes, it does illustrate that several failure mechanisms combine to produce a region of available life. One of the goals of life-prediction methods is to define this region.

PHASES OF THE LIFE-PREDICTION PROGRAM

The three major phases of the Lewis life-prediction program for turbine components are illustrated in Fig. 4. These phases are in various stages of development, as will be discussed in subsequent sections of this report. The first phase includes materials tests such as uniaxial tensile, creep, and mechanical fatigue. These tests are conducted on very simple specimens and are supplemented by static and cyclic furnace oxidation studies. Basic methods for predicting life have been developed from the resulting data. Thermal-fatigue tests on relatively simple wedge specimens in fluidized beds are used to evaluate these methods.

In the second phase of the program, evaluation of life-prediction methods continues in burner rig tests directed toward a better simulation of the hot gas environment of an engine. Wedge specimens are used to study cyclic oxidation behavior and to evaluate methods for predicting coating life. Airfoil specimens are used to evaluate thermal-fatigue life predictions in a simulated engine environment for complex geometries. As a result of burner rig tests, the life-prediction techniques are expanded or modified to integrate additional factors such as high gas velocity, rapid temperature transients, stress concentrations, combustion products, etc.

The third and final phase of the program is the prediction of lives for prototype components tested in engines and rigs. This provides the best evaluation of life-prediction methods and the first step in developing improved turbine components.

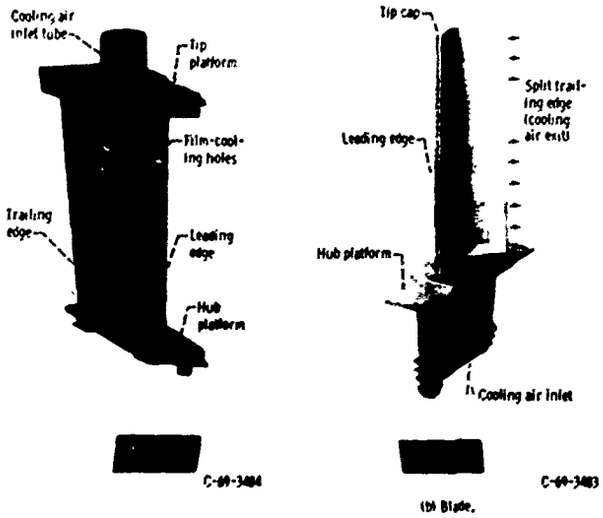

Figure 1. Typical cooled turbine components.

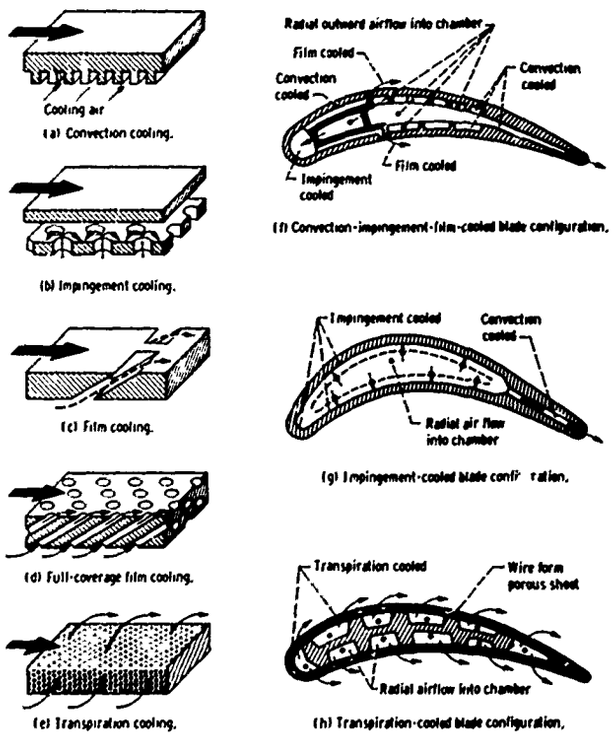

Figure 2. Complex turbine blade configurations required for various cooling methods.

PHASE I: DEVELOPMENT OF PREDICTION METHODS THROUGH MATERIALS STUDIES

The purpose of the first phase of the general program is to develop a prediction method for each of the potential failure modes in its "pure" form and then to integrate these methods into a unified life-prediction technique. Each failure mode requires detailed study to understand the damage mechanisms and to describe the damage process quantitatively. Quantitative description is the basis of any life-prediction method.

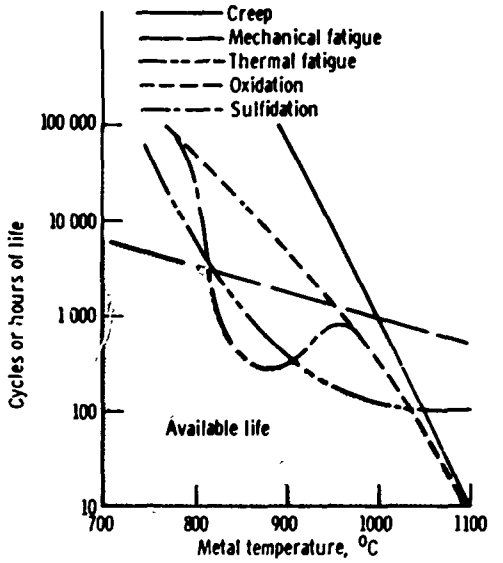

Figure 3. Factors influencing turbine component life.

Materials studies are usually conducted on small samples (coated and uncoated) under carefully controlled laboratory conditions. These conditions are seldom as severe as engine service unless temperatures, stresses, or environments are deliberately altered to accelerate damage. The assumption is made that the engine environment may increase damage rates, but the damage mechanisms remain the same. Thus, life-prediction methods developed from materials studies must provide for the changing of rates to suit engine service.

BASIC MECHANICAL TESTS AND DATA ANALYSIS

Test procedures for obtaining conventional tensile, creep-rupture, and mechanical-fatigue data are widely used and well documented. These tests are usually isothermal, and they provide the basic strength and deformation information that characterize the material. Methods have been developed for interpolation and extrapolation of these data. For example, time-temperature parameters for the analysis of creep-rupture data have been studied extensively at Lewis (12-14). Methods are also required for applying isothermal test data to cycles that are not isothermal. Two such methods now being used to predict thermal-fatigue life are the Method of Universal Slopes (15) for mechanical fatigue and the Method of Life Fractions for creep (14,16).

Method of Universal Slopes–This is an empirical equation relating cyclic life to strain range, using tensile ductility, ultimate tensile strength, and Young's modulus. It is used

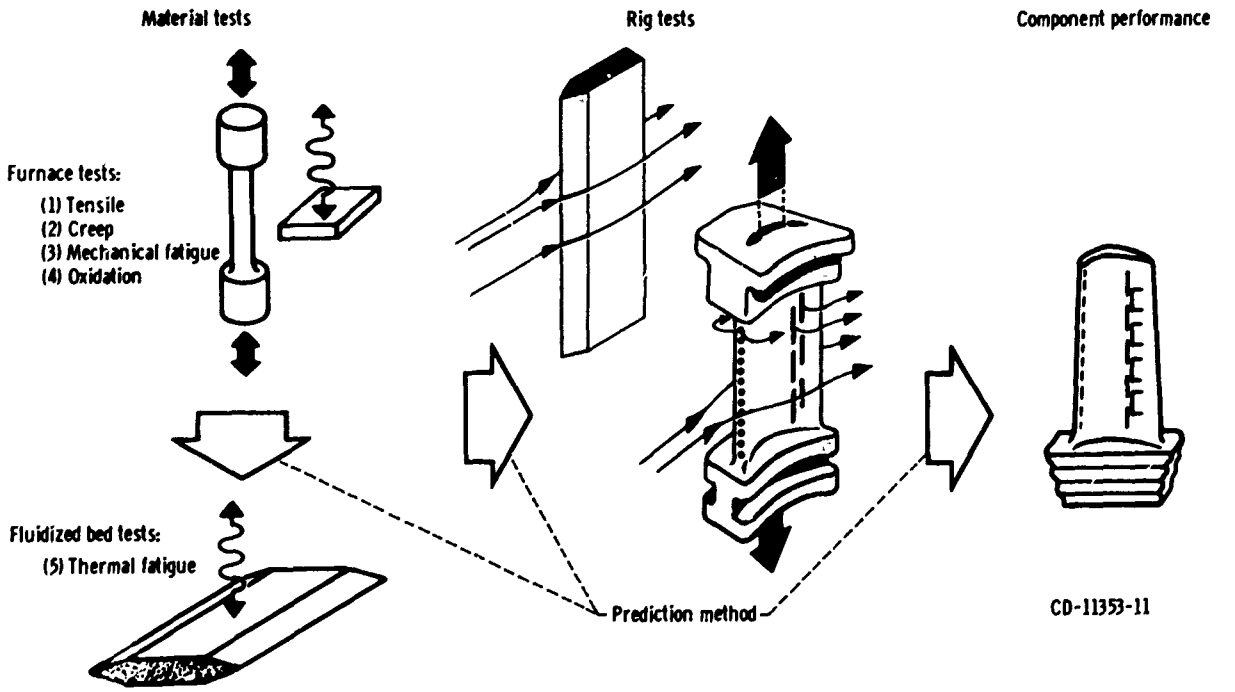

Figure 4. Turbine component life-prediction program.

to predict failure in the pure fatigue mode. Temperature is assumed to affect fatigue life indirectly, through its effect on tensile properties. Time effects such as creep and oxidation are assumed to be absent. For nonisothermal cycles, the temperature in the cycle that gives the shortest calculated life is used.

Method of Life Fractions–This is a rule for calculating creep-rupture life under cyclic conditions of temperature and stress. The cycle is divided into small time intervals, each having a nominal temperature and stress, and thus a nominal rupture time. The fraction of life consumed in each interval is then assumed to be the ratio of the interval time to the rupture time. The life fractions are summed for a complete cycle to obtain the damage per cycle. The reciprocal of this sum is assumed to be the cyclic life in the pure creep mode.

Other methods for characterizing the resistance of materials to low-cycle fatigue are being studied at Lewis. One of the most promising of these is Strainrange Partitioning (17,18). With this method, any inelastic strain cycle, no matter how complex, can be subdivided into four basic components. These components are unique combinations of plastic and creep strains. They are related independently to cyclic life by equations that are generalizations of the well-known Manson-Coffin equation. A linear life fraction rule is used to sum the damages resulting from each of the strain range components. Failure is assumed to occur when the summation of life fractions equals unity. This method has the potential of guiding the generation of fatigue data (17), improving the understanding of fatigue mechanisms, and interpreting the effects of frequency, hold time, temperature, and environment.

OXIDATION TESTING IN FURNACES

The vast majority of oxidation studies have been conducted under isothermal, noncyclic conditions so as to continuously measure weight gain of oxygen per unit area of the specimen. These data were then used to calculate an oxygen pickup or scale growth rate constant, a number long used as an index of oxidation resistance. Recently, a few programs have explored the influence of thermal cycling on the scaling and spalling behavior of turbine alloys (20,21). Such studies have shown that thermal cycling accelerates surface attack, promotes spalling of oxide scales, and eventually results in weight loss rather than gain in the specimen. Of special importance is the observation that protective coatings are often consumed during thermal cycling, when isothermal tests showed little or no consumption. For these reasons, Lewis has adopted the use of cyclic furnace testing of coated turbine alloys as the first step in establishing their oxidation resistance and coating behavior.

A typical cyclic oxidation furnace facility is shown in Fig. 5. Specimens are suspended from platinum wires to minimize the influence of the support material on oxide scale composition. Each specimen is in its own tube to eliminate cross contamination from oxide vapors. The transfer mechanism lifts the specimens out of the furnace for slow cooling to room temperature. A small cup is moved into place beneath each specimen so that the oxide spall can be collected for analysis. Cycles are usually 1 hour long, to approximate an average flight cycle. Furnaces of this type are operated around the clock, unattended, with periodic interruptions for weighing of specimens and collecting of spalled oxide.

Cyclic oxidation tests indicate that coating failures are usually preceded by the thinning and subsequent breaking up of a key protective layer or phase (22,23). These observations are described in more detail in the appendix and have led to the concept of "layer break-up" for predicting coating life. This concept is now in its early stages of development. Hopefully, it will provide a model for the calculation of the pure coating life from its composition and the cyclic environment.

THERMAL-FATIGUE TESTING IN FLUIDIZED BEDS

The thermal-fatigue resistances of various alloys and coatings are being determined under contract at the Illinois Institute of Technology Research Institute, using the fluidized-bed technique (24,25). The objectives of this continuing program are (1) to determine the comparative resistances of the latest alloys, coatings, and claddings of interest for turbines, and (2) to provide carefully controlled data for development and evaluation of life-prediction methods.

Figure 6(a) is a schematic view of the facility and of a typical group of double-wedge specimens. Two beds are used, one each for heating and cooling. A bed consists of a retort filled with fine sand through which air is pumped. The flow of air causes the sand particles to develop a churning, circulating action. The large mass of the beds and their mixing action promote uniform, high heat-transfer rates, making them ideal for thermal-fatigue studies. Fluidized beds were first used for this prupose at the National Gas Turbine Establishment in England in 1958. Since that time the technique has become widely accepted for evaluating both materials and components.

Typical data on some turbine materials are shown in the bar chart in Fig. 6(b). The most crack resistant alloys were either directionally solidified or coated or both. Tests continue on the best of these alloys plus 20 new alloys and conditions, bringing to 38 the total number of systems being evaluated.

Figure 6(c) shows a typical comparison between calculated and observed thermal-fatigue lives. The method of life calculation is explained briefly in the next section. The alloy is B 1900, with and without an aluminide coating. Tests of this type have verified the life-calculation method for simple thermal-fatigue tests of the fluidized-bed type.

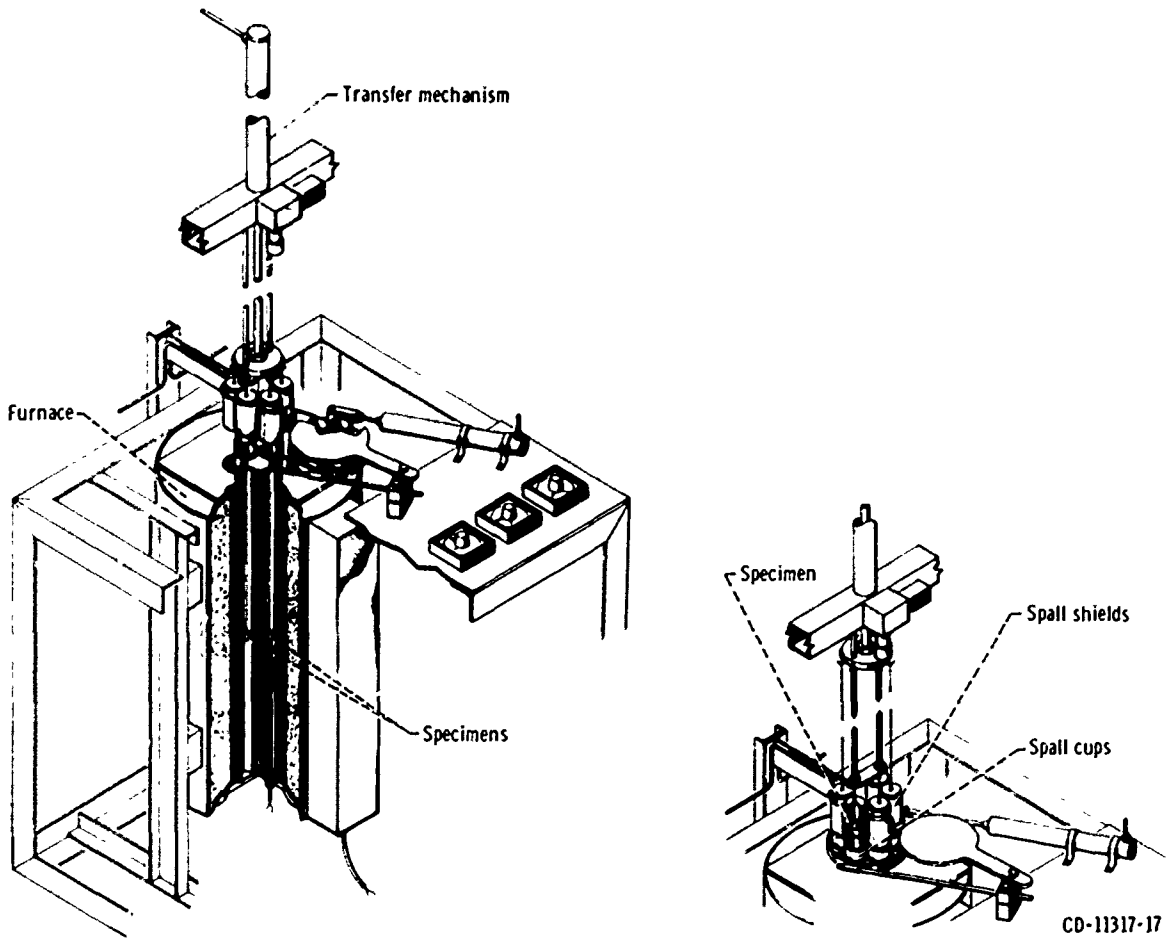

(a) Specimens in heating position.

(b) Specimens in cooling position.

Figure 5. Cyclic oxidation test facility.

TOWARD A UNIFIED LIFE-PREDICTION METHOD

The materials testing phase of the program has led to the conclusion that a life-prediction method for turbine components must unify fatigue, creep, and oxidation. The first two of these failure modes have already been combined in a computer code for predicting thermal-fatigue life. Figure 7 shows a schematic diagram of this code which is called THERMF1. Calculations start with a thermal and stress analysis for both transient and steady-state conditions, including plasticity and creep. This is often the most difficult step in the life analysis of a complex component. On the basis of this analysis, two lives are calculated: (1) a fatigue life, using the Method of Universal Slopes and the tensile properties of the material, and (2) a cyclic creep life, using the Method of Life Fractions and the creep-rupture properties of the material. These two methods were described briefly at the beginning of this section. The fatigue and creep lives are then combined to give the thermal-fatigue life, assuming a simple linear interaction (26,27).

Figure 8 shows the progress to date in using THERMF1 to calculate the thermal-fatigue lives of coated and uncoated specimens tested in fatigue machines, fluidized beds, and burner rigs (28). Calculated and observed lives agree within a factor of two for 114 of the 125 tests examined thus far. The error is distributed approximately in a log normal fashion and reflects both the inaccuracies in the calculations and the experimental effort. Twenty of these tests were on simulated turbine blades tested in a Mach 1 burner rig, which will be described later in the report. Distribution of error in these tests is similar to that in Fig. 8 for all of the tests.

Only a few of the tests analyzed thus far have included long hold times at elevated temperature. For this reason, it has not been necessary to include the oxidation failure mode directly. However, life analysis of actual turbine components will require that THERMF1 be expanded to include this mode, particularly for coatings. When this is done, a unified method will be available for predicting the lives of prototype components under service conditions.

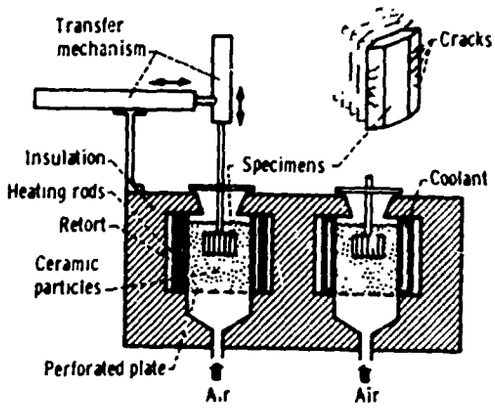

(a) Fluidized bed facility and specimens.

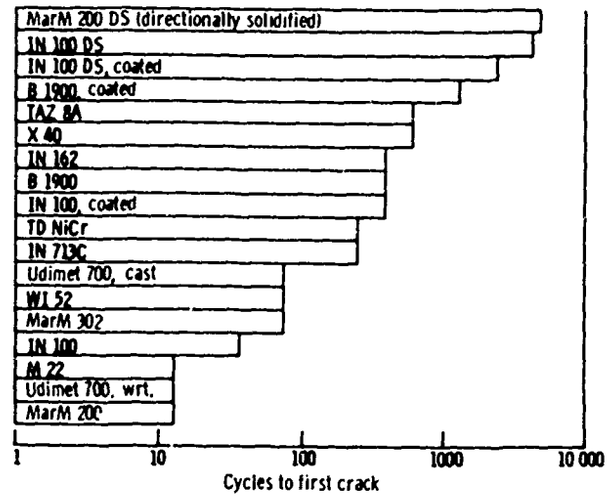

(b) Comparative thermal fatigue resistance of typical turbine materials. Bed temperatures, 320° and 1090° C; 6-minute cycle.

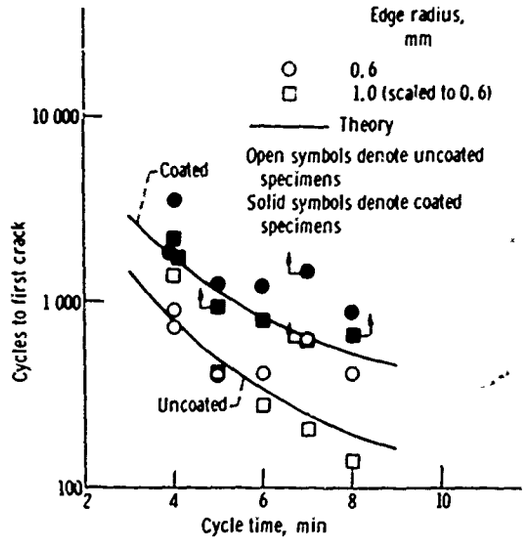

(c) Theoretical and experimental thermal fatigue lives for B 1900. Bed temperatures, 320° and 1090° C.

Figure 6. Thermal fatigue testing using the fluidized-bed technique.

PHASE II: EVALUATION OF PREDICTION METHODS THROUGH BURNER RIG STUDIES

OPEN-JET BURNER RIGS

Open-jet burner rigs, which burn jet fuel or natural gas, are the simplest facilities that can provide the combustion environment, gas velocities, and thermal gradients similar to those encountered in actual engines. Because the specimens are not enclosed, their temperature distributions can be readily observed and strains can often be measured optically. The specimens can be moved out of the burner exhaust for cooling, which allows the burner to operate at steady state, prolonging its life.

Two types of open-jet rigs are in operation at Lewis: large Mach 1 burners with mass flows of 0.5 kilogram per second and small burners with mass flows less than 0.07 kilogram per second. Three large and nine small burner rigs are presently available. One of the large rigs uses natural gas; all the remaining rigs use jet fuel.

A large Mach 1 burner rig is shown in Fig. 9 (29). A rotating specimen holder supports eight wedge specimens in front of the burner nozzle, inside clam-shell radiation shields. For cooling, the specimen holder moves downward, positioning the specimens in front of the sonic cooling air stream. The three Lewis rigs of this type are used for studies on oxidation, coating, cladding, and thermal fatigue. Two

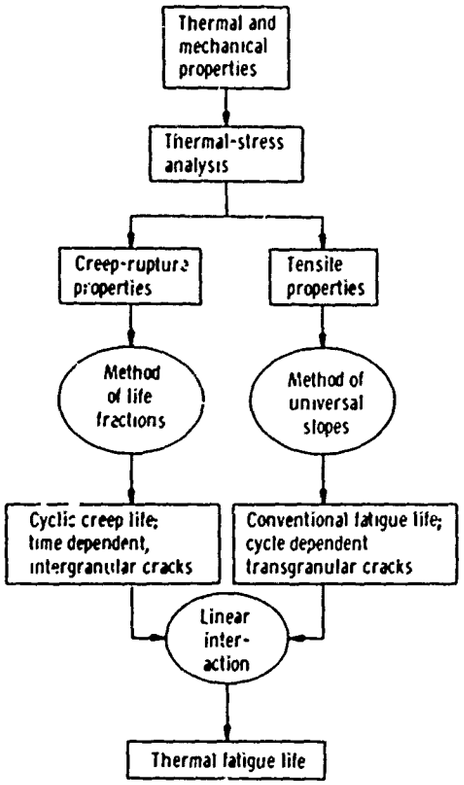

Figure 7. Schematic diagram of THERMF1, a computer code for calculating thermal fatigue life.

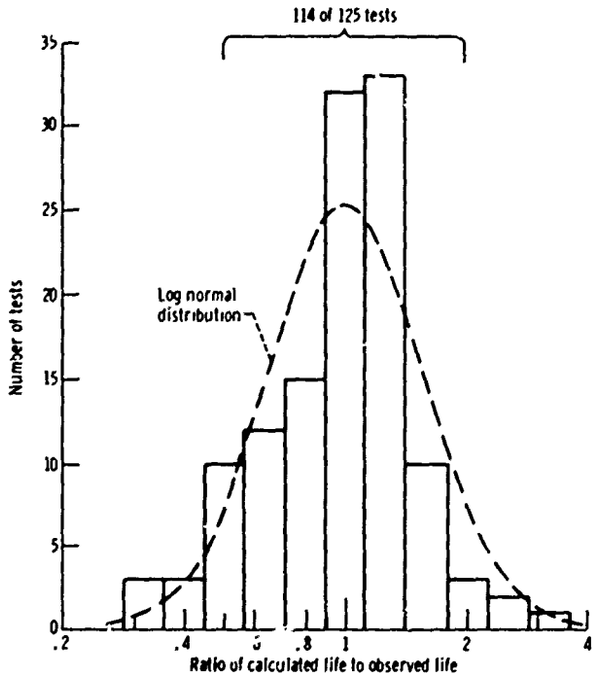

Figure 8. Progress in calculating life of thermal fatigue specimens using THERMF1.

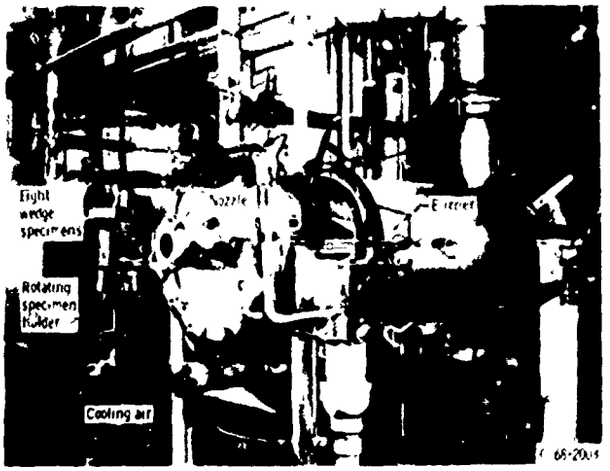

(a) General view of rig

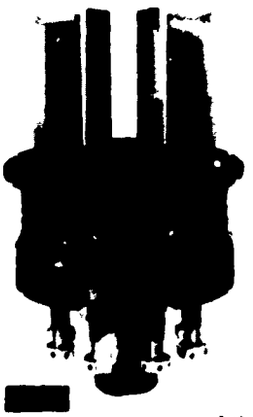

(b) Wedge specimens in holder. C-68-7269

Figure 9. High-velocity open-jet burner rig for oxidation and thermal fatigue studies.

of the rigs have provisions for salt injection for sulfidation studies.

Oxidation tests–Tests have shown that bare alloy oxidation and coating degradation occur at significantly higher rates in the Mach 1 rigs than in cyclic oxidation furnaces (23,29-31). For example, Fig. 10 presents a comparison of the weight changes in aluminide coated B 1900 under the two test conditions. At 1090°C, cyclic furnace specimens showed a small weight gain followed by a very gradual weight loss. The rig tests, however, produced an immediate, rapid weight loss. Coating consumption rates have been found to be 10 to 20 times higher in the burner rig. However, the same sequence of growth, consumption, and break up has been observed. This is discussed further in the appendix.

Creep-rupture tests–Burner heating nas been found to increase creep as well as oxidation rates and reduce rupture times (32). Figure 11(a) shows one of the Lewis burner rigs for creep-rupture testing. It is a conventional lever-loaded creep machine fitted with a small (0.07 kg/sec) jet-fueled burner. Specimens are conventional

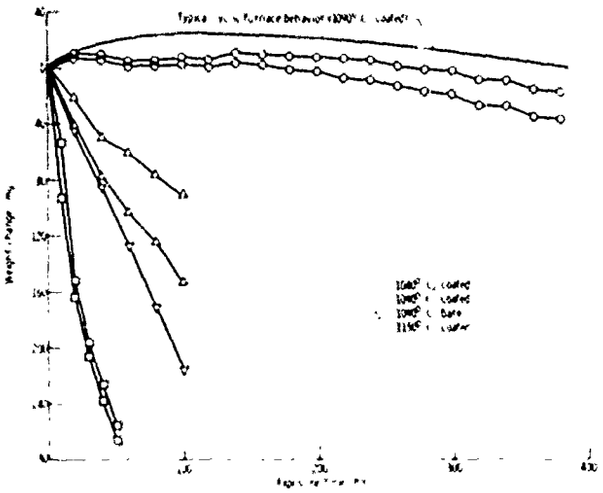

Figure 10. Weight change of B 1900 specimens during cyclic burner-rig oxidation compared with cyclic furnace behavior. Minimum temperature, 20°C; 1 cycle per hour.

6-millimeter-diameter, uniaxial test bars. The small size of the burner requires that auxiliary electrical resistance heating be used to keep the test section at a uniform temperature. The power leads can be seen in Fig. 11(b). A similar rig using a large Mach 1 burner does not require the auxiliary heating.

Comparison of rupture lives in a burner rig and in a furnace is shown in Fig. 11(c). Burner heating has drastically reduced the rupture times for the same stress and temperature combinations. At 980°C the burner heated life - only 10 percent of the furnace life for two turbine alloys, one of which was aluminide coated. At 1040°C only 5 percent of the furnace life was obtained. These data suggest that creep rates are 10 to 20 times higher than those in the furnace tests, increases very similar to those observed for oxidation. The two phenomena are closely related, and studies are under way to determine the relationship.

As explained previously, the Method of Life Fractions has been used to calculate cyclic creep life. One part of this method is the calculation of creep-rupture life as a function of temperature and stress. This is usually done by means of empirical formulas called time-temperature parameters. When calculating the creep life of a component in a moving gas environment, these parameters should be corrected in accordance with data similar to that given in Fig. 11(c). When this is done, cyclic creep life in a turbine environment can be accurately calculated using the Method of Life Fractions.

Thermal-fatigue tests–Simulated turbine blades, both cooled and uncooled, are being tested in a burner rig to evaluate life-prediction methods for turbine components (32). The test facility is shown in Fig. 12(a). A loading fixture has been added to a large burner (of the type shown in Fig. 9(a)) to allow the application of simulated centrifugal loads. The entire loading fixture pivots to move the airfoil specimen between heating and cooling positions. Cyclic heating and cooling in this rig produce high thermal stresses and leading-edge cracks similar to those found in turbine components.

Specimen shape and typical data are shown in Fig. 12(b). Cyclic life is shown as a function of the leading-edge temperature at steady state for coated and uncoated IN 100. Theoretical lives, calculated using THERMF1 are also shown in the figure. Agreement between experiments and theory is good. The agreement verifies the computer code and its applicability to turbine components. Studies are now being carried out to include stress concentrations such as film cooling holes.

HOT GAS TUNNEL

High gas pressure is one aspect of the turbine environment that is lacking in the open-jet burner tests. To include this factor, a fully automated, programmable, hot-gas tunnel rig has been constructed for thin-walled, cooled airfoils (2). Both the specimens and the environment represent a turbine component more closely than those in the open-jet rigs. Pressure levels can be raised to 11 atmospheres–an important factor in sulfidation studies. The mass flow rate is approximately 1.0 to 2.2 kilograms per second, which produces realistic heat fluxes through the airfoil walls. Fig. 13(a) presents a schematic view of this rig. Fig. 13(b) shows a typical cooled, symmetrical airfoil specimen in the test section. The tunnel is equipped with a fatigue machine capable of applying steady loads of 130 kilonewtons and cyclic loads of ±44 kilonewtons at frequencies up to 60 hertz. The combustor exhaust gases can be cycled in temperature from 540°C to as high as 1650°C. Cooling air can be heated to 650°C to simulate a compressor bleed condition.

Life tests are now being conducted on aluminide coated IN 100 airfoil specimens under various conditions of temperature, load, coolant flow, and hold time. These data will be used for the final evaluation of a unified life-prediction method before using the method to calculate the lives of prototype turbine components.

PHASE III: APPLICATION OF PREDICTION METHODS TO TURBINE COMPONENTS

HIGH TEMPERATURE TURBINE TECHNOLOGY PROJECT

The third phase of the program is predicting the lives of prototype components tested in advanced rigs and engines. This phase is one part of a major research program at NASA-Lewis–the High-Temperature Turbine Technology Project. The objective of this project is to develop advanced gas turbines with increased performance and reliability, compared

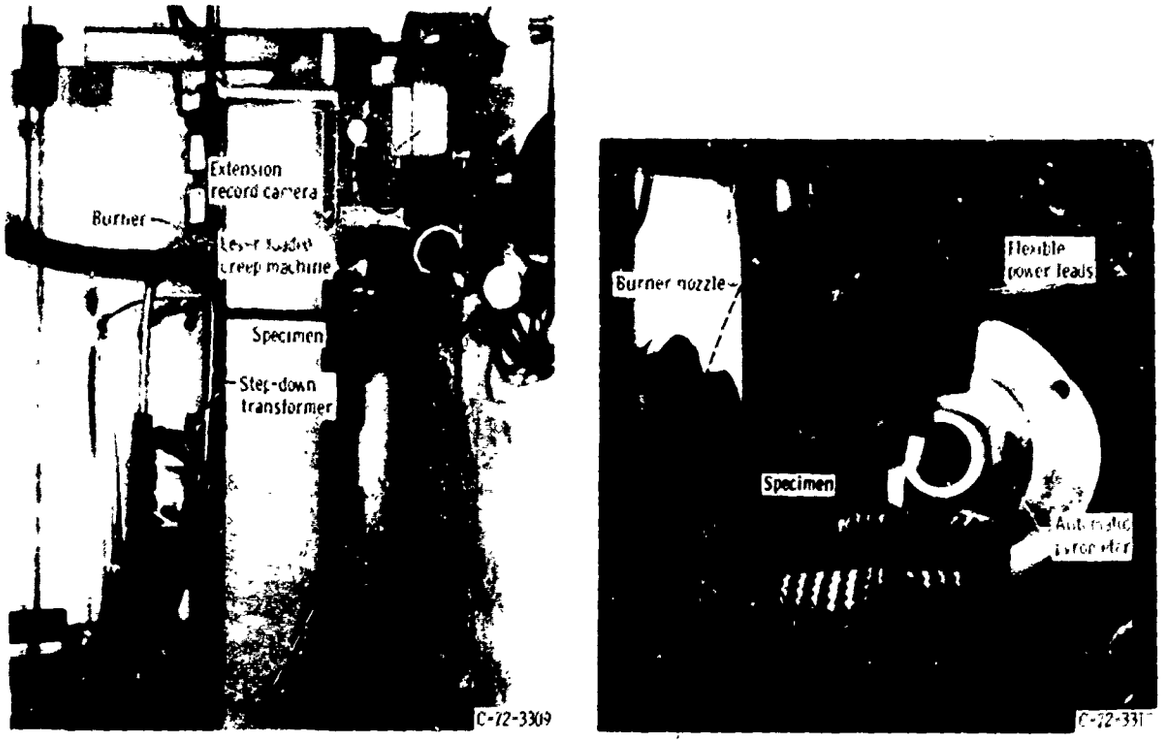

(a) Typical view of rig.

(b) Test section.

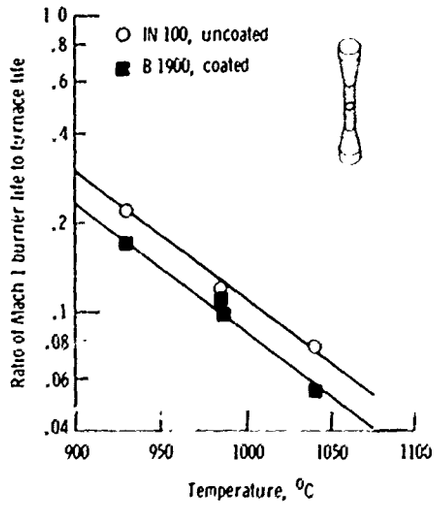

(c) Typical data showing effect of burner heating on creep-rupture life.

Figure 11. Creep-rupture testing using burner rig.

with the best of present-day turbines. The project includes research on cooled turbine heat transfer, aerodynamics, and life. Other technical areas involved are mission analysis, materials and fabrication, mechanical design, rig and engine operations, instrumentation development, and data reduction.

The turbines under investigation range in size from relatively large ones, which would be applicable to supersonic cruise turbojets, to very small turbines with a flow capacity of only 0.5 to 1 kilogram per second, which could be used on small aircraft. Intermediate sized turbines under investigation include those applicable to high-pressure cores of engines for military multimission aircraft and advanced subsonic cruise commercial transports. Turbines for helicopter engines of about 1500 shaft horsepower are also included in the project.

(a) General view of rig.

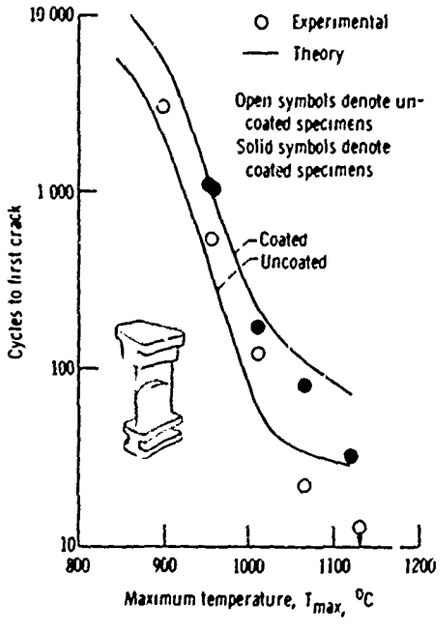

(b) Theoretical and experimental thermal fatigue lives for IN 100 airfoil specimens. Heating time, 3 minutes; rapid air cooling to 75° C.

Figure 12. Thermal fatigue testing of simulated turbine blades using high-velocity burner rig.

In the third phase of the program, lives will be predicted for turbine components tested in four facilities: a static cascade rig, a modified J75 research engine, a high-pressure - high-temperature turbine rig, and the Lewis propulsion systems laboratory.

STATIC CASCADE RIG

A static cascade rig originally designed for heat-transfer studies (1,2,33) is being modified for a vane life testing program. This program will provide the first comparison at Lewis between predicted and observed lives of actual cooled engine components. The cascade rig is shown in Fig. 14. It was designed for continuous operation at an average inlet gas temperature of 1350°C and pressures up to 11 atmospheres. It can be operated at temperatures up to 1650°C for short times.

As shown in Fig. 14(b), the specimen pack contains four vanes of J75 size. Test data are obtained from the central two vanes. The outer two vanes are slave vanes, which act as flow channels and radiation shields. The test and slave vanes have separate cooling air systems. This allows preheating of the test vane cooling air to about 650°C to simulate compressor bleed air. The two slave vanes can also receive more cooling than the test vanes, to ensure longer life.

MODIFIED J75 RESEARCH ENGINE

Life studies on actual blades and vanes will be conducted in the research engine shown in Fig. 15(a) (1,2,33). Only the high-pressure spool of the basic J75 engine is used. This modified engine can operate for long periods of time at an average turbine inlet temperature of 1350°C. A cross-sectional diagram of the turbine test section is shown in Fig. 15(b). The standard uncooled single-stage turbine of the J75 high-pressure spool has been replaced with a single-stage air-cooled turbine. Five of the 72 vanes and five of the 76 blades are test components. The remaining blades and vanes are slave components provided with more cooling than the 10 test parts to ensure longer life. Several special features are incorporated in the turbine section to make a versatile test bed. These features include the following:

1. Independent metering of cooling air to the test and slave components from either the compressor or from an external air supply,
2. Individual replacement of all airfoils without removing the turbine disk,
3. Extensive instrumentation for gas temperatures, gas pressures, and metal temperatures on both blades and vanes.

Up to this time, the engine has been used exclusively for turbine cooling studies. A program of life tests in this engine is now in its early stages. One of the goals of this program is to develop improved vanes and blades using life prediction methods verified by rig tests.

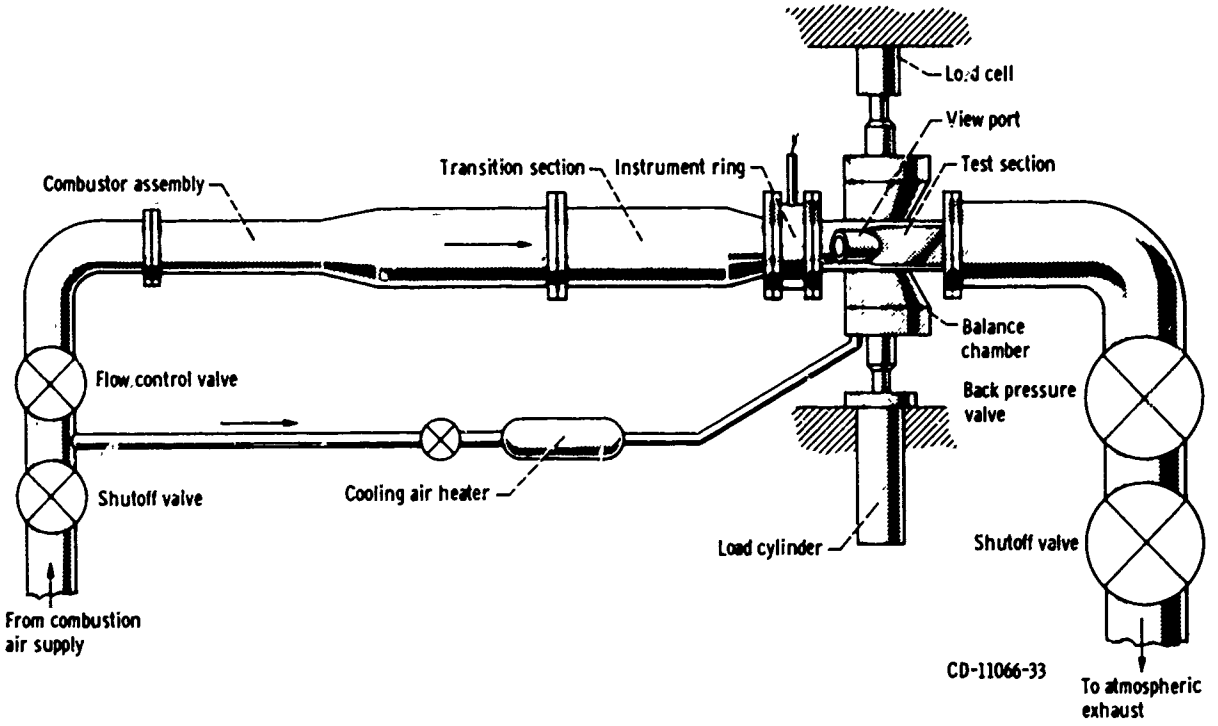

(a) Schematic view, showing major components.

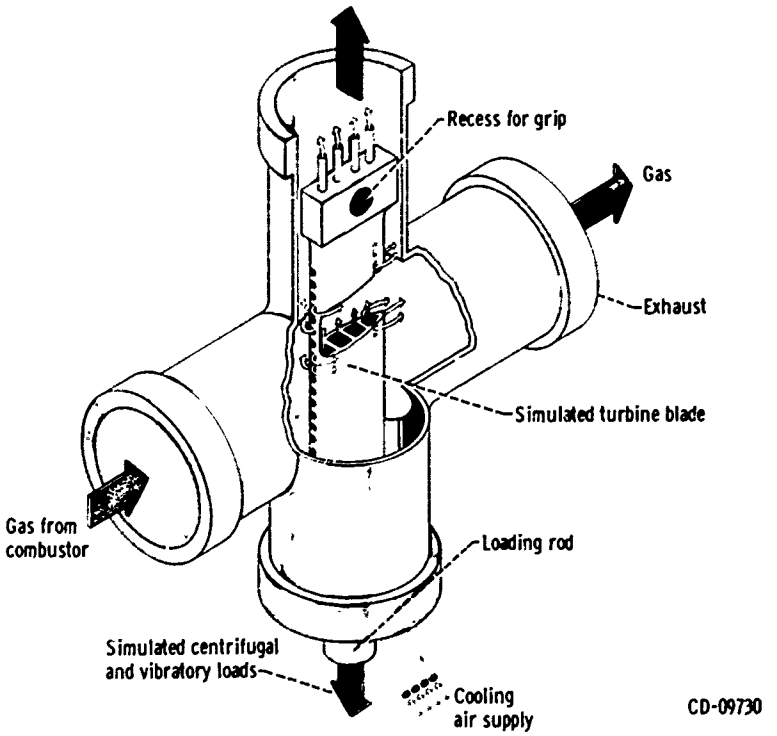

(b) Test section, showing simulated turbine blade.

Figure 13. Hot-gas tunnel rig for life testing of simulated turbine blades and vanes.

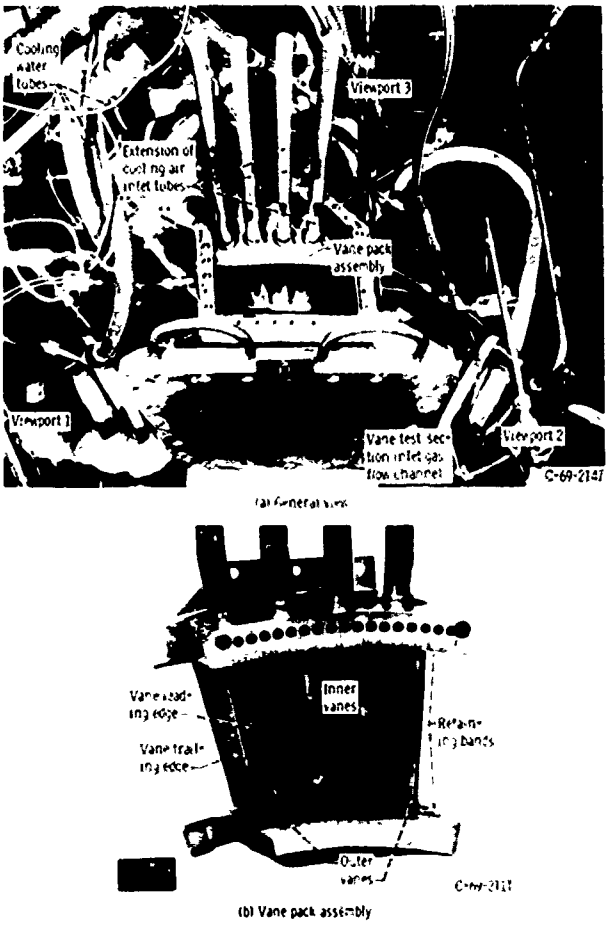

(a) General view.

(b) Vane pack assembly.

Figure 14. Static cascade rig for testing cooled turbine vanes.

HIGH-PRESSURE - HIGH-TEMPERATURE TURBINE TEST RIG

The NASA-Lewis Research Center is now designing and building an advanced turbine test rig that will operate at the high temperatures and pressures expected in future engines (2). In the turbine test section of this facility, gas temperatures may reach 2000°C, and pressures may be as high as 40 atmospheres. The facility will consist of a combustor, a single-stage turbine, a water brake power absorber, an auxiliary compressor system with integral turbine drives, and the required service, control, and instrument systems. The turbine will have a tip diameter of approximately 50 centimeters, a blade span and chord of about 4 centimeters, and a shaft speed of 17,600 rpm. The combustor, turbine disk, blades, and vanes will all be replaceable in the facility.

PROPULSION SYSTEMS LABORATORY

Performance testing of engines and components will be conducted in the propulsion systems laboratory shown in Fig. 16. Here large commercial and military engines can be operated under simulated altitude, speed, and temperature conditions. New designs to increase performance, minimize noise, and reduce pollution will be evaluated. Life predictions will be made for critical components to improve the reliability of these test engines.

CONCLUDING REMARKS

This report has reviewed the turbine component life-prediction program at the NASA-Lewis Research Center. The program is composed of a wide variety of on-going studies covering many aspects of materials research, environmental testing, and component development. It is divided into three general phases in various stages of completion.

Much progress has been made in the first phase: The development of life-prediction methods through materials studies. The basic modes of failure such as fatigue, creep, and oxidation are sufficiently well understood at this time to be described quantitatively. Computer codes are being written to include these failure modes in a unified manner.

A limited amount of progress has been achieved in the second phase of the program: the evaluation of prediction methods through combustion rig studies. Material properties are being measured in high-velocity gas atmospheres, and simulated turbine components are being tested in thermal fatigue.

The third phase of the program is now in the planning stage: the application of a unified life-prediction method to prototype turbine components in rigs and engines. This is the area where increased effort would be of greatest benefit. To be successful, this phase must involve program planners and specialists alike in mission analysis, materials, component design, fabrication, test operations, maintenance, and repair.

REFERENCES

1. Anon.: Aircraft Propulsion, NASA SP-259, 1971.
2. John N. B. Livingood, Herman H. Ellerbrock, and Albert Kaufman, 1971 NASA Turbine Cooling Research Status Report, NASA TM X-2384, 1971.
3. Jack B. Esgar, "Turbine Cooling: Its Limitations and Its Future," NASA TM X-52801, 1970.
4. Anon.: Aerospace Structural Materials, NASA SP-227, 1970.
5. John C. Freche and Robert W. Hall, "NASA Programs for Development of High-Temperature Alloys for Advanced Engines," *J. Aircraft*, vol. 6, no. 5, Sept.-Oct. 1969, pp. 424-431.
6. John C. Freche, "Materials for Jet Engines. Vehicle Technology for Civil Aviation: The Seventies and Beyond," NASA SP-292, 1971, pp. 85-106.
7. S. S. Manson, "New Directions in Materials Research Dictated by Stringent Future Requirements," NASA TM X-67885, 1971.
8. Salvatore J. Grisaffe and John P. Merutka, "Coatings for Aircraft Gas Turbine Engines and Space Shuttle Heat Shields; A Review of Lewis Research Center Programs," NASA TM X-68007, 1972.
9. J. Marin and K. Ohui, "A Review of Research on Low-Cycle Fatigue," Pennsylvania State Univ. (NASA CR-68704), Aug. 1965.

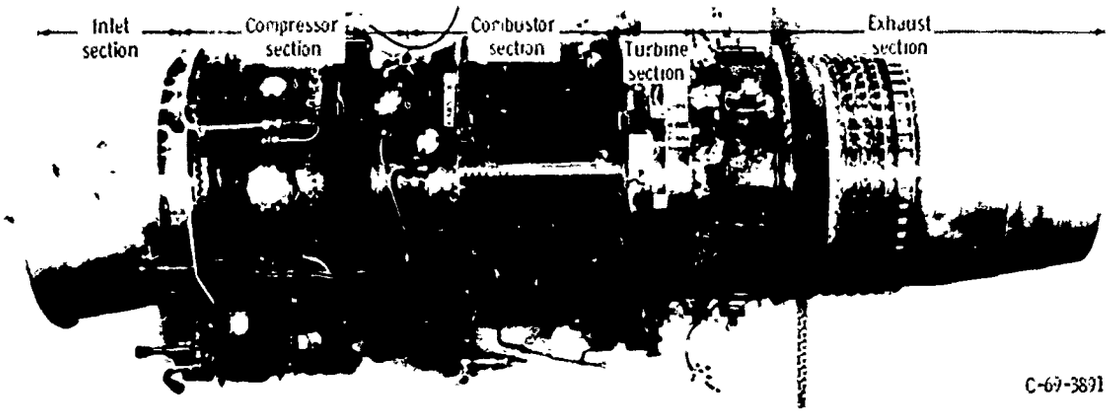

(a) General view of engine (modified J75 turbojet).

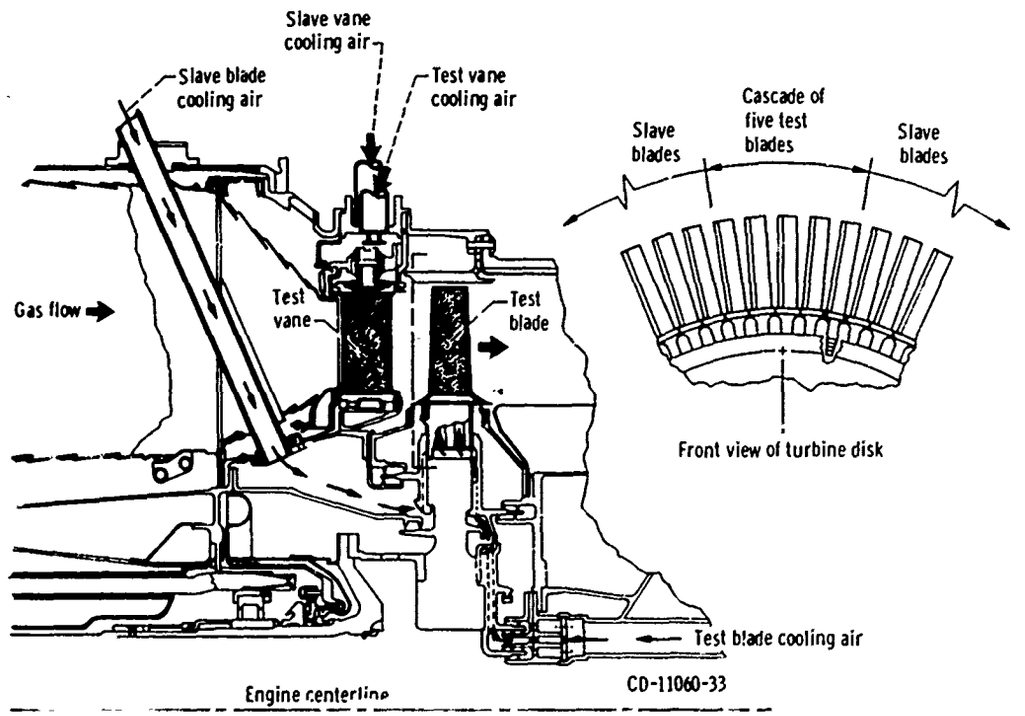

(b) Schematic of turbine section, showing test blades and vanes.

Figure 15. Research engine for life testing of turbine components.

10. S. S. Manson, *Thermal Stress and Low-Cycle Fatigue*, McGraw-Hill Book Co., Inc., 1966.
11. Alex..nder Mendelson, *Plasticity - Theory and Application*, Macmillan Co., 1968.
12. S. S. Manson and C. R. Ensign, "A Specialized Model for Analysis of Creep Rupture Data by the Minimum Commitment, Station-Function Approach," NASA TM X-52999, 1971.
13. S. S. Manson, "Time-Temperature Parameters–A Re-Evaluation and Some New Approaches. Time-Temperature Parameters for Creep-Rupture Analysis," Publ. D8-100, ASM, Jan. 1970, pp. 1-114.
14. David A. Spera, "A Linear Creep Damage Theory for Thermal Fatigue of Materials," Ph.D. Thesis, Univ. Wisconsin, 1968.
15. S. S. Manson, "Fatigue: A Complex Subject–Some Simple Approximations," *Exp. Mech.*, vol. 5, no. 7, July 1965, pp. 193-226.
16. David A. Spera, "Calculation of Thermal-Fatigue Life Based on Accumulated Creep Damage," NASA TN D-5489, 1969.
17. S. S. Manson, G. R. Halford and M. H. Hirschberg, "Creep Fatigue Analysis by Strain-Range Partitioning," Symposium on Design for Elevated Temperature Environment, ASME, 1971, pp. 12-28 (NASA TM X-67838).
18. G. R. Halford, M. H. Hirschberg and S. S. Manson, "Temperature Effects on the Strainrange Partitioning Approach for Creep-Fatigue Analysis," NASA TM X-68023, 1972 (to be published in ASTM STP 520, 1972).

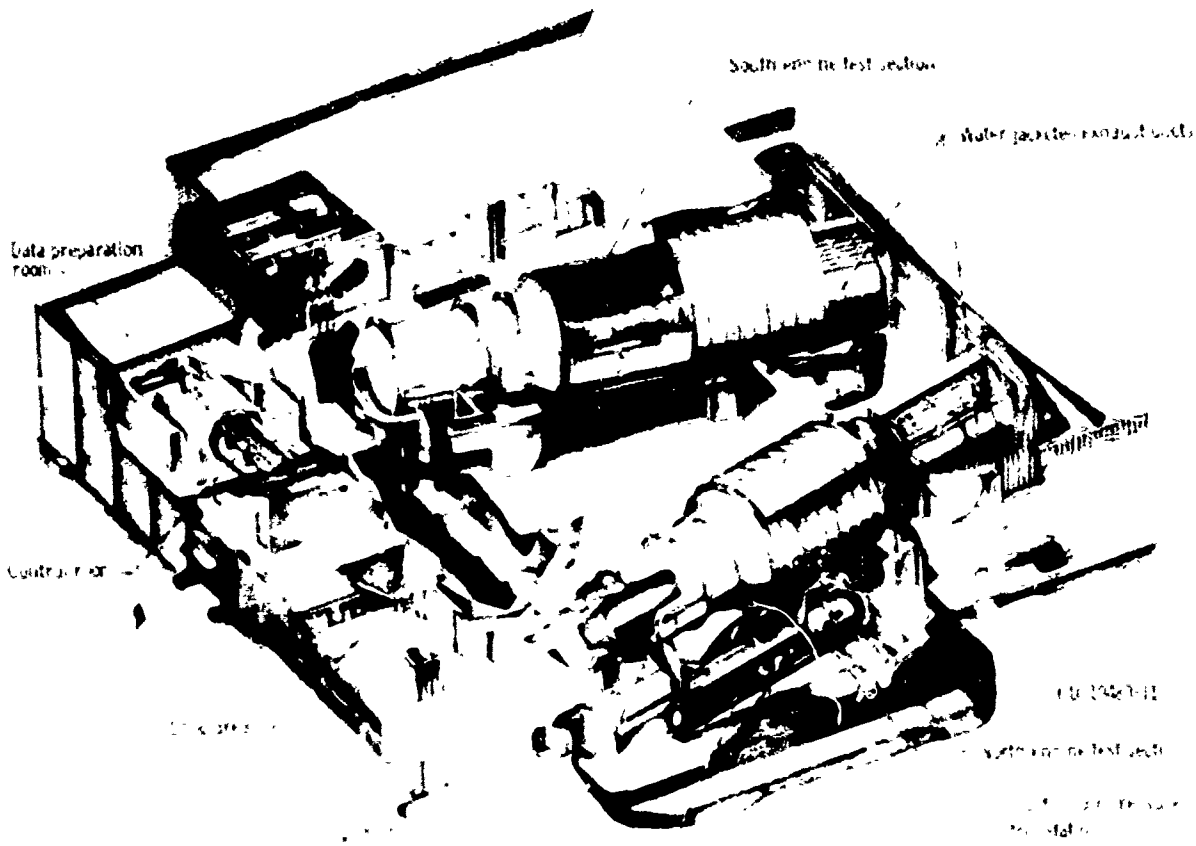

Figure 16. Propulsion systems laboratory for testing large turbofan and turbojet engines.

19. S. S. Manson, "The Challenge to Unify Treatment of High Temperature Fatigue–A Partisan Proposal Based on Strain-range Partitioning," to be published in ASTM STP 520, 1972.
20. Daniel L. Deadmore, "Observations on the Cyclic and Isothermal Oxidation of WI-52 and IN-100," NASA TM X-2195, 1971.
21. Hubert B. Probst, "Effect of Environment on Erosion-Corrosion Processes," Aerospace Structural Materials, NASA SP-227, 1970, pp. 279-294.
22. Salvatore J. Grisaffe, Daniel L. Deadmore and William A. Sanders, "Furnace and High-Velocity Oxidation of Aluminide-Coated Cobalt Superalloy WI-52," NASA TN D-5834, 1970.
23. Stanley R. Levine, "Cyclic Furnace and High-Velocity Oxidation of an Aluminide-Coated High-Strength Nickel Alloy (B-1900)," NASA TM X-2370, 1971.
24. Maurice A. H. Howes, "Thermal Fatigue Data on 15 Nickel- and Cobalt-Base Alloys," Rep. IITRI-B6078-38, IIT Research Inst. (NASA CR-72738), May 1970.
25. David A. Spera, Maurice A. H. Howes and Peter T. Bizon, "Thermal-Fatigue Resistance of 15 High-Temperature Alloys Determined by the Fluidized-Bed Technique," NASA TM X-52975, 1971.
26. David A. Spera, "The Calculation of Elevated-Temperature Cyclic Life Considering Low-Cycle Fatigue and Creep," NASA TN D-5317, 1969.
27. S. S. Manson, G. R. Halford, and D. A. Spera, "The Role of Creep in High-Temperature Low-Cycle Fatigue. Advances in Creep Design," A. I. Smith and A. M. Nicolson, eds., Applied Science Publ. Ltd., 1971, pp. 229-249.
28. David A. Spera, "Comparison of Experimental and Theoretical Thermal-Fatigue Lives for Five Nickel-Base Alloys," NASA TM X-68051, 1972 (to be published in ASTM STP 520).
29. James R. Johnston and Richard L. Ashbrook, "Oxidation and Thermal Fatigue Cracking of Nickel- and Cobalt-Base Alloys in a High Velocity Gas Stream," NASA TN D-5376, 1969.
30. Carl F. Lowell and William A. Sanders, "Mach 1 Oxidation of Thoriated Nickel-Chromium at 1204 C (2200 F)," NASA TN D-6562, 1971.
31. V. S. Moore, W. D. Brentnall and A. R. Stetson, "Evaluation of Coatings for Cobalt- and Nickel-Base Superalloys," Vol. 2, Rep. RDR-1474-3, Solar Div., International Harvester (NASA CR-72714), July 1970.
32. D. A. Spera, F. D. Calfo and P. T. Bizon, "Thermal Fatigue Testing of Simulated Turbine Blades," NASA TM X-67820, 1971.
33. Howard F. Calvert, Reeves P. Cochran, Robert P. Dengler, Robert O. Hickel and James W. Norris, "Turbine Cooling Research Facility," NASA TM X-1927, 1970.

Appendix

MECHANISMS OF COATING FAILURE

It has been observed that coating failures are usually preceded by a certain sequence of changes in composition and structure (22,23). Figure 17 shows typical changes in the microstructure of a coated turbine alloy, caused by cyclic oxidation. The system shown in the figure is an aluminide coating deposited on a B 1900 substrate (a typical cast nickel-base alloy). As shown in Fig. 17(a), the coating actually consists of four distinct layers between the surface oxide and the B 1900 substrate. It has been determined that oxidation protection in this coating is obtained primarily from layer II, composed of nickel-monoaluminide, NiAl. If the NiAl layer is broken, rapid oxidation of the substrate begins. Thus, the thickness and integrity of the NiAl layer is critical to the oxidation resistance of coated turbine components.

Two simultaneous processes combine to change the thickness of the NiAl layer: (1) a growth process that thickens the layer at the II/III interface, through inward diffusion of aluminum and outward diffusion of nickel and (2) a consumption process that thins the layer at the I/II interface, through oxidation and depletion.

The growth process is generally dominant in the early stages of exposure to high temperature. In Fig. 17(a), after 100 1-hour cycles at 1090°C, the NiAl layer is approximately 50 percent thicker than it was at the start of testing. The consumption process then becomes dominant. In Fig. 17(b), layer II has become much thinner after 400 1-hour cycles. Finally, after additional exposure, the NiAl layer breaks up (see Fig. 17(c)), opening paths for the oxidation of the substrate. This layer breakup can be considered to be the start of a coating failure, as proposed by Grisaffe (31).

The processes of growth and consumption leading to breakup are shown graphically in Fig. 18 for aluminide coated B 1900. Starting from an initial thickness of 43 micrometers, the layer grows to a peak thickness that is strongly dependent on the exposure temperature. The higher the temperature, the smaller the net amount of growth above the initial thickness. After reaching its peak thickness, the NiAl layer becomes thinner at a rate that is assumed to be constant for a constant temperature. The consumption rates shown in the figure were calculated using the Arrhenius equation:

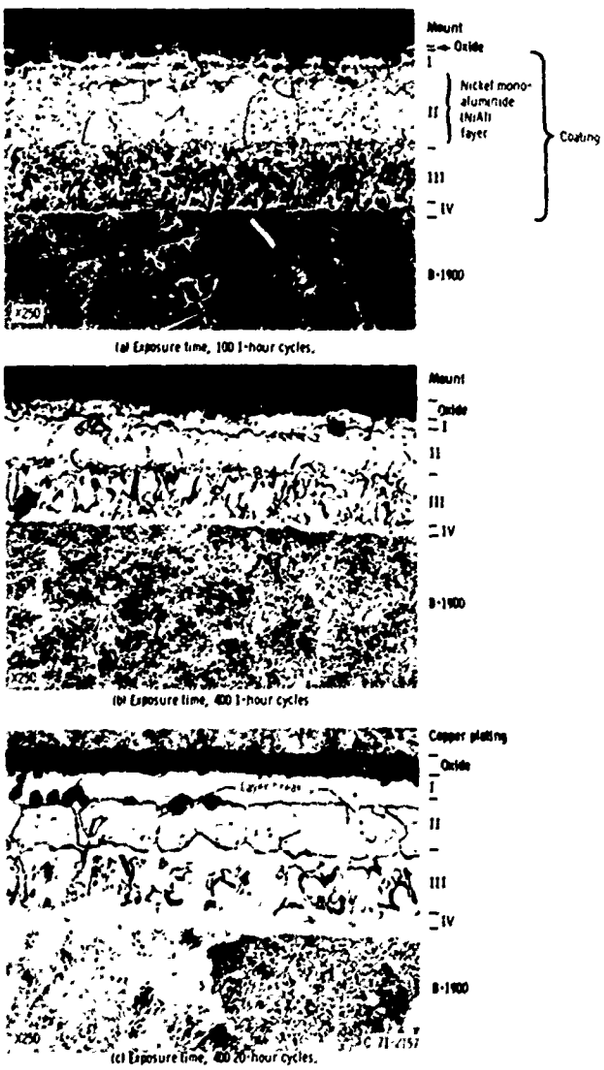

Figure 17. Changes in coating microstructure during cyclic furnace oxdation. Temperature, 1090°C; slow cooled hourly to 50°C.

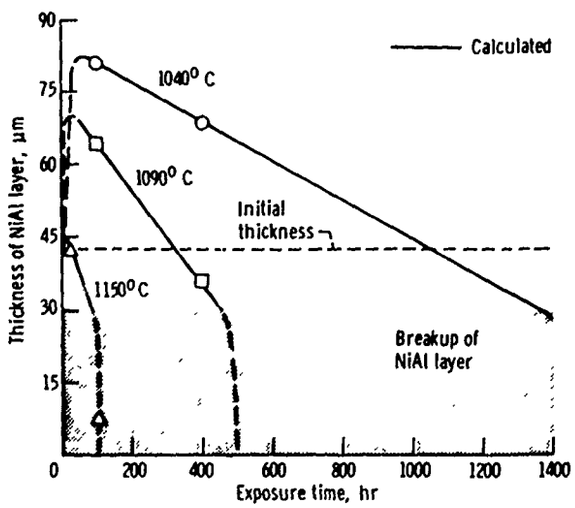

Figure 18. Growth, consumption, and breakup of nickel monoaluminide (NiAl) layer during cyclic furnace oxidation. Substrate, B 1900; slow cooled hourly to 50°C.

$$\frac{dh}{dt} = Ae^{-Q/RT}, \qquad h_b \leq h \leq h_{max}, \qquad \mu m/hr$$

where

h	thickness of NiAl layer, μm
t	exposure time, hr
A	curve-fit constant, μm/hr
Q	activation energy, J/mole
R	universal gas constant, J/mole-K
T	exposure temperature, K
h_b	thickness below which breakup occurs, approximately 30 μm
h_{max}	peak layer thickness, μm

The activation energy Q was found to be approximately equal to that for the diffusion of nickel in NiAl.

The indicated breakup thickness of 30 micrometers is a preliminary value measured for NiAl. Once breakup occurs, consumption of the broken layer continues at an increasing rate, as is indicated by the dashed lines in Fig. 17. Similar thickness data have been reported for aluminide coated WI-52, a cobalt-base alloy (22).

The concept of layer breakup is an attempt to quantitatively describe the processes shown in Fig. 17 and 18. With this concept the pure coating life could be calculated from its composition and a knowledge of the growth rates, consumption rates, and minimum unbroken layer thickness.

The same sequence of structural changes has been observed in burner rig specimens, but at much higher rates. Similarities can be seen between the microstructures of a typical wedge-shaped specimen (Fig. 19) and a typical furnace specimen (Fig. 17) of the same alloy and coating. Figure 19 shows a NiAl layer that has grown in thickness after 100 1-hour cycles on the side of the wedge specimen in a lower temperature region. However, in a hotter region near the leading edge (Fig. 19(b)), the layer has become thinner and broken. On the leading edge itself, in the area of severest spalling, the protective NiAl layer has been completely consumed. Similar comparisons have been made between rig and furnace tests of aluminide coated WI-52 (22). However, the differences in rates were not as great as for the aluminide coated B 1900. It can be concluded, then, that the concept of layer breakup might also be used to predict coating life in a Mach 1 gas stream using increased rate constants.

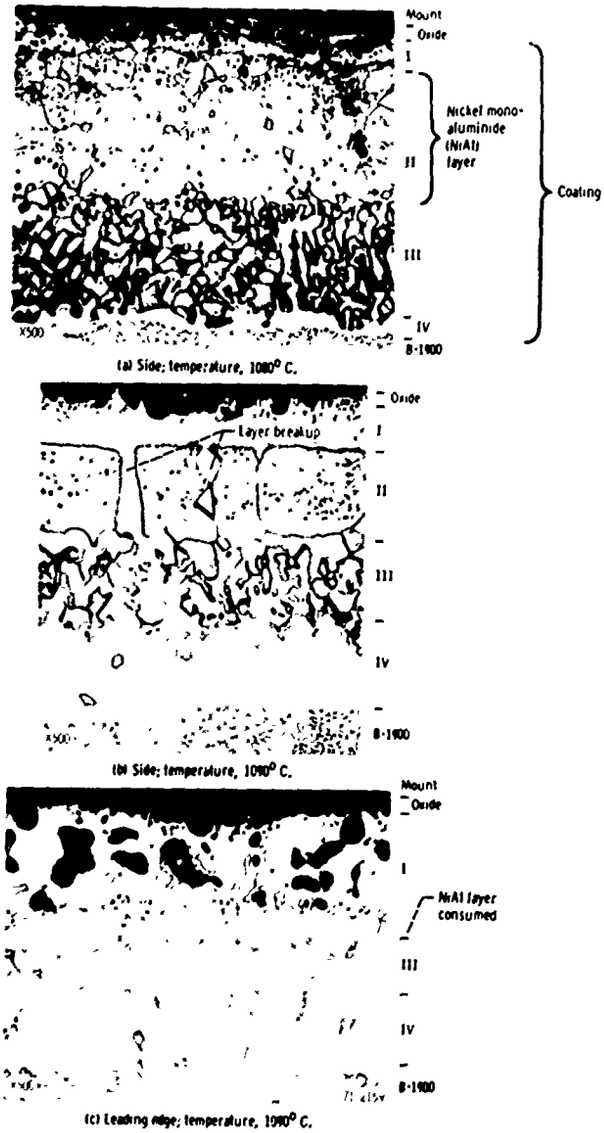

Figure 19. Changes in coating microstructure during cyclic burner-rig oxidation. Maximum temperature, 1090°C; 100 1-hour cycles; aluminide coating on B 1900 substrate.

Discussion:

LIFE PREDICTIONS OF TURBINE COMPONENTS: ON-GOING STUDIES AT THE NASA-LEWIS RESEARCH CENTER

Dr. Murray Kaufman
General Electric
Lynn, Massachusetts

The work described is essential to permit more accurate life prediction for gas turbine blades and vanes. The use of the high pressure hot-gas tunnel rig, the static cascade rig and the research engine as test vehicles to aid in verification of prediction methods is extremely valuable and probably unique. Since the paper is only a review of the types of programs in progress, and not a detailed technical study, it is difficult to offer specific suggestions. However, a few comments can be made that may help in guidance or evaluation of the programs.

1. The Method of Universal Slopes used to calculate cyclic life includes tensile properties (ductility and strength) among its parameters, yet many nickel-base alloys are subject to great changes in these properties as a function of exposure to elevated temperature. They may lose or gain in properties depending on the exposure conditions and the test temperatures. The Method must be able to cover such changes.

2. The Method of Life Fractions for calculation of creep-rupture cyclic life is in common use. Careful cyclic rupture tests on various alloys have shown that this rule is not sufficiently accurate for direct application. Depending on the exact sequence of temperature-load conditions and on the alloy itself, life percentages of well under or over 100% have been found reproducibly. Any use of the Life Fraction method should be based on the proper fraction for the alloy and mission.

3. Oxidation (and hot corrosion) testing is often reported in terms of weight gain. However, for practical use where mechanical properties are important, the depth of attack (localized or general) is the major factor determining the effective load carrying capacity remaining and should be measured and reported.

4. Thermal fatigue is a critical design parameter, and a reliable calculation method would be extremely desirable. The simple linear combination of the Universal Slopes + Life Fractions does not seem sufficiently accurate, with a range of 9:1 in predicted:actual life among the results shown. Perhaps the corrections suggested in 1 and 2 above can help make the agreement closer. Actual engine thermal fatigue conditions are more complex than the disc-type test, and the use of the more advanced rigs will be very helpful in extending the prediction methods. Inclusion of oxidation/corrosion effects into these calculations is desirable, but will be difficult. Oxidation at the tip of a crack (or even an incipient crack) is more rapid than on a stress-free surface, and initiation and progression of a thermal fatigue crack is easier at an oxide: these interactions should be considered.

5. The apparent great loss of creep-rupture life in a burner rig atmosphere is quite surprising. Over ten-to-one losses (even when coated) were sustained. Engine experience does not indicate effects of such magnitude. One of the aspects of the testing that may contribute to the loss is the use of a constant load. As oxidation decreases the effective cross section of the specimen, the true stress increases. A small stress increase represents a large life decrease. For coated material, exposure during test causes base metal-coating interdiffusion, and the additional phases found below the original boundary may be detrimental to creep resistance. Some good explanations should be made for this loss.

6. The concepts used to describe aluminide coating life are very good. Several different coating/alloy combinations should be investigated, since there is a variety of coating microstructures that are produced in the different processes. The variation in structures may have some effect on diffusion and life. It can be noted that the use of diffusion constants to determine NiAl deterioration to Ni_3Al are more appropriate to calculate corrosion life than for oxidation life. In a corrosive environment, any break in the NiAl layer, as by conversion at the grain boundary to Ni_3Al, may result in rapid attack at that point. However, the NiAl would still have a long life remaining in an oxidizing environment.

Marine Turbine Corrosion, Rig Evaluation and Engine Experience

K. Page and R. J. Taylor
Rolls-Royce Limited, Industrial and Marine Division
Ansty, Nr. Coventry

1. INTRODUCTION

The first Rolls-Royce aero derived gas turbine entered marine operational service in 1958. This was a Proteus engine installed in a Brave class patrol boat. However, our first marine experience dates from 1953 when HMS Grey Goose was commissioned with experimental RM 60 engines. Since 1958 a total of over 350,000 operational hours have been accumulated at sea with a total of 300 engines of four different types.

The purpose of this paper is to review some of this experience relevant to the performance of critical turbine and stator blade materials and coatings, and to outline our current programmes and philosophy for the selection of new materials for uprated versions of the engines and also to extend the lives at current ratings.

It should be noted that this paper is a broad engineering presentation of the information, rather than a detailed metallurgical discussion of the materials and coating technology or mechanisms of corrosion.

2. SUMMARY OF OPERATING EXPERIENCE

Table I summarises the applications and operational experience for the four types of engines currently on marine use.

One half of the running time at sea has been accumulated on hovercraft with two types of engine, Proteus and Gnome. The operating environment for Hovercraft is particularly severe due to high levels of sea spray generated during particular modes of operation.

In addition to engine experience at sea, a large number of operating hours have been accumulated in industrial applications, primarily electrical generation, and where the environment is either close to the sea, the atmosphere is polluted with sulphurous compounds, or there have been high levels of salts present in the fuel.

This has resulted in limitations on turbine life due to corrosion to a greater or lesser degree dependent on severity of environment.

It is most difficult to be specific in trying to correlate experience on corrosion obtained with the above factors, but typically the Industrial Avon H.P. blade life can be reduced from around 4000 hours with little corrosion on a "good" site to 1000-1500 hours with severe corrosion where the above factors are present.

3. CURRENT BLADE MATERIALS AND COATINGS

3.1 ROTOR BLADE MATERIAL

At the time when aero service engines were first adapted for marine and industrial applications, the rotor blade material most widely in use by Rolls-Royce was N 105. This material was retained for the marine applications with the engine rating adjusted conservatively to provide several thousands of hours predicted creep life and with due recognition of our knowledge on sulphidation at elevated temperatures. It was perhaps fortuitous that the bulk of our aero blade experience was, at that stage with this higher chrome content material which provides reasonable basic corrosion resistance in the marine environment. Whilst we continued to build up our marine experience, the aero side in recent years have moved towards the more advanced high strength casting alloys with low chrome content, and a penalty in sulphidation resistance. As a result of this we could for the future no longer rely directly on the aero programmes for new corrosion resistant blade materials.

3.2 BLADE COATING

Pack aluminising is applied as the standard coating for blades in the critical positions to thickness limits of .0007"-.0015".

3.3 NOZZLE MATERIALS AND COATINGS

Current material for the nozzle guide vanes is X 40 which at an early stage replaced the then standard aero materials such as Nimocast 90 and C 242. Again pack aluminising is applied as the standard coating for all applications.

Table I
Summary of Operating Experience

Engine	Application	No. of Engines Installed Service	Max. Turbine Entry Temp. °K	Corresponding Max. Blade Temp. °C	Operational Hours at Sea
Olympus 24500 BHP	Frigates Destroyers Corvettes	20	1165	830-850 (1530-1560°F)	10,000
Proteus 4250 BHP	Fast Patrol Boats Gunboats Torpedo Boats Hydrofoils Hovercraft	107	1145	820 (1510°F)	217,000
Tyne 4250 BHP	Frigates Destroyers Hydrofoils	5	1170	825 (1520°F)	1,685
Gnome 1050 BHP	Hovercraft	49	1100	750-800 (1380-1560°F)	123,000

4. CORROSION OF BLADES IN SERVICE

In section 2 a summary of our background experience is given in terms of engine hours. Some results from this background are worth illustrating.

Figure 1, Proteus Engine–H.P. blades in X 40 and N 105 pack aluminised, 1000 hours shore trials, max. turbine entry temp. 1180°K.

Figure 2, Proteus Engine –H.P. blades in X 40 and N 105 pack aluminised, 1500 hours Hovercraft operation, max. turbine entry temp. 1145°K.

Figure 3, Proteus Engine–H.P. blades in G 64, 2000 hours industrial operation in salt environment, max. turbine entry temp. 1145°K.

Figure 4, Proteus Engine–H.P. nozzles in X 40 with and without pack aluminising, 1500 hours Hovercraft operation, max. turbine entry temp. 1145°K.

Figure 5, Proteus Engine–Comparison of "marine" and "industrial" corrosion on H.P. turbine blading, 1500 hours.

Figure 6, Industrial Avon–Corrosion at 1900 hours on N 115 H.P. blade, pack aluminised with high levels of salt in fuel, max. operating turbine entry temp. 1170°K.

Figure 7, Proteus Engine–H.P. blade N 105 corroded remote from max. temperature profile on blade aerofoil, industrial operation.

Figure 8, Olympus Engine–Marine shore trials at 1225°K turbine entry temperature. Corrosion at 1000 hours, with comparison between thin and thick pack aluminising (.0007" to .0015") respectively. Material N 115.

Figure 9, Proteus Engine–Further evidence of effect of pack aluminising layer thickness on Proteus engine Hovercraft application, 1500 hours, 1145°K.

The inspection of corroded components, of which the above are representative, and correlation with the relevant field environment as far as this is possible permits some broad conclusions to be made.

- Surprise at the relative good performance of G 64 in the Proteus, related to its lower chrome content (ref. Fig. 3).
- There is obvious benefit in carrying the maximum thickness pack aluminising coating, as illustrated on the Olympus and Proteus blading, provided it is effectively diffused to ensure coating cracking does not occur reducing the overall life of the blade in fatigue (ref. Figs. 8, 9).
- In general the wart-like corrosion associated with fluxing on the blade (650°C approx.), is more typical of worst industrial operations where a high level of atmospheric pollution and suspected fuel contamination is present (ref. Figs. 5, 6, 7). It is interesting to note that much higher levels of corrosion on the I.P. and L.P. stages, which are run at lower temperature, have occurred specifically on the Avon engine associated with a polluted atmosphere. We believe this may be the result of a generally more aggressive condition resulting in oxidation at temperatures below the sulphidation threshold (approx. 700°C).
- Local high concentrations of salt passing through to the turbine can be deleterious to life. This may be caused by breakdown of air intake filters in high humidity conditions or fired washing of marine engines at infrequent intervals. On the Proteus engine we have demonstrated in

X. 40 NIM. 105

X. 40 NIM. 105

Figure 1. Comparative corrosion attack on Nimonic 105 and X 40 material (pack aluminised) H.P. rotor blading trials evaluation at N.G.T.E. Pyestock. Proteus Marine Engine P 10016, 975 hours running with "salt in fuel" (0.6 ppm), blade metal temperature 870°C max.

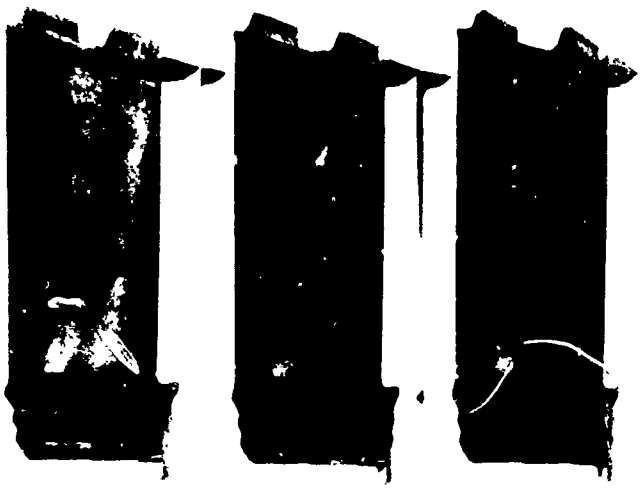

Figure 2a. Vac melted X 40 H.P. rotor blades pack aluminised—service evaluation in the SRN4 Hovercraft. Proteus Engine No. P10128 after 1525 hours running, blade metal temperature—850°C max.

Figure 2b. Nimonic 105 material H.P. rotor blades pack aluminised showing severe corrosion attack after 1260 hours running in the SRN4 marine Hovercraft. Proteus Engine P10131, blade metal temperature—850°C max.

the field that blade life can be doubled by deletion of fired washing by adopting crank wash procedures on a cold engine. This latter procedure has now been our primary washing method for approximately two years.

- In general the severity of corrosion on the blading is related in severity to the temperature profile, but occasionally corrosion has occurred on N 105 more severely in the colder regions around the hub and tip. This is illustrated in Fig. 7 of a Proteus H.P. turbine blade from industrial operation. We must conclude from this that corrosion can occur at temperature levels much lower than normal peak sulphidation temperatures usually shown by rigs (ref. Fig. 7).

Salt levels acceptable to the engine.

- Where salt levels in fuel have exceeded 0.6 ppm sodium in industrial applications, sulphidation of turbine blading has been severe.

4711006589	Part No.	B. 203785
HR Alloy Mat. 2053 (N. 105) Pack aluminised Precision forging	Specification	Jessops G. 64 BACF 433 Vacuum melt Precision casting Pack aluminised
	Las Palmas Experience	
10088	Engine No.	10085
July 69 in T. S. 5	Installed	Aug. 69 in T. S. 1
April 70	Removed	June 70
Low Power	Reason	Reduction gear snag
2053 hours	R/T total	1991 hours
2035	Generation	1968
576	Starts	551
3. 56	Hrs. /Start	3. 60
2120	Average load	2100
19-29°C	Ambient (Outside)	19-28°C
485-520°C	Obs. E. G. T.	495-520°C
10960-11500	Obs. C. R. P. M.	11160-11440
Cold soak only	Washing	Cold soak wash
Knitmesh	Int. Filters	Vokes manual roll on.
Result - Catastrophic corrosion		Result - Concave pack aluminising completely removed - form penetration in order of 0. 015"

Figure 3. Industrial Proteus 1st row turbine rotor blades. Comparison of N 105 & G 54 material, site—Las Palmas, different engines.

a. X 40 uncoated H.P. vanes—showing catastrophic hot cororsion attack.

b. X 40 pack aluminised H.P. vanes—showing characteristic hot corrosion attack.

Figure 4. Proteus Marine—1525 hours in Hovercraft SRN4, Engine No. 10128, vane metal temperature—approximately 900°C.

Marine Installation
F.P.B.

Industrial Site
Marine Atmosphere

Figure 5. Nimonic 105 pack aluminised H.P. blades showing concave form attack on a marine engine compared with the wart-like growths on land based engines. Proteus Marine Installation—F.P.B., 610 hours, Proteus Industrial—Las Palmas—1022 hours, blade metal temperatures—850°C max.

CONCAVE FORM

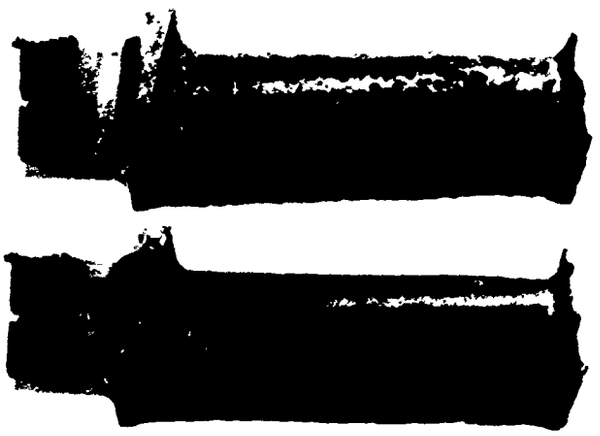

CONVEX FORM

Figure 6. Nimonic 115 H.P. blades showing typical form of corrosion attack experienced on land based engines subjected to high level of salt in fuel. Avon Industrial Engine 37015 after 1900 running hours.

Figure 7. Nimonic 105 H.P. blades showing corrosion attack remote from the maximum temperature profile at mid-chord position. Proteus Industrial Engine P10003-1, EX S.W.E.B. site Lynton—running time 576 hours.

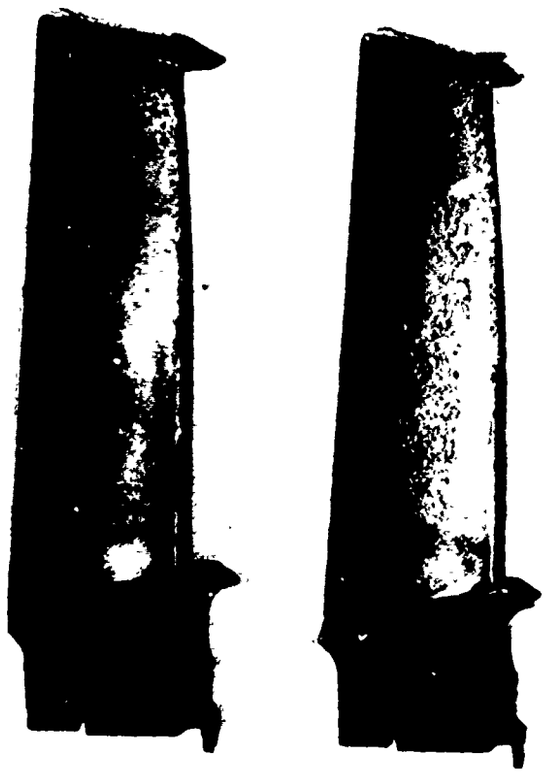

Figure 8. Nimonic 115 pack aluminised H.P. blades showing corrosion attack on good blades (normal Pt/Al thickness) and bad blades (0.00075 inch thickness). Olympus Marine TM3, shore trials engine 951 hours running (409 hours with salt injection) 0.01 ppm salt in air plus 0.6 ppm salt in fuel. Blade metal temperatures—880°C max with temperature of around 830°C under shroud.

● On Marine shore trials engines, where salt is introduced into the engine at 0.01 ppm salt in air (equivalent to about 0.25 ppm sodium in fuel), and associated with a fuel having a low sodium content, the level of corrosion has been less severe.

We believe in the longer term, that to obtain really long life in a marine environment it is necessary to have not more than 0.3 ppm sodium in the fuel and 0.01 ppm salts in the air supplied to the engine. On larger ships, as opposed to Hovercraft and Hydrofoils, we would expect the latter figure to be very much less for high percentages of the operating time.

We would emphasise that a wide scatter in turbine life can be achieved in service for apparently identical installations and operational roles. Whilst salt in air and fuel has been recorded, washing methods and general servicing requirements standardised, not enough specific knowledge has been obtained to permit a full appreciation of the factors involved.

It is important in the future that more detailed monitoring, on a continuous basis is programmed, and in particular, covering the widest possible range of engine application.

Figure 9. Nimonic 105 pack aluminised HP blades showing severe corrosion attack on 0.0007 inch thick pack aluminised blades. Proteus Marine Hovercraft Engine P10131, 1260 hours blade metal temperature–850°C max.

5. NEW MATERIALS AND COATINGS

5.1 GENERAL PHILOSOPHY

The Company is committed for the immediate future to higher ratings on the Olympus and Tyne engines in the marine field, and the Olympus and Avon for industrial applications. In the longer term new engine projects, both ex-aero engine derived, and basic new design are currently under evaluation.

Apart, therefore, from the requirement to provide improved life for existing service engines, a more fundamental reason for improvement exists, and where higher levels of blade cooling is essential.

With the development of cast materials which have sulphidation resistance at least equivalent to the Nimonic series of forging materials, notably N 105, and adequate creep strength for marine applications, the Company decided to take advantage of the more efficient cooling which could be achieved with cast cooled blade designs in relation to a forged material equivalent. We believe it would have been unwise to pursue this policy if the basic sulphidation resistance of possible casting materials had been worse than current materials, and placed reliance solely on lower blade surface temperatures. At the same time Rolls-Royce considered basic cast cooled blade technique had been adequately proven.

It was also decided that for any future uprated, or new designs of engine we would limit the maximum blade surface temperature within 825°C. This figure has been derived from our overall service experience to date.

The difficulty of properly simulating engine operating conditions in a static corrosion rig has influenced our thoughts on material evaluation, and we regard such testing as an initial coarse screen for ranking materials and coatings prior to engine evaluation. The more representative the rig can be made, e.g. high pressure, the more valuable this initial assessment will be.

Due to the wide scatter on severity of corrosion in service it is believed essential for final engine test evaluation to be conducted in "rainbow" turbines, using existing blade materials and coatings as a datum.

Rolls-Royce has not pursued any policy of accelerated engine testing for material comparisons, as our interpretation from rig tests at various levels of temperature and salt concentrations do not suggest such tests conducted on an engine would be meaningful to interpret accurately the relative improvements which may appear in service engines.

Because of these difficulties, and our present limited knowledge on the factors promoting sulphidation, we consider that the engine test evaluation referred to above should be carried out in the field on service engines at the earliest opportunity.

In conjunction with the Ministry of Defence endurance tests of approximately 2500 hours on complete engine modules are carried out. These tests are aimed at establishing overall reliability, and whilst valuable information on turbine corrosion is obtained, it relates primarily to life evaluation on existing turbine standards.

The above policy has also been influenced by:

- There is no requirement to demonstrate predicted improvement to a certifying authority to the same extent as necessary within the aero concept. This, therefore, permits field trials to start earlier.
- The high degree of cooperation the Company receives from customers for service evaluation, both in terms of preferred environment and in areas where high utilization will be achieved.

5.2 OVERALL PROGRAMME

As previously mentioned the materials now regarded as standard for our existing marine engines are pack aluminised X 40 for the first stage nozzle guide vanes and pack aluminised N 105 for the first stage rotor blade.

The basic programme for improvement beyond this stage may be summarised as follows:

a) Select a blade material suitable for cast air cooled blades for uprated engines. Based on corrosion rig and other laboratory testing discussed below, this material has now been selected as In 738, with M 432 as an alternative. Blades are now being cast for the first uprated engine development programmes, on the uprated Tyne and Olympus for marine and the Olympus and Avon for industrial application. This material will also be used in some guide vane positions where X 40 does not provide an adequate strength margin.

b) Evaluate the preferred material, pack aluminised In 738, and M 432 in existing service engines if possible, where blading is not air cooled, tooling exists, or is relatively simple, and time scales and costs for introduction are small. The basic evaluation in this context will

i) establish improvements for existing engine ratings
ii) be valid for future higher ratings which are being achieved with increased cooling, and where blade surface temperatures will be within existing experience.

c) Evaluate readily available vendor coatings on both current and new materials in combustion rigs and current engines, and if justified standardise on one of them instead of pack aluminising.

d) Evaluate in the combustion rigs 3 and 4 element coatings now in the initial development phase, and when justified proceed to engine evaluation.

e) Evaluate the newer high strength, high chrome, materials such as In 792.

Of course, in practice the work is not necessarily phased in the orderly manner described, since for example coatings which show initial promise may well rapidly advance to engine field evaluation, or materials may be selected to solve particular problems on one engine in advance of their use on other engines.

Current position on the above overall programme is discussed in 5.3 and 5.4 below.

Briefly, we have completed rig evaluation of materials for engine ratings required in the immediate future, and are now introducing these materials into existing service engines where possible on the basis outlined in 5.2(b).

With regard to alternative coatings, evaluation of existing vendor coatings, and some experimental coatings are now being trialled in service.

5.3 RIG TESTING

Work on new materials for engines for the Royal Navy is funded by MOD(N). At present this is carried out at 3 sites, as follows:

1) Rolls-Royce Laboratories at Derby in Aero Division.
2) Rolls-Royce Laboratories at Bristol in Aero Division.
3) Admiralty Materials Laboratories at Poole Dorset.

A brief summary of some of the results of these programmes is given below.

Rolls-Royce Derby Laboratory Work

This work has been directed as phase (a) in 5.2 of the programme to select a material for cast air cooled blades for the Tyne RMIC Engine with max. rating of 1285°K T.E.T. which is now entering the initial development phase.

Three candidate materials, In 738, M 432 and U 700 were selected for evaluation of their corrosion resistance in both the uncoated and pack aluminised condition, and for a laboratory assessment of other properties such as creep rupture strength. To provide a comparative basis, N 105 used for corrosion, and In 100 for castability assessment.

Corrosion Testing–Corrosion tests were conducted in a low pressure combustion rig. Rod specimens 7 mm diameter are arranged in a cylindrical assembly which is then rotated at 1300 rpm and the exhaust from the combustion chamber directed at the centre of the specimens.

Salt solution (using synthetic salt or DEF 1053) is sprayed into the air before combustion to give a concentration of 4 ppm. The fuel used is a medium gas oil to specification BBS 2869. The thickness of the coating for the pack aluminised samples was .0008"/.0015". It should be noted that the Tyne RMIC cooled blade surface temperature range at maximum rating is 780°C to 825°C.

The results of the tests at 820°C and 870°C are given in Figs. 10 and 11. It will be seen that at 820°C the penetration experienced by all three candidate materials in the uncoated condition was less than .0005" in 600 hours under these accelerated conditions, and all were considerably less than N 105. In the coated condition all except In 738 seem to have suffered an increase in the depth of attack, with U 700 and N 105 having penetrated the aluminised layer.

At 870°C, which is thought to be near the peak sulphidation temperature for most metals, all three materials show a significant increase in the depth of attack in the uncoated condition, but still considerably less than the attack on Ni 105. The pack aluminised samples all show a low rate of attack with no penetration of the coating. However, the Ni 105 samples showed a severe off centre attack i.e., at a lower temperature portion of the sample.

This evidence suggests that Ni 105 suffers its peak attack at temperatures lower than for the other materials, that is at 820°C or lower. It also suggests that the rate of attack of Ni 105 is very much greater after the first 50 to 120 hours of rig running (at these accelerated corrosion conditions). This is consistent with previously observed results on this rig which indicate an extended incubation period for Ni 105 compared with other mateirals. These earlier results, using aviation kerosine as the fuel and with 4 ppm salt injection are shown in Figs. 12 and 13.

A number of anomalies are again apparent, for example the very low attack experienced by uncoated U 700 using

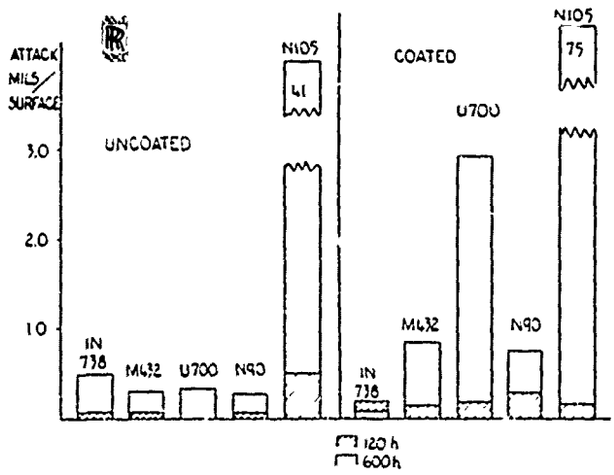

Figure 10. Corrosion resistance–820°C, 4 ppm salt (with diesel fuel).

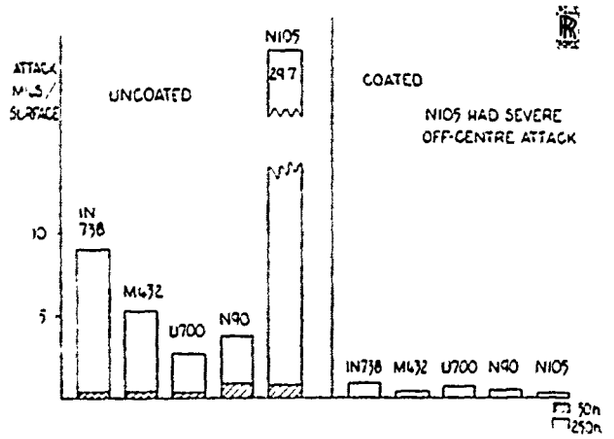

Figure 11. Corrosion resistance–870°C, 4 ppm salt (with diesel fuel).

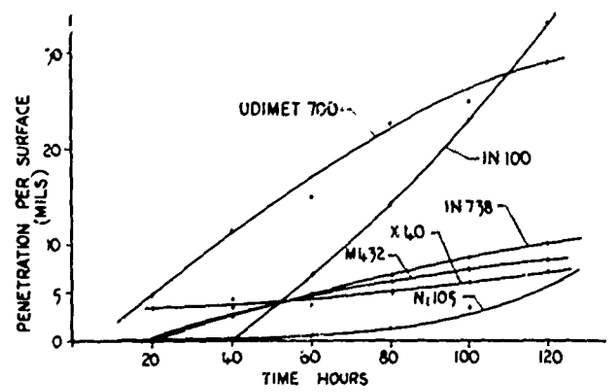

Figure 12. Corrosion rate of uncoated specimens at 870°C, 4 ppm synthetic sea salt in air (aviation kerosine fuel).

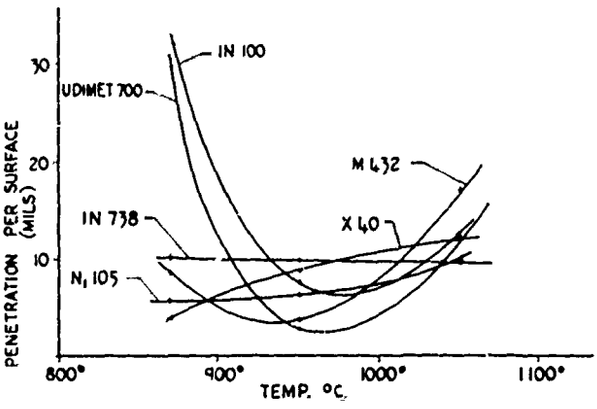

Figure 13. Corrosion depth of uncoated specimens after 120 hours, 4 ppm synthetic sea salt in air (aviation kerosine fuel).

diesel fuel compared with the high level of attack with previous tests using kerosine.

Material Properties–In addition to the corrosion tests, this programme also covered other material properties, the most important of which were creep rupture strength, creep consistency, coating adhesion (pack aluminising) and castability, thin wall strength and fatigue of hollow specimens. Some results of these tests are shown in Figs. 14 and 1..

Typical 100 hour stress rupture data show In 738 and M 432 to be much the same, with U 700 slightly inferior. On creep consistency M 432 proved to be the best with good resul also being obtained for In 738. However, the U 700 samples tested proved to be very poor for consistency.

The coating adhesion tests were carried out on half rhombic specimens tested in a spinning rig for 6000 cycles at 1050°C. These showed U 700 to be the best with In 738 also quite satisfactory, but M 432 gave poor performance. However, since the corrosion attack on M 432 at 1050°C is quite severe, this could have an adverse influence on these results and it is expected that acceptable results wil be obtained at the lower temperatures seen by the rotor blades.

Castability–Casting tests were deliberately carried out on an existing aero intricately cooled blade and this showed that U 700 is much better than In 100, In 738 is comparable to In 100, and M 432 is very poor. However, previous casting tests with solid blades showed M 432 to be satisfactory and it is thought that the material will also be satisfactory for blades with the relatively simple cooling configurations designed for the next series of engines. Additional casting trials with more representative blade designs are now in hand.

Some results for tensile and fatigue properties are shown in Figs. 16 and 17. These indicate that M 432 and In 738 are the best with U 700 less satisfactory.

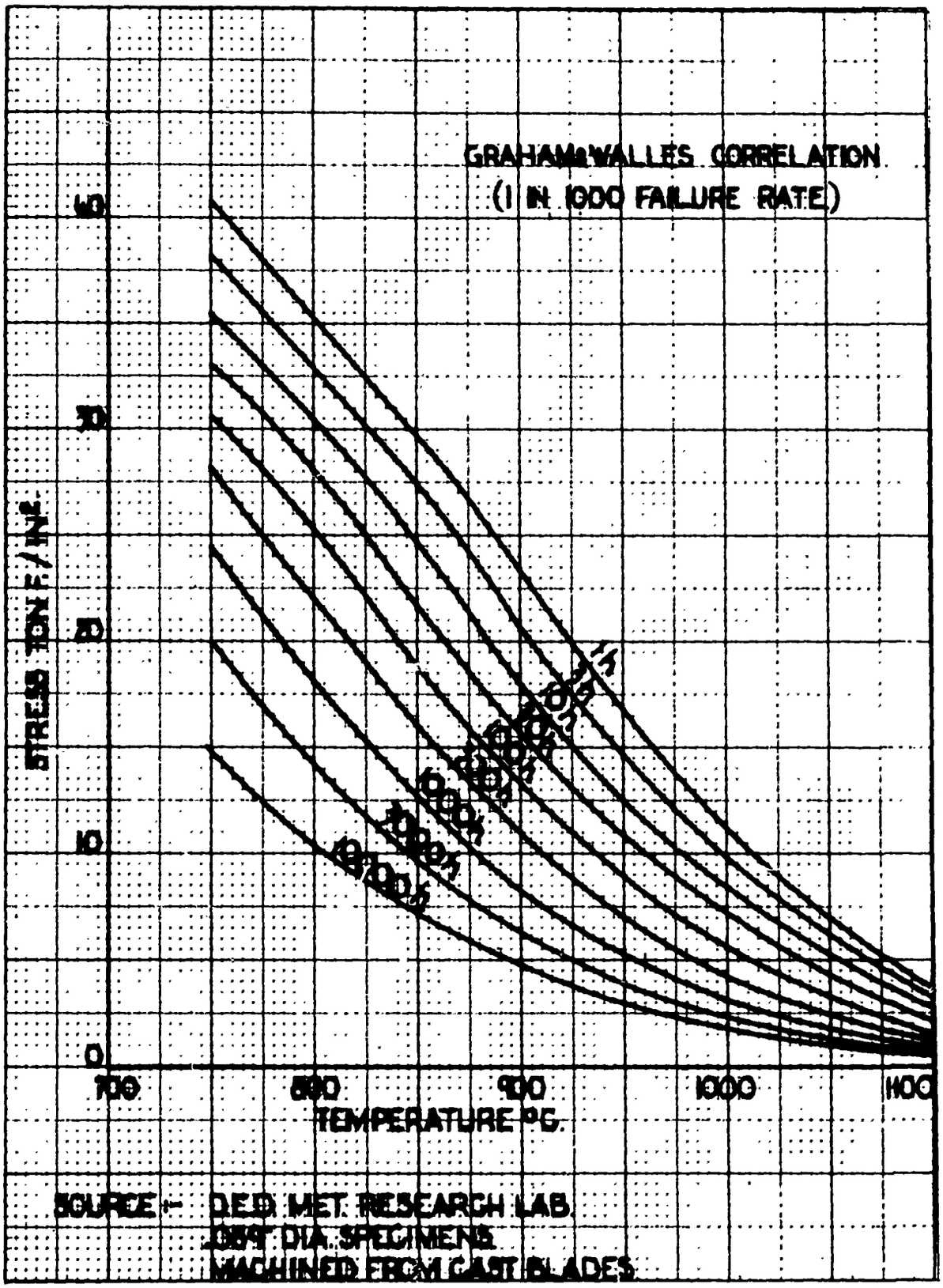

Figure 14. Estimated minimum stress rupture properties.

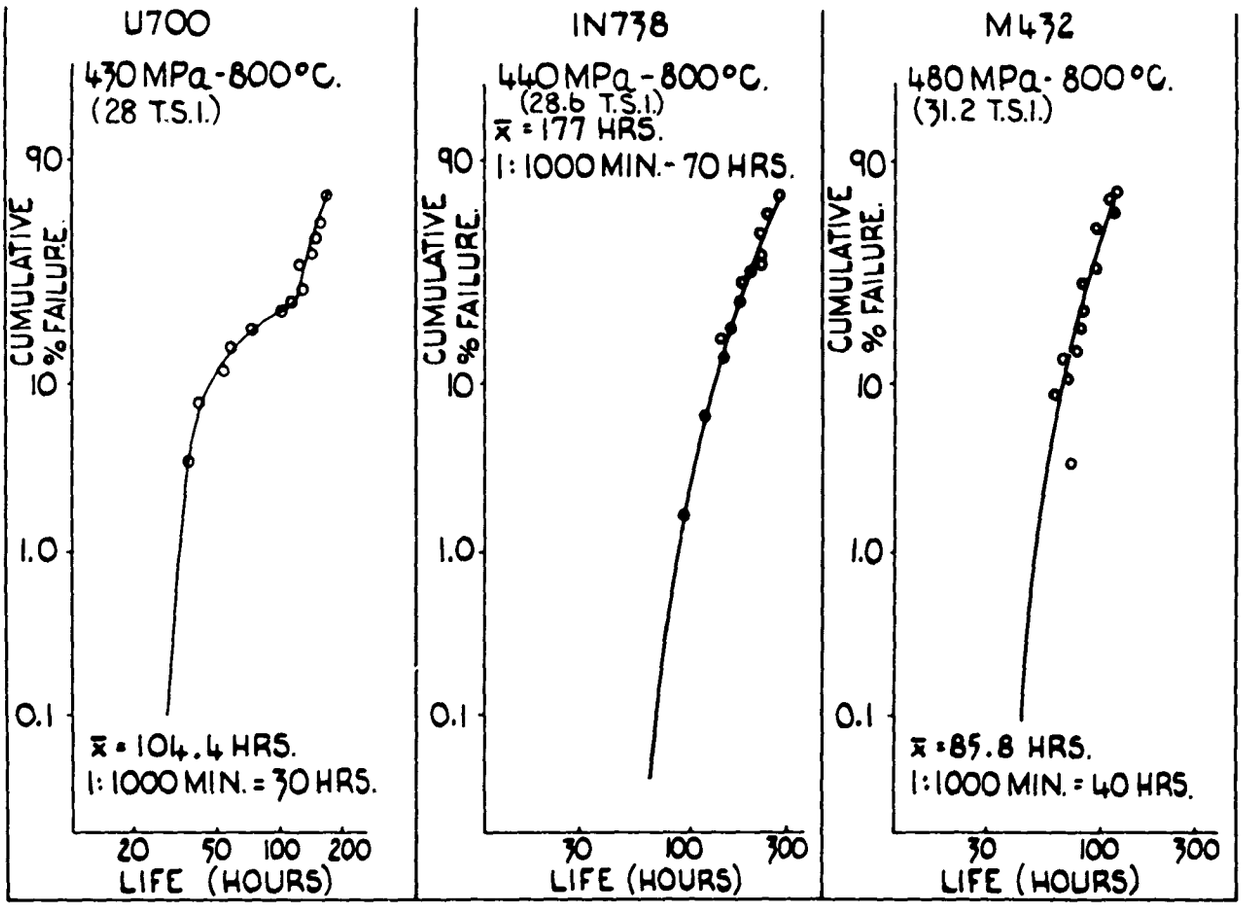

Figure 15. Creep consistency.

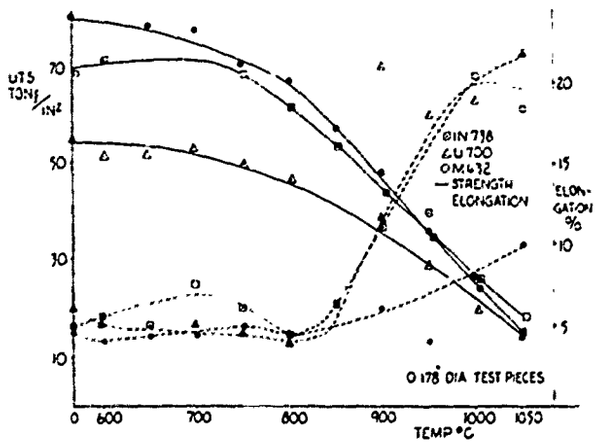

Figure 16. Tensile strength & elongation—comparative.

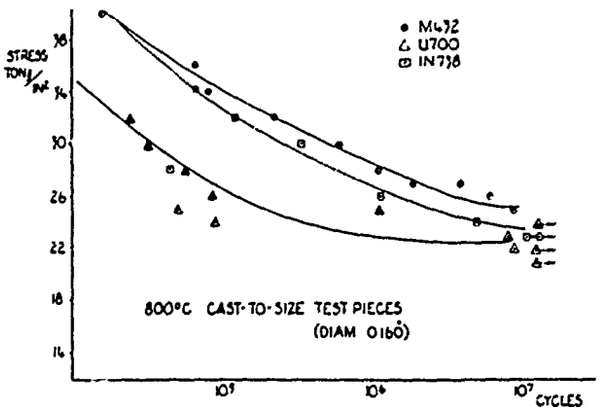

Figure 17. Rotating bend fatigue—comparative.

Rolls-Royce Bristol Laboratory Work

This work is directed at phases c and d in 5.2 mentioned previously, that is the corrosion rig evaluation of alternative coatings to our standard pack aluminising process. At the moment the programme is directed mostly at identifying improved coatings for the current blade material Ni 105, but also includes tests on pack aluminised alternative materials.

The main test procedure consists of 3 furnace cycles of 18 hours each at 850°C on specimens that are first washed and weighed and then coated with 1 mg/cm^2 Na_2SO_4 prior to each cycle. This is followed by a further 72 hours at 850°C and finally cleaning by blasting with fine alumina abrasive. The cycle is repeated until the coating shows signs of failure.

Additional furnace tests at 850°C have been carried out using an alternative procedure in which the application of sodium chloride replaces erosion as the means of removing the protective scale.

Low pressure burner rig tests using 10 ppm salt in air have also been conducted on pack aluminised samples of the candidate materials.

The results of the programme to date are given in Table II. These show that pack aluminised In 738 has significantly improved corrosion resistance compared with pack aluminised Ni 105 and Ni 115. Also for Ni 105, alternative coatings can be identified which show considerable potential

Table II
Rolls-Royce Bristol Laboratory Work
Merit Rating of Materials/Coatings From Results to-Date

Material/Coating 1.5-2.0 thous. in.	Sodium Sulphate/ Erosion 850°C Coating Life Hrs.	Sodium Sulphate/ Sodium Chloride 850°C Coating Life Hrs.	B.E.D. Burner Rig (10 ppm salt)* 870°C Depth of Penetration in 400 Hours
N 105 Pt-Al (LDC2)	1500		
X 40 P.Al.	1500	125	
X 40 Cr-Al (H. 1.15)	1250	375+	
N 105 Ta-Cr-Al	1250-1500	375	
In 587 P.Al.	1250	125	
N 105 Cr-Al (H. 1.15)	1250	250	
In 738 P.Al.	1000-1250	125	0.8 Thous. ins.
N 105 CoCrAlY (Vac. Hyd. slurry)	500-1000		
N 105 (Cr) + Al (MDC 701)	875-1000		
M 432 P.Al	875 1000	125	1.1 Thous. ins.
N 105 Cr-Mn-Al	875		
N 105 Mn-Si-Al	750-875		
N 105 P.Al.	500-625		1.4 Thous. ins.
N 115 P.Al.	500		1.2 Thous. ins.

*Injected as Portland seawater supplied by the Admiralty Materials Laboratory.

improvement over pack aluminising, and these coatings will be engine evaluated as quickly as possible. Microsections of the pack aluminised samples tested on the burner rig are shown in Fig. 18.

Erosion has been identified as an important factor in the overall resistance of the coatings, and additional tests were carried out with the erosion cycle included after each 125 hours. These results are shown in Table III, and it is interesting to note that the previous order of merit of the retested coatings was reversed and the Mn-Si-Al coating was now superior to the Ta-Cr-Al and Al coatings.

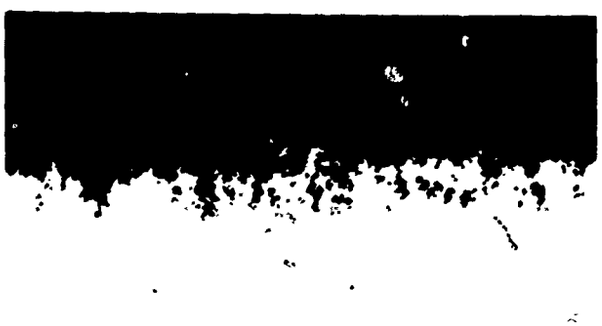

N105 P.Al, X500, 3760

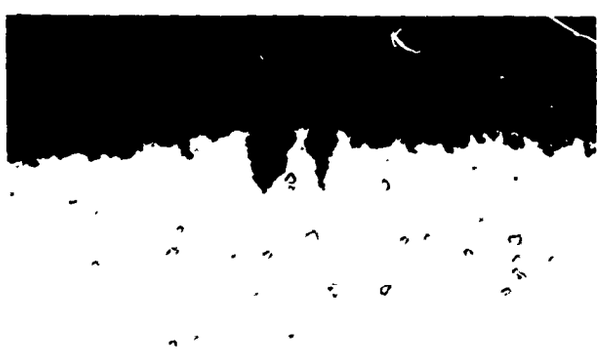

Mar-M 432 P.Al, X500, 3759

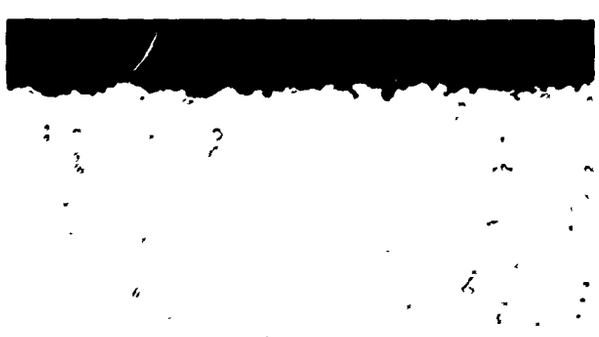

In 738 P.Al, X500, 3757

Figure 18. Rolls-Royce Bristol Laboratory burner rig tests. 400 hours at 850°C, 10 ppm salt with kerosine.

Table III
Effect of Erosion on Coating Life

Material/ Coating .0015" to .002" thick	Sodium Sulphate Furnace Tests Coating Life–Hrs.	
	One erosion cycle per 125 hours	4 erosion cycles per 125 hours
Ni 105 Ta-Cr-Al	1250-1500	425
Ni 105 Mn-Si-Al	750-875	750
Ni 105 P. Al	500-625	375

A.M.L. Corrosion Tests

The A.M.L. corrosion tests are carried out in a low pressure combustion rig using Diesofuel and with natural seawater injected in to the air to provide a concentration of 0.1 ppm salt in air at the test section. The gas velocity onto the specimens is about 1200 ft/sec, and for these initial tests non rotating cascade specimens were used.

Tests at 850°C for 200 hours have shown the average weight loss for uncoated specimens when corrected for rig position factors (20% maximum correction) to be:

In 738	.297 gms
M 432	.122 gms
Ni 90	.094 gms
Ni 105	.091 gms

The relative positions of uncoated In 738 and M 432 is consistent with the results obtained on the Rolls-Royce Derby rig, and the low attack on Ni 105 is consistent with an extended incubation period at this temperature and the low level of salt contamination.

In similar tests at 850°C, pack aluminised samples of In 738, M 432 and Ni 105 all performed in a similar manner.

A further comprehensive programme is being carried out covering a range of coatings from Rolls-Royce pack aluminising to currently available vendor coatings and experimental 3 and 4 element coatings, which will be tested on Ni 105, N 115, In 738, M 432, X 40 and M 509. For these tests, rod type specimens will be used and rotated in a similar manner to the Derby rig–A range of representative blade and vane temperatures will be investigated, and degree of penetration will be used as the performance criterion instead of weight loss.

Selection of Preferred Material--Whereas the information generated by the above programmes was limited and not entirely consistent, it was sufficient coupled with information derived from literature surveys for us to identify In 738 as the preferred material for current engine evaluation

and use in the next series of engines. Further information is now being generated on this material, in particular the effects of thin cast sections coupled with pack aluminising on the mechanical properties. In addition further work will also be directed at assessing the influence of heat treatment cycle and amounts of interdiffusion on the thin wall properties of In 738 when coated with alternative vendor and experimental coatings. Weldability and brazing trials are also being conducted.

5.3 TEST EVALUATION

Marine Shore Trials–Proving of Existing Blade and Nozzle Material

In conjunction with the Ministry of Defence, shore trials are carried out on current marine engines simulating operational requirements.

Tests have been completed for the initial rated Olumpus engines, where approximately 2500 hours were achieved by 1968.

Current shore trials programmes for the higher rated Olympus at 1220°K Turbine Entry Temperature and for the Tyne RMIA at 1170°K, are in progress. Both have completed approximately 1500 hours.

Nominally our objectives are to obtain 2500 hours endurance, and subsequently extend the trials to keep in front of operational experience in service.

Where possible, we will introduce into these trials alternative coatings, ref. (c) and (d) in section 5.2, and possibly cast blading in existing form in In 738.

Material Evaluation on Engine Trials

In agreement with the philosophy defined in 5.2 Inco 738 and M 432 solid cast blades, pack aluminised, are being introduced on a trials basis on to existing engines.

The primary areas are:

- Marine Proteus–In 738 and M 432 are now being trialled on Hovercraft, fitted in a "rainbow" set with the existing proven X 40 blade material. These are pack aluminized.
- Industrial Avon–In 738 sets of H.P. blading will be available for service engine evaluation early 1973.
- Industrial/Marine Olympus–In 738 blades will be available for limited service evaluation early 1973.

Coating Evaluation–Existing Coatings

Industrial Avon–From the rig evaluation work on coatings within the Aero Divisions and A.M.L. we have introduced on a trials basis a number of vendor and experimental coatings on existing nozzle and blade materials, fitted in rainbow sets. The primary coatings under relative evaluation are:

Nozzles (C 242)–H 115, MDC 701, MDC 9, CODEP B1, P3 Aluminised plus Ceramic RW 132J30C. (R.R. Exp.)

Rotor Blades (N115)–H 115, MDC 7, MDC 9, CODEP B1, MDC 701 "Thick" pack aluminising, Blades coated with stellite X 40.

Marine Proteus–In the short term, we will be introducing In 738 and M 432 rotor blading on a trials basis in Hovercraft application with MDC 701 and H 115 coatings.

As soon as manufacturing techniques for the preferred Mn-Si-Al and Ta-Cr-Al coatings have been established, we will introduce these into services engines on existing blade designs.

Environment Conditions

In conjunction with above work we are implementing a parallel programme on more detailed and continuous recording of salt contamination in fuel and air supplied to the engine.

Salt levels upstream and downstream of both air and fuel filtration systems will be recorded in more detail than in previous exercises, and particularly in conjunction with improved air filtration systems. This will be on both marine and industrial sites to obtain a wide range of contaminant levels.

We consider work to progressively reduce salt ingestion is of equal importance, and we need to establish more specifically the levels at which corrosion may be effectively eliminated, and whether these are achievable.

6. CONCLUSIONS

1. In order to properly assess the realtive merits of alternative materials and coatings it is preferable to test engines with rainbow turbines in the actual operational environment.

2. More extensive field monitoring of engine operating environments and running schedules is necessary in order to obtain a better understanding of the relative importance of various factors influencing corrosion.

3. A better understanding of the relative importance of salt in fuel and salt in air is also required.

4. Engine cleaning or washing techniques can have a significant effect on hot end component life, and increased development effort in this area is required.

Discussion:

MARINE TURBINE CORROSION, RIG EVALUATION AND ENGINE EXPERIENCE

Paul A. Bergman
General Electric, Lynn, Massachusetts

I would compliment the authors on an interesting and information paper on hot corrosion, particularly the coverage of considerable field experience. In addition, their ambitious plans are commendable relative to "rainbow" testing of various alloys and coatings in field engines and extensive monitoring of engine operating environments and running schedules. This type of information is vital to the ultimate success of gas turbines operating in marine environments.

Salt Concentrations–The authors have delineated 10 ppb sea salt as a critical maximum amount in order to achieve really long life parts. On large ships, much less than 10 ppb would be expected most of the time. Our experience mostly based on aircraft engine operation in marine environments including considerable helicopter service would support some figure of about 10 ppb at least for times of 1000 to 2000 hours although not much accurate information is available.

In the past, gas turbines have been corrosion tested with unrealistically high sea salt concentrations, e.g. 300 ppb. In many of these tests even the most corrosion resistant materials were subject to severe effects in 100 to 300 hours. The current trend in this country is to require longer engine tests at lower and more realistic salt concentrations. For example, the Military Specification for Ships (MIL-E-17341C) specifies 50% of testing time at 3 ppb salt, 45% at 7 ppb, 3% at 16 ppb and 2% at 30 ppb. Testing times are 1000 or 3000 hours.

Temperatures–The minimum temperature of corrosion is a provocative subject due in part to the variable engine conditions, diverse corrosive environments and the lack of accurate information. The authors have shown a variability in the minimum corrosion temperature apparently based on different corrosion conditions but a temperature of 1515°F (825°C) was implied. Would the authors confirm, deny or modify the minimum temperature of significant corrosion in the marine environment encountered in ship and hovercraft applications?

Our service information indicates that in a practical sense the threshold temperature of corrosion is about 1500°F since no major problem is known to exist at lower temperatures at least in 1000 to 2000 hours. Only relatively shallow depths of sulfidation have occurred at lower temperatures under normal conditions. However, the minimum temperature of corrosion may be as low as about 1350°F based on longer operating times, low vanadium (.5 ppm) fuels, possibly local reducing conditions and the use of less resistant alloys. Higher vanadium fuels could lower the minimum temperature further.

The authors indicate that their new design concept would limit the blade surface temperature to about 1515°F by air cooling in order to minimize corrosion. This design feature seems to be a severe penalty to pay.

Alloys–It is noted that aluminized N105 and X-40 are the primary materials used but reference is made to N115, C242, Nimocast 90 and G64. Would the authors indicate a ranking of these materials and others and, if possible, quantify the alloy behavior in terms of expected life in normal marine environments? In addition, does coating X-40 improve its corrosion performance? It is our experience in aircraft gas turbines to coat X-40 mainly for oxidation resistance at higher temperatures, i.e. above 1800°F. At lower temperatures where sodium sulfate deposits and hot corrosion occurs, X-40 has an excellent resistance to the environment without any coating.

It is noted that in burner rig testing U700 showed a better corrosion resistance than Inco 738 when diesel fuel was consumed but an inverse ranking occurred with kerosene. Our burner rig tests with a variety of fuels have consistently denoted U700 (or Rene 77) as moderate in corrosion resistance–better than IN 100 and Inco 713 but not as good as the new group of alloys containing 13 to 16% chromium along with balanced or high ratios of titanium to aluminum like Inco 738 and Rene 80 and probably M432 and N115. However, all of these latter alloys probably have relatively less oxidation resistance. Engine experience has supported the corrosion ranking at least in regard to IN 100, Inco 713, Rene 77 and Rene 80. In the opinion of the writer, the validity of the test is questionable when U700 shows a good resistance to a hot corrosion environment unless it really is an oxidation oriented test. However, this type of controversy supports the need for engine data especially the "rainbow" type of testing. Nevertheless, the quality of laboratory testing should be continually improved rather than rationalized.

Coatings–The authors show that in lab testing, nickel aluminide coated specimens are subject to greater amount of attack at 1515°F (825°C) than the uncoated specimens. We have likewise seen this behavior in rig testing. Would the authors comment on the possible mechanism and the ramifications of the phenomenon in field engines?

Sputter Deposited Coatings for Marine Gas Turbine Blades and Vanes

John Fairbanks
Naval Ship Engineering Center, Hyattsville, Maryland

Edward McClanahan and Ray Busch
Battelle-Northwest, Richland, Washington

BACKGROUND

The US Navy is committed to extensive use of gas turbine engines for propulsion from the mid-1970s through the 1980s. The high power-to-weight ratio, compactness and rapid response of the gas turbine virtually dictate its use for hydrofoil and surface effect ships and craft and make it a prime candidate for large non nuclear vessels.

The major problem with gas turbines operating in the marine environment is sulfidation corrosion in hot-section components. Sulfidation currently restricts time between overhaul to about 4000 hours. This life is obtained by vapor deposited Co-Cr-Al-Y coatings and by limiting the first-stage average metal temperature to about 1530°F. Current aircraft engines have average metal temperatures of 1850°F, however, the superalloys used in these engines have significantly lower sulfidation resistance than those used in marine gas turbines. As a result of some laboratory testing, one engine manufacturer predicts about a 30% reduction in life with a 60°F increase in average metal temperature above 1530°F (1).

Performance of marine gas turbine engines can be dramatically improved by operating with higher turbine inlet temperatures. For example, an increase in power output of about 17% could be obtained with a 100°F increase in temperature. Thus, it is highly desirable for the naval application of gas turbines to increase the turbine inlet temperature without incurring an engine life penalty. In fact, improved engine life is highly desirable from a naval vessel on-station capability viewpoint.

The current coating production art employs electron-beam evaporation from a continuously fed rod source. The electron beam is focused on the top surface of the alloy rod to form a liquid pool, while the rod is fed at a rate to maintain a constant rate of evaporation, as shown schematically in Fig. 1. Turbine blades are rotated in the evaporant cloud until the deposited coating is about 5 mils thick. Such coatings on blades and vanes have provided significant improvements in marine gas turbine performance and life. However, the current-art vapor deposition processes have several disadvantages for coating turbine blades and vanes, which include the following: Deposition is by line-of-sight from a small area source, thereby limiting the areas that are coated. The vapor pressure of the alloy constituents must not differ from each other by more than 10^3, or dual sources must be used to avoid the formation of a "distilled" coating. The vapor deposited coating has a columnar structure which requires modification by post-deposition heat treatment. Early experience in the Callaghan with vapor deposited coatings indicated columnar structure provided paths for corrosive agent migration to the blade substrate. The evaporation process has a low material efficiency; i.e., most of the evaporated material is deposited on chamber walls, thus restricting consideration of expensive elements as alloy constituents.

The Navy wants improved marine gas turbine reliability, increased engine performance with respect to power output and fuel consumption, and increased time between overhauls. The use of the sputtering process for blade and vane coating holds significant potential to achieve some of the above goals. A program with Battelle-Northwest has been initiated to develop and evaluate sputtered coatings on blades and vanes. The Naval Ship R&D Center, Annapolis, will conduct extensive burner rig and mechanical tests to evaluate the coatings. A review of the history of sputtering and a description of the process is in order.

SPUTTERING HISTORY

Deposition of thin films by sputtering has a history dating back to a paper by Wright in 1877 (2). Generally, until the 1940s the interest in sputtered films was primarily for optical and protective coating applications. The appearance of the active semiconductor in the late '40s stimulated the miniaturization of the related passive devices (resistors, capacitors, etc.). Thin films allowed reduction in size, but such films required close control of electrical, chemical and mechanical properties. At this point deposition by sputtering received increased attention.

Coincidently, basic investigations of sputtering were conducted by several researchers, in particular G. K. Wehner

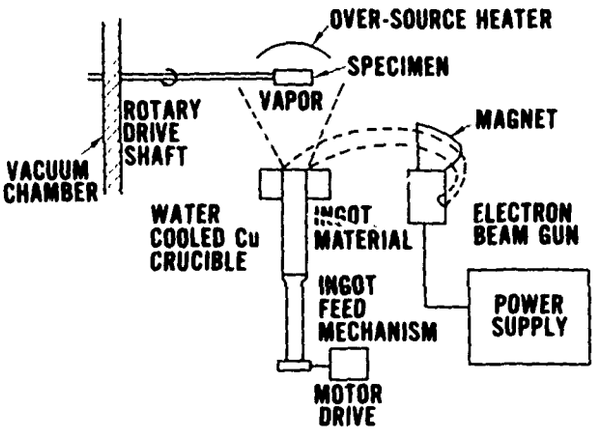

Figure 1. The vapor deposition coating process.

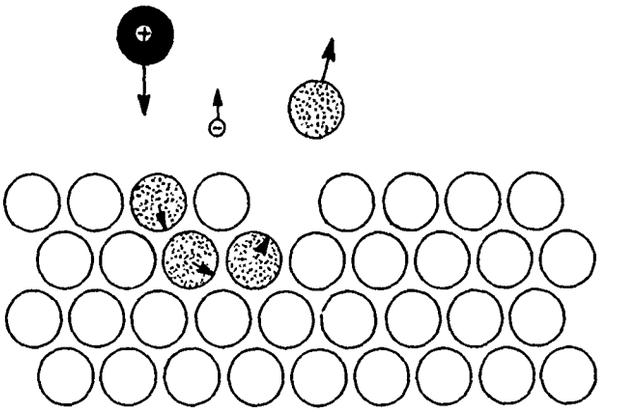

Figure 2. Basic sputtering mechanism.

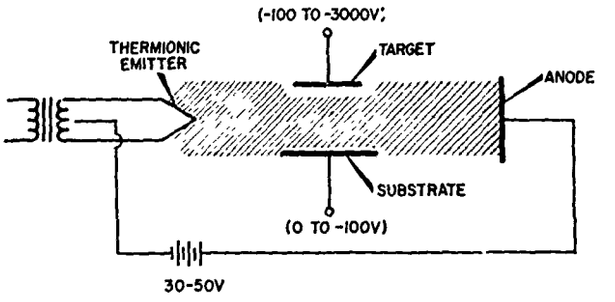

Figure 3. Thermionic supported discharge for triode sputtering.

and co-workers. In 1955 Wehner (3) suggested the possibility of using radio frequency power for sputtering of insulators which was demonstrated five years later. The development of sputtering has occurred rapidly and continuously to the present time. Generally the applications use thin films, such as integrated circuits for the electronics industry, and thin corrosion-resistant coatings for razor blades, to name a couple of many applications.

Deposits in the range of several mils thickness were usually not considered practical because of the low deposition rate associated with sputtering. However, with supported discharge (or triode sputtering) equipment much higher deposition rates have been attained, permitting deposit thicknesses of several tens of mils. Battelle-Northwest has developed numerically controlled equipment for sputter deposition at high rates on large areas and various geometries.

SPUTTERING MECHANISM

Experimental evidence, particularly that obtained from sputtering of single crystals indicates the sputtering phenomenon is a momentum transfer process.

Figure 2 shows a simple model illustrating momentum transfer through binary collisions. Sputtering is conveniently carried out in noble gas discharges where positively charged ions are drawn out of the plasma by applying a negative potential to an immersed electrode. Atoms ejected from this target or cathode may be collected on surfaces placed adjacent to the target.

Figure 3 is an electrical diagram of a typical triode sputtering apparatus. The chamber is evacuated and backfilled with argon or krypton to a pressure of several millitorr. Next, a potential of 40-50 volts is applied between the heated tungsten filament and the anode. The discharge is produced by ionizing collisions made by the electrons before they are collected at the anode. The discharge current is controlled by the filament temperature. A negative potential (50-100 volts) applied to the substrate causes the positive ions to bombard its surface for cleaning. The deposition begins when a negative potential 100-3000 volts is applied to the target. The substrate may be allowed to "float" or biased negatively if desired. Typical substrate biasing is about -15 volts but in no case more negative than -75 volts.

Sputtering of ceramics or insulators is a little more complex. An impressed negative charge on the target surface is quickly neutralized by incoming positive ions. A solution is to apply a radio frequency (RF) potential to the back of the target. This approach takes advantage of the difference in ion and electron mobilities. A net negative charge is developed on the surface proportional to the peak-to-peak RF potential. During the greater portion of the RF cycle the surface is ion bombarded, while the loss of charge is replenished by electrons during the small remaining portion of the cycle.

The resultant average negative potential of the surface allows successful sputtering of insulators and the energy of the impinging ions can be varied and controlled by changing the peak-to-peak RF potential applied.

POTENTIAL ADVANTAGES OF SPUTTER DEPOSITED COATING ON TURBINE BLADES

The deposition by sputtering of overlay coatings on marine gas turbine blades and vanes offers several significant advantages over evaporation or aluminiding. 1) The blades can be atomically cleaned immediately prior to deposition by "sputter etching." This procedure is the most thorough cleaning technique known. 2) The target used in sputtering can be designed to coat complex geometries. A possible scheme to coat a vane pair is shown as Fig. 3. The design of targets for coating a specific geometry involves considerable art as well as science. 3) The sputtered coating, by virtue of its high energy deposition, has much greater adhesion than vapor deposited coating. 4) There are indications that sputter coatings on blades will not require heat treatment thus reducing the blade-coating interdiffusion region. 5) Sputter deposition coating structure can be controlled precisely thereby incorporating a high reliability potential for coating reproducibility.

One of the general advantages of sputtering is that it can be used to deposit practically any material or combination of materials, uniformly or in laminated or graded structures. This results from the fact that sputtering is a momentum transfer mechanism that does not require coating material phase change. This removal of a number of restrictions on candidate materials or alloy constituents for turbine blade coating provides a tremendous potential for improved coatings.

POTENTIAL DISADVANTAGES

There are several possible problem areas. The one most commonly raised is low deposition rate and high equipment cost. However, improvements in equipment have led to deposition rates of greater than 2 mils thickness per hour for materials similar to those used here. Also, the equipment is numerically controlled, so relatively low rates do not imply high labor costs. Finally, a large number of blades can be simultaneously coated. One possible target geometry for multiple blade coating is shown as Fig. 4. This effectively reduces the equipment cost.

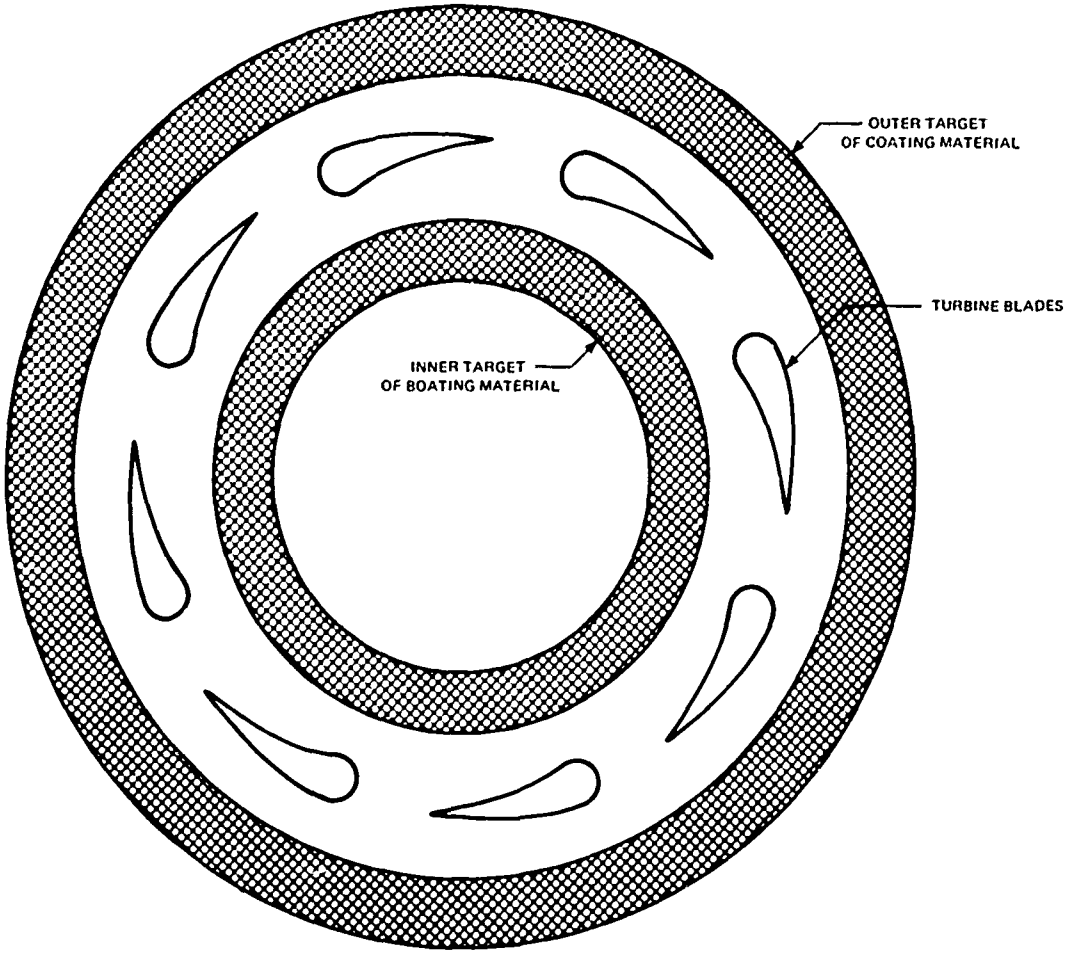

Figure 4. A possible target geometry for multiple blade coatings by sputtering.

A second problem area is the incorporation of sputtering gas (e.g. argon) in the sputtered deposits. Such incorporation does occur. Although it can be reduced to low levels by selection of the deposition parameters, in a given program the range of acceptable parameters may be determined by other factors, e.g. the deposit grain structure. The concentration of argon in sputtered blade coatings will be measured, and evaluation of the coatings will reveal if these concentrations are harmful or beneficial.

PROGRAM DESCRIPTION

The program consists of two main parts; one dealing with metallic coatings of the CoCrAlY type and the other with thermal barrier coating systems based on stabilized zirconia.

In the metallic coating section, pins for burner rig testing will be coated under a range of deposition parameters and with small composition modifications. The objective is to produce coatings with a non columnar structure, and to correlate this structure with coating performance in the burner rig. The principal deposition parameters are deposition rate, substrate temperature and substrate (electrical) potential, or bias. The substrate temperature will depend upon deposition rate and bias, unless cooling techniques are employed. The composition modifications visualized are small percentage additions of materials which will increase the amount of second phase present under the deposition conditions, thereby modifying the grain growth characteristics. Results from this work will be used to establish parameters for coating of turbine blades for engine tests. A sufficient number of blades will be coated to obtain process data suitable for the design of production coating equipment.

The objective of the thermal barrier coating section of the program is a coating system, with a stabilized zirconia outer layer, which will remain bonded to the superalloy substrate through the temperature range encountered by turbine blading. Several approaches to this objective will be investigated, including modification of the thermal expansion of the zirconia, the establishment of a favorable stress system, and the use of interlayers. Two types of interlayer are under consideration—a ductile metal intended to absorb the residual expansion mismatch, and a layer of graded thermal expansion intended to distribute the mismatch over a finite thickness rather than permitting it to occur at a discontinuous interface.

Again, variation of deposition parameters will be used to influence the properties of the coatings. Additional parameters particular to this section are the thickness and composition of the interlayers, and the composition and stress state of the zirconia.

The most successful of these approaches will be utilized in the production of coated pins for burner rig testing, and mechanical test specimens.

PRELIMINARY RESULTS

The results of a limited number of preprogram experiments indicate that CoCrAlY coatings can be produced with the desired composition and noncolumnar grain structure. They also indicate that a very high order of coating adherence can be obtained without the use of high substrate temperatures or post-deposition heat treatment. No experiments have as yet been performed with the thermal barrier coatings.

REFERENCES

1. Personnel Communication, R. Shaw, Pratt and Whitney Aircraft Corp. May 1972.
2. A. K. Wright, *Am. Journal Sci. Arts* 13, 49 (1877).
3. G. K. Wehner, *Advan. Electron Phys.*, 7 239 (1955).

Discussion:

SPUTTER DEPOSITED COATINGS FOR MARINE GAS TURBINE BLADES AND VANES

R. C. Krutenat
Pratt & Whitney Aircraft, Div. United Aircraft Corporation
East Hartford, Connecticut

I. INTRODUCTION

P&WA™ has developed over a period of the last 5 years overlay coating technology and in recent months has demonstrated production coatings capability for electron beam evaporated CoCrAlY type materials for sulfidizing environments. At the same time development efforts have focused on alternate techniques for overlay coatings by sputtering and arc plasma spray. Considerable attention has been given to the sputtering process because of its broad materials capability. Extensive efforts aimed toward increasing deposition rates have not been as fruitful as originally hoped. The electron beam deposition process has afforded greater short term capability in spite of the apparent advantages of sputtering. As more understanding of the compositional requirements of overlay coatings become known, sputtered deposits undoubtedly will be needed to complement present capability.

We will address comments on the preceding paper first to disadvantages of electron beam vapor deposition, then to advantages of sputtering.

II. COMMENTS ON DISADVANTAGES OF ELECTRON BEAM DEPOSITION

The line-of-sight restriction of electron beam deposition has been cited as a limitation to the need for providing protection to vulnerable nonairfoil areas of turbine hardware. Although this was certainly true during the early months of CoCrAlY production it is now apparent that P&WA™ can provide shroud and platform coatings at very little extra cost by articulation of hardware during coatings. Internal passages and cooling hole exits of course are still restrictions, but they are also restrictions in the sputtering techniques as well.

The vapor pressure requirements of alloying components will be a continuing problem in the electron beam vapor process. The vapor eminating from the liquid pool is governed by the Langmuir equation:

$$W_i = K\alpha_i P_i^{\circ} X_i \gamma_i \left(\frac{M_i}{T}\right)^{1/2}$$

Where α is the evaporation coefficient, P_i is the vapor pressure of the pure element, X_i is the mole fraction of the element in question, γ_i is the activity coefficient and M is the atomic mass. Although vapor pressures are known, the more important factors are the evaporation and activity coefficients which are only poorly known even for binary alloys. Fundamental studies in the area would be helpful for several alloy systems of interest.

The columnar structures cited as a detrimental artifact of vapor deposition require explanation. It must be pointed out that only an open columnar structure is detrimental to coating performance, that is, individual grains separated by open boundaries. A closed columnar structure can be grown by avoiding rotation of the substrate which guarantees no shadowing from neighboring crystals. However, it is apparent that this is not a practical alternative for uniformly coating the type of complex turbine components we are considering. Gas scattering techniques and so-called "ion plating" techniques may provide the multiplicity of virtual vapor sources needed to produce more desirable structures. Again, post-coating treatments of current production CoCrAlY suffice to close an open columnar structure. It has been our experience that these types of structural defects can also be observed in sputtered deposits under certain conditions of substrate temperature and deposition rate, sputtering pressure and angle of incidence.

Material recovery efficiency in evaporation is low and could be considered a restriction for expensive alloy constituents. However, recently we have shown that it is possible to recover and reuse, after melting and recasting, nearly all of the collectable condensate without detriment to coating performance.

III. COMMENTS ON ADVANTAGES OF SPUTTERING

There is no doubt that atomically clean interfaces are more desirable for promoting adherence effects in thin films and such effects have been adequately substantiated by others. Adequately clean interfaces can be prepared in sputtering with no prior sputter etching provided that proper substrate preheating is used followed by deposition at the preheat temperature.

Sputter etching may give rise to surface roughening that may be replicated in the coating and also introduce trapped sputtering gases in the substrate alloy. If coating deposition is then made at temperatures below about 400°C the coating may blister on subsequent heating to service temperature.

An additional reason for providing some substrate heating during deposition is to overcome by minimal interdiffusion the stresses caused by thermal mismatch between coating and substrate. Films deposited at ambient temperature in excess of 1 mil in thickness are very prone to delaminate.

Sputter coated blades may indeed not require heat treatment from the standpoint of correcting processing induced structural defects. Present experience on electron beam vapor deposited coatings indicates that post-coating processing and heat treatments adequately correct such deficiencies. However, there are also indications that certain post-coating treatments may provide operating advantages relating to the mechanism of corrosive attack. These requirements may hold also for sputter deposited coatings. Sputter coated parts can have defects caused by (1) deposition at improper intermediate temperatures and (2) by failures to remove large, that is, nonatomic sized particles from the surface. Becuase it is neccssary to maintain substrate temperatures of at least 400°C to avoid argon occlusion into the deposits a means of heating a large number of blades is required in the sputtering equipment. Overheating of deposits can also modify both coating structure and composition. Figure 1 shows the effect of deposition temperature on sputtered CoCrAlY. At 850°C a typical structure is observed. However as substrate temperatures are increased to 1150°C a single phase beta structure results because the chromium, being less soluble in the growing beta is rejected and reevaporated. As the flux of CoCrAlY vapor is increased adequate chromium supersaturation in the vapor phase near the surface can be maintained such that chromium rich γ phase continues to nucleate and grow at this temperature.

The deposition rate by sputtering of complex coating alloys will be governed chiefly by the thermal conductivity of the alloy and the presence in its composition of low vapor pressure constituents. If rotation of hardware is also required the effective deposition rate is the flat plate rate divided by π. Our estimates indicate that the maximum reasonable deposition rate for a CoCrAlY type alloy will be about 2 mils per hour based on the thermal characteristics of this type of material. Although sputtering maintains an advantage for deposition of every conceivable desirable element or compound this advantage is not available without sacrifice of deposition rate. Alloy sputtering coefficients are reduced by presence of low vapor pressure constituents. Finally, we wish to point out that we are convinced that useful coatings can be deposited by the sputtering technique. Figure 2 shows a single phase NiCrAlY deposit with an appealing structure and diffused interface that demonstrated the expected high temperature oxidation resistance in test.

In our view it is still desirable to construct a sputtering system with pilot plant capability to learn what problems are associated with production sputtering of thick films and to determine the cost effectiveness of such an operation. The most effective use of the technique may well be as an initial step to provide certain required elements at the surface that can be incorporated into a coating structure by subsequent pack cementation processing.

With regard to thermal barrier coating it should be pointed out that plasma spraying is an effective, proven low cost technique for applying modified zirconias to stationary components in gas turbines. Further development studies should offer the 100°F increase in metal temperature suggested to be desirable for marine applications without sacrifice of protectivity from sulfidation attack.

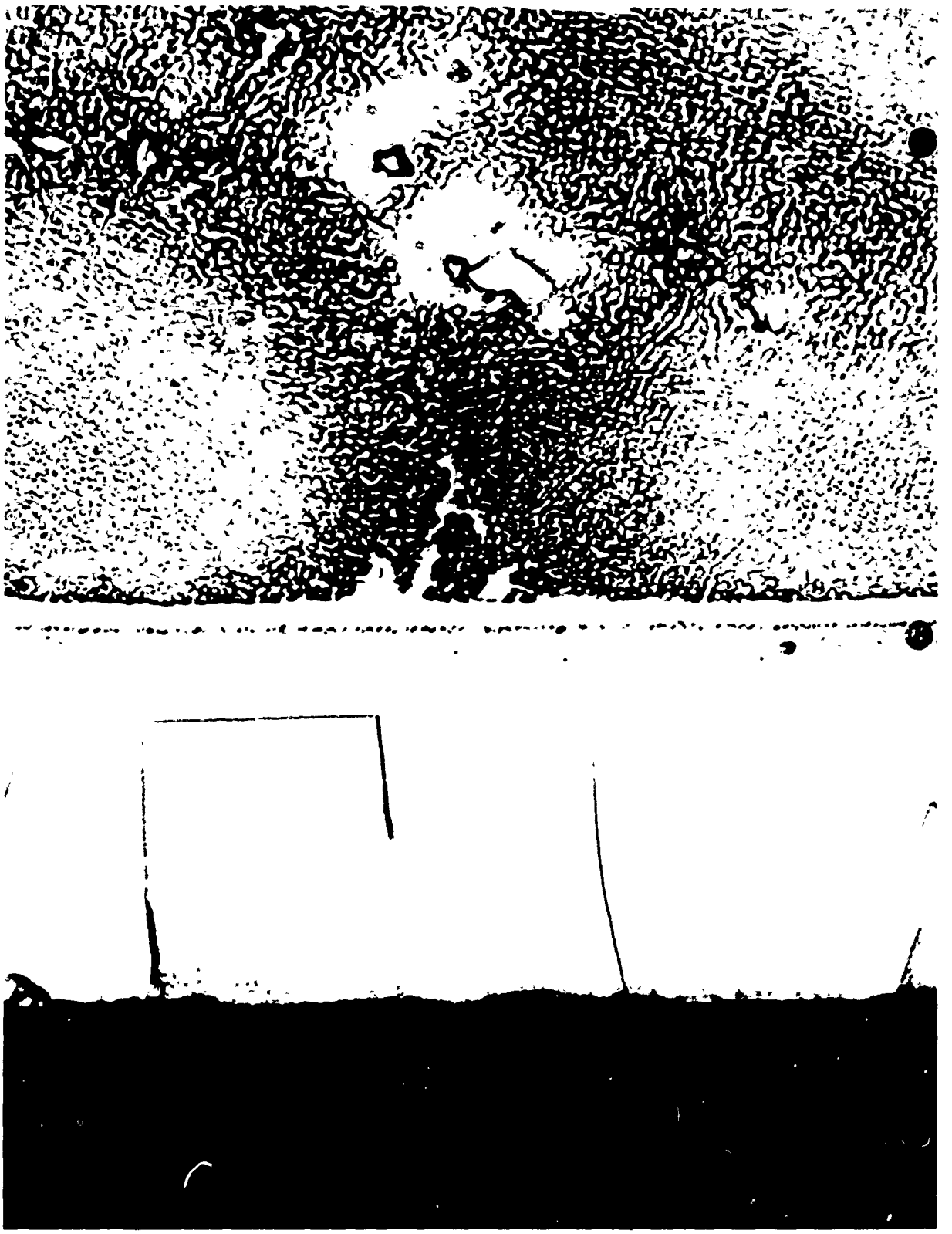

Figure 1. Effect of deposition temperature on sputtered Co-Cr-Al-Y at 850°C (upper left), 950°C (upper right), 1050°C (lower left) and 1150°C (lower right).

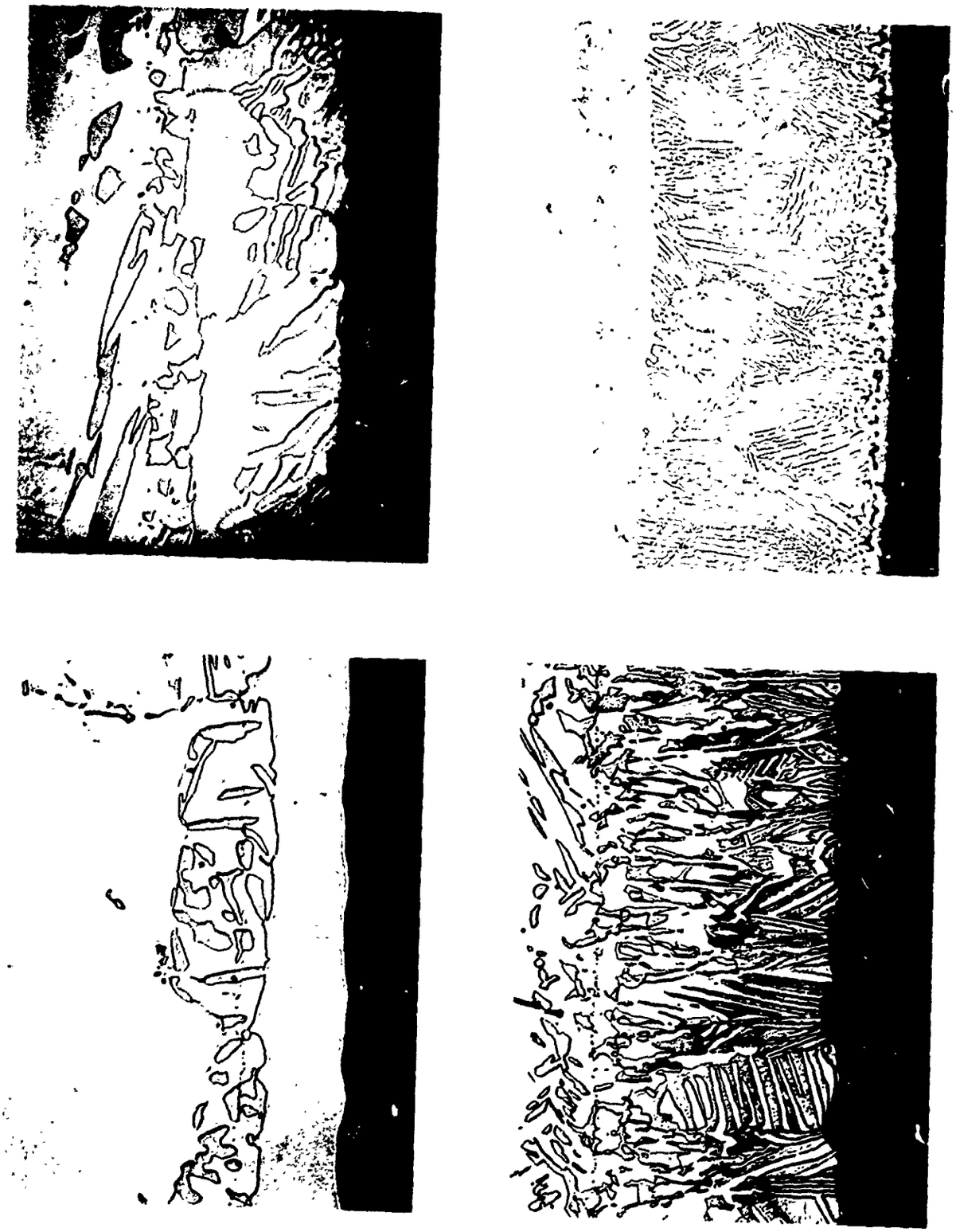

Figure 2. Single phase sputter deposited Ni-Cr-Al-Y coating.

Discussion:

SPUTTER DEPOSITED COATINGS FOR MARINE GAS TURBINES AND VANES

Dr. Gottfried K. Wehner
University of Minnesota

Sputtering involves the transfer of materials in an atom by atom fashion. What is deposited on a substrate must have the same composition unless something gets lost in the process. So if one has a closed system comprised of concentric spheres one will come up with the same composition even if the sticking coefficients of the deposits are different for the different components. This is not the case with a system wherein the material can escape to other parts such as in a system with parallel plates. However, as the size of the plates gets very large, one approaches the approximate condition of a closed system.

Sputtering permits deposition of virtually any compositions. Many things in the metallurgical field can now be done by sputtering which are not possible with other types of coating equipment. Transferring materials atom by atom, one has the potential of developing some very interesting new materials. For instance, some recent sputtering work with Cu and Mo has produced some depositions with unusual properties.

Many advances in development and applications in sputtering have been made in recent years. For instance, Western Electric has sputtered many square kilometers of tantalum in the fabrication of integrated hybrid circuits. They have developed equipment such that the substrates are continuously fed through the sputtering system on a belt-type mechanism.

A classical sputtering application at least from the financial perspective, has been the coating of razor blades. The edges of approximately 50,000 razor blades can be coated in a single pump down. However, the 250Å-thick razor blade coating is significantly different than the nominal 5 mil alloy coating on a turbine blade!

I was amazed to see the quantity of sputtering equipment on display at the recent Vacuum Society Conference and exhibit in Chicago. Equipment was available for sputtering in all directions and configurations with a variety of techniques. However, Ed McClanahan and his group at Battelle-Northwest have something unique in sputtering. They have developed the triode sputtering system with very high deposition rates over large surfaces. No such systems are commercially available. I think the potential of the triode sputter system is enormous! I also favor the triode system for research sputtering as it affords better control. For instance, one can sputter at lower gas pressures and increase the plasma density to much higher values. In fact, one can deposit about 15,000Å per minute which can not be easily achieved with the conventional diode sputtering system.

Ten years ago there were many parameters in sputtering that were so confusing that the process was not well understood. However, the picture has changed considerably in the past decade and we know now how to make use of many of these parameters.

Sputter etching or cleaning is another important application. But cleaning is not always advantageous. We recently found an interesting case where we deposited Mo on Al substrates in an ultra high vacuum system. Studies of the Mo coating with Auger Electron Spectroscopy showed that Mo does not adhere well to the atomically clean Al surface. However, when the Mo is deposited on oxidized Al the Mo adheres very well. So in some cases, it appears that in coating of metal the oxide film may be beneficial for better adherence.

The columnar structure encountered often in vapor deposition can be influenced in sputtering by biasing the substrate with a negative voltage. An interesting approach here is to use pulse biasing so that one can apply higher negative voltages to the substrate for short intervals without resputtering off the substrate more than arrives. This interesting possibility has not been investigated yet. Also, the effect of imbedded Ar in the coatings should be investigated to determine its beneficial or detrimental effects. New surface analysis techniques provide better means to understand what is going on the in sputtering process. For example, we are studying sputter deposition in situ Auger Electron Spectroscopy in order to identify the constituents at the interfaces responsible for poor adherence.

We are accumulating a wealth of new information which was not possible 4 years ago. With better understanding of the process one can foresee much further progress and useful applications.

Session III

TEST, EVALUATION AND MAINTENANCE

Session Chairman:

Jim Newhart
Naval Air Propulsion Test Center, Philadelphia, Pa.

THURSDAY, OCTOBER 26, 1972

Test Methods in Hot Corrosion

H. Doering
General Electric
Schenectady, New York

INTRODUCTION

Testing the resistance of hot section components to corrosive contaminants in actual gas turbines under controlled conditions is both expensive and difficult. As a result, a number of laboratory tests intended to simulate the hot section environment of gas turbines have been designed and used over the past 25 years.

Each of these tests has its own advantages and limitations with respect to the chemical and aerodynamic factors in the turbine environment and the capability of studying all or part of the corrosion reactions that may take place.

This paper describes some of these various tests, evaluates their advantages, and discusses the factors necessary to obtain a better correlation between results and the prediction of maintenance costs in gas turbines due to the deterioration of hot section components.

TEST OBJECTIVES

There appear to be three purposes for conducting both engine and laboratory tests although it is obvious that these are interrelated:

MATERIAL SCREENING

Although a given laboratory test may not be capable of predicting the precisely quantified corrosion behavior of alloys and coatings in a turbine, it can at least rank the relative resistance of susceptability to a variety of contaminants. Numerous commercial and development alloys have been tested in a number of tests for just this purpose. Generally, the agreement has been good enough only to identify materials at either end of the corrosion resistance spectrum. Some of the guidelines for alloy development have evolved from such tests.

TYPE AND LEVEL OF CONTAMINANT

A further purpose for testing is to examine the effect of Na, V, K, Pb, S, Cl, etc. on the deterioration of one or more alloys and coatings. In addition, varying quantities and combinations of such contaminants are also examined at a number of temperatures. The results of such tests often form the bases of specifications which limit the amount of contaminant that should be ingested with fuel or air if hot section replacement costs are to be maintained at an acceptable level.

MECHANISMS AND KINETICS

The examination of the micromorphological changes that take place during corrosion, the nature of corrosion products, as well as the kinetics of the surface reactions are all obvious purposes of laboratory testing.

It is generally agreed that only through a thorough understanding and quantification of corrosion reactions can a rational basis for material development and prediction of turbine maintenance be obtained.

LABORATORY TESTS:

It has been said that there exist as many recipes for borscht as there are or have ever been Russians. In like manner, there are as many laboratory tests and versions thereof, each with its justifiable purpose, as there are or have been investigators in this problem area of hot corrosion. It is not possible to describe all herein but rather to classify the various types and then describe in a general way the relative costs, capabilities, and limitations to achieve simulation as well as some of the factors that should be considered in rendering their results more relevant to the prediction of turbine reliability.

The correlation between material behavior in an engine and that in a test can be developed either empirically or, if contributing phenomena are sufficiently well understood, on a more rational basis.

THE GAS TURBINE

Before one can assess the validity of laboratory test results, a review of the environmental factors that are known and/or thought to be of importance to corrosion are needed:

1. Metal temperatures and fluctuations
2. Gas temperatures and fluctuations
3. Gas velocity with respect to a given part
4. Gas pressure
5. Metallic contaminant concentration, e.g. Na, V, K, Pb, etc.
6. Chemical potentials of S, O. Cl, etc.
7. Concentration of abrasive particles.

In addition to these environmental factors, the life of the hot section component will be affected by three design factors:

1. Allowable metal loss
2. Geometry of the given component
3. Material of construction.

If these environmental and design factors are well defined, then it is possible to predict under given operating conditions and contaminant concentration levels the following:

1. The chemistry of stable condensed species on the metal surface.
2. The probable deposition rate, dm/dt, of such condensable species onto the surface of a hot section component of a given geometry and temperature residing in a gas stream of known pressure, velocity, temperature, chemistry, etc.

With both the type and the amount of condensed species specified, one can proceed to construct laboratory tests with more confidence that the results obtained therefrom can be used to predict actual turbine part corrosion during operation.

HIGH PRESSURE/VELOCITY TESTS

Originally designed for the development and study of gas turbine combustors, several high pressure full flow test stands have been constructed. With the advent of corrosion problems these have been modified to test materials under a variety of temperatures and contaminant levels.

The exact duplication of the environment seen by rotating buckets is somewhat in question particularly if one considers the effect of centrifugal forces on liquid deposits.

The partial pressures of all gas species should be exactly the same as in a turbine operating at comparable pressures.

HIGH VELOCITY TESTS

The velocities generated by the rigs used in these tests (up to mach one) were originally intended to investigate the expected effects of erosion in addition to corrosion. Since these operate at atmospheric pressure, the duplication of partial pressures is possible for any component for which the partial pressure is less than one atmosphere under turbine operating conditions. Thus, if it is of interest only to control one such gas component, e.g. SO_2, then these tests can be said to "duplicate" turbine environments.

A further requirement in using these tests to duplicate turbine environments is the generation and control of uncombusted carbon particles. Unless combustion mixtures and residence times are similar to a given turbine, both the effect of local reducing conditions and erosion can give misleading results.

Because of their fairly high air requirements, these tests remain expensive but considerably cheaper than high pressure tests.

BURNER RIG

This class of tests will be defined as those tests which expose the specimen to combustion products at atmospheric pressure and at velocities not more than one-tenth as great as the velocity in the hot section of a turbine.

These tests are relatively inexpensive, possess the capability of testing many specimens at one time for long periods of time and have the flexibility of exposing specimens to a wide variety of temperatures, gas and liquid or solid species.

If one is content to draw more than empirical correlations between corrosion rates obtained herein with burner rigs and those in gas turbines, then, a thorough understanding of the chemistries and deposit mechanisms is essential. As with high velocity tests, one can in part control these chemistries by adjusting contaminant levels and gas compositions.

THERMOGRAVIMETRIC TESTS

These tests measure the change in weight with time of a specimen suspended in a furnace and exposed to a given gas or gases. The specimens may be simultaneously coated with a deposit; e.g., Na_2SO_4. The changes in weight give insight to the kinetics of corrosion reactions, and permit the study of incubation periods and the effect of exposure to changing gas compositions. These tests permit the exposure of only one specimen at a time but give far more information on kinetics than other types of tests.

Again, the correlation of results with gas turbines depends on a duplication of the environment with respect to the amount and chemistries of deposited species and the equilibrium partial pressure of gases.

CRUCIBLE TESTS

These tests, in which specimens are immersed in a crucible containing molten salt, are the cheapest and fastest of all. The molten salt composition to which a specimen is exposed is quite variable, while the control of gas composition to

the specimen is immersed in the salt. Therefore, the results are very difficult to extrapolate to turbine conditions. These tests are useful to screen materials with respect to corrosion resistance, and to investigate the effect of various combinations of contaminants.

Several modifications of crucible tests are currently in use. These include the measurement of electrochemical potentials between a specimen and a reference electrode. These measurements can be further extended to make anodic/cathodic polarization measurements to deduce a corrosion current, i_{corr}, or to investigate the potentiodynamic polarization with the application of the potentiostat to investigate the protective nature of oxide films.

A further modification is the addition of carbon to a melt in order to obtain reducing conditions or the intermittent dipping and withdrawal of a specimen into a melt to simulate the thin films of deposits that exist on turbine parts.

RELATIVE MERITS OF METHODS

Table I is compiled to compare the simulation capabilities of each class of test from both an aerodynamic and chemical point of view. In addition, each class of test is compared with respect to cost and speed of obtaining results.

The selection of a test method depends on what objective is sought. The prediction of engine part deterioration is best accomplished by actual engine tests themselves and as a first approximation by high pressure tests. The kinetics and microstructural changes of corrosion in specific environments can perhaps best be studied by TGA experiments. A qualitive ranking of alloys and coatings can most economically be obtained through the use of burner rigs and crucible tests.

A further consideration in selecting a test method is based on the comparison of the cost of the consequences of *not* having the correct prediction of hot section component life and the cost of making absolutely sure that the prediction is correct. If, for example, a turbine manufacturer or user would lose $10 if his buckets failed prematurely but the cost of making absolutely sure that they would perform as contracted is $20, including the time lost, then there is an obvious basis for not selecting the most expensive highest simulating test. On the other hand, if reliability is of utmost concern, then testing of the turbine itself becomes mandatory.

Table I
Test Simulation and Cost

Type of Test	Simulation[1] with respect to					Cost	Test Time
	Chemistry		Aero Dynamics				
	gas[2]	s/l[3]	P[4]	V[5]	dm/dt[6]		
Engine	10	10	10	10	10	1	1
High Pr. & Vel.	10	9	10	9	8	2	2
High Velocity	5	8	4	9	7	3	7
Burner Rigs	5	7	3	2	4	7	8
TGA	5	6	3	1	2	7	3
Crucible	2	5	1	1	1	10	10

Notes:
[1] Numbers between 1 & 10 based according to:
10 = best simulation of given factor; lowest cost; shortest test time
1 = worst simulation; highest cost; longest test time
[2] gas refers to partial pressure of SO_2, O_2, N_2, etc.
[3] s/l = solid or liquid condensed species
[4] P = pressure of system
[5] V = velocity of gases
[6] dm/dt = rate of deposit of condensible species

CONCLUSIONS

The valid interpretation and extrapolation of results obtained in laboratory tests depends on an understanding of how well each simulates the chemical and aerodynamic variables present in an engine. Factors such as gas pressures, temperatures, and velocities as well as the chemical potential of oxygen and sulfur intuitively have important influences on the effects of contaminants on alloys and coatings at given components temperatures.

A rigorous correlation between the behavior of materials in laboratory tests and the behavior in engines is continually sought. The Navy is in a most enviable position to develop this correlation by conducting a systematic series of engine tests with "rainbow" hot section configurations to evaluate a number of materials under identical environments. As a first step, engine tests can be empirically correlated with burner rigs, TGA and crucible tests. But the extrapolation of results beyond specific conditions of engine and laboratory tests carries considerable uncertainty unless studies to develop kinetic models of the interaction between gas turbine environments and materials are concurrently developed and evaluated.

Discussion:

TEST METHODS IN HOT CORROSION

William E. Young
Westinghouse
Pittsburg, Pennsylvania

There can be no question that corrosion testing in a gas turbine operating under service conditions represents the ultimate in reliability but it is an expensive choice when one considers that a modern industrial gas turbine may consume over 20 tons of the test fuel in an hour. As a result of the crucible test was proposed many years ago as the ultimate in simplicity, but as pointed out in the paper the crucible test departs further from simulation than any other method. Alternatives then are rig and passage tests.

The most recent of the laboratory tools for studying reaction kinetics is the TGA and as the author states, simulation may be rather poor. We have used this apparatus as well as its companion DTA. The DTA should be an excellent tool for measuring ash fusion temperatures but in the past there has frequently been a problem in interpretation. This problem can be simplified by using the ash fusion apparatus shown in Fig. 1. It is essentially a hot stage microscope which has been used for more than 20 years examining both ashed fuel samples and scrapings of blade deposits. One can generally obtain some insight as to the deposit forming characteristics and potential corrosivity of a fuel. Its greatest reliability takes place with ash or deposit whose formation and subsequent stability is independent of pressure and the associated gas composition. Some thought has been given to pressurizing the furnace and providing an appropriate combustion gas envelope. This would make it a more useful and reliable tool.

The burner and rig tests as pointed out offer a wide range of simulation, cost, and reliability. In theory it should be possible to exactly simulate engine conditions for both stationary and rotating parts although admittedly it is usually done for only the stationary. We have run both the low velocity atmospheric pressure rigs and passage tests that closely simulate gas turbine operating conditions. The low pressure and velocity rigs were intended for

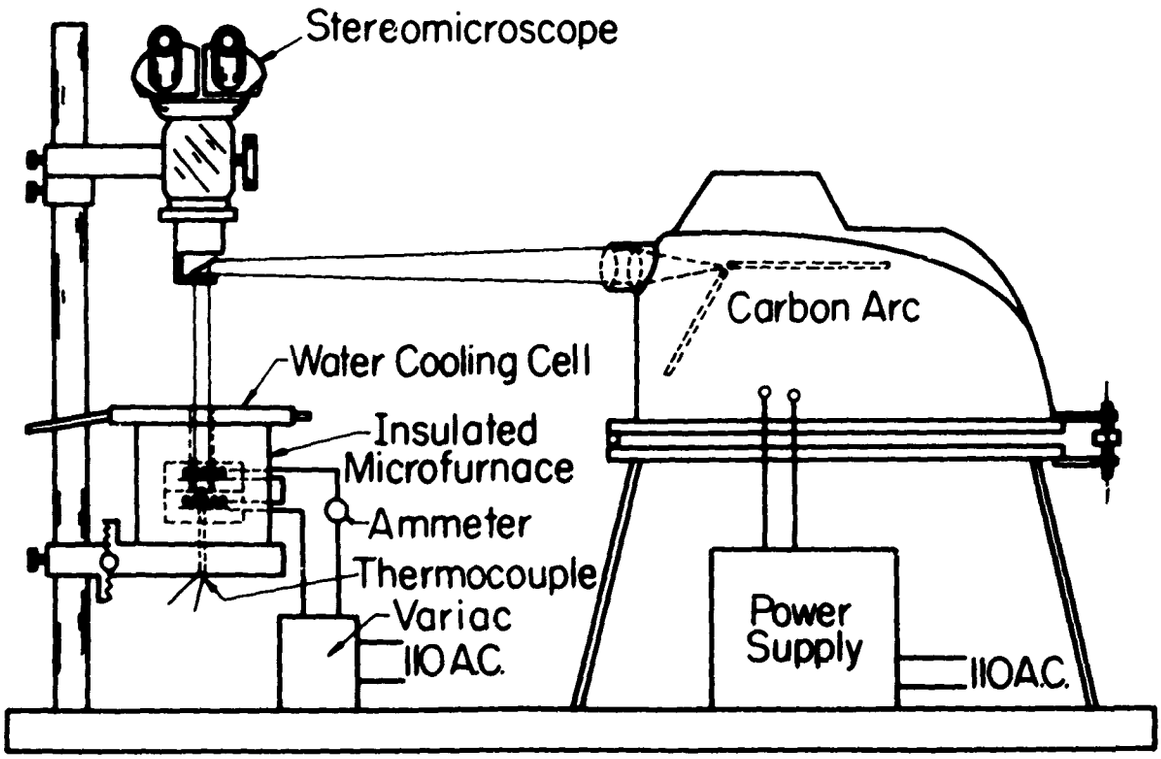

Figure 1. Ash fusion apparatus.

screening and for rating alloys under a range of conditions. Unfortunately as will be shown this screening was not always reliable.

Figure 2 shows a comparison of results for three pieces of test apparatus and the alloys X-45 and U-500. Although the data are plotted as functions of stream velocity it is likely that the pressure also contributed to the reversed ratings of the two alloys at the higher velocity condition. Similar information is shown in Fig. 3. Here X-45 is seen to be one of the better alloys as indicated by the low pressure low velocity rig, but the worst alloy at higher pressures and velocities. There are explanations of these results based, for example, on adherence of the protective oxide layers, but these curves are intended to show only that whereas the simple test rigs give reliable ratings for some alloys, there are occasional exceptions. It should also be mentioned that these ratings are all on a weight loss basis. Metallographic analyses sometimes produce different results as C. J. Spengler will point out in his discussion of the last paper of the day.

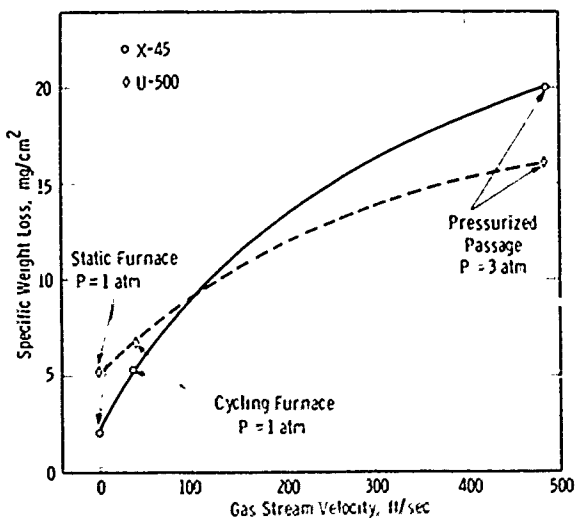

Figure 2. Effect of gas stream velocity on the oxidation rate of X-45 and U-500 tested at 1800°F for 150 hours.

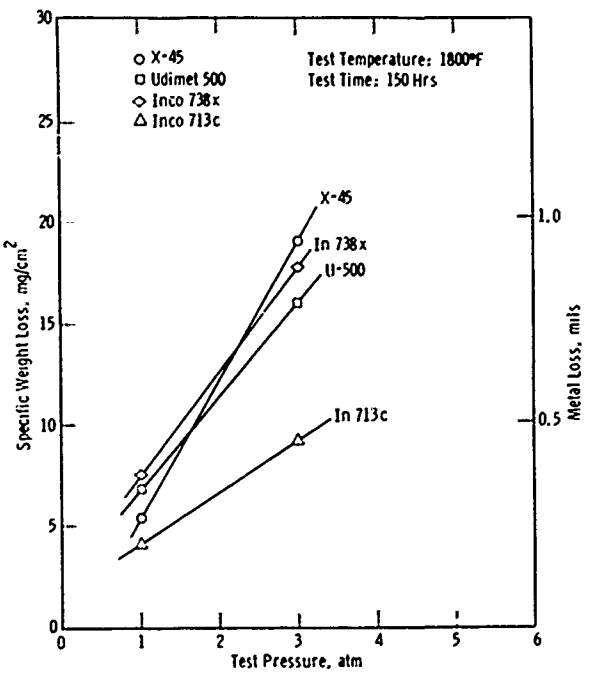

Figure 3. Effect of pressure on the oxidation rate of superalloys.

Another characteristic difference in the two rigs is shown by an examination of Figs. 4 and 5. Fig. 4 seems to indicate an incubation period, particularly for U-500. This is not in evidence for the high pressure high velocity rig in Fig. 5. In fact, the indicated rates are higher for the first 200 hours and then tend to decrease. This points to the possibility of overly conservative ratings based on short time tests. One could question whether or not the curves might again change slope if the testing time were to be extended. Our present feeling is that this is not likely. Extrapolation of these curves seems to fit reasonably well with field observations in operating turbines. Unfortunately, we cannot state conclusively that this is the case for hot corrosion. It is generally very difficult to measure and correlate the amount of attack against time and conditions in an operating turbine which may be experiencing load variation and changes in fuel quality. This suggests another possible tool for predicting the occurrence and progression of attack, the "dipstick."

Figure 6 shows the dipstick which is simply a collection of sleeves of the various alloys used in the hot section of the turbine, mounted on a thermocouple probe, and inserted near the turbine inlet. In theory, this should give a very reliable indication with frequent periodic inspections of what to expect in the turbine. To date it has not been completely successful in its predictions. It seems to be quite sensitive to velocity and temperature profiles in the passage, and specimens of the same material spaced only a few inches apart react quite differently.

Finally I would like to comment briefly on Table I which presents a very interesting comparison and rating of the various test methods. If one adds the ratings horizontally for each type of test another column of unweighted totals is obtained, namely, 52, 50, 43, 36, 27, and 30 for the six types. The engine is best with the rating of 52 as might be expected, and the high pressure high velocity passage, a close second with 50. However, if one takes the

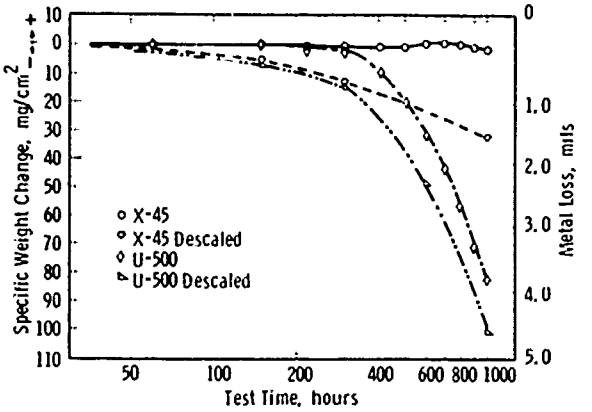

Figure 4. Weight change of U-500 and X-45 alloys oxidation tested at 1800°F in the cyclic furnace.

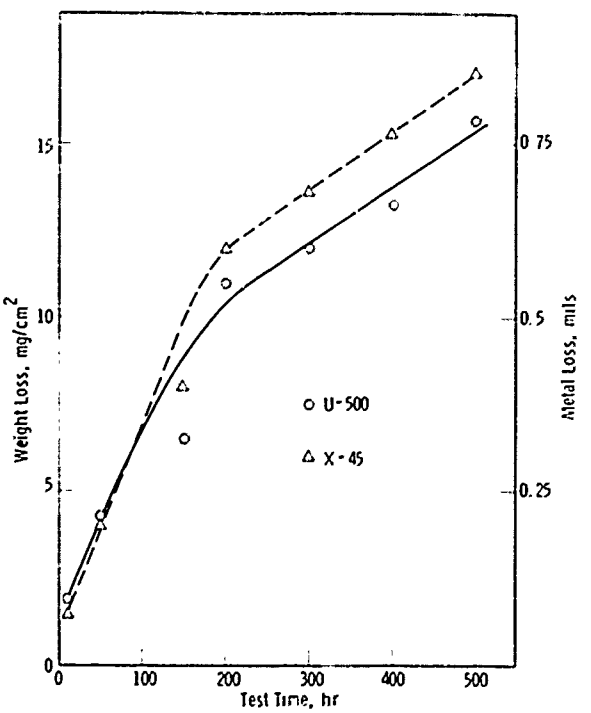

Figure 5. Oxidation rate of X-45 and U-500 tested in the pressurized passage at 1600°F gas temperature and 3 atmospheres pressure.

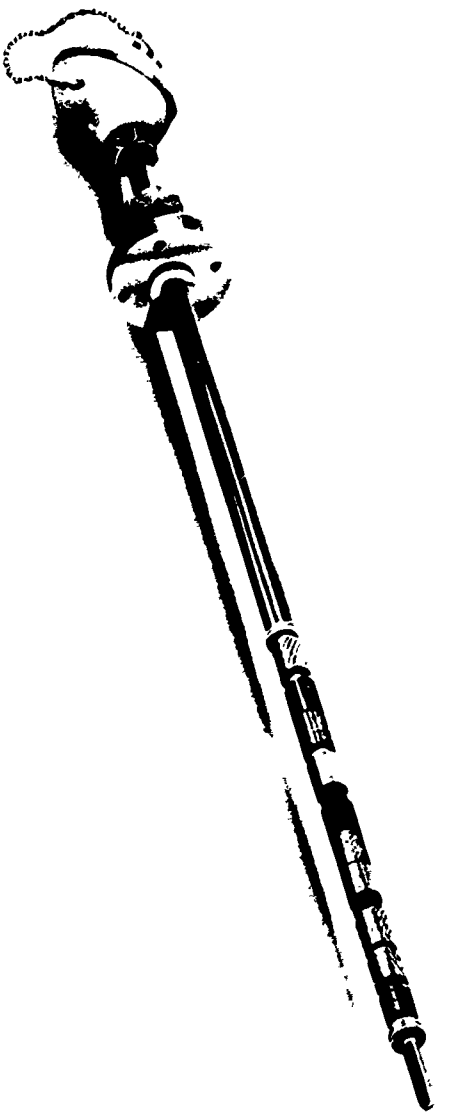

Figure 6. Dipstick.

position that the high velocity and pressure test is not much more expensive than the burner rigs (by comparison with the engine test) a cost number of 6 might be assigned. Similarly the time to obtain data is not far different from that of the burner rig and again a 6 might be assigned. On this basis of ranking the high pressure and velocity rig totals 58 compared to 52 for the engine. It has won out by nearly equaling the simulation of the engine and clearly surpassing it on the basis of cost and time of test. With this laboratory technique then, the investigator is in a position to tell the engine designer that if he maintains the design conditions prescribed by the test and if the turbine user operates with the prescribed fuel, trouble-free operation should occur over the predicted life of the turbine.

Discussion:

TEST METHODS IN HOT CORROSION

S. J. Dapkunas
Naval Ship R & D Center, Annapolis, Maryland

Harvey's paper has given a general view of many things of which we are well aware and which have been brought out in these presentations and especially in the question sessions. His analysis of test methods has concentrated on the ability of laboratory test to simulate engine conditions. The question of how much reliance can be placed on these tests remains to be answered.

This discussion would, perhaps, be a good place to renumerate some of the points on testing which have been brought up during this conference.

The question of a quantitative correlation of laboratory test data with material data obtained from actual engine testing has not been graphically presented. It would seem that with the enormous amount of laboratory testing done by engine manufacturers that some correlations could have been presented.

It is not to be expected that data obtained from one type of rig test to another should be quantitatively correlatable. However, I believe it was shown in the round-robin burner rig tests conducted a few years ago that results obtained in different rigs were qualitatively correlatable. That is to say, the general ranking of alloys was the same from one rig to another. It is probably quite unrealistic to desire that results from one rig to another be quantitatively equal since the various rigs have been designed to simulate different types of engines under varying conditions.

The point brought up by Irv Bessin that much of what is observed after engine testing may be an effect of transient conditions could conceivably make the results obtained by steady-state testing even more questionable.

The point of duration of test has arisen on two separate occasions. Mr. Conde has pointed out that the comparative curves given for different materials are often misleading since they do not approach the time frame normally associated with engine operations. The same question arose in the discussion of what constitutes failure in a coating test, i.e., what happens to base material when a coating is penetrated. The same arguments can be made for short time/high contaminant burner rig tests vs. long time/low contaminant burner rig tests.

Mr. Rausch's comment that very much the same questions about testing were asked six years ago and pretty much the same answers given shows that the problem we are dealing with probably does not have a simple or universal solution. However, new materials have been developed and put into operation. This would indicate that although laboratory results and engine testing data may not correlate well, we have learned to interpret what may be crude results and have, thereby, improved material properties. We may well have reached the point where empirical testing to develop more corrosion resistant materials is reaching its limit, in which case we may well be forced to learn to play "Goward's game," i.e., developing new materials from first principles.

One theme which has run throughout this meeting has been that in order to accurately predict material behavior in operation we try to isolate particular phenomena which we personally feel to be of greatest importance. This was evident in the testing done by Bornstein, DeCrescente and Roth who have taken a different approach to mechanism studies from that taken by Conde or Spaciel and is certainly true of the analysis of the effect of Δt taken by Bessin in contrast to Young.

Probably the most productive way for many of these problems of test interpretation and correlation to be resolved would be to have more conferences of this type or perhaps a round-robin test wherein rig and engine results are compared.

Development of Repair and Reprocess Coatings for Air Cooled Nickel Alloy Turbine Blades

J. V. Peck
TRW Incorporated
Cleveland, Ohio

ABSTRACT

The work described in this paper, sponsored by the Air Force Materials Laboratory, was conducted to develop and characterize coating compositions, processing techniques and resulting properties for: (1) repair of localized damage to diffused aluminide coatings on nickel base turbine alloys and (2) re-application of coatings to worn turbine blades during engine overhaul.

A multiphased effort was pursued to develop a stripping procedure for removing used commercial aluminide coatings and to develop a coating process which could be used for both recoating and repair coating. A comprehensive test program was also conducted to compare the environmental performance of reprocess and repair coatings and to evaluate the effects of new coatings on the mechanical properties of thin section substrate relative to the corresponding properties of the original coatings.

A chemical stripping procedure was developed for removing remnant Jo-Coat from B-1900 and INCO-713C and CODEP C-2 from IN-100 and U-500 without significant substrate attack. Grit blasting was found to be satisfactory for partial stripping wherein only surface scale and oxides required removal. A vacuum fired slurry slip pack coating process using 56Cr-44Al powder as a source material was developed which was capable of affecting both complete recoatings as well as repair coatings to locally damaged areas.

Environmental performance of reprocess and repair coatings was excellent. However, mechanical properties of thin section substrate/coating composite structures were markedly debased by the original coatings, engine simulated exposure and recoatings. The reduction in properties is directly related to a loss in load bearing cross section due to coating formation, diffusion during exposure and stripping plus recoating. While this effect may not represent a serious problem for solid blades where the substrate-to-coating thickness ratio is high, it does suggest a potential problem in thin section hardware, such as cooled coated turbine blades as well as vanes where substrate-to-coating thickness ratios are relatively low.

INTRODUCTION

Economic pressures and increasing hardware costs have motivated both commercial and military aircraft turbine users and manufacturers to seriously consider the feasibility of using reprocessed engine components. While repair and reprocessing of some stationary hardware has been established as an economically and technologically sound practice, similar operations on rotating hardware such as turbine blading have not been as readily accepted. This, of course, is largely due to the more stringent demands placed on the mechanical and metallurgical properties of rotating components. Nevertheless, efforts have been made over the past 3 to 5 years to develop procedures and design data necessary to insure safe and reliable operation of reprocessed turbine blades. While progress in this area has been cautiously slow, some engine users are routinely employing repaired and recoated parts and considerable R&D activity is being aimed at expanding the list of allowable repairs and repairable parts. In many instances, engine manufacturers are incorporating overhaul and repair technology in the design of advanced engines.

One of the many aspects of the O&R activity is stripping and recoating of coated nickel base turbine blades. It is often necessary to remove a portion or all of an aluminide coating because it is either spent and no longer protective or its presence hinders other repairs. In other instances, it may be necessary and/or advisable to affect a repair of localized damage without subjecting an otherwise acceptable blade to complete strip and recoat processing.

This paper discusses the various aspects of strip and recoat operations relative to processing as well as attendant effects on recoated substrate environmental performance and mechanical properties. The major portion of the work upon which this paper is based was performed under Air Force Materials Laboratory sponsorship[1,2].

STRIPPING

Stripping may be defined as the removal of a part or all of a surface coating by any one of several methods. Two types of stripping are generally encountered: partial and complete. The characteristics of these processes are illustrated in Fig. 1. Partial stripping consists of removing surface scale and aluminum oxides leaving a portion of the original coating and a clean surface capable of accepting an overcoat. Complete stripping, on the other hand, removes

[1] AFML Contract F33615-69C-1662, N. Geyer and J. Crosby, AFML Program Managers.

[2] E. E. Jones and J. V. Peck, "Development of Repair and Reprocess Coatings for Air Cooled Nickel Alloy Turbine Blades," AFML-TR-71-278, December 1971.

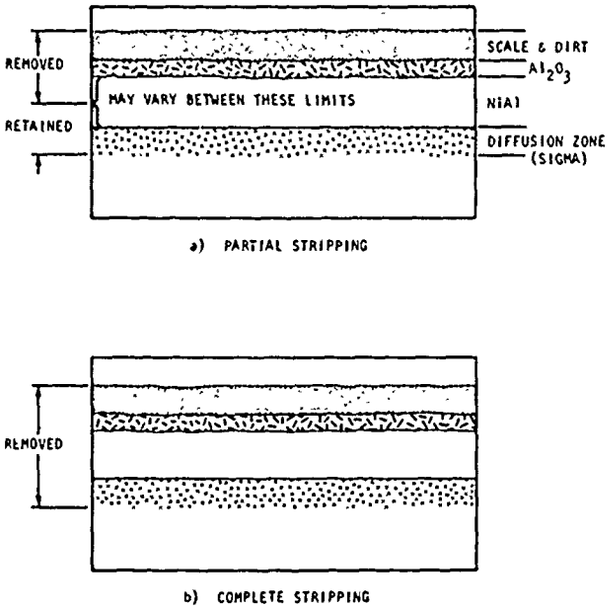

Figure 1. Schematic illustration of partial and complete stripping.

not only the entire coating but also the diffusion layer between the coating and base material (substrate).

Partial stripping can be most easily achieved by merely grit blasting under controlled conditions. Using a heat tint inspection which will disclose the presence of remnant oxides, grit blast operations can be adjusted and/or repeated until a uniform gold heat tint coloration of coated areas is achieved. Subsequent light vapor abrasion and a hot water rinse to remove heat tint oxides generally results in a suitable surface for overcoating.

Complete stripping can also be accomplished by grit blasting but the relatively slow removal rate, particularly of the thicker (>2.0 mils) coatings, makes this operation slow and expensive. In addition, efficient grit blasting can produce uneven removal and create considerable damage to exposed substrate surfaces as well as excessive stock removal if not precisely controlled.

Consequently, most complete stripping operations attempt to utilize chemical solutions which readily attack the remnant nickel aluminide and, at the same time, are relatively passive with regard to the substrate material. Ideally, a stripping solution should be totally inert relative to the substrate and highly active relative to the coating. Unfortunately, such ideal solutions are not available. In the AFML program, an attempt was made to provide a stripping bath which would attack the aluminide at a rate which would allow economical operation yet be slow enough that substrate attack in areas of thin coatings and uncoated root sections would be limited to less than 0.5 mil.

Several commercial stripping products were evaluated on as-coated and oxidation exposed coated nickel base alloys and found to produce either excessive substrate attack or were unable to remove the diffusion zone (sigma + carbide).

A laboratory stripping bath was developed which combined nitric acid and a commercial product, Turco Nitradd, with procedures shown in Table I. This process completely removed the coating and diffusion zone in about 1 hour with virtually no substrate attack as shown in Fig. 2. Exposure beyond one hour (1.5 hours) produced substrate attack to a depth of only 0.2 mil. Subsequent vapor abrasion to remove the smut resulting from the strip also removed the affected substrate. The results obtained with this procedure and stripping bath duplicated results obtained with other proprietary procedures developed by the engine manufacturers which obviously cannot be described in this paper.

The above procedure and most other processes require the removal of surface oxides which markedly resist the corrosive action of the strip bath. This present limitation, which must be resolved, presents no particular problem when dealing with solid hardware since such hardware, if not previously cleaned for inspection, may be easily prepared for chemical stripping by grit blasting. The limitation does become a real problem, however, when processing hollow hardware, particularly those designs containing very fine passages. Not only must grit abrasion be avoided because of the danger of entrapping particles, but internal passages cannot be adequately cleaned by mechanical means. Thus, there remains a need for stripping procedure which will attack substrate and coating oxides and one which does so in a manner that will not result in the formation of adherent smut or large scale particles.

As the process description implies, stripping results in stock removal to varying extents. Generally, an aluminide coating adds to overall part dimensions and also reduces the thickness of the unaffected substrate. For example, a 3 mil coating may be expected to add 2 mils per side to the

Table I
Laboratory Stripping Procedure

1. Dry blast with 320 grit Al_2O_3.
2. Immerse in stripping solution.

   Solution: Nitric acid–30% volume.
   Turco 4104 - 1.0 - 1.5% by volume.

   Temperature: Room temperature.

   Time: 1.5 hours.

   Agitation: Mixer.
3. Spray rinse to remove smut.
4. Vapor blast to clean up using Novaculite 625 at 70 psi open line pressure.
5. Rinse.
6. Dry.

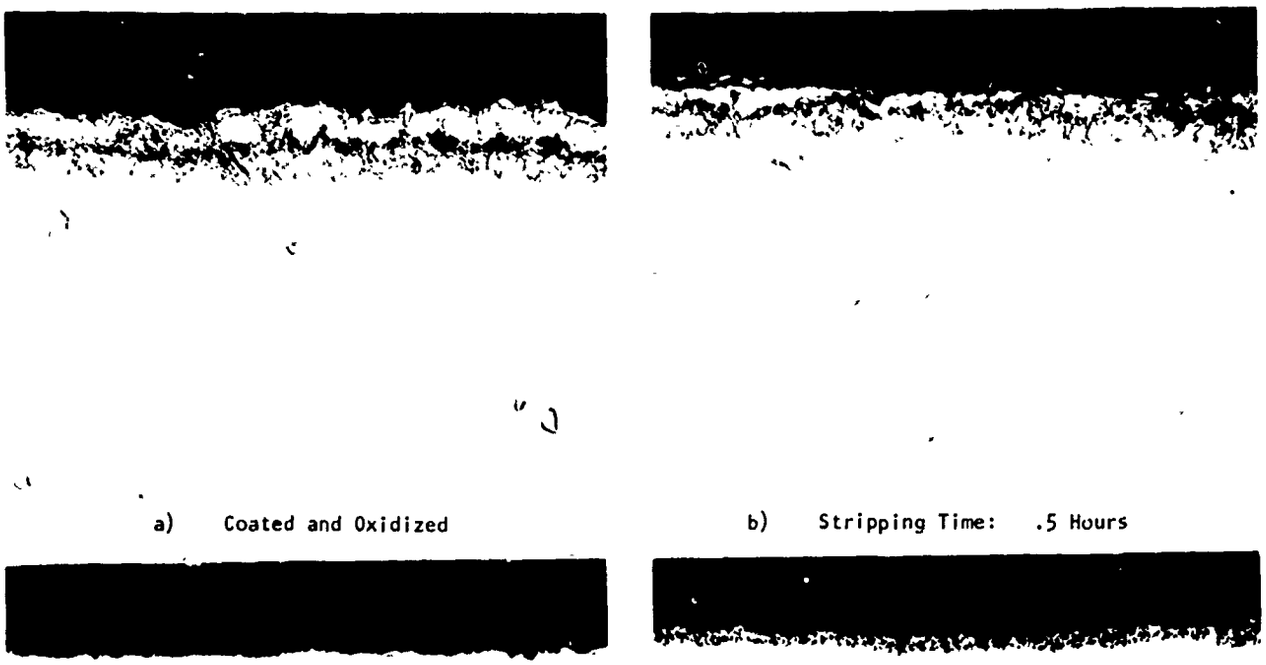

a) Coated and Oxidized

b) Stripping Time: .5 Hours

c) Stripping Time: 1.0 Hours

d) Stripping Time: 1.5 Hours

Figure 2. Effect of stripping time on coating removal using Nitric Acid + Turco Nitradd (500X, Approx.)

overall thickness and reduce the substrate thickness by 1 mil per side. Depending on the aluminum content of the coating, the substrate thickness will be further reduced by inward aluminum diffusion during high temperature usage. Therefore, complete stripping of a three mil coating after sufficient high temperature exposure may be expected to result in a total stock removal of 4 to 5 mils per side, 2 to 3 mils of which would be coating affected substrate.

Since aluminide coatings are considered to be non-load bearing, coating and complete stripping may be expected to reduce the load bearing thickness of the base metal by a total of 4 to 6 mils. This coupled with another 2 to 3 mils per side loss due to subsequent recoating and exposure could easily reduce the load bearing cross sectional thickness by as much as 12 mils. Experimental work on commercially coated alloy specimens which were exposed in air to 1750°F for extended periods indicated total thickness losses in the range of 4 to 5 mils/side. Subsequent work on actual engine operated turbine blades indicated that a loss of 3 to 4 mils per side could be expected. In this work, the chord widths of about 400 blades were measured before and after stripping. The average loss of pre-stripped chord width was 7 mils; i.e., 3.5 mils/side.

In view of the above discussion, complete stripping should be approached with some degree of caution. Firstly, it should only be used when necessary. Partial stripping is an attractive alternate since it does not remove substrate stock and the remnant coating is considered an impediment to further diffusion into the substrate from the recoat. Secondly, the complete stripping operation must be done with sufficient control so as to minimize unnecessary substrate stock removal. Thirdly, turbine blades should be dimensionally checked prior to complete stripping to insure the presence of sufficient stock to accommodate the inherent losses.

RECOATING

A properly stripped blade or vane may be recoated in much the same manner as original hardware. In general, completely stripped hardware will be recoated in exactly the same manner as new hardware, whereas partially stripped hardware requires a somewhat thinner coating to assure meeting maximum specified dimensions.

In the work conducted by TRW for the AFML, a coating system was desired which could be used as an overcoat (recoat) as well as a repair coat. For this application a slurry slip pack coating was selected. This process consists of applying a slurry comprised of Cr-Al alloy powder suspended in a lacquer to the surfaces of the hardware by either spraying, dipping or troweling; the latter being more appropriate for affecting repairs of local coating damage.

After applying the slurry, the piece is heated slowly to about 800°F in vacuum to drive off the organic vehicle. After about 15 minutes at 800°F, the evacuated chamber is back filled with argon to a pressure of 150 torr and the work heated to 1950°F and held at temperature for about 1.0 hour. Since this process produces a coating rich in Ni_2Al_3 and $NiAl_3$, the work is subsequently diffusion heat treated at one atmosphere and 1950°F for an additional three hours to diffuse the aluminum into the substrate and thereby convert the coating to predominantly NiAl.

The microstructures of a recoated nickel base alloy after partial and complete stripping are shown in Fig. 3. The coatings are basically the same with the exception that the recoat on partially stripped substrate is slightly thicker, the diffusion zone somewhat thicker and coarser and there are more carbides within the NiAl matrix. It is suspected that the carbides in the recoat on partially stripped substrate are traceable to the original coating. They appeared in all overcoats regardless of substrate or original coating.

Simulated repair coatings were produced by creating a defect in an original coating and subsequently oxidizing the defected specimen. After oxidation exposure the defected area was grit blasted with a fine stream of abrasive from a 0.018 inch diameter nozzle to remove oxidation products. A slurry of coating material was applied to the defect area by troweling and the part heat treated as described previously. The repair coating sequence is shown in Fig. 4.

A typical microstructure is presented in Fig. 5. In the most severe case wherein the substrate was penetrated by the damage/oxidation/cleaning sequence, a surface depression of between 5 and 8 mils resulted. On the other hand, when damage was repaired prior to oxidation, a surface depression less than 0.5 mil was encountered as shown in Fig. 6.

ENVIRONMENTAL PERFORMANCE

Coupon specimens of each coated alloy were oxidized then partially or completely stripped, recoated with the

a) Partially Stripped

b) Completely Stripped

Figure 3. Al(Cr) recoated oxidized nickel-base alloys, etched. (500X, Approx.)

slurry Al(Cr) system and subjected to static oxidation at 1750°F along with as originally coated specimens. The results shown as total weight change after the indicated exposure times are summarized in Table II. The recoated B1900 exhibited essentially the same oxidation behavior as the original coating. Recoated IN-100 exhibited about the same weight gain as B1900 after 150 hours; however, compared to the original coating, a significant reduction in oxygen pickup was noted. Metallographic examination of the specimens after exposure indicated no substrate attack and a remnant coating having considerable additional protective potential.

Hot corrosion/sulfidation resistance was determined in a 0.6 Mach test rig (Fig. 7) which simulates an engine environment. To accelerate the corrosion attack, sulfur is added to the Jet A fuel (0.4 w/o) and synthetic seawater is injected into the combusted gases (3.5 ppm chloride). Temperature is regulated by fuel/air ratio control to provide a seven-minute cycle consisting of the following profile:

1 minute heatup + 2 minutes at 1750°F+
1 minute heatup + 1 minute at 2050°F+
2 minutes air cool.

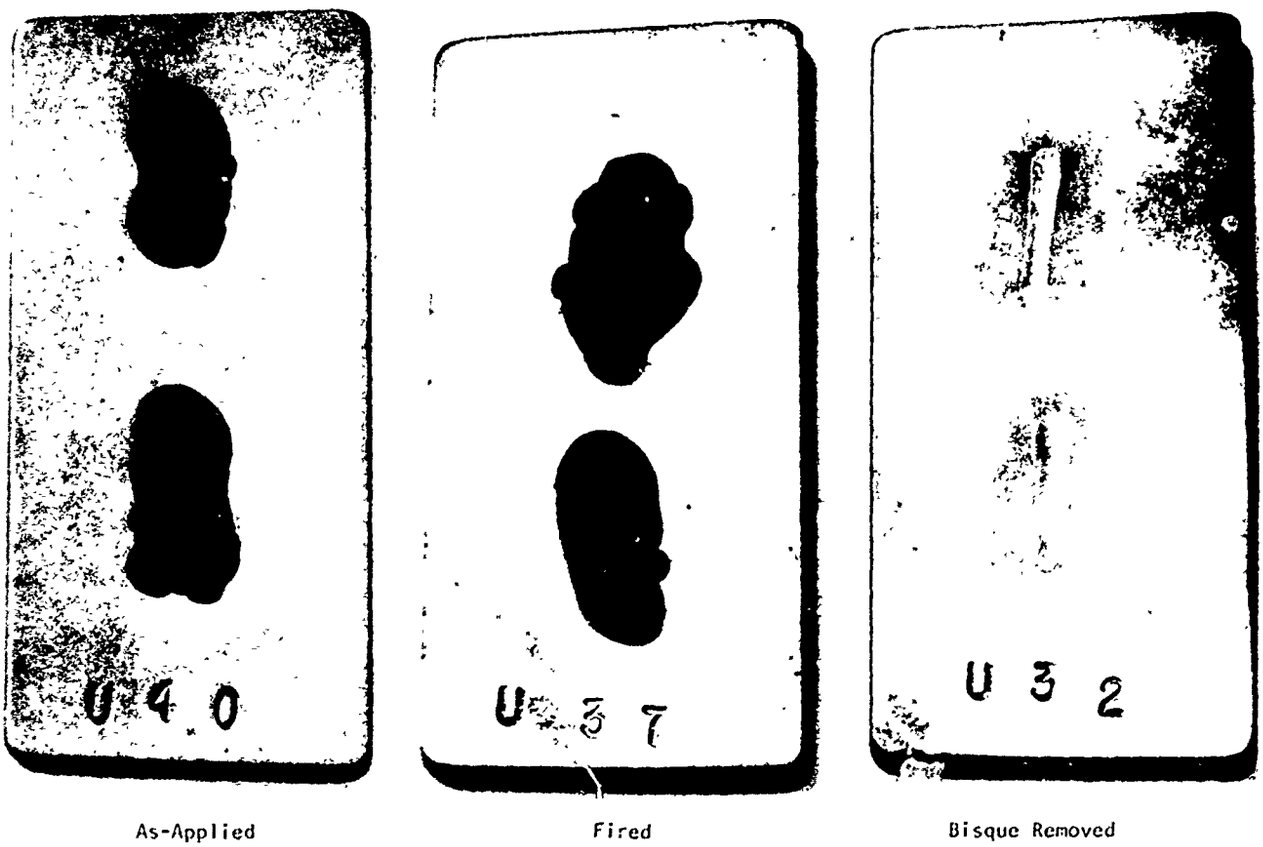

Figure 4. Repair coating sequence.

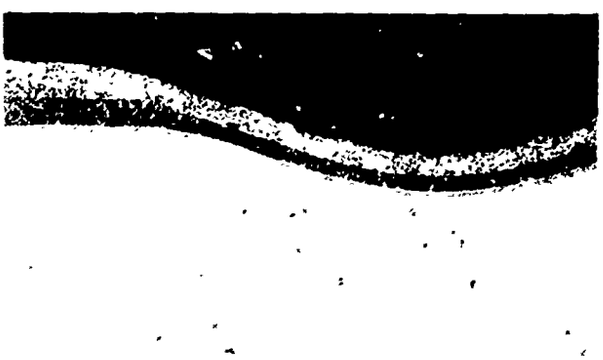

Figure 5. Repair coating on severely damaged and oxidized coating, 100X. (Approx.)

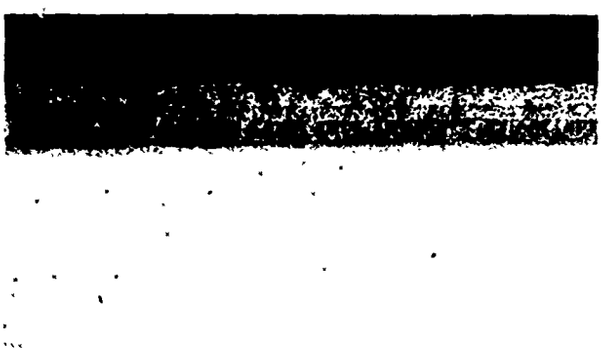

Figure 6. Repair coating on a damaged specimen which was repaired prior to oxidation exposure, 100X. (Approx.)

Prior to stripping and recoating, test specimens were rig tested for a period of time approximately 75 percent of the normal coating life under the above test conditions. The results of these, summarized in Fig. 8, show the recoat to be as effective as the original coating. Differences between the lives of partially and completely stripped specimens are considered insignificant as they are within a normal scatter range.

Thermal shock tests conducted in the rig shown in Fig. 8 consisted of heating airfoil shaped specimens to 1750°F in 60 seconds and air blasting for 30 seconds. Sepcimens were cycled to failure which generally consisted of substrate exposure caused by coating cracking and spallation. The results indicate that the recoated life of B1900 was about 88% of the original coating life and the life of recoated IN-100 was about 50% of the original coating.

Table II
1750°F Static Oxidation Resistance of Recoated Ni Base Alloys

Substrate	Condition	Exposure Time (hrs)	ΔW Mg/cm^2
B1900	Original Coating	500	+0.3
B1900	Partial Strip & Recoat	500	+0.3
B1900	Complete Strip & Recoat	500	+0.2
IN-100	Original Coating	150	+1.3
IN-100	Partial Strip & Recoat	150	+0.5
IN-100	Complete Strip & Recoat	150	+0.5

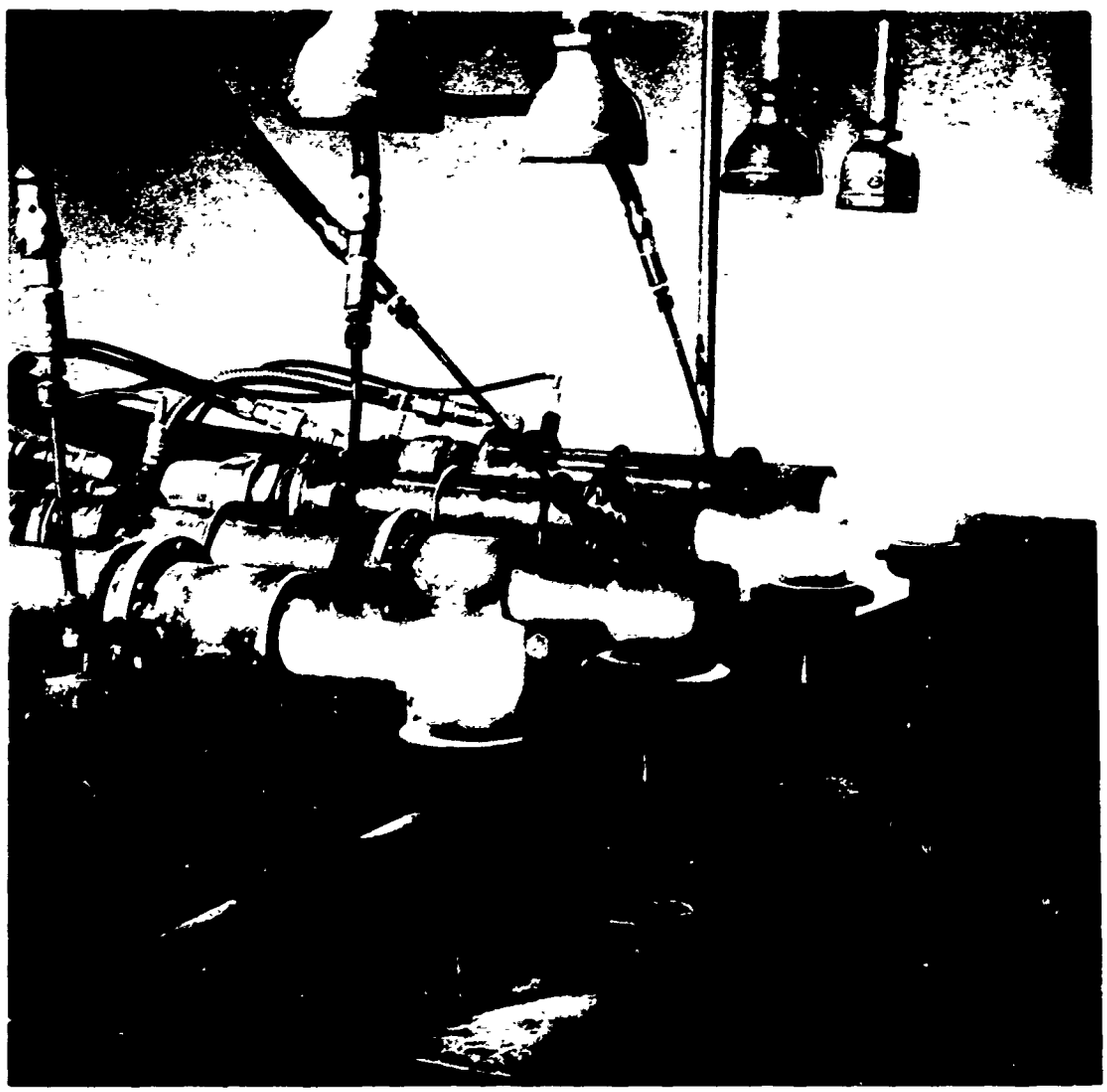

Figure 7. Gas turbine environmental simulators.

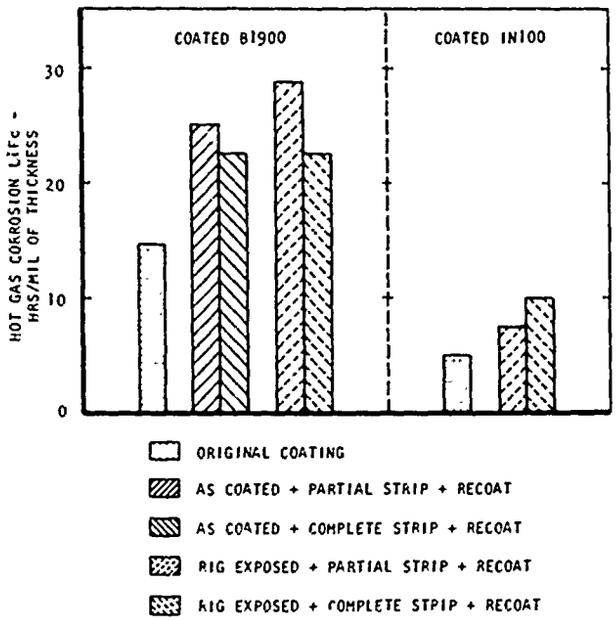

Figure 8. Hot gas erosion/corrosion resistance of reprocessed coatings.

MECHANICAL PROPERTIES

The mechanical properties of coated and recoated base metal were calculated on the basis of original substrate dimensions so as to illustrate the reduction in load bearing area caused by the various strip and recoat processes. Representative 1800°F tensile and stress-rupture properties are shown in Tables III and IV, respectively. Coated B1900 exhibited a progressive degradation due to coating and exposure. Stripping and recoating produced no further degradation of the oxidized properties but failed to restore as-coated strengths. Coated IN-100 system also displayed a loss in strength due to coating with no further degradation due to oxidation exposure. Strip and recoat operations provided a modest increase in strength. Tensile ductility was substantially reduced by the strip and recoat operation. This, however, may be characteristic of the coating rather than due to the processing itself.

The stress-rupture lives at 1800°F and 20 ksi exhibited the same general pattern as tensile strengths. The rupture ductility of the specimens, however, did not reflect a loss due to coating or recoating, but an increase. The increase

Table III
1800°F Tensile Properties

Coating/Substrate	Condition*	U.T.S. (ksi)	0.2% Y.S. (ksi)	Elongation (%-1")
Co Coat/B1900	Uncoated	64.2	49.6	10.0
	Coated	57.5	44.0	8.6
	Coated + Oxid.	49.8	37.9	5.0
	C+Ox+P.S.+R.C.	52.8	38.4	4.2
	C+Ox+C.S.+R.C.	50.1	40.3	1.8
Codep C-2/IN-100	Uncoated	56.3	41.2	5.6
	Coated	53.7	38.5	9.2
	Coated + Oxid.	54.0	39.1	3.7
	C+Ox+P.S.+R C.	58.8	48.6	3.5
	C+Ox+C.S.+R.C.	54.5	49.4	1.9

*B1900 oxidation exposed (Oxid) at 1750°F/500 hrs.
IN100 oxidation exposed (Oxid) at 1750°F/150 hrs.
C – Coated.
Ox – Oxidized as above.
P.S. – Partial Strip.
C.S. – Complete Strip.
R.C. – Recoated–Slurry Slip Pack Process.

Table IV
1800°F Stress Rupture Data (20 KSI)

Coating/Substrate	Condition*	Life (hrs)	Elongation (%)
Jo-Coat/B1900	Uncoated	172.7	4.5
	Coated	141.9	8.7
	Coated & Oxid.	39.2	9.4
	C+Ox+P.S.+R.C.	74.2	11.4
	C+Ox+C.S.+R.C.	61.7	12.0
Codep C-2/IN-100	Uncoated	147.9	2.0
	Coated	96.1	7.6
	Coated & Oxid.	64.0	6.1
	C+Ox+P.S.+R.C.	50.9	7.3
	C+Ox+C.S.+R.C.	45.6	6.4

*B1900 oxidation exposed (Oxid) at 1750°F/500 hrs.
IN-100 oxidation exposed (Oxid) at 1750°F/150 hrs.
C – Coated.
Ox – Oxidized as above.
P.S. – Partial Strip.
C.S. – Complete Strip.
R.C. – Recoated–Slurry Slip Pack Process.

in rupture ductility with corresponding loss in load bearing ability suggests that the thermal treatments experienced by the substrate during coating, oxidation exposure and recoating are influencing its properties. The low tensile ductility, on the other hand, may be the result of a strain rate sensitivity of the coating.

In an attempt to determine the effects of a strain/oxidation environment on subsequent recoat properties, coated B1900 was prestrained to a permanent elongation of 1.5% at 1800°F, oxidized at 1750°F for 500 hours, stripped and recoated and finally tested for stress rupture life. On actual turbine blades, the maximum allowable total stretch varies from 0.01 to 0.02 inch for 3 to 4 inch chord lengths. Considering a 3.5 inch chord length, a permanent strain of 1.5% as used in this work, would produce a stretch of 0.053 inch; i.e., a stretch 2 to 5 times greater than allowed.

The results, a portion of which are shown in Fig. 9, indicate that prestraining generally increased stress rupture life and reduced rupture elongation. The apparent improvement in strength properties and reduced ductility must be related to changes which occurred in the substrate since any coating related effects were removed by stripping. It is possible that prestraining produced a strain induced grain boundary precipitation of carbides which were not solutioned during the recoating and diffusion thermal cycles and act to pin grain boundaries to improve creep and stress-rupture properties while reducing elongation at rupture.

RECOATING BLADES

Several engine operated blades of the type shown in Fig. 10 were stripped, repaired and recoated. The blade in the center of Fig. 10 contained a leading edge crack which was blended out (not to specification) and the blade on the right is air-cooled with no coating on the internal passages.

The blades were grit blasted to remove surface oxides, stripped using previously described techniques and coated by the slurry slip pack process. The hollow blade was coated on the inside surfaces during recoat by packing fine Cr-Al alloy powder into the cavities. The dry powder was the same as used to prepare the slurry. The resulting blades are shown in Fig. 11.

While this exercise was performed to demonstrate the capability of the stripping and recoating operations, the effects of these operations on the hollow hardware were of

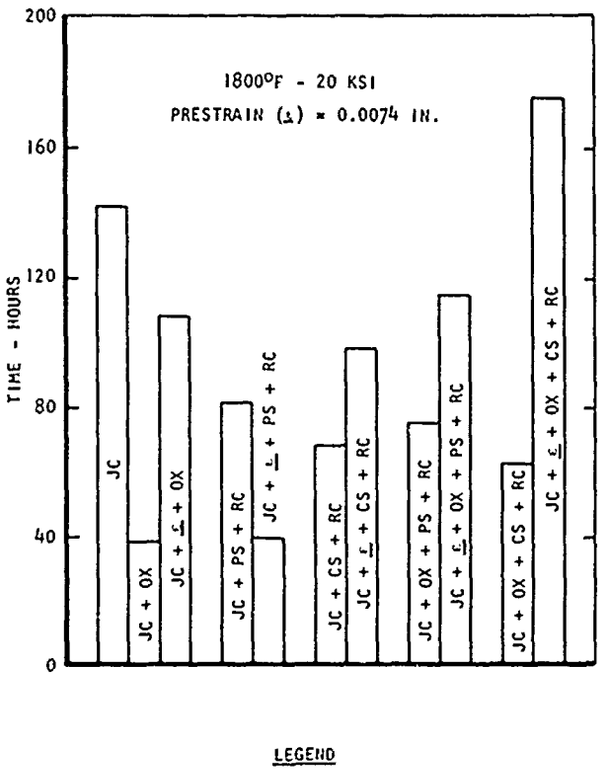

Figure 9. Effect of prestrain and oxidation on the stress rupture lives of as-coated and stripped plus recoated B1900.

Figure 10. Typical engine used turbine blades as-received.

Figure 11. Engine operated blades after complete stripping and recoating with the Al(Cr) slip pack.

particular concern. In the as-received (engine operated) condition, the internal surfaces contain subsurface and surface oxides, whereas the outer surfaces contain appreciable remnant coating as shown in Fig. 12. The appearance of the blade and coating microstructure indicates that these blades were removed from service for reasons unrelated to the coating. In other words, had coating depletion been the dominant reason for scrapping this blade, one would expect appreciably more oxidation on internal surfaces.

The appearance of the surfaces after stripping and recoating, Fig. 13, indicate a normal coating structure on the outer surfaces. The internal surfaces, however, contain oxides in the coating which are attributed to those caused by engine usage and which were not removed by stripping. While the amount of oxides shown in Fig. 13 may not appear to be particularly troublesome, it should be reemphasized that this blade was not removed from service because of a coating problem.

Oxidation

(a) Hole

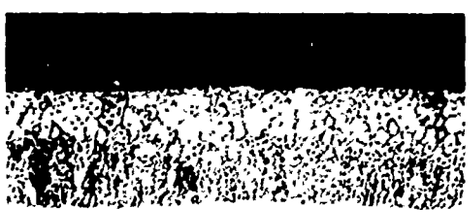

(b) Outside Surface

Figure 12. Engine operated cooled turbine blade showing absence of coating on hole surfaces and outside surface coating, 500X. (Approx.)

SUMMARY

This paper has attempted to summarize work done in the laboratory at TRW for the AFML and to indicate areas which require additional efforts. Stripping and recoating of solid hardware can be accomplished by relatively conventional methods. The work reported herein utilized laboratory stripping techniques and a coating which while a development coating (not commercial) is considered representative of those systems being currently used on the majority of turbine blades. It must, therefore, be emphasized that the other coatings can and, in many cases ,are being used as reprocess coatings.

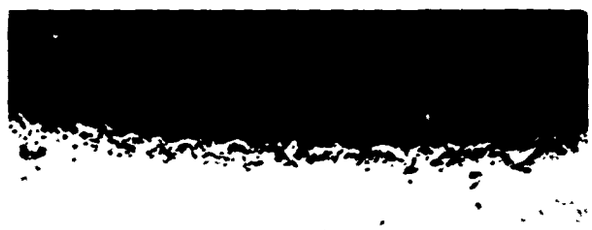

(a) Hole

(b) Outside Surface

Figure 13. Stripped and recoated engine operated blade. Stripped with Nitric and Turco solution and recoated with slip pack Al(Cr), 500X. (Approx.)

Three areas of particular concern require additional R&D activity. The first deals with the effects of exposure, stripping, recoating and reexposure on mechanical properties of the substrate/coating composite structure. Substrate stock losses associated with recoating as well as superimposed thermal effects must be correlated with section thicknesses. The influence of substrate losses on the strengths of various substrate thicknesses is dramatic as shown in Figs. 14 and 15, particularly in the thin sections encountered in hollow hardware. These curves illustrate theoretical losses in the load carrying ability of reprocessed substrates relative to their original capability ignoring heat treat effects.

The second area requiring considerable attention is stripping. Processing procedures and stripping solutions must be developed which will remove surface oxides and aluminide coatings with no substrate attack and without the use of abrasives. Furthermore, stripping solutions must be such as to affect a solutioning of oxides and coating as opposed to descaling to prevent entrapment of particles within the passages of hollow hardware.

The third area involves hole coating. Large cavities and passages may be coated by placing powders into them and affecting a diffusion coating. However, the more intricate design of high performance blades and vanes utilizing a multitude of very small holes and passages preclude such coating techniques. A new process is therefore needed to uniformly, reliably, efficiently and economically coat holes and passages which does not require the introduction of particulate material.

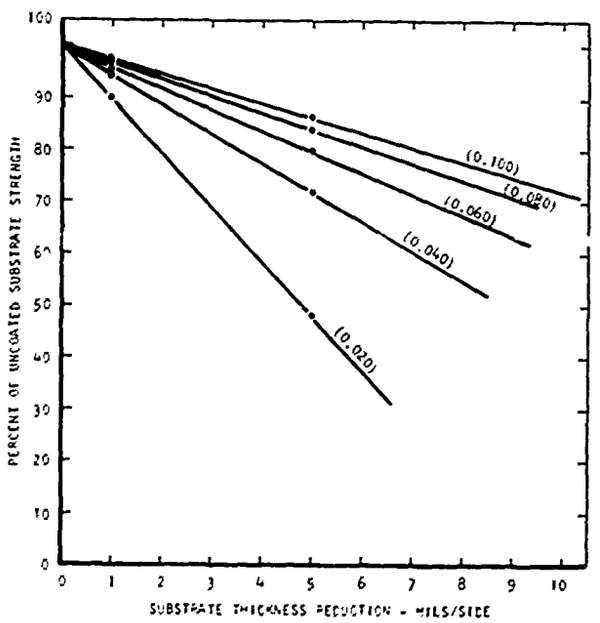

Figure 14. Effect of substrate thickness reduction on the load bearing ability of the substrate.

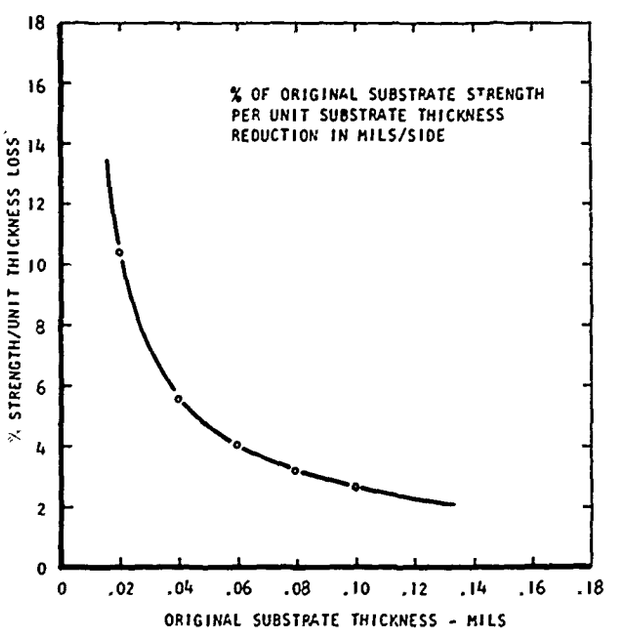

Figure 15. Effect of original substrate thickness on the reduction in load bearing ability per unit thickness loss.

The AccuRay KET* Process for the Detection of Microdefects

William C. Eddy, Jr.
Industrial Nucleonics Corporation, Federal Systems Division
Columbus, Ohio

The determination of the maximum time between overhaul of jet engines is set principally by two differing types of engine wear. If mechanical damage and abuse are neglected, an engine will require overhaul at a point where incremental wear items are at their maximum limits. Turbine blade coatings, bearings, accessory drives, and burner cans are all typical of subsystems that age progressively in engine operation to the point that overhaul is indicated. This type of wear is characterized by its predictable nature and freedom from catastrophic failures. While these aging parts do affect overhaul life, it is the structural strength of rotating components that generally determines the time between overhaul (TBO) of modern day jet engines.

Failure of any rotating component almost invariably results in an in-flight shutdown, if not the near catastrophic destruction, of the engine and possibly adjacent airframe. The consequences of in-flight mechanical failure are such that the airline industry and the government have essentially set "zero" as a target goal for incidence of in-flight failure.

Considering the number of parts in an engine and the broad distribution of statistical fatigue failure, it is very obvious that a few "early failures" become the controlling element in determination of engine overhaul periods.

The TBO is highly dependent on the incidence of in-flight failure which relates directly to the maintenance facility's ability to spot and remove defective parts during overhaul. An operator is torn between an ultra-conservative approach in which he throws away everything and, essentially, assembles a new engine from parts around an old serial number, and an approach which places a heavy reliance on nondestructive inspection techniques–replacing only those parts which have demonstrable defects. Such an obvious procedure has two main drawbacks. Present nondestructive inspection techniques are unable to give reliable results when operated at the limits of their sensitivity, and the limits of the detection sensitivity may be too close to failure of the part to do much more with the information than use it to discard obviously bad parts.

In any critical part, the period between inspections can never exceed the time between detection probability and failure–and this period in practice must be reduced to achieve some safety factor. To illustrate, fluorescent dye penetrant can detect turbine disc cracking at some 75% of the fatigue life; if the shortest life that can be expected is 10,000 hours, then discs with over 7,500 hours would have to be limited to some number less than 2,500 hours in any succeeding overhaul period to prevent 74% disc passing inspection with a forecast life of only 2,500 hours. This, in itself, would not be objectionable if all discs had about the same forecast life, but one major jet engine manufacturer has suggested that if he could reliably detect 3% *early failure* turbine discs, it could extend the fleet time limit of this part by a factor of four. The common thread in all of these determinations is the time at which the "age" of a part can be predicted reliably.

With good sensitivity, not only the damage can be measured but with knowledge of parts service time to date, the 3% which brings down service life of the group also can be found. As the margin between detection and failure grows, so does the probability that the part can be reinstalled *regardless* of the total life of the part. The airlines today have millions of dollars of parts in warehouses which fit into this special division of purgatory–parts which they cannot prove to be bad, but which they also cannot prove to be good. This paper is about a new process which has the sensitivity necessary to give a sound engineering basis for continuing these parts in service.

Four years ago, Industrial Nucleonics began working on a radioactive gas penetrant inspection technique that now offers a significant improvement in nondestructive inspection for critical part evaluation and may lead to a means of using productively the phenomenon known as low cycle fatigue.

Cracks, as they are known in the aircraft industry, are actually a manifestation of part failures rather well along in the aging process. Generally speaking, cracks having lengths of 1/32 inch and some reasonable depth, of say 5-10 mils, can be detected with conventional nondestructive inspection techniques. However, before these "large" cracks appear, the material undergoes metallurgical changes which, at about 30-40% of the fatigue life, present themselves as microcracks–cracks having dimensions measured in millionths of an inch with depths nearer to 1/2 to 1 mil.

Typically, cracks which can be detected with high resolution dye penetrants are those produced in the last 30% of

*Registered service marks of Industrial Nucleonics Corporation.

life. Parts with cracks this large are actually in the early stages of failure.

The AccuRay KET radioactive gas penetrant process takes advantage of the fact that all materials have surface-adsorbed gases which can be replaced with radioactive gases. The concentrations of these gases in cracks and porosity are detectable using conventional film autoradiography or electronic scanning.

Presently, the process is being run as a batch operation with the following major steps being taken. The parts to be inspected are loaded into a pressure tight container which is evacuated to a normal laboratory vacuum. The parts are allowed to outgas for 30 to 60 minutes. Kr-85 (actually, 95% Kr-84 and 5% Kr-85) is admitted to the chamber at room temperature. After a brief soaking in krypton, the gas is removed and the parts are readied for imaging (Fig. 1). The sensitivity of this process when compared to other techniques is almost frightening to a material scientist.

Inherent in a system capable of measuring defects with dimensions measured in millionths of an inch is the requirement for some enlargement of the image. A crack that small cannot be seen visually, so, logically, it is assumed that its image cannot be seen unless it is enlarged by some large factor.

The nuclear character of our penetrant solves this problem for us very neatly. Unlike visible light, the radiation given off in a crack is not constrained to a free path but can pass through a small amount of metal laterally around the crack. Figure 2 shows this rather convenient property of the radioactive gas penetrant.

This enlargement factor varies but the image is generally between 5-10 mils and is somewhat dependent on the density of the material being inspected. The enlargement can be as much as 10^4 on a crack of 10^{-6} inches–large defects are increased by a nearly constant 5-10 mils and have negligible size distortion.

In optical microscopy, image size magnification is achieved at the expense of a proportional reduction in viewing area. A KET presentation does not have this inherent limitation. All defects are shown on an area basis in their proper relationship with micro defects enlarged to a convenient viewing size. Significantly, the whole part can be seen and not just some highly magnified section. Most defects have a third dimension that often cannot be detected by a purely surface measurement.

Volume, area open to surface, and crack cleanliness are important factors in determining the adequacy of a liquid penetrant inspection. The KET process with its extremely small atom can penetrate and coat the walls of all but atomically small defects, a pinhole well below optical resolutions can serve as an access for krypton gas to inside passages. Crack contaminants, long a serious variable in dye penetrants, actually help enhance a crack with the KET process. Since the KET process is predicated on coating the surfaces with adsorbed gases, the presence of foreign material in a crack serves to provide more adsorption sites and, therefore, provides a greater signal. Last, the penetrating radiation allows subsurface defects to be detected on the surface of the part.

SENSITIVITY

The KET process apparently can measure clean cracks in stainless steel (worst case) having widths of 1 to 5 millionths of an inch and depths of less than 1 mil. Cracks of this size

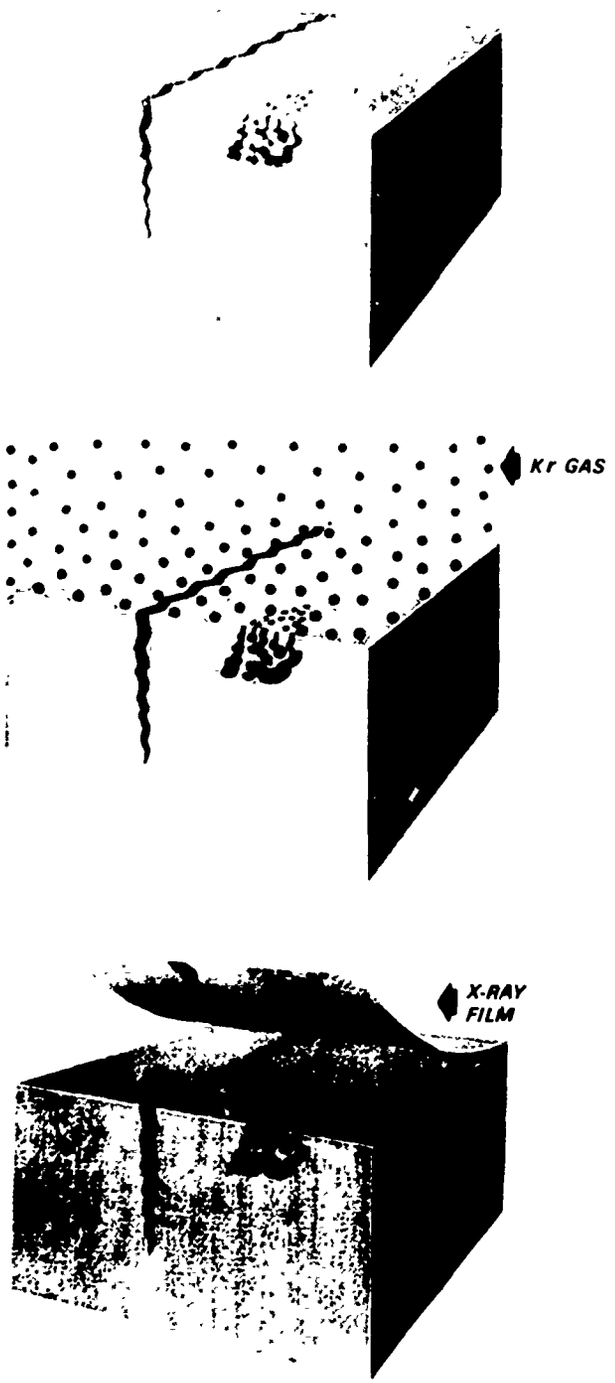

Figure 1. Sequence of steps in the AccuRay KET process.

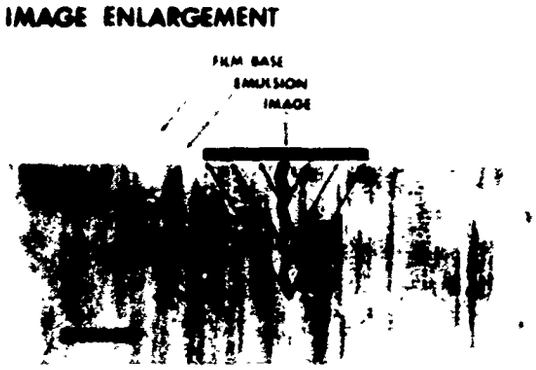

Figure 2. The penetrating nature of radiation provides an effective image enlargement.

are generally created in low cycle fatigue at about 40% of service life.

Conventional high resolution dye penetrants start to fall apart at 0.5 mil, and crack cleanliness is very important This corresponds to about 70% fatigue life (Figs. 3, 4, and 5).

The KET process is extremely sensitive to porosity or three-dimensional type defects. Figure 6 illustrates two sleeve bearings from an Air Force turbine engine that has been failing to give normal operating life since the engine was first produced.

Figure 3. KET autoradiograph of low cycle fatigue specimen at 30% fatigue life.

Figure 4. KET autoradiograph of low cycle fatigue specimen at 50% fatigue life.

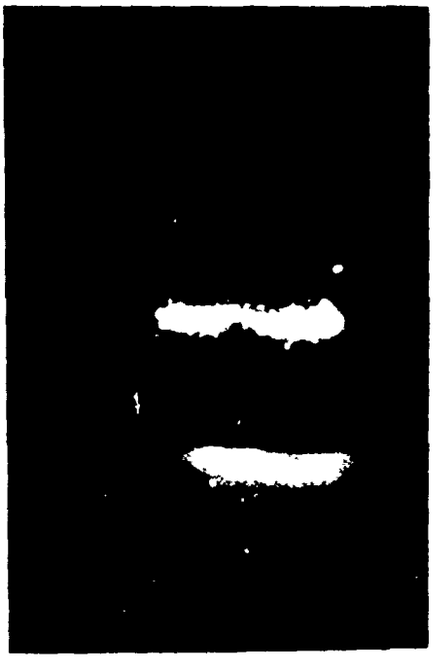

Figure 5. KET autoradiograph of low cycle fatigue specimen at 70% fatigue life.

A great deal of money was spent on this item attempting to reengineer the engine to remove cavitation erosion from the bearings–over $17,000,000 was spent on this part in addition to the damage to machinery caused by its failure before it was inspected using the KET process. The photographs clearly show that the bearing has a serious case of subsurface porosity. Simple fatigue failure of vapor-loaded porosity areas caused metal erosion closely simulating cavitations.

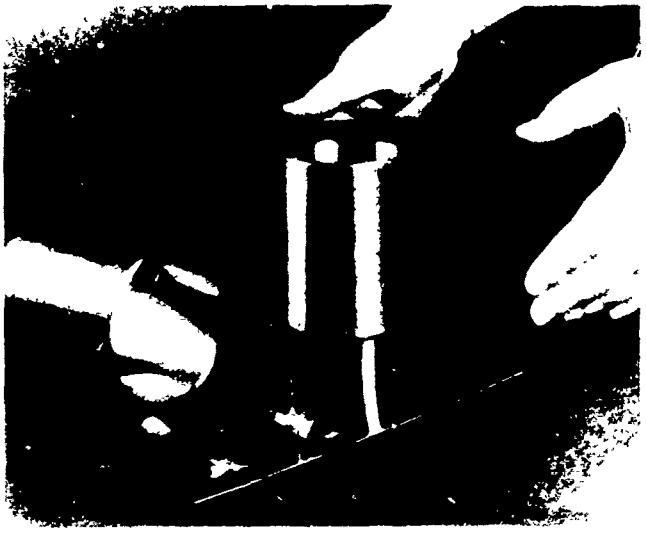

Figure 6. Air Force turboprop sleeve bearing with autoradiographs showing subsurface porosity.

Figure 7. Sectors of a T-53 compressor disc with indications of cracks shown by arrows.

Figure 7 is a reproduction of an Army turbine compressor wheel which was sectioned into four pieces. There is some dispute as to the cause of failure (whether it is high or low cycle fatigue or possibly stress corrosion induced). There is no doubt, however, that the cracks are being missed in conventional nondestructive inspections.

These discs are a classic illustration of the superiority of the new process. The cracks in these parts are not only very small, they are also generally filled with oxides and have proven nearly impossible to find with dye penetrants. The illustration clearly shows the high signal-to-noise present.

One of the more common questions regarding this process deals with confusion caused by an overabundance of data. This has never been a problem. One of the best illustrations of this is a microscopic anomaly which was found in a shot peened area of a jet engine turbine disc, Fig. 8. The defect was continuous through the specimen and had a width of approximately 10 millionths of an inch, a depth of 1 mil, and was buried in a matrix of cracks having depths on the order of 0.5 mil (shot peened damage). The photomicrograph in Fig. 8 shows the area of the cracks and its lesser neighbors. The scanning electron microscope photograph shows the cracks after 0.5 mil has been polished from the surface. The remaining crack correlated well with the KET data (all SEM and metallurgy work done by Battelle Memorial Institute).

LOW CYCLE FATIGUE

One of the very earliest applications of the radioactive gas penetrant process was comparison testing of the KET process with more or less conventional technologies such as dye penetrant, eddy current, and ultrasonics. While looking for fairly large cracks, we found that the KET process was very sensitive to measuring the even smaller cracks and crack nucleations that anteceded these larger defects. As noted previously, the first disc work that we did was with General Electric on a high time CJ-805 disc, with Battelle classifying the defects as being in the low cycle fatigue range. This started the users agitating for application of the process to what we now call fatigue life prediction.

Although our first work in low cycle fatigue was with General Electric, it was not until American Airlines' interest and early Pratt & Whitney test programs that we became aware of extreme sensitivity that the KET process had in measuring damage done in the very low percentage cycle life of parts. Figure 9 shows three of seventeen specimens in the original low cycle fatigue evaluation of the KET process against stress penetrant. The normal fatigue life of these specimens approximated 65,000 cycles and it was easy to see that even on the 1,000 cycle, which is a nominal two percent of fatigue life, the early microcracks are discernible. Similar data from another manufacturer's disc alloy is shown in Fig. 10.

The requirement for exhaustive empirical testing before use of life extended discs, the variety of discs available and the varying service environments dictate a lengthy engineering program with a considerable amount of engine testing. Some of this testing can obviously be cut short by use of existing high time discs, but there is no way to test "cycles to failure" after defect detection other than in a test cell. Ferris wheel testing and spin pit work can define these parameters but in the end, actual discs will have to be run to near failure. This is both expensive and time consuming.

The two charts, Fig. 11 and 12, were used in a talk given to ATA last September on life extension of discs. Figure 11 represents the integrated waste of disc hardware based on retirement of all discs at cycle life with only 0.2% of these discs being at nominally 85% of fatigue life. We hope to show that by the simple expedient of moving back the threshold for detection sufficiently to allow an overhaul

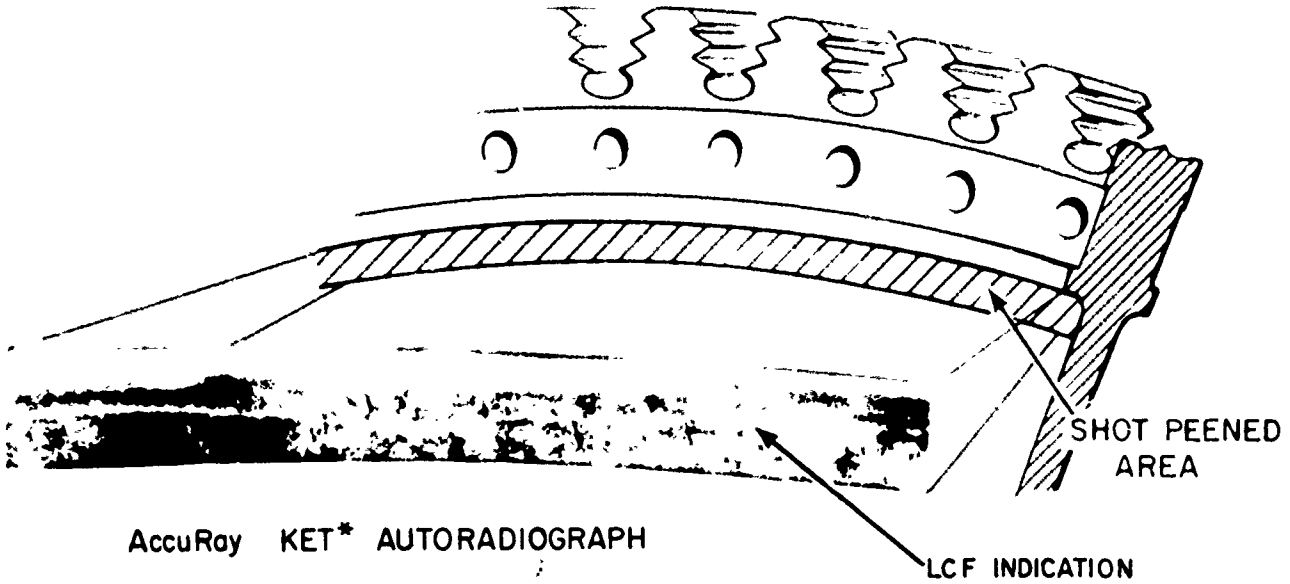

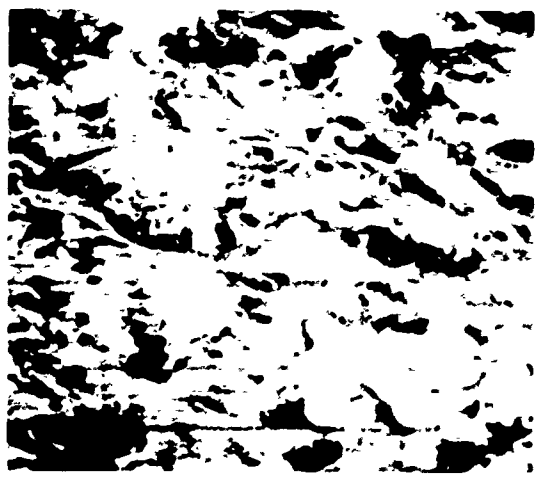

PHOTOMICROGRAPH OF
SHOT PEENED SURFACE

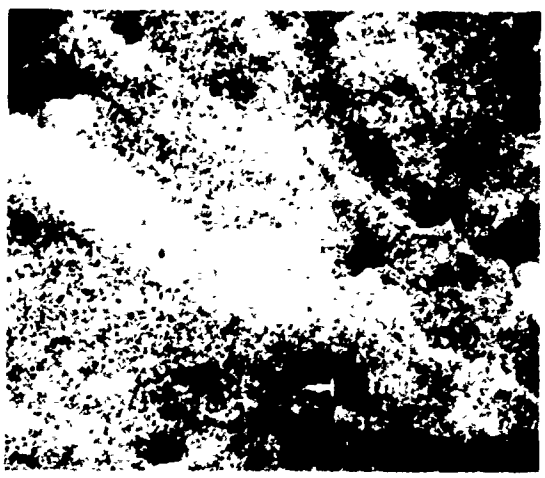

SCANNING ELECTRON MICROSCOPE
0.5 MILS OF SURFACE REMOVED

Figure 8. Scanning electron microscope reveals anomalies approximately 10 micro-inches wide and 1.3 mils deep which correlate with KET autoradiograph. Note the rough texture of the shot peened surface.

cycle, we can effectively eliminate cycle limitations on discs and utilize the entire integral of the disc life curve. The curve shown here illustrates what happens if you simply reject 3% "early failure" discs at the present cycle life limitation. You should be able to get a four-fold life improvement at no degradation of safety.

The second chart, Fig. 12, is somewhat a compilation of *actual* KET process data on a variety of turbine disc materials from work at both General Electric and Pratt & Whitney. What is significant is its resemblance to a nomograph (Fig. 13) prepared by Schijve and included in ASTM 495. Our data, wholly empirical, produced a striking correlation to the theoretical crack sizes predicted but never previously seen in service materials. The discovery of the Schijve data added a great deal of confidence to our empirically derived data.

POROSITY

Our beginning work in porosity started almost simultaneously with AVCO and General Electric. Both programs were given impetus by test cell failures of air-cooled turbine blades in experimental engines.

The AVCO blade was a first stage high pressure turbine blade from the, then, experimental main battle tank engine.

SPEC #	7	8	9
CYCLES	20,000	33,000	1,000

EVALUATION OF LOW CYCLE FATIGUE DETECTION CAPABILITY
AccuRay KET* vs STRESS PENETRANT

Nickle Base Crouse Specimens

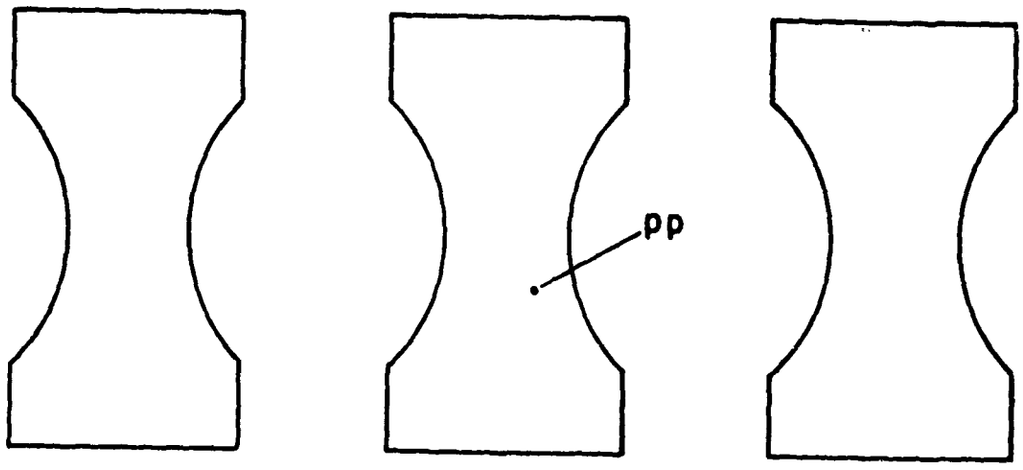

STRESS PENETRANT RESULTS

Figure 9.

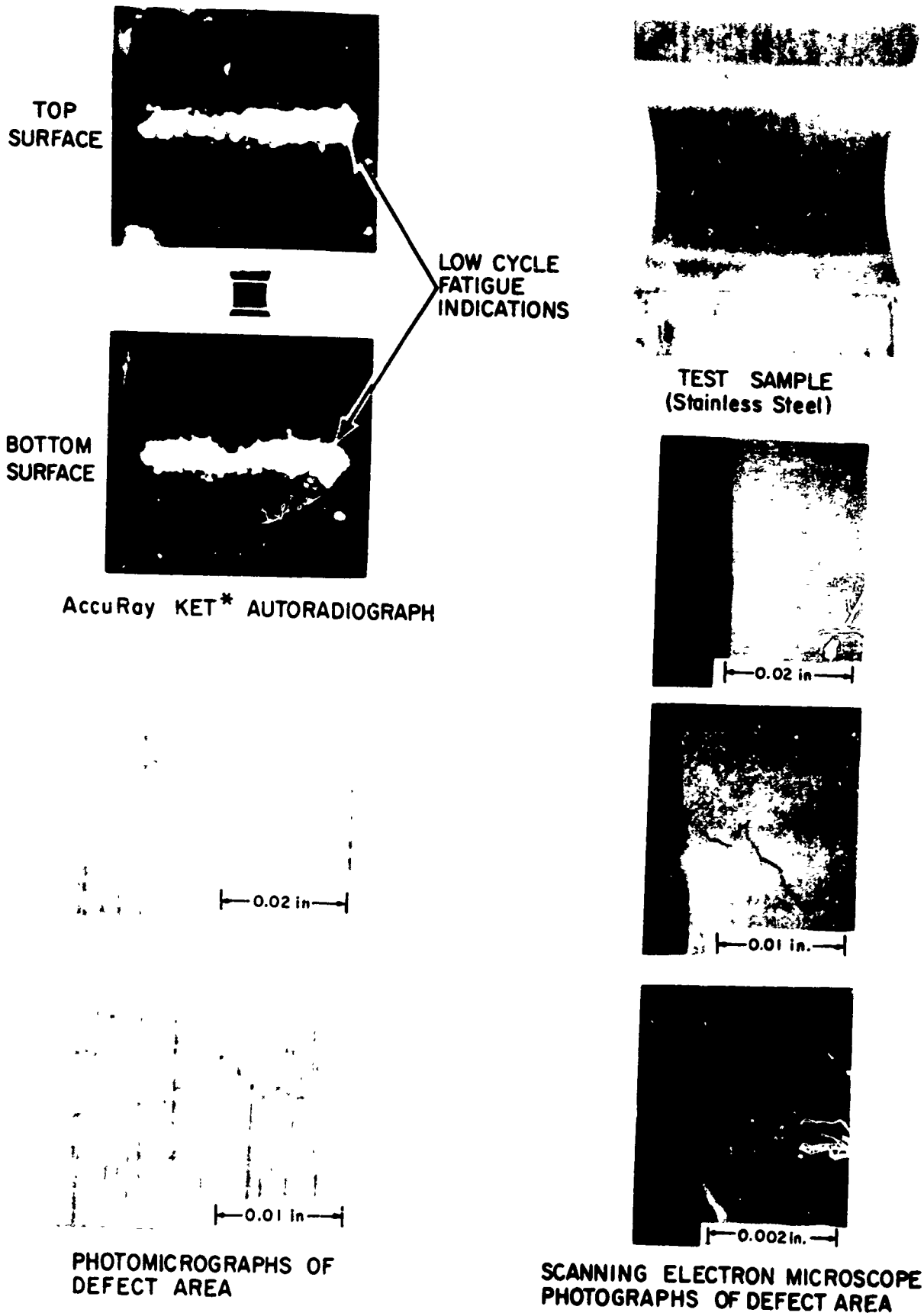

Figure 10. Low cycle fatigue test sample.

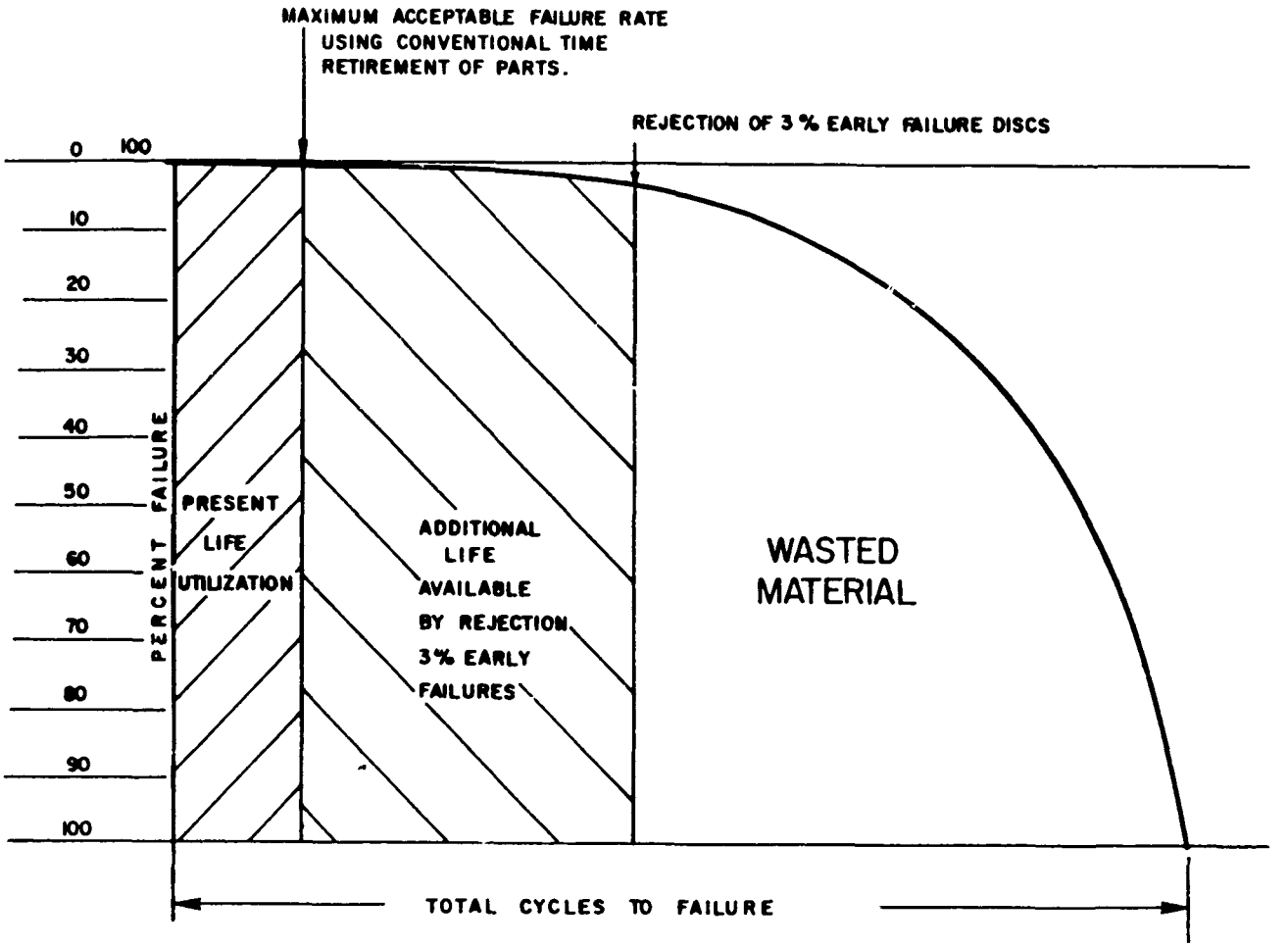

Figure 11.

Figure 14 shows a general outline of the blade. The cast recess in the base was designed into the blade to accommodate fixturing. The blades were, in general, failing in the cast recess area; metallurgical analysis showed the blade failures to have originated in dendritic porosity. Dendritic porosity, incidentally, comes from the Latin meaning "treelike," and it is characterized in metal solidification by the presence of catacombs of sharp, treelike porous cavities which result in high stress concentrations.

The metallurgical confirmation of our findings of porosity was extremely good, and this, coupled with the low acceptance rate, forced AVCO to go back to the casting vendor to regate the blade along with effecting design changes which elimir ed the recess. With these changes the porosity problem stopped immediately and the blade went on to provide very good service. To our knowledge, the blade is free of this problem today.

The General Electric work was very similar in that General Electric had the contract for the SST engine, and early in the test cell life, three of the engines had second stage HPT blade failures. Like the AVCO blade, metallurgy indicated that failure had proceeded from localized areas of dendritic porosity. General Electric had thrown the porosity problems into their NDI department to develop processes and techniques for detecting amd measuring porosity.

One blade in particular had been used as a "guinea pig" in this testing and had been x-rayed over 75 times, in addition to being run many times through eddy current and ultrasonics by the best technicians available to General Electric with no defects detected. The KET process detected two major areas of porosity and a host of other small indications which, at that time, were not defined by Industrial Nucleonics as porosity. Figure 15 is one of the first autoradiographs made of this GE4 blade and is somewhat unusual; rather than immerse the blade in krypton, the blade was filled with krypton. For this reason, we are getting a composite autoradiograph showing the inside-out X-ray. The two areas of concern are shown, located as they should be, in the thicker metal sections at the confluence of the thin metal skin and the thicker metal structure of the spar.

A second autoradiograph shown in Fig. 16 is a KET process autoradiograph which was furnished to General Electric to orient metallurgy. Figure 16 is self-explanatory.

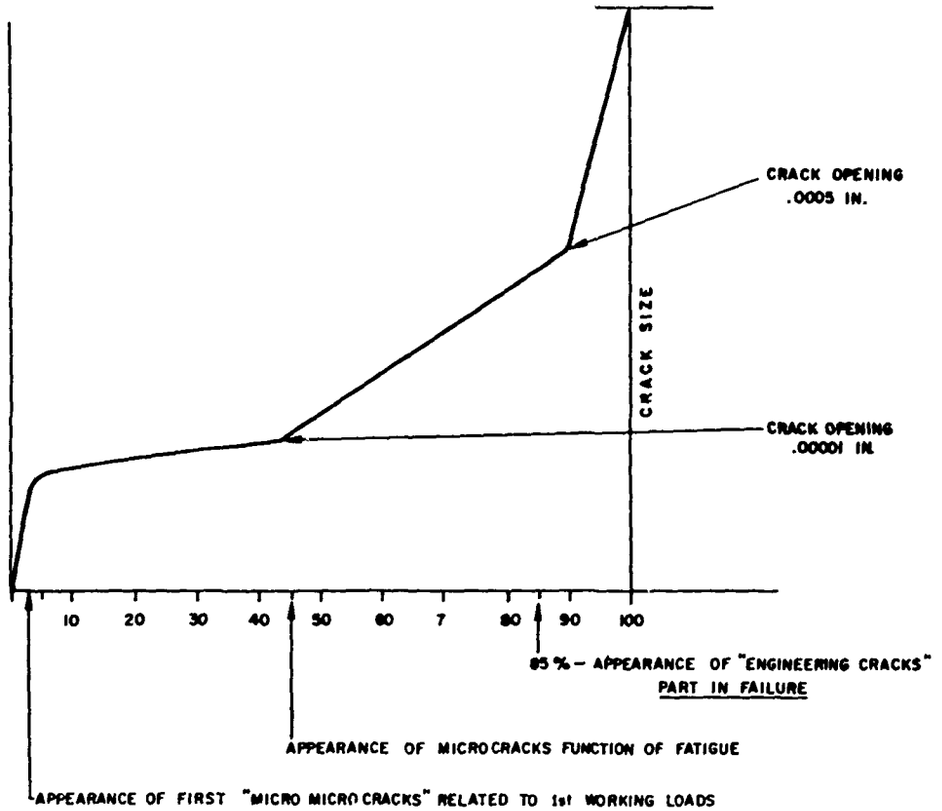

Figure 12.

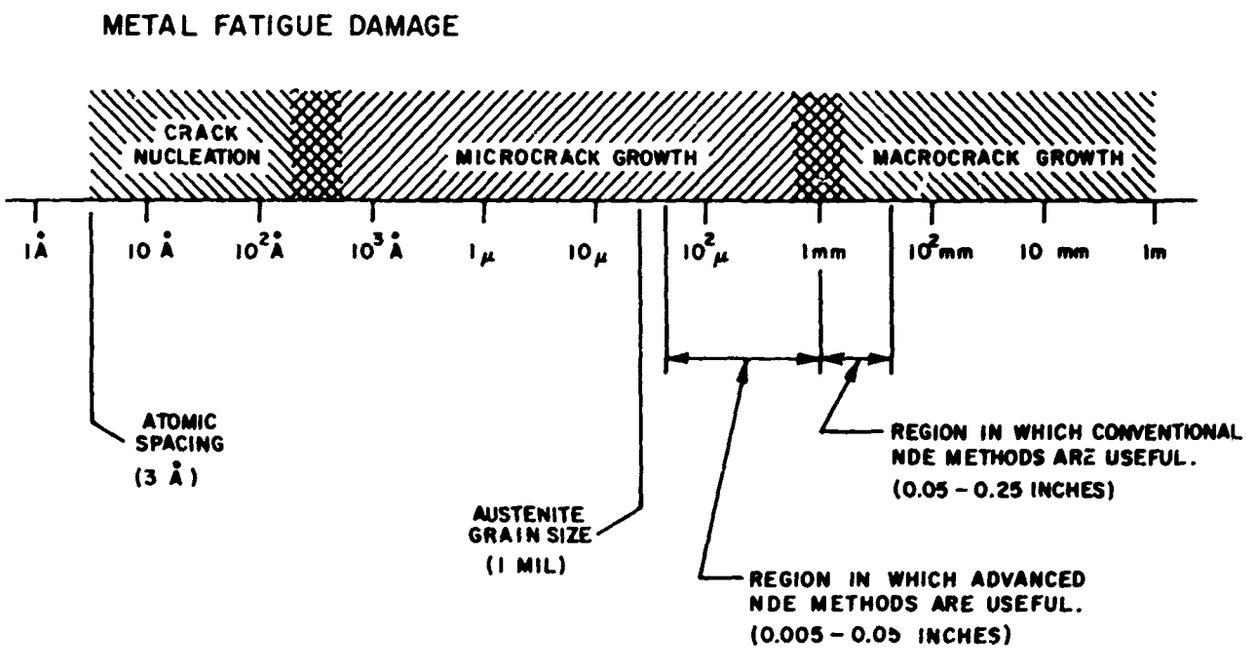

Figure 13. Schijve's scale of crack dimension.

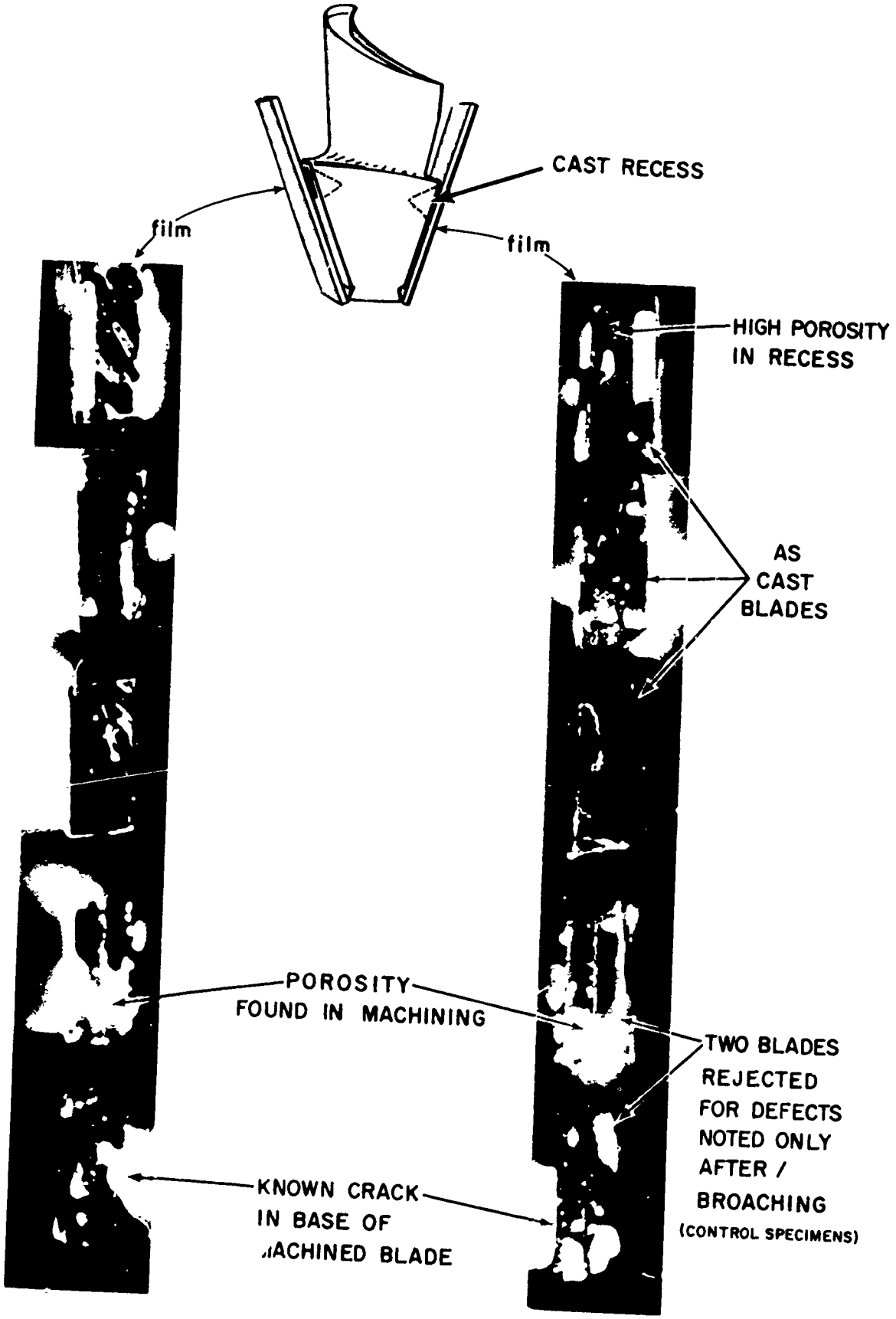
CAST RECESS
film
film
HIGH POROSITY
IN RECESS
AS
CAST
BLADES
POROSITY
FOUND IN MACHINING
TWO BLADES
REJECTED
FOR DEFECTS
NOTED ONLY
AFTER /
BROACHING
(CONTROL SPECIMENS)
KNOWN CRACK
IN BASE OF
MACHINED BLADE

Figure 14.

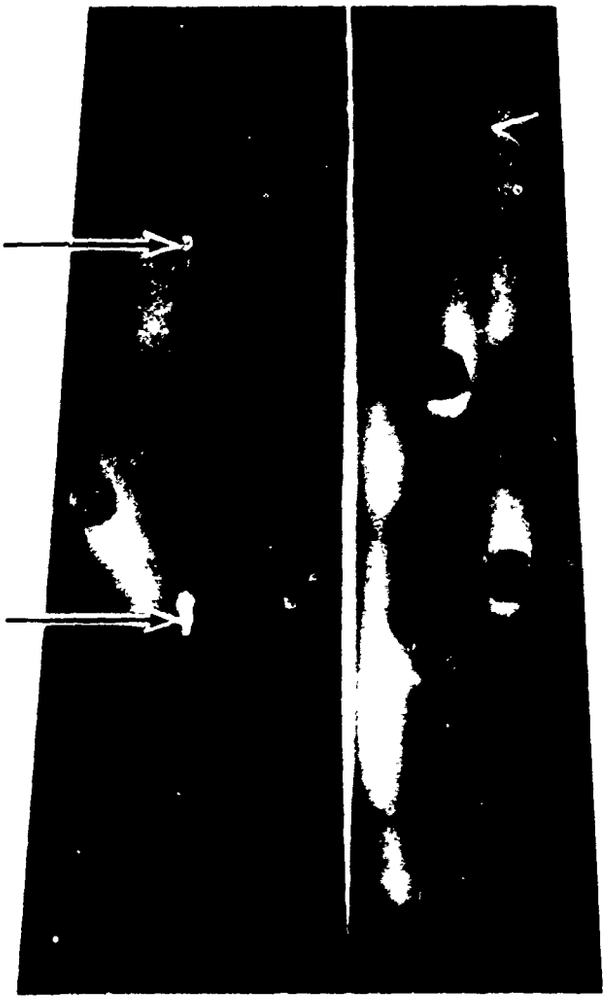

Figure 15. Autoradiograph of hollow turbine blade filled with KR85 showing 2 large dendritic defects.

General Electric moved quickly to have us inspect a whole series of GE4 blades. Figure 17 is a good example of the process refined for GE4 blades to show basically subsurface porosity. In the blade shown, there are seven areas of porosity sufficiently large to cause rejection of the blade.

The majority of engine manufacturers are now coming to treat dendritic porosity as a structural strength problem in that it is felt the porosity provides the nucleus for low cycle fatigue failure in turbine blades. In essence, the sharp edges of the porosity acts as stress risers or crack nucleation sites with failure occurring over some extended period of life. More succinctly stated, a turbine blade may be extremely safe for 500 to 600 hours but may be destined to fail at higher operating lifetimes.

We are at a point now where the engine manufacturers agree that the KET process can give near unity confidence for the detection of casting anomalies (hot tears included). We are also confronted with an industry that has not quite determined what to do with the data even though the new technology engine blade problems indicate it is now of significance.

CONCLUSION

Although a relatively recent development in the field of NDI, the AccuRay KET process has already demonstrated a significant improvement over conventional NDI techniques in a number of applications. Specifically, the process has demonstrated capabilities in the following areas:

1. The detection of low cycle fatigue will permit the replacement of time/cycle removal of components with condition removal of components which will result in significant economic savings for both military and commercial engine users.

2. The reliable detection of microporosity in castings will make possible the manufacturing of difficult to cast superalloys in a technically desirable complex configuration.

3. The reliable detection of microdefects will permit advanced fabrication technology to design highly complex components with the assurance that manufacturing defects will be detected prior to the component being incorporated into an engine.

4. The detection of microdefects will also permit designers to reliably reduce their overdesign which is now required to compensate for defects; this will result in significant material and weight savings in addition to increased performance.

5. Significant improvement appears to exist in proving the reliability of advanced bonding techniques in diffusion bonding, inertia welding, electron beam welding, etc. It would appear that the KET process will also be able to detect defects in advanced components such as composite materials, powder metallurgy materials, and ceramic materials.

The feasibility of the KET radioactive gas penetrant inspection process to effectively and efficiently work in these areas has generally been demonstrated; however, much work remains to be accomplished. Programs to complete this work are presently being rapidly established with interested parties who have the application and need for this advanced NDI technology.

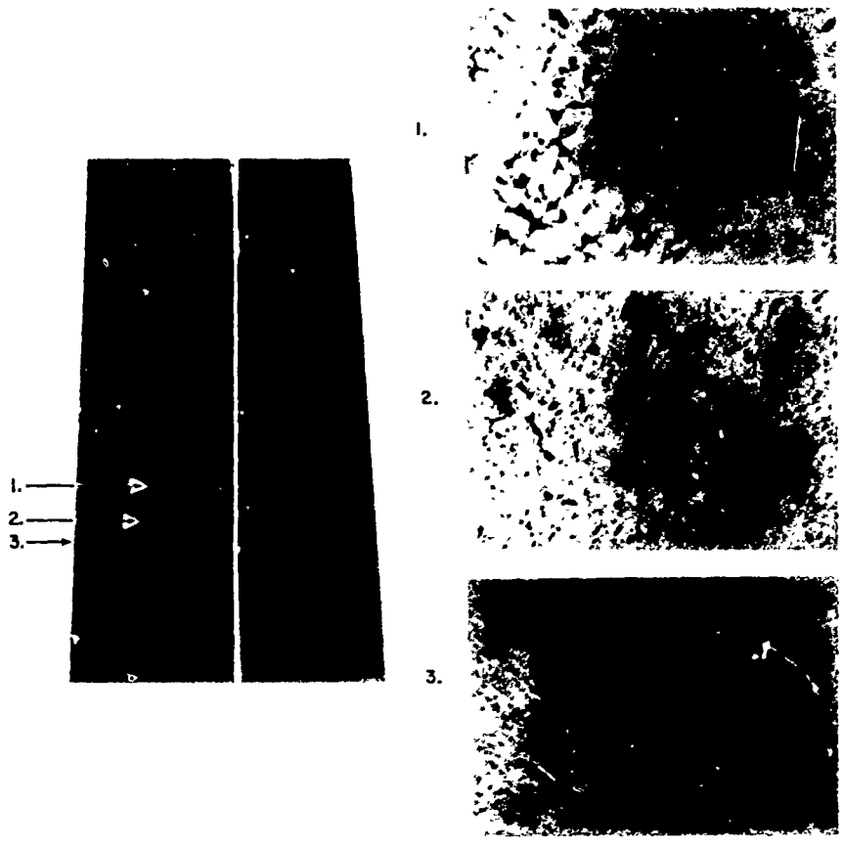

Figure 16. AccuRay KET autoradiograph of large hollow turbine blade showing metallurgy of indicated sections. In this, and 31 other sections no defect was found which was not shown by the KET process and all KET indications were verified.

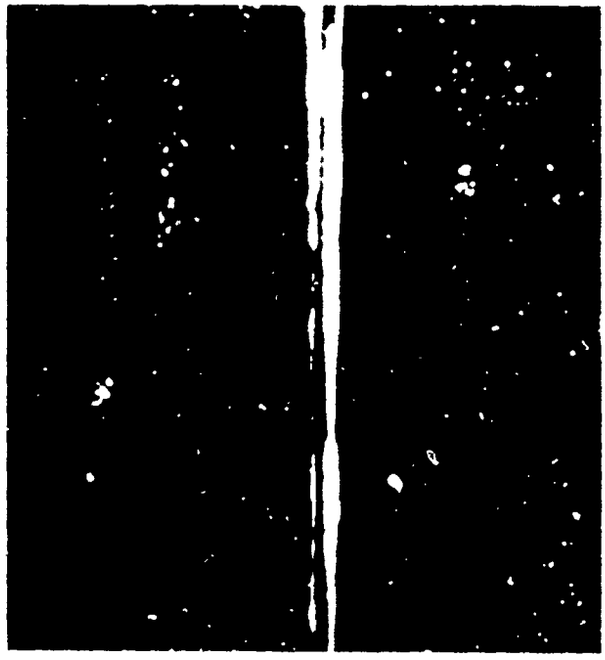

Figure 17. Shrink defects located up to 30 mils below the surface in a hollow investment casting. Vertical line caused by wrapping film around the component.

Discussion:

THE ACCURAY KET PROCESS FOR THE DETECTION OF MICRODEFECTS

Anthony P. Pontello

The excellent paper presented by Mr. Eddy on the "AccuRay KET process for the Detection of Microdefects" gives light to a new area in nondestructive testing. The use of a radioactive gas penetrant offers a means of capturing microdefects in metals previously difficult to detect using normal NDT equipment. However, in nondestructive testing, manufacturers and the like, think of quality and economy as being synonymous. Most principles of nondestructive testing strive for the shortest time possible in detecting flaws. Extension of test times means added dollars in cost. The KET process needs approximately 30 to 60 minutes of preparation time to outgas the subject items. What is the total time to conduct an average test on a turbine disc, for example? It appears that the longer the subject item the longer is the preparation time for outgassing the object. This could possibly hold true even in cases where small porosity flaws (caused by entrapped gases in manufacturing) require extensive time to be outgassed. What effect, if any, would the KET process have on those discontinuities which have not been completely outgassed?

The sensitivity of the AccuRay KET process seems to be significantly greater than that of the liquid penetrant dye test technique. It is possible that the sensitivity of the gases is so great that detection of a seam or forging lap, considered not detrimental to a turbine blade or disc, be interpreted as a flaw and the item be discarded prematurely? A distinction should possibly be made to differentiate between those metal castings that are acceptable or non-acceptable when using the KET process. Possibly a table with accompanying photographs giving statistical results of previous tests conducted on the component sections of jet engines could serve as a guide in defining microdefects inherent in metals.

The KET process seems to have wide applications in the Aerospace industry. It is generally acknowledged that means are available today which will indicate cracks, holes and other types of casting or molding flaws in turbine blades. However, few, if any, test methods are available to detect the degree of sulfidation that takes place under the spalling of vapor blasted turbine blades. The KET process, having the potential to penetrate crack contaminants could possibly be applicable in detecting whether sulfidation has occurred under the spalling of the blade and the degree of sulfidation which has taken place. The spalling, which in essence acts a surface contaminant, should provide more adsorption sites for the gases over the sulfidated area. The sensitivity of the KET process seems to have the capability of revealing any changes in alloy composition due to chemical attack or depletion of any constituents in the alloy.

Mr. Eddy's paper has clearly demonstrated the capability of the KET process. Further studies should reveal numerous applications in the area of nondestructive testing centered on jet engines and their component parts.

Service Corrosion Problems Produced in the Test Cell

W. W. Wagner
Naval Air Propulsion Test Center
Trenton, New Jersey

INTRODUCTION

After many years of upgrading materials and coatings and after time consuming and extensive retrofits to engine configurations, the Naval Air Systems Command (NAVAIR) decided that the best approach to corrosion control of gas turbine engines was not in the expensive after-the-fact retrofits but in appropriate preventive initial design followed by testing. It was established that in environments representative of service conditions the engine manufacturer (supplier) must give greater consideration during the design phase to materials degradation. In addition, it also was believed that the Navy also should have a check on the end product. In this respect, NAVAIR authorized the Naval Air Propulsion Test Center (NAPTC) to prepare and evaluate new requirements for the gas turbine engine salt corrosion testing specification.

RECENT SERVICE PROBLEMS

The myriad of materials problems identified with the gas turbine engine are almost always found after the engine has been subjected to service conditions. Concerning ourselves with only the corrosive effects, the results are startling. The scope ranges from corrosion of exterior housings, functional accessories, accessory hardware, moving parts such as variable geometry, airfoil pitting in the compressor, to the catastrophic hot corrosion of turbine vanes and blades. The following are examples of typical corrosion problems the Navy is experiencing with service engines as established by inspection of engines returned for overhaul. These examples will serve to illustrate the variety of materials problems connected with the gas turbine engine.

A. Fuel Controls–Fuel controls have exhibited heavy internal corrosion. Rusting can be found internally on gears, cams, springs, pistons, piston sleeves, and other functional parts. Such corrosion can be caused by an inadequate preformed packing seal which allows moisture into the control or from the aspirator and inlet air temperature sensing tubes. In the latter case, humid, saline air is free to enter the control during normal engine operation. Obviously, more corrosion resistant materials should be employed in the affected areas of the fuel control.

B. Turboprop Engine Gear Box–Original material selected was magnesium since Navy aircraft use was not anticipated. The gear box and accessory drive housings have exhibited destructive corrosion in Navy service use to the extent that the engines were returned to overhaul with gaping holes in the housings. An organic-type coating designed to protect the magnesium was inadequate in a salt-air environment.

C. Turbojet Engine Compressor Variable Geometry–The linkages which control engine airflow function by means of a series of stainless steel bushings, sleeves, and levers. Pitting and crevice corrosion have caused these parts to seize particularly after even short periods of nonuse. Both the type of lubricant and frequency of lubrication are critical for maintaining free movement of the variable geometry.

D. Turbine Nozzles–Air-cooled turbine nozzle assemblies, fabricated of INC 713C, have experienced severe hot corrosion even on low time engines. Sulfidation of the substrate occurs wherever a premature oxidation or spalling of the typical aluminide pack-type coating has taken place. In the case of one engine, the premature coating breakdown has been attributed to a substrate overtemperature due to cooling hole blockage. The vane temperature profile resulted in internal corrosion of the cooling holes and extensive diffusion of the coating into the substrate.

E. Hot Corrosion of Turbine Hardware–Generally, the most difficult materials problem to understand and certainly the most catastrophic in scope is the hot corrosion, specifically sulfidation, found to some degree in all turbine engines. Hot corrosion in Navy engines is compounded by the wide variety of materials and coatings used and by insufficient evaluations of these materials through bench tests. More than any other component design or material selection, hot section gas path hardware requires full-scale engine testing in a realistic service environment prior to service introduction.

INADEQUATE MATERIALS QUALIFICATION PRIOR TO SERVICE INTRODUCTION

The current military specification for aircraft gas turbine engines includes a Corrosion Susceptibility Test which consists of the following:

A. The engine and all components shall have operated for at least 150 hours of endurance equivalent to a Military Qualification Test (MQT).

B. A synthetic sea salt solution is sprayed into the engine while motoring at a rotor speed of 300-500 RPM, until a mist of the spray exists from the exhaust nozzle. The engine exterior also is thoroughly wetted with salt spray.

C. The engine is allowed to stand idle for one week, then the procedure (item B above) is repeated following which the engine is again allowed to remain inoperative a second week.

D. The engine is disassembled sufficiently to determine the extent and degree of corrosion.

At best, this entire technique is superficial when compared to the more exacting demands of engine operation in the fleet. The resultant corrosion produced by this test consists mainly of low temperature oxidation. The significant parameters of high temperature, high pressure, high gas velocities, and the products of combustion associated with real-situation engine operation are not accounted for. However, it is these parameters which produce the most destructive forms of corrosion. A new engine or model configuration subjected to the previously described test will usually satisfactorily qualify as being corrosion resistant, yet the same engine may be plagued by materials problems after Naval aircraft service operation.

SIMULATING SERVICE-TYPE CORROSION

The NAPTC, in proposing the new corrosion susceptibility test for gas turbine engines, has attempted to define a more meaningful and comprehensive materials evaluation based on engine operation at atmospheric environments in realistic conditions. The proposed full-scale engine test is an accelerated test from the standpoint of high temperature engine operation because of the similarity to an MQT cycle and also with respect to the salt-air concentration. During this test, the engine is exposed to a 200 PPB SS/AIR concentration for a total of 150 hours of engine operation and also for 350 hours of dynamic soaking. During dynamic soaking, the engine is inoperative but is exposed to a 200 PPB salt-air concentration. Corrosive effects representative of service engines are produced through this testing procedure because both the operational environment and the modes of fleet operation are simulated. In designing the test cell, it was imperative that close control of temperature, humidity, and salt-air concentration of the engine ingested air was maintained throughout the test cycle to insure a realistic simulation of the actual operational environment. Incorporating the ability to soak an engine both dynamically and statically enabled realistic simulation of the various modes of operation during fleet operations. Inoperative aircraft parked on an aircraft carrier flight or hangar decks are constantly exposed to high salt-air concentrations. The proposed dynamic soak exposes the gas turbine engine to this environment. Also significant to engine external corrosion is the hot, humid bath the engine receives just sitting in the aircraft nacelle after completion of a mission. The static soak incorporated in the proposed test procedure is intended to simulate this conditon.

PROPOSED SALT CORROSION SPECIFICATION TEST

Specification AS-2864 requires that a full-scale engine 150-hour endurance test be conducted in a controlled salt-air environment. The test is based on a 48-hour corrosion test cycle, and it is comprised of 25 such cycles. Each cycle consists of six hours of engine operation, 14 hours of dynamic soak, and 24 hours of static soak. Within the 48-hour test schedule, the engine is operated for three hours followed by a 2-hour shutdown period, seven hours of dynamic soaking, and 12 hours of static soaking. The 48-hour corrosion test cycle is outlined in Fig. 1. Figure 1 shows the relationship of salt solution, temperature, and relative humidity to the test operating conditions. During both engine operation and dynamic soak phases the engine is exposed to a 200 PPB salt-air concentration and a minimum ambient air temperature and relative humidity of 50°F and 73%, respectively. The static soak consists of maintaining the engine ambient air temperature at 110 ± 10°F and the relative humidity in excess of 90%. Figure 2 shows a typical shaftpower engine operating cycle. During this cycle the engine is operated at maximum power (highest TIT) for 16% of the time. The development of this proposed specification test is traced in an earlier NAPTC paper[1]. This paper described the initial NAPTC attempts to evaluate gas turbine engine corrosion susceptibility from testing in a natural environment to the final test cell controlled environment.

BENCH TESTING

Although existing literature lists many innovative and seemingly thorough material and design configuration test methods, it must be understood (and is verified by our full-scale engine testing) that the results are mostly analytical and wholly comparative in nature. At NAPTC various forms of bench testing are employed as a screening device, a preview of materials performance, or an added look-see at the behavior of one material or coating versus another. The burner rig has been a useful testing device for comparing

Phase No.	Duration of Phase Hours	Test Engine Condition	Salt Solution Injected (ppb)	Engine Ambient Air	
				Temperature °F (min)	R.H. % (min)
1	3[1]	Operating	200[2]	50	75
2	2	Not Operating	0	Atmospheric	Atmospheric
3	7	Dynamic Soak Not Operating	200[2]	50	73
4	12	Static Soak Not Operating	0	110 ± 10°F	>90
5	3[1]	Operating	200[2]	50	73
6	2	Not Operating	0	Atmospheric	Atmospheric
7	7	Dynamic Soak Not Operating	200[2]	50	73
8	12	Static Soak Not Operating	0	110 ± 10°F	>90

[1]During shutdown, while the engine is decelerating from idle, the salt solution shall continue to be sprayed into the engine until the rotor has come to rest.
[2]The test facility blower system will provide the flow of salt-laden air over and through the engine.
[3]Engine inlet and exhaust openings shall remain open for all phases of the test cycle.

Figure 1. 48-hour corrosion test cycle

high temperature strength and hot corrosion resistance for both current and future generation superalloys. In addition, the ability to add extraneous pollutants to the products of combustion makes the burner rig an ideal bench test in the study of corrosion mechanisms. The salt bath cabinet is useful as a materials screening device because it yields results quickly and inexpensively. There are numerous advantages to bench-type testing and above all they are necessary to the normal development of materials improvement. However, even though test methods and equipment can be standardized, results are often open to interpretation. Rig test results can be disguised by so many test variables that interpretation or stacking of results is often misleading through a maze of statistical analyses Proof of the fallacies resulting from bench-type testing or even inadequate full-scale engine qualification is the materials degradation once the engine is introduced to service conditions. The NAPTC feels that the proposed full-scale test in a controlled environment is the ultimate test for gas turbine engine materials performance.

RECENT TEST RESULTS

Recently the specification test was conducted on a model T58-GE-10 turboshaft engine in the NAPTC salt corrosion facility. A final report (2) describes the test methods and results. A summary of the materials problems associated with this engine and an analysis of corrosive effects produced by the test can best be described by reviewing post-test conditions of the major engine sections.

A. Engine Exterior–Figure 3 shows that the uncoated AM-355 compressor casing exhibited heavy oxidation as did the four variable geometry rings. Test results indicated a need for coating the compressor casings. Other external corrosion problem areas identified by the test were the second stage turbine casing and T_5 thermocouple harness, pressure and dump valve, starter bleed valve, and A/I valve. After eight test cycles, the A/I valve froze in the closed position due to internal corrosion. The failure of the valve was identical to that reported on service engine valves. As a result more corrosion resistant materials were incorporated

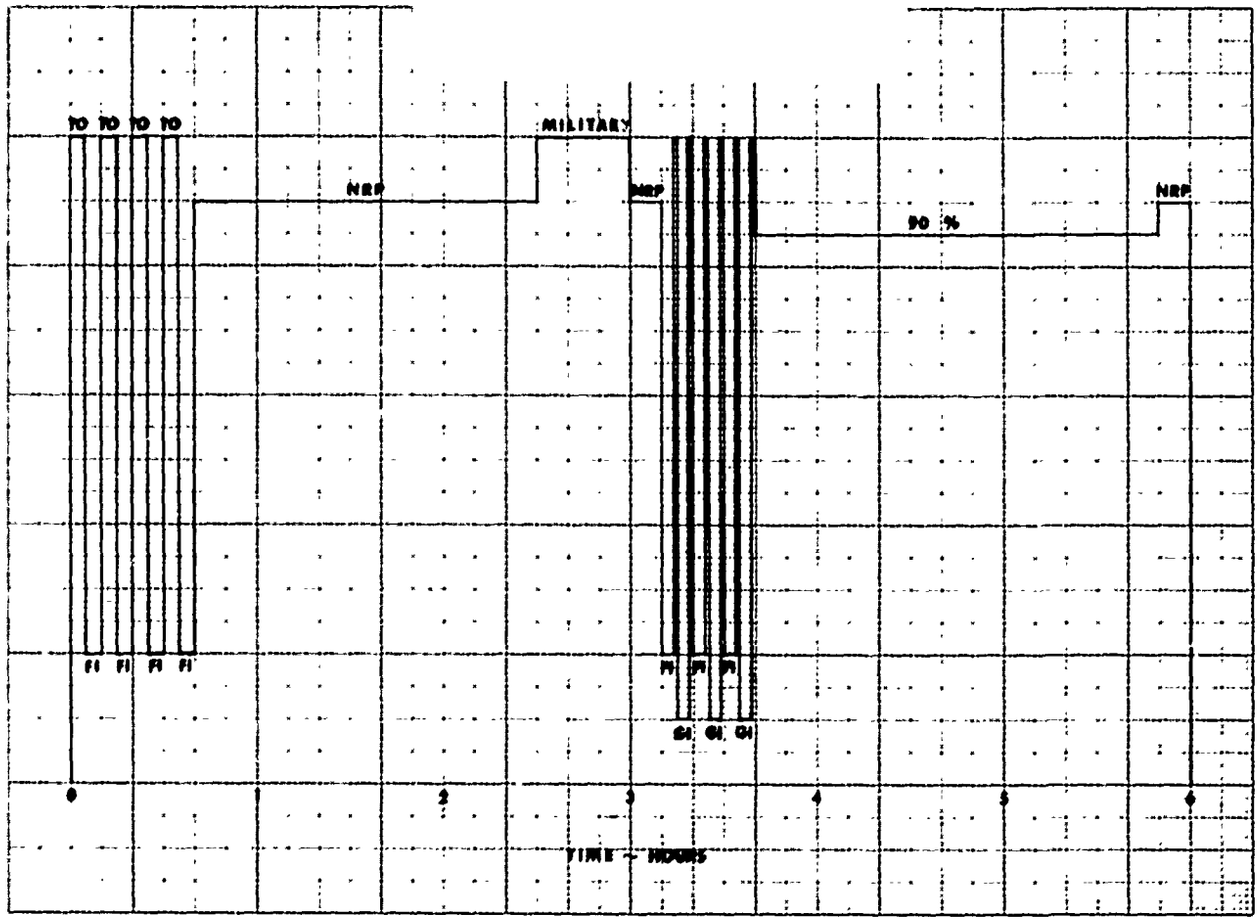

Figure 2. Salt corrosion test engine operating cycle T58-GE-10 S/N200045.

in the valve. This further verifies that the test procedure does indeed simulate an operational environment. In a subsequent report (3), the NAPTC evaluated the redesigned valve and offered recommendations for further improvements.

B. Compressor Stators–AM-355, the standard material for T58 compressor stators, was evaluated using both coated and uncoated airfoils. The uncoated AM-355 vanes exhibited considerable pitting of the airfoils, in the root area, and at the tips. Again, this same degree of pitting was revealed on high time service engines. Of the coated airfoils, a Sermetel W coating offered adequate protection against the substrate pitting, but Aluminized Nubelon & Solaramic coatings were unsatisfactory. A segment of 403 SS vanes proved to be inferior to the AM-355 material; however, a segment of uncoated INCO 718 vanes was unaffected by the test. Figures 4 and 5 show the contrasting post-test conditions of the leading edge of an Aluminized Nubelon coated AM-355 vane and an uncoated INCO 718 vane, respectively.

C. Compressor Blades–Uncoated AM-355 blades exhibited pitting in excess of serviceable limits. This same condition in service engines resulted in a change to coated blades. INCO 718 compressor blades, as well as stators were evaluated for future use and showed no evidence of corrosive attack. Based on corrosive resistance, INCO 718, which does not require a protective coating, is now an excellent candidate for a compressor airfoil material. The test also verified the improved performance of A-286 as a locking screw material. The original SAE 420 screw was inadequate in both corrosion and wear resistance.

D. Turbine Nozzles–INCO 713C coated with the MDC-1 coating has been the standard configuration for the first stage turbine nozzles in T58 engines. Test results, Fig. 6, showed the MDC-1 coating to be inadequate for protection of the INCO 713C substrate. The coating was removed on areas of the leading edge and concave surface. Localized eruptions along the leading edges and massive sulfide scales along the concave surfaces of the vanes showed this material/coating system to be inadequate in the real operational environment. Figure 7 is a microphotograph of the typical cracking found on the leading edges in the first stage nozzle. A gas temperature of 1750°F was sufficient to cause coating spalling since a metallurgical analysis revealed no change in

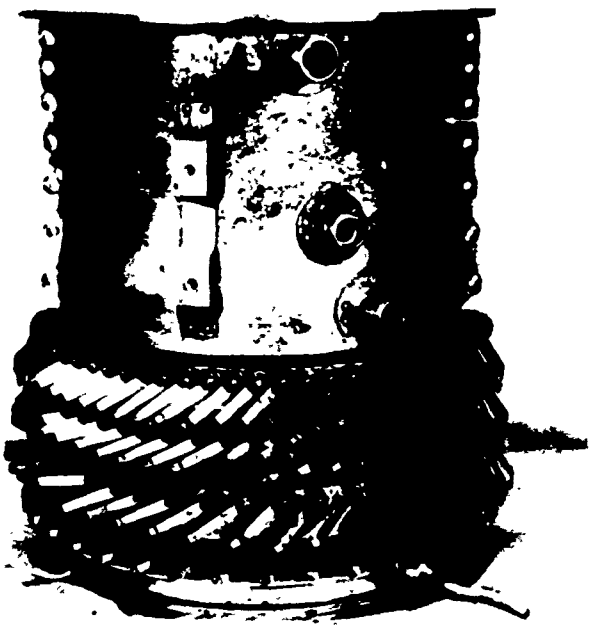

Figure 3. Post-test condition of T58-GE-10 engine upper compressor casing.

the as-cast structure of the substrate due to overtemperature operation.

One segment of uncoated X-40 vanes, also shown in Fig. 6, proved satisfactory in resisting the corrosive environment. The cobalt-base oxide which formed over the substrate was a hard, rough layer exhibiting good adherence qualities. No sulfidation was evident with the X-40 material; however, a minor grain boundary attack was observed metallurgically. The second stage nozzle, shown in Fig. 8, is uncoated INCO 713C and is exposed to a gas temperature 1550°F. As is evident in Fig. 8, the corrosive attack varied greatly around the nozzle with some partitions more severly sulfidated than in the first stage. Figure 9 shows leading edge delamination on one of the more severely attacked partitions. The obvious conclusion was that a protective coating was necessary in the second stage. Prior to the test, the existence of the same condition in service engines resulted in the use of an MDC-1 coating on the INCO 713C substrate for the second stage nozzle.

E. *Turbine Buckets*–The first stage buckets of SEL material coated with MDC-1 were in satisfactory condition. The coating remained intact with very little evidence of corrosive attack. First stage buckets of Rene 80 coated with Codep C-2 proved to be inadequate due to coating spalling.

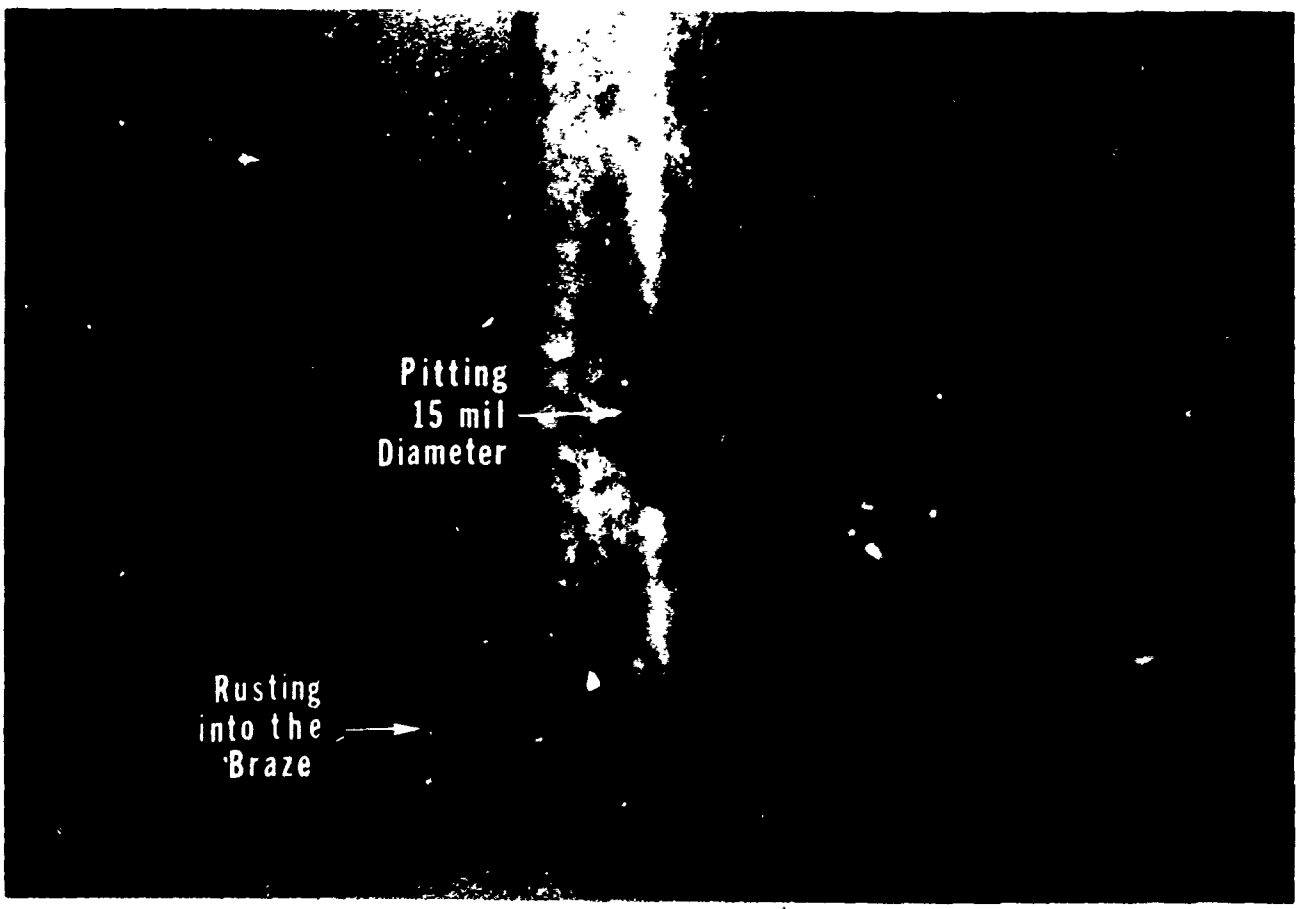

Figure 4. Post-test condition of T58-GE-10 engine. An EGV at the leading edge–Aluminized Nubelon coated AM-355 (30X).

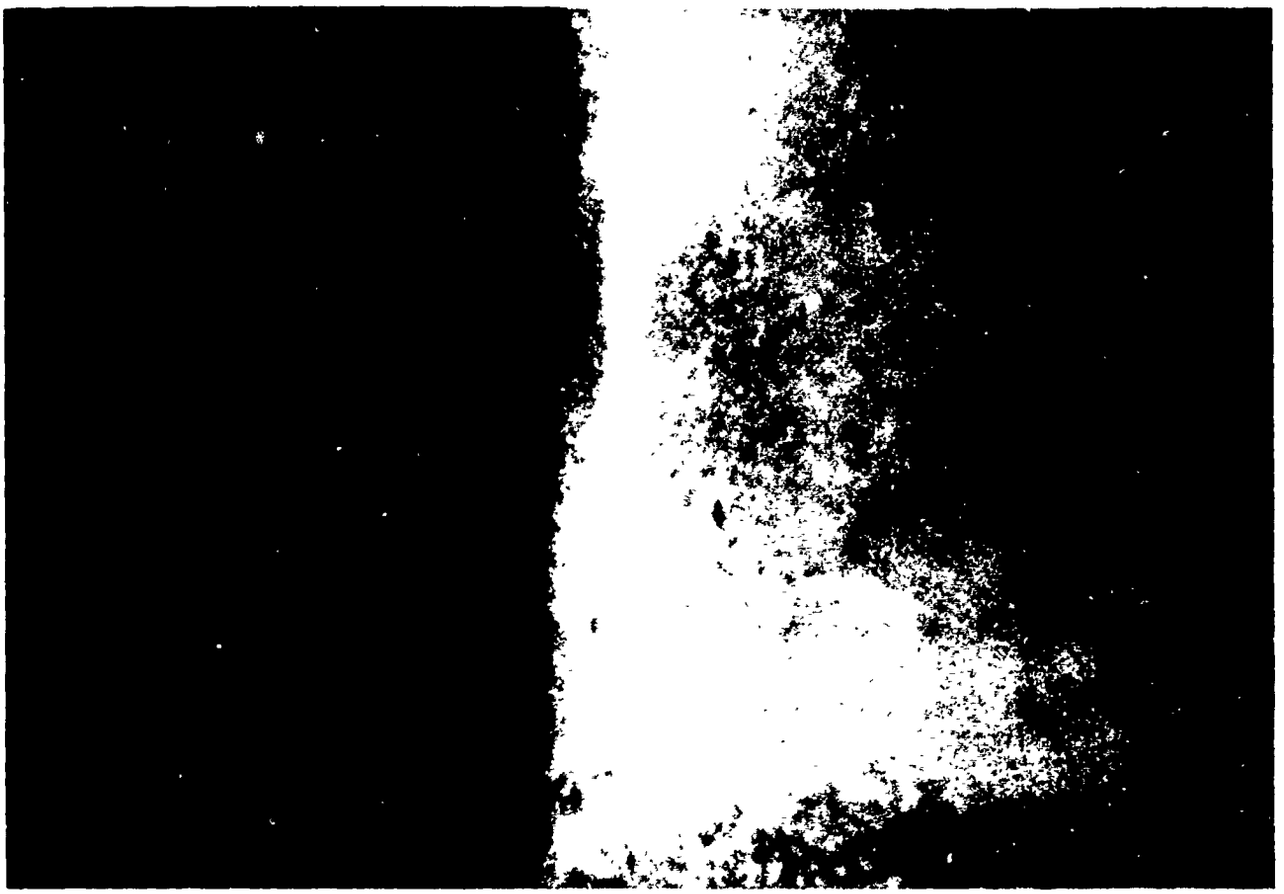

Figure 5. Post-test condition of T58-GE-10 engine. Eighth stage compressor vane leading edge—uncoated INCO 718 (30X).

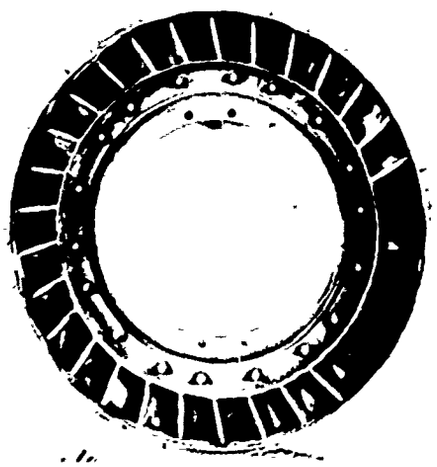

Figure 6. Post-test condition of T58-GE-10 engine. First stage turbine nozzle assembly (leading edge).

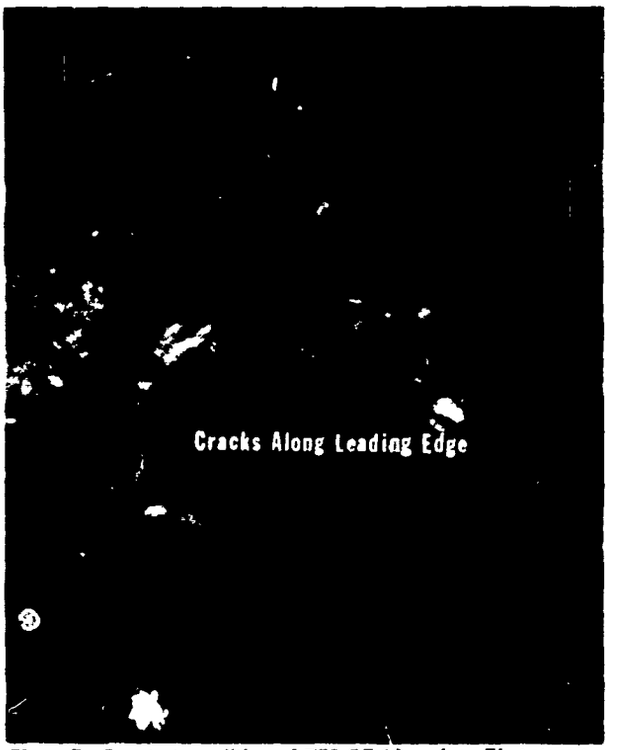

Figure 7. Post-test condition of T58-GE-10 engine. First stage turbine partition—leading edge cracking—MDC-1 coated INCO 713C (30X).

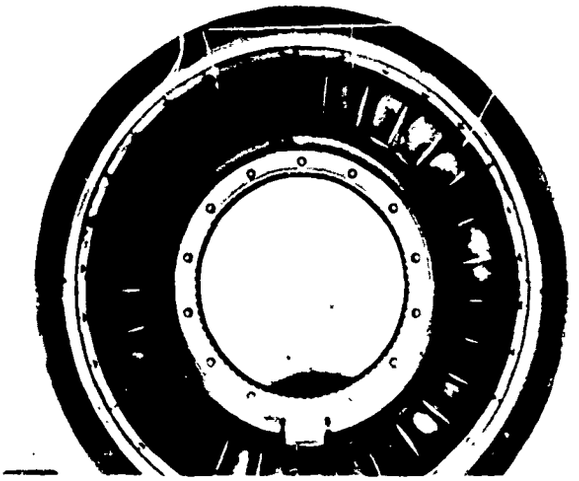

Figure 8. Post-test condition of T58-GE-10 engine. Second stage turbine nozzle assembly (leading edge)—uncoated INCO 713C.

The coating was completely removed on both the leading and trailing edges as well as the entire concave surfaces. Attack in the form of classical sulfidation was present in the substrate in the areas where the coating had been removed. The second stage buckets were uncoated SEL material and exhibited traces of sulfidation along the leading edges and over the concave surfaces. This condition emphasized the need for a protective coating on the second stage buckets.

The primary objective of the test program was achieved by identifying corrosion problem areas on the T58 engine similar in type and degree to those presently found in service engines. As substantiated by the test results, the proposed specification test does identify components which are susceptible to corrosion in service.

OTHER TEST ADVANTAGES

In addition to engine qualification testing, this test procedure is an ideal device for advancing the state-of-the-art in gas turbine materials. The test, by the stringent environmental conditions it imposes upon the engine, even more than flight testing, represents the ultimate criteria for materials and design configuration evaluation prior to service introduction. Accordingly, newer generation superalloys and new coating processes can be investigated with good assurance of future success or failure in service. Once the physical properties and basic engineering data have been established on a new material through the standard bench tests, the material can be evaluated for its operational performance. This would lead to a much needed quicker acceptance of new materials. As the T58 engine test reveals, from corrosion consideration alone, INCO 718 should be the compressor airfoil material in current model engines and INCO 713C is really inadequate for the higher temperature turbine components. In another recent NAPTC test (4),

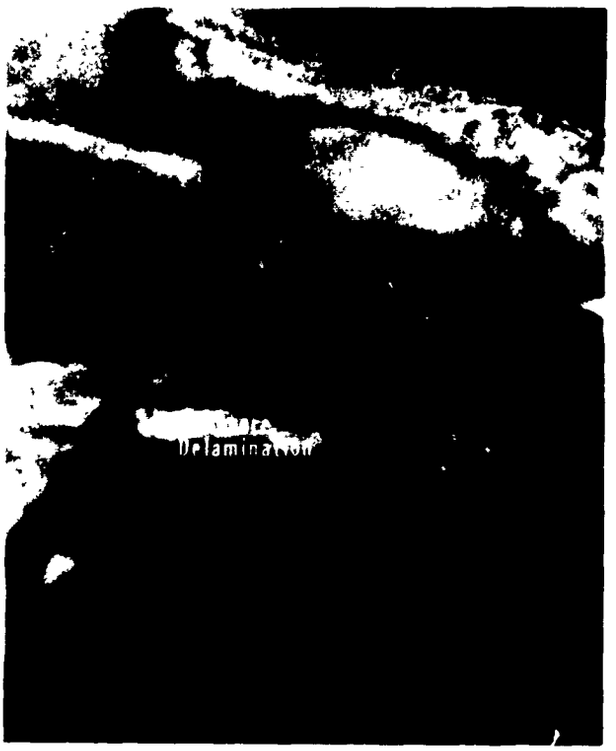

Figure 9. Post-test condition of T58-GE-10 engine. Second stage turbine partition—leading edge delamination—uncoated INCO 713C (15X).

the relative performance of several material/coating systems for the T58 first stage nozzle was investigated. The results showed a new proposed coating inferior to the present coating on the INCO 713C substrate; the cobalt X-40 material again was considered superior to the nickel-base INCO 713C and the potential of a viable coating strip and recoat process was established for NARF applicability. Such comparative analysis is further justification for this type test.

HOT CORROSION

Latest generation superalloys have kept abreast with today's demands on higher gas turbine engine operating temperatures with the necessary increase in high temperature strength. However, the higher turbine inlet temperatures and the tendency to a reduced chromium content in newer alloys have made the corrosion resistance of these alloys inadequate. Growing concern for the hot corrosion susceptibility of superalloys has moved the technology priority back into the areas of coating composition and processes. Compounding the problem of hot corrosion in Navy gas turbine engines is the large number of different materials and coatings utilized in turbine applications. If it was possible to standardize on a limited number of alloys, maintenance and overhaul procedures could be greatly simplified. For example, relative few materials could be

scaled for particular temperature range applications; consequently, all engines would use a universal material for similar applications. Concerning hot section coatings, it appears even more practical to develop a coating offering the required protection for a select number of alloys. Ideally it could be reduced to two coatings, one suitable for nickel-base alloys and one for cobalt alloys. The fact that each engine manufacturer requires his own proprietary coating adds to the complexities and reduces the opportunity for immediate state-of-the-art improvements.

SUMMARY

The corrosion resistance performance of gas turbine engine materials has in the past only been revealed through service operation. Although bench-type testing of materials and design configurations is a necessity for the development of both materials and coatings designed for gas turbine application, bench testing is considered primarily an initial screening device. Analytical studies of hot corrosion mechanisms and comparative analysis of candidate materials is the forte of the burner rig. Unfortunately, analytical investigations, often misinterpreted in statistical analyses, have not always correctly determined the strength or weaknesses of candidate materials in gas turbine engine applications. An actual service operation environment coupled with component interrelationship only achieved in full-scale engine testing is considered to be the only proven method of predicting materials performance. Since the test results obtained were representative of service engines, the proposed specification test reviewed in this paper is considered a comprehensive and necessary evaluation of gas turbine engine materials.

REFERENCES

1. J. E. Newhart and W. W. Wagner, "The Development of a Full-Scale Aircraft Turbine Engine Controlled Environment Corrosion Test," NACE, 1972.
2. W. W. Wagner and J. E. Newhart, "Evaluation of Corrosive Effects on a T58-GE-10 Engine in a Controlled Salt Air Environment," NAPTC-AED-1961, 1972.
3. W. W. Wagner, "Corrosion Resistance of Model T58 Engine Anti-Icing Valve ECP A10 Configuration," NAPTC AEP 22:WWW 13700 Ser 556, 1972.
4. J. E. Newhart and W. W. Wagner, "Material/Coating Systems Performance of T58-GE-10 Engine First Stage Turbine Nozzle," NAPTC AEP 22:JEN/WWW 13700 Ser 557, 1972.

Discussion:

SERVICE CORROSION PROBLEMS PRODUCED IN THE TEST CELL

C. J. Spengler
Westinghouse Research Laboratories

Mr. Wagner points out that the principal shortcoming of testing in the laboratory is the failure to predict reliably actual service performance hence the cost of engine testing is certainly justified for coatings and alloys intended for application in aircraft turbines. Reliable predictions are especially important because the safety of humans is a concern.

Engine testing, however, for marine propulsion or stationary land-based application may not be economically feasible. Certainly, in the area of electrical power generation a large land based unit may require 26,500 liters of fuel oil per hour for operation. Hence, there is economic incentive to use a test facility such as the pressurized passage that can be operated on about 48 liters of fuel per hour.

Essentially, what I will comment on is applicable to larger stationary gas turbines but should be applicable also to aircraft gas turbines. Specifically, are the significant fallacies that result from laboratory-type tests that seek to predict hot corrosion performance in turbines a matter of not reproducing the corrosion mechanism, or is it failure to initiate or accelerate the attack, or, are there reversals in material behavior even with reproduction of the correct hot-corrosion mechanism?

With regard to accelerated engine testing, there is the effect of eventual coating/alloy interaction on the corrosion-attack resistance of protective coatings, not to say anything about the effects corrosion of the coating has on fatigue life, thermal or otherwise, that cannot be expected to show up in the accelerated engine test. Therefore, some reliance has to be put on a laboratory test with ultimate justification based on actual engine operation.

The question to be asked then is how can testing under simulated turbine conditions be made reliable. We at Westinghouse, a number of years ago, conducted a comparison of hot corrosion in laboratory tested and long-time service exposed nickel-, cobalt-, and iron-based alloys either as inlet guide vanes, rotating blades, or as part of corrosion monitors, to determine which features of hot corrosion attack had to be reproduced in order to extrapolate with a high degree of confidence from those observations made in short-time laboratory tests to the performance anticipated under long-time service conditions.

The study looked at a number of the features of hot corrosion attack (Fig. 1) and showed the following. For uncoated alloys on evaluation of initial and final microstructure of the unattacked portions of the various alloy

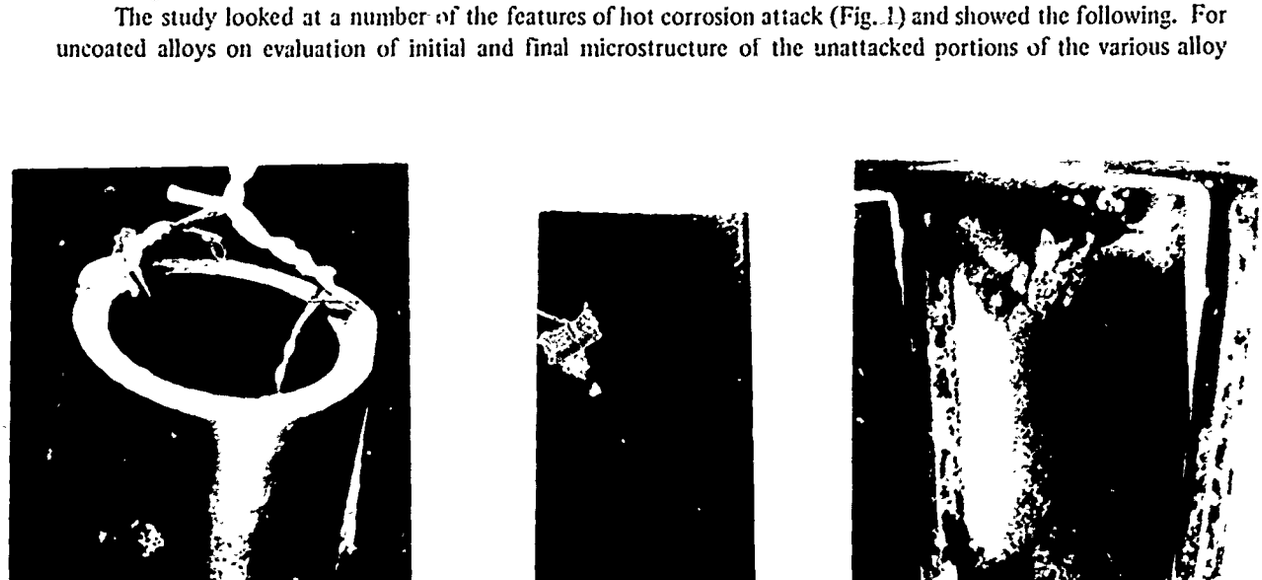

Figure 1. Photographs of corrosion tested specimens from (a) combustion furnace, (b) turbine simulator, and (c) gas turbine vane.

specimens indicate that for a particular alloy the corrosion behavior is affected only to a minor degree by variations in microstructure and the presence of sigma.

Eventual massive grain boundary carbide precipitation did lead to preferential corrosion along the boundaries but the attack rarely exceeded a few grain diameters except in certain wrought alloys.

The characterization of the corrosion attack, as shown in Fig. 2, differentiated between deposits (mainly of foreign origin), scales (predominantly non-metallic reaction products of the alloy), affected alloy region (the near-surface region of the specimen which exhibits a modified microstructure and composition as a result of the corrosion attack), and the unaffected base alloy. Special effort, as illustrated in Fig. 3, was made to determine the variations in chromium content with respect to variations in alloy composition, test condition, and location on the test specimen. The pressurized passage produced chromium-depletion profiles on the shock paddies that approximated those of the inlet guide vanes.

The composition of the outer scale, as demonstrated in Fig. 4, was found to depend on the amount of condensed salt. The amount of salt also established the nature of the subscale features. In alloys tested under static conditions with artificially applied salt deposits there was a complicated sequence to the chemistry of the various sulfides present across the affected alloy region while the same alloys tested in the turbine simulator and actual gas turbine with salts condensed from the gas stream had one or at most two types of sulfide present. The burner rig sometimes failed to initiate hot corrosion attack in some of the more corrosion resistant alloys such as X-45.

In short, the study indicated that a characterization of a particular alloy in terms of its anticipated corrosion behavior necessitated information on (1) chromium-depletion in the affected alloy region, (2) the microstructure of this region, and (3) the phases in this region and composition of the scale. These factors were met in the pressurized passage at longer test times (>150 hr) when the weight change curve showed a steady rate of weight loss. The corrosion penetration then could be taken as a guide to the anticipated susceptibility of an alloy or coating to corrosion attack.

The pressurized passage more consistently than the burner rig produced the type of hot corrosion attack and variation in attack that is similar to that in an actual gas turbine. The static test rigs with salt-dipped specimens

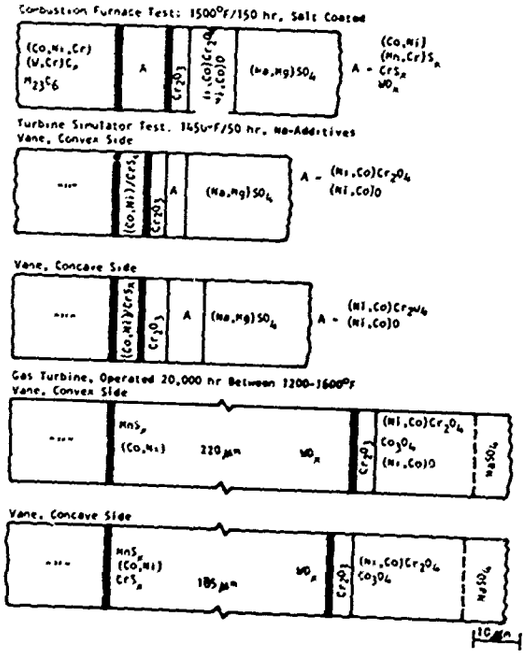

Figure 2. Schematic representation of principal phases found in Co-based alloy, X-54, exposed to laboratory tests and long-time turbine operating conditions.

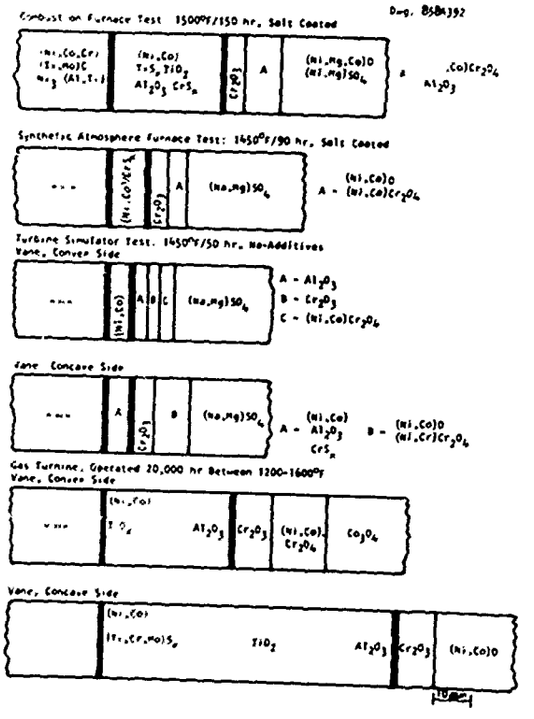

Figure 3. Schematic representation of principal phases found in Ni-based alloy (11-500), exposed to laboratory tests and long-time turbine operating conditions.

reproduced the attack only found in gas turbines subject to exceptionally heavy salt deposits. The average penetration rates from the pressurized passage for different levels and ratios of combined sodium and vanadium now being determined are considered to be a reliable indication of anticipated engine performance for both coated and uncoated superalloys.

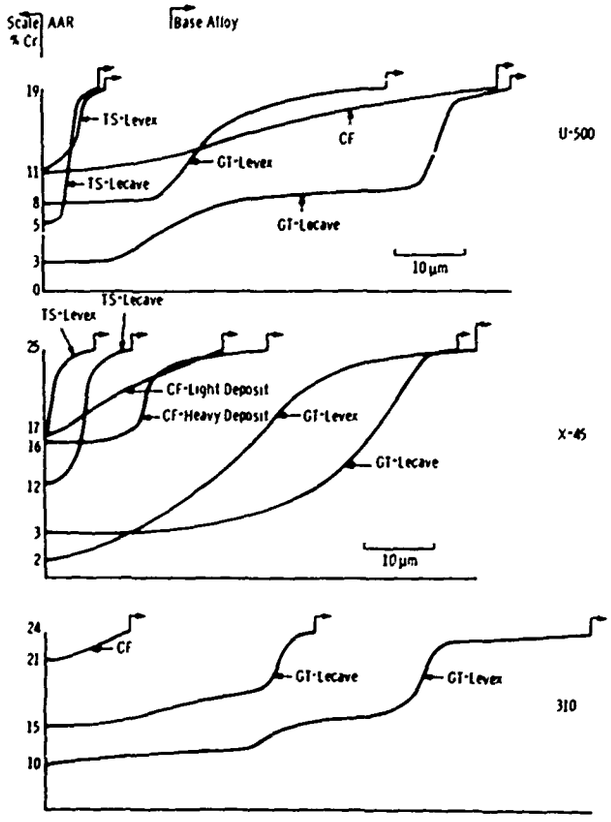

Figure 4. Chromium-concentration profiles across affected alloy region (AAR) of U-500, X-45, and 310, tested in turbine simulator (TS), combustion furnace (CF), and gas turbine (GT) corrosion tests.

Discussion:

SERVICE CORROSION PROBLEMS PRODUCED IN THE TEST CELL

Bernard J. Rogus

I have only a few brief remarks in keeping with the spirit of the hour.

I think it fitting that the conference end with the views of an engine user. It must be held constantly in mind that engine use is what our business is all about. At NAVSECPHILADIV we are concerned about engine use in Naval applications. In this light, I completely ascribe to the views from Trenton that full scale engine testing is essential to the whole picture. Possible benefits were clearly described.

However, in the paper it was implied that the proposed accelerated corrosion test cycle may well be the ultimate test and that it could be used to help establish universal materials for all engines. A few words of caution may be in order concerning absolute or ultimate value criteria.

It is true that burner rig tests are subject to different interpretations. Our recent attempt at Round Robin testing has verified this. However, I'm sure that most of us agree burner rig tests are valuable as a screening device. What is probably needed is burner rig improvement and standarization rather than rationalization of results.

An engine test is really a systems test. But an engine test may also be likened to a burner rig in which all components are being evaluated at one time. A multiple specimen burner rig if you will.

In this view, many of the shortcomings of burner rig tests could well follow through to ultimate engine tests unless we standardize test conditions so that they will be acceptable to all as being conclusive. Many questions arise which need to be answered before an ultimate test cycle can be written, especially for such short time tests. For example, some questions are:

1. What type fuel do we use in the engine test? What sulfur content should be specified? What V content?
2. Are the salt concentrations really capable of being standardized? What size aerosols are to be allowed to the engine? How is the engine to be positioned in the test chamber for static and dynamic tests?
3. What are the most effective time cycles for such an engine test? Is it possible that more realistic cycles could later be evolved? If so, we could be headed into the same maze that we now have with the burner rigs. These are only a few questions which arise.

With regard to the paper, it is suggested that visible corrosion effects may not be the best absolute measure. The presence of visible corrosion may well point out a potential problem area. It may not present a ready answer. Substitution of materials should not be made based on visual corrosion effects alone. Factors such as fatigue strength, creep, and stress rupture need be considered and these are not amenable to short time engine tests. What may be indicated is the need for a design or configuration change.

In conclusion, engine testing is a vital part of the whole picture. The benefits to be gained from engine testing are real, valuable, and cost economical. An absolute or ultimate engine test cycle may yet be far away and universal materials for all engine applications may be farther still.

U S GOVERNMENT PRINTING OFFICE : 1974 O - 531-743